B DECAYS AT THE LHC

CERN–TH/2000–101
hep–ph/0003238

Conveners*: P. Ball, R. Fleischer, G.F. Tartarelli, P. Vikas, G. Wilkinson*
Contributing authors*: J. Baines, S.P. Baranov, P. Bartalini, M. Beneke, E. Bouhova, G. Buchalla, I. Caprini, F. Charles, J. Charles, Y. Coadou, P. Colangelo, P. Colrain, J. Damet, F. De Fazio, A. Dighe, H. Dijkstra, P. Eerola, N. Ellis, B. Epp, S. Gadomski, P. Galumian, I. Gavrilenko, S. George, V.M. Ghete, V. Gibson, L. Guy, Y. Hasegawa, P. Iengo, A. Jacholkowska, R. Jones, A. Khodjamirian, E. Kneringer, P. Koppenburg, H. Korsmo, N. Labanca, L. Lellouch, M. Lehto, Y. Lemoigne, J. Libby, J. Matias, S. Mele, M. Misiak, A.M. Nairz, T. Nakada, A. Nikitenko, N. Nikitin, A. Nisati, F. Palla, E. Polycarpo, J. Rademacker, F. Rizatdinova, S. Robins, D. Rousseau, W. Ruckstuhl, M.A. Sanchis, O. Schneider, M. Shapiro, C. Shepherd-Themistocleous, P. Sherwood, L. Smirnova, M. Smizanska, A. Starodumov, N. Stepanov, Z. Xie, N. Zaitsev*
Acknowledgements*: Thanks to M. Battaglia, M. Ciuchini, A. Deandrea, G. Eigen, A. Lenz, D. Liko, L. Moroni, N. Neufeld and D. Wyler who also contributed to the workshop.*

Abstract
We review the prospects for B decay physics at the LHC as discussed in the 1999 workshop on Standard Model physics at the LHC.

Contents

1 THEORETICAL INTRODUCTION **1**
1.1 CP Violation in the B System 1
1.2 Rare B Decays 8
1.3 Other B Physics Topics 9

2 EXPERIMENTAL OVERVIEW **9**
2.1 Introduction 9
2.2 Luminosity 11
2.3 Monte Carlo Generators, Simulation Methods and Assumed Cross-Sections 11
2.4 Proper Time Resolution 12
2.5 Particle Identification 12
2.6 Triggers 13
2.7 Flavour Tagging 14

3 BENCHMARK CP MODES **17**
3.1 Extracting β from $B_d \to J/\psi\, K_{\rm S}$ 17
3.2 Probing α with $B_d \to \pi^+\pi^-$ 23
3.3 Extracting α from $B \to \rho\pi$ Modes 28
3.4 Extracting $2\beta + \gamma$ from $B_d \to D^{(*)\pm}\pi^{\mp}$ Decays 31
3.5 Extracting $\gamma - 2\delta\gamma$ from $B_s \to D_s^{\pm}K^{\mp}$ Decays 36
3.6 Extracting γ from $B \to DK$ Decays 37

4 THE "GOLD-PLATED" DECAY $B_s \to J/\psi\,\phi$ **40**
4.1 Theoretical Aspects 40
4.2 Experimental Studies 45
4.3 Conclusions 48

5 NEW STRATEGIES TO EXTRACT CKM PHASES **48**
5.1 Extracting γ from $B \to \pi K$ Decays . . . 49
5.2 Extracting γ from $B_{s(d)} \to J/\psi\, K_{\rm S}$ Decays . . . 57
5.3 Extracting γ from $B_{d(s)} \to D^{+}_{d(s)} D^{-}_{d(s)}$ Decays . . . 60
5.4 A Simultaneous Determination of β and γ from $B_d \to \pi^+\pi^-$ and $B_s \to K^+K^-$ . . . 63
5.5 Conclusions . . . 67

6 SYSTEMATIC ERROR CONSIDERATIONS IN CP MEASUREMENTS **67**
6.1 Introduction . . . 67
6.2 Sources and Categories of Systematic Bias . . . 67
6.3 Use of Control Channels . . . 69
6.4 Application to the $\rm B_d \to J/\psi K^0_S$ Sample . . . 72
6.5 Other Measurements and Conclusions . . . 72

7 B–$\bar{\rm B}$ MIXING **72**
7.1 Hadronic Matrix Elements from Lattice Calculations . . . 73
7.2 The Mass Difference ΔM . . . 76
7.3 The Width Difference $\Delta\Gamma$ . . . 76
7.4 Measurement of B^0_s Oscillations . . . 77

8 RARE DECAYS **79**
8.1 $B^0 \to \mu^+\mu^-$ . . . 81
8.2 $B \to K^*\gamma$ . . . 83
8.3 $B \to K^*\mu^+\mu^-$ . . . 86
8.4 Inclusive Decays . . . 91
8.5 Conclusions . . . 93

9 THEORETICAL DESCRIPTION OF NON-LEPTONIC DECAYS **93**
9.1 Non-Factorizable Contributions to $B \to J/\psi K^{(*)}$ . . . 94
9.2 Dispersion Relations for B Non-Leptonic Decays into Light Pseudoscalar Mesons . . . 96
9.3 QCD Factorization for Exclusive Non-Leptonic B Decays . . . 98

10 B_c PHYSICS **101**
10.1 B_c Lifetime and Inclusive Decays . . . 101
10.2 Leptonic and Radiative Leptonic B_c Decays . . . 102
10.3 Semileptonic B_c Decay Modes . . . 102
10.4 Non-Leptonic Decay Modes . . . 103
10.5 B_c Decays induced by FCNC Transitions . . . 104
10.6 CP Violation in B_c Decays . . . 104
10.7 Experimental Considerations . . . 104
10.8 Concluding Remarks . . . 104

11 CONCLUSIONS **105**

1 THEORETICAL INTRODUCTION[1]

The exploration of physics with b flavoured hadrons offers a very fertile testing ground for the Standard Model (SM) description of electroweak interactions. One of the key problems to be studied is the phenomenon of CP violation, which, although already discovered in 1964 by Christenson, Cronin, Fitch and Turlay in the neutral kaon system [1], is still one of the experimentally least constrained phenomena. Another main topic is the study of rare b decays induced by flavour changing neutral current (FCNC) transitions $b \to s, d$, which are loop-suppressed in the SM and thus very sensitive to new-physics effects.

During the last few years, B physics has received a lot of attention, both from theorists and experimentalists, and we are presently at the beginning of the B factory era in particle physics. The BaBar (SLAC), BELLE (KEK) and HERA-B (DESY) detectors have already seen their first events, and CLEO-III (Cornell), CDF-II and D0-II (Fermilab) will start taking data in the near future (see [2] for a recent experimental overview). Although the physics potential of these experiments is very promising, it may well be that the "definite" answer in the search for new physics in B decays will be left for second-generation B experiments at hadron machines. In the following, we will give an overview of the B physics potential of the LHC experiments ATLAS, CMS and LHCb, with the main focus on SM physics.

1.1 CP Violation in the B System

Among the most interesting aspects and unsolved mysteries of modern particle physics is the violation of CP symmetry. Studies of CP violation are particularly exciting, as they may open a window to the physics beyond the SM. There are many interesting ways to explore CP violation, for instance through certain rare K or D meson decays (a very recent comprehensive description of all aspects of CP symmetry and its violation can be found in Ref. [3]). However, for testing the SM description of CP violation in a quantitative way, the B system appears to be most promising [4, 5, 6].

1.1.1 The SM Description of CP Violation

Within the framework of the SM, CP violation is closely related to the Cabibbo–Kobayashi–Maskawa (CKM) matrix [7, 8], connecting the electroweak eigenstates (d', s', b') of the down, strange and bottom quarks with their mass eigenstates (d, s, b) through the following unitary transformation:

$$\begin{pmatrix} d' \\ s' \\ b' \end{pmatrix} = \begin{pmatrix} V_{ud} & V_{us} & V_{ub} \\ V_{cd} & V_{cs} & V_{cb} \\ V_{td} & V_{ts} & V_{tb} \end{pmatrix} \cdot \begin{pmatrix} d \\ s \\ b \end{pmatrix} \equiv \hat{V}_{\rm CKM} \cdot \begin{pmatrix} d \\ s \\ b \end{pmatrix} . \tag{1.1}$$

The elements of the CKM matrix describe charged-current couplings, as can be easily seen by expressing the non-leptonic charged-current interaction Lagrangian in terms of the electroweak eigenstates (1.1):

$$\mathcal{L}_{\rm int}^{\rm CC} = -\frac{g_2}{\sqrt{2}} \left(\begin{array}{ccc} \bar{u}_{\rm L}, & \bar{c}_{\rm L}, & \bar{t}_{\rm L} \end{array} \right) \gamma^\mu \, \hat{V}_{\rm CKM} \begin{pmatrix} d_{\rm L} \\ s_{\rm L} \\ b_{\rm L} \end{pmatrix} W_\mu^\dagger \quad + \quad h.c., \tag{1.2}$$

where the gauge coupling g_2 is related to the gauge group $\mathrm{SU_L}(2)$ and the $W_\mu^{(\dagger)}$ fields describe the charged W bosons.

In the case of three generations, three generalized Cabibbo-type angles [7] and a single *complex phase* [8] are needed in order to parametrize the CKM matrix. This complex phase allows one to accommodate CP violation in the SM, as was pointed out by Kobayashi and Maskawa in 1973 [8]. A closer look shows that CP-violating observables are proportional to the following combination of CKM matrix elements [9]:

$$J_{\rm CP} = \pm \, \mathrm{Im} \left(V_{ik} V_{jl} V_{il}^* V_{jk}^* \right) \quad (i \neq j, \, l \neq k) \, , \tag{1.3}$$

[1] Section coordinators: P. Ball and R. Fleischer, with help from G. Buchalla and L. Lellouch.

which represents a measure of the "strength" of CP violation in the SM. Since $J_{\rm CP} = \mathcal{O}(10^{-5})$, CP violation is a small effect. However, in scenarios of new physics [10], typically several additional complex couplings are present, leading to new sources of CP violation.

As far as phenomenological applications are concerned, the following parametrization of the CKM matrix, the "Wolfenstein parametrization" [11], which corresponds to a phenomenological expansion in powers of the small quantity $\lambda \equiv |V_{us}| = \sin\theta_{\rm C} \approx 0.22$, turns out to be very useful:

$$\hat{V}_{\rm CKM} = \begin{pmatrix} 1-\frac{1}{2}\lambda^2 & \lambda & A\lambda^3(\rho - i\eta) \\ -\lambda & 1-\frac{1}{2}\lambda^2 & A\lambda^2 \\ A\lambda^3(1-\rho-i\eta) & -A\lambda^2 & 1 \end{pmatrix} + \mathcal{O}(\lambda^4). \tag{1.4}$$

The terms of $\mathcal{O}(\lambda^4)$ can be taken into account systematically [12], and will play an important rôle below.

1.1.2 The Unitarity Triangle(s) of the CKM Matrix

Concerning tests of the CKM picture of CP violation, the central targets are the *unitarity triangles* of the CKM matrix. The unitarity of the CKM matrix, which is described by

$$\hat{V}_{\rm CKM}^{\dagger} \cdot \hat{V}_{\rm CKM} = \hat{1} = \hat{V}_{\rm CKM} \cdot \hat{V}_{\rm CKM}^{\dagger}, \tag{1.5}$$

leads to a set of 12 equations, consisting of 6 normalization and 6 orthogonality relations. The latter can be represented as 6 triangles in the complex plane, which all have the same area [13]. However, in only two of them, all three sides are of comparable magnitude $\mathcal{O}(\lambda^3)$, while in the remaining ones, one side is suppressed relative to the others by $\mathcal{O}(\lambda^2)$ or $\mathcal{O}(\lambda^4)$. The orthogonality relations describing the non-squashed triangles are given as follows:

$$V_{ud}\,V_{ub}^* + V_{cd}\,V_{cb}^* + V_{td}\,V_{tb}^* = 0 \tag{1.6}$$

$$V_{ud}^*\,V_{td} + V_{us}^*\,V_{ts} + V_{ub}^*\,V_{tb} = 0. \tag{1.7}$$

The two non-squashed triangles agree at leading order in the Wolfenstein expansion, i.e. at $\mathcal{O}(\lambda^3)$, so that we actually have to deal with a single triangle at this order, which is usually referred to as "the" unitarity triangle of the CKM matrix [14]. However, in the LHC era, the experimental accuracy will be so tremendous that we will have to take into account the next-to-leading order terms of the Wolfenstein expansion, and distinguish between the unitarity triangles described by (1.6) and (1.7), which are illustrated in Fig. 1. Here, $\overline{\rho}$ and $\overline{\eta}$ are related to the Wolfenstein parameters ρ and η through [12]

$$\overline{\rho} \equiv \left(1 - \lambda^2/2\right)\rho, \quad \overline{\eta} \equiv \left(1 - \lambda^2/2\right)\eta. \tag{1.8}$$

Note the angles of the triangles, in particular those designated by α, β, γ and $\delta\gamma$. These will be referred to frequently throughout this report. The sides R_b and R_t of the unitarity triangle shown in Fig. 1(a) are given as follows:

$$R_b = \left(1 - \frac{\lambda^2}{2}\right)\frac{1}{\lambda}\left|\frac{V_{ub}}{V_{cb}}\right| = \sqrt{\overline{\rho}^2 + \overline{\eta}^2} = 0.41 \pm 0.07, \tag{1.9}$$

$$R_t = \frac{1}{\lambda}\left|\frac{V_{td}}{V_{cb}}\right| = \sqrt{(1-\overline{\rho})^2 + \overline{\eta}^2} = \mathcal{O}(1). \tag{1.10}$$

1.1.3 Non-Leptonic B Decays and Low-Energy Effective Hamiltonians

With respect to testing the SM description of CP violation, the major rôle is played by non-leptonic B decays, which can be divided into three decay classes: decays receiving both "tree" and "penguin" contributions, pure "tree" decays, and pure "penguin" decays. There are two types of penguin topologies:

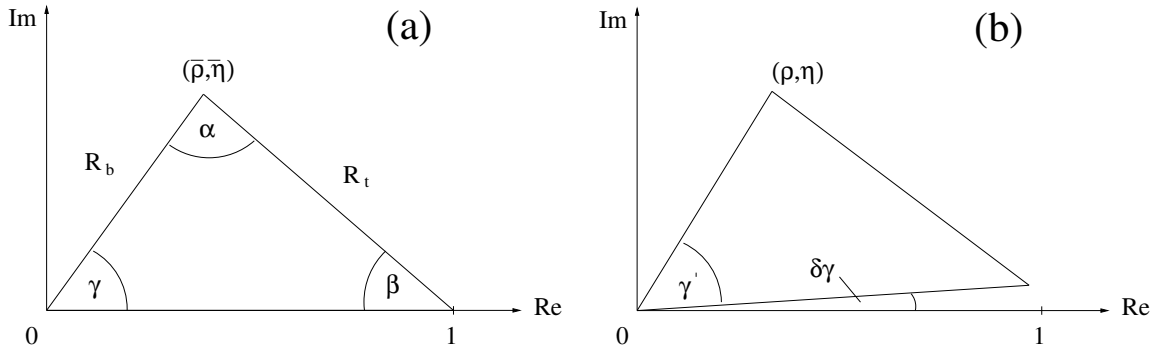

Fig. 1: The two non-squashed unitarity triangles of the CKM matrix: (a) and (b) correspond to the orthogonality relations (1.6) and (1.7), respectively.

gluonic (QCD) and electroweak (EW) penguins, which are related to strong and electroweak interactions, respectively. Because of the large top-quark mass, also the latter operators play an important rôle in several processes [15, 16, 17].

In order to analyse non-leptonic B decays theoretically, one uses low-energy effective Hamiltonians, which are calculated by making use of the operator product expansion, yielding transition matrix elements of the following structure:

$$\langle f|\mathcal{H}_{\text{eff}}|i\rangle \propto \sum_k C_k(\mu)\langle f|Q_k(\mu)|i\rangle\,. \tag{1.11}$$

The operator product expansion allows one to separate the short-distance contributions to this transition amplitude from the long-distance ones, which are described by perturbative Wilson coefficient functions $C_k(\mu)$ and non-perturbative hadronic matrix elements $\langle f|Q_k(\mu)|i\rangle$, respectively. As usual, μ denotes an appropriate renormalization scale.

In the case of $|\Delta B| = 1$, $\Delta C = \Delta U = 0$ transitions, which will be of particular interest for the exploration of CP violation in the B system, we have

$$\mathcal{H}_{\text{eff}} = \mathcal{H}_{\text{eff}}(\Delta B = -1) + \mathcal{H}_{\text{eff}}(\Delta B = -1)^\dagger, \tag{1.12}$$

where

$$\mathcal{H}_{\text{eff}}(\Delta B = -1) = \frac{G_{\text{F}}}{\sqrt{2}}\left[\sum_{j=u,c} V_{jq}^* V_{jb}\left\{\sum_{k=1}^{2} Q_k^{jq}\, C_k(\mu) + \sum_{k=3}^{10} Q_k^{q}\, C_k(\mu)\right\}\right]. \tag{1.13}$$

Here $\mu = \mathcal{O}(m_b)$ is a renormalization scale, the Q_k^{jq} are four-quark operators, the label $q \in \{d, s\}$ corresponds to $b \to d$ and $b \to s$ transitions, and k distinguishes between current–current ($k \in \{1, 2\}$), QCD ($k \in \{3, \ldots, 6\}$) and EW ($k \in \{7, \ldots, 10\}$) penguin operators. The calculation of such low-energy effective Hamiltonians has been reviewed in [18], where the four-quark operators Q_k^{jq} are given explicitly, and where also numerical values for their Wilson coefficient functions can be found.

1.1.4 B–$\bar{B}$ Mixing

The eigenstates of flavour, $B_q = (\bar{b}q)$ and $\bar{B}_q = (b\bar{q})$ ($q = d$, s), degenerate in pure QCD, mix on account of weak interactions. The quantum mechanics of the two-state system, with basis $\{|1\rangle, |2\rangle\} \equiv \{|B_q\rangle, |\bar{B}_q\rangle\}$, is described by a complex, 2×2 Hamiltonian matrix

$$\mathbf{H} = \mathbf{M} - \frac{i}{2}\mathbf{\Gamma} = \begin{pmatrix} M & M_{12} \\ M_{12}^* & M \end{pmatrix} - \frac{i}{2}\begin{pmatrix} \Gamma & \Gamma_{12} \\ \Gamma_{12}^* & \Gamma \end{pmatrix} \tag{1.14}$$

with Hermitian matrices $\mathbf{M}$ and $\mathbf{\Gamma}$. The off-diagonal elements in (1.14) arise from $\Delta B = 2$ flavour-changing transitions with virtual (M_{12}) or real intermediate states (Γ_{12}), in the latter case corresponding to decay channels common to B and $\bar{B}$.

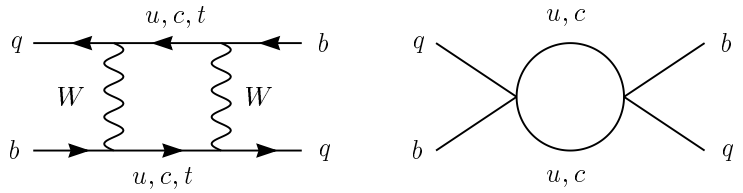

Fig. 2: (a): General box diagram describing B–$\bar{\text{B}}$ mixing. (b): Special case of diagram (a) with internal u and c, whose absorptive part determines Γ_{12}.

Diagonalizing (1.14), one obtains the physical eigenstates B_H ('heavy'), B_L ('light') and the corresponding eigenvalues $M_{H,L} - \frac{i}{2}\Gamma_{H,L}$. The mass and width differences read

$$\Delta M_q \equiv M_H^{(q)} - M_L^{(q)} = 2|M_{12}^{(q)}|, \qquad \Delta\Gamma_q \equiv \Gamma_H^{(q)} - \Gamma_L^{(q)} = \frac{2\mathrm{Re}(M_{12}^{(q)*}\Gamma_{12}^{(q)})}{|M_{12}^{(q)}|}\,. \tag{1.15}$$

ΔM is positive by definition, $\Delta\Gamma$ is defined in such a way that a negative value[2] is obtained in the SM for the case of B_s, where a sizeable width difference is expected. In the SM, the off-diagonal elements M_{12} and Γ_{12} inducing B mixing are described by the box diagrams in Fig. 2.

Detailed numerical results will be given Sec. 7; here we only summarize a few important general characteristics of $\Delta B = 2$ second-order weak processes. The relative size of the various contributions is controlled by CKM quantities and quark masses. With $\lambda_i^{(q)} = V_{iq}^* V_{ib}$, and denoting the magnitude in powers of the Wolfenstein parameter λ, we have $\lambda_u^{(d)} \sim \lambda_c^{(d)} \sim \lambda_t^{(d)} \sim \lambda^3$ for B_d, and $\lambda_u^{(s)} \sim \lambda^4$, $\lambda_c^{(s)} \sim \lambda_t^{(s)} \sim \lambda^2$ for B_s. Because the box amplitude strongly grows with large ($\gg m_b$) internal quark masses m_i, proportional to m_i^2 for $m_i \gg M_W$, it is clear, considering the above CKM hierarchy, that the top-quark contribution completely dominates the *dispersive part* M_{12}. The remaining contributions ($i = u$, c) are safely negligible for both the B_d and B_s system. Since m_t, $M_W \gg m_b$, M_{12} is described by an effectively local interaction already at scales far above m_b. External mass scales can thus be neglected and the resulting $\Delta B = 2$ effective Hamiltonian is governed by a single operator. It acquires the simple form

$$\mathcal{H}_{\text{eff}}^{\Delta B=2} = (V_{tq}^* V_{tb})^2 C\,(x_t)\,(\bar{q}b)_{V-A}(\bar{q}b)_{V-A} \tag{1.16}$$

with C the short-distance Wilson-coefficient and $x_t = m_t^2/m_W^2$, whence M_{12} is obtained as

$$M_{12} = \frac{1}{2M_B}\langle B|\mathcal{H}_{\text{eff}}^{\Delta B=2}|\bar{B}\rangle. \tag{1.17}$$

For the *absorptive part* Γ_{12} the situation is more complicated. First of all, the top contribution, dominant for M_{12}, cannot contribute to Γ_{12}, since, by kinematics, top quarks are forbidden as on-shell final states in B decays. Γ_{12} is then determined by the (absorptive parts of) box diagrams with up and charm quarks. Both up and charm are important for B_d because $\lambda_u^{(d)} \sim \lambda_c^{(d)}$. In the case of B_s, the up-quark sector is negligible ($\lambda_u^{(s)} \ll \lambda_c^{(s)}$). In calculating Γ_{12}, the heavy W boson lines can be contracted to form two local $\Delta B = 1$ four-quark interactions (Fig. 2(b)). By contrast, u and c are lighter than the relevant scale of the process ($\sim m_b$) and cannot be integrated out, unlike the top quark in M_{12}. Consequently, Γ_{12} is given as the matrix element of a non-local (or 'bi-local') product of two local $\Delta B = 1$ Hamiltonian operators $\mathcal{H}_{\text{eff}}^{\Delta B=1}$, the usual effective weak Hamiltonian describing B decays:

$$\Gamma_{12} = \frac{1}{2M_B}\langle B|\mathrm{Im}\, i\int d^4x\, T\,\mathcal{H}_{\text{eff}}^{\Delta B=1}(x)\mathcal{H}_{\text{eff}}^{\Delta B=1}(0)|\bar{B}\rangle\,. \tag{1.18}$$

[2]Note that also the opposite sign convention for $\Delta\Gamma$ is used in the literature.

To lowest order in the strong interaction, (1.18) corresponds to the absorptive part (Im) of the diagram in Fig. 2(b). Taking the absorptive part inside the formal expression (1.18), the T-product is transformed into an ordinary product of the two factors $\mathcal{H}_{\rm eff}^{\Delta B=1}$. Inserting a complete set of hadronic final states f gives

$$\Gamma_{12}^{\rm (hadron)} = \sum_f \langle B|\mathcal{H}_{\rm eff}^{\Delta B=1}|f\rangle\langle f|\mathcal{H}_{\rm eff}^{\Delta B=1}|\bar{B}\rangle, \tag{1.19}$$

where one recognizes the usual expression for a decay rate, generalized here to the off-diagonal entry Γ_{12}. This connection, which allows one to write Γ_{12} in (1.18) as the absorptive part of the $\bar{B} \to B$ forward scattering amplitude, is known as the optical theorem. $\Gamma_{12}^{\rm (hadron)}$ does, however, escape direct calculation, which instead starts from (1.18): taking advantage of the large momentum $\sim m_b \gg \Lambda_{\rm QCD}$ flowing through the internal u and c quark lines of the box diagram, one expands the operator product into a series of local operators [19]:

$$\Gamma_{12}^{\rm (quark)} = \frac{1}{2M_B}\,\langle B \mid \mathrm{Im}\, i\int d^4x\, T\,\mathcal{H}_{\rm eff}^{\Delta B=1}(x)\mathcal{H}_{\rm eff}^{\Delta B=1}(0) \mid \bar{B}\rangle = \frac{1}{2M_B}\sum_n \frac{C_n}{m_b^n}\langle B \mid Q_n^{\Delta B=2} \mid \bar{B}\rangle\,. \tag{1.20}$$

The identification of the exact $\Gamma_{12}^{\rm (hadron)}$ with the approximation $\Gamma_{12}^{\rm (quark)}$ based on the heavy quark expansion is equivalent to the assumption of local quark-hadron duality ('local' in this context refers to the fact that the large energy scale m_b is, in practice, a fixed number, rather than a variable allowing for the consideration of some ('global') averaging procedure). When viewed as a function of m_b, $\Gamma_{12}^{\rm (hadron)}$ is expected to include terms of the form $\exp(-(m_b/\Lambda_{\rm QCD})^k)\,\sin((m_b/\Lambda_{\rm QCD})^k)$. Such oscillating and exponentially suppressed terms are related to the opening of new decay channels as m_b is increased. They are however completely missed in $\Gamma_{12}^{\rm (quark)}$ to any finite order in the heavy quark expansion, which is just a power series in $\Lambda_{\rm QCD}/m_b$. Of course, for asymptotically large $m_b/\Lambda_{\rm QCD} \to \infty$, these terms vanish much faster than power corrections. In any case $\Gamma_{12}^{\rm (quark)} \to \Gamma_{12}^{\rm (hadron)}$ in the strict limit $m_b \to \infty$. Nevertheless, for realistic values of m_b those terms may introduce a deviation of $\Gamma_{12}^{\rm (quark)}$ from the correct $\Gamma_{12}^{\rm (hadron)}$ (beyond the omission of higher power corrections). This error is referred to as a violation of local duality. Theoretical knowledge from first principles about duality violating contributions is so far rather limited. Interesting general discussions and further information can be found in Refs. [20, 21, 22].

1.1.5 CP Violation in Neutral B Decays into CP Eigenstates

The description of CP violation in terms of weak phases becomes particularly simple for decays of neutral B_q mesons ($q \in \{d, s\}$) into CP self-conjugate final states $|f\rangle$, satisfying the relation

$$(\mathcal{CP})|f\rangle = \pm\,|f\rangle. \tag{1.21}$$

In this case, the corresponding time-dependent CP asymmetry can be expressed as

$$\begin{aligned}\mathcal{A}_{\rm CP}(t) &\equiv \frac{\Gamma(B_q^0(t)\to f) - \Gamma(\overline{B_q^0}(t)\to f)}{\Gamma(B_q^0(t)\to f) + \Gamma(\overline{B_q^0}(t)\to f)} \\ &= 2\,e^{-\Gamma_q t}\left[\frac{\mathcal{A}_{\rm CP}^{\rm dir}(B_q\to f)\cos(\Delta M_q t) + \mathcal{A}_{\rm CP}^{\rm mix}(B_q\to f)\sin(\Delta M_q t)}{e^{-\Gamma_{\rm H}^{(q)}t} + e^{-\Gamma_{\rm L}^{(q)}t} + \mathcal{A}_{\Delta\Gamma}(B_q\to f)\left(e^{-\Gamma_{\rm H}^{(q)}t} - e^{-\Gamma_{\rm L}^{(q)}t}\right)}\right],\end{aligned} \tag{1.22}$$

where $\Delta M_q \equiv M_{\rm H}^{(q)} - M_{\rm L}^{(q)}$ denotes the mass difference between the B_q mass eigenstates, and $\Gamma_{\rm H,L}^{(q)}$ are the corresponding decay widths, with

$$\Gamma_q \equiv \frac{\Gamma_{\rm H}^{(q)} + \Gamma_{\rm L}^{(q)}}{2}\,. \tag{1.23}$$

In Eq. (1.22), we have separated the "direct" from the "mixing-induced" CP-violating contributions, which are described by

$$\mathcal{A}_{\rm CP}^{\rm dir}(B_q \to f) \equiv \frac{1-|\xi_f^{(q)}|^2}{1+|\xi_f^{(q)}|^2} \quad \text{and} \quad \mathcal{A}_{\rm CP}^{\rm mix}(B_q \to f) \equiv \frac{2\,{\rm Im}\left\{\xi_f^{(q)}\right\}}{1+|\xi_f^{(q)}|^2}\,, \tag{1.24}$$

respectively. Here direct CP violation refers to CP-violating effects arising directly in the corresponding decay amplitudes, whereas mixing-induced CP violation is due to interference effects between B_q^0–$\overline{B_q^0}$ mixing and decay processes. Whereas the width difference $\Delta\Gamma_q$ is negligible in the B_d system, it may be sizeable in the B_s system [23, 24], thereby providing the observable

$$\mathcal{A}_{\Delta\Gamma}(B_q \to f) \equiv \frac{2\,{\rm Re}\left\{\xi_f^{(q)}\right\}}{1+|\xi_f^{(q)}|^2}, \tag{1.25}$$

which is not independent of $\mathcal{A}_{\rm CP}^{\rm dir}(B_q \to f)$ and $\mathcal{A}_{\rm CP}^{\rm mix}(B_q \to f)$:

$$\left[\mathcal{A}_{\rm CP}^{\rm dir}(B_s \to f)\right]^2 + \left[\mathcal{A}_{\rm CP}^{\rm mix}(B_s \to f)\right]^2 + \left[\mathcal{A}_{\Delta\Gamma}(B_s \to f)\right]^2 = 1. \tag{1.26}$$

Essentially all the information needed to evaluate the CP asymmetry (1.22) is included in the following quantity:

$$\xi_f^{(q)} = \mp\, e^{-i\phi_q}\, \frac{\sum\limits_{j=u,c} V_{jr}^* V_{jb} \langle f|\mathcal{Q}^{jr}|\overline{B_q^0}\rangle}{\sum\limits_{j=u,c} V_{jr} V_{jb}^* \langle f|\mathcal{Q}^{jr}|\overline{B_q^0}\rangle}\,, \tag{1.27}$$

where

$$\mathcal{Q}^{jr} \equiv \sum_{k=1}^{2} Q_k^{jr} C_k(\mu) + \sum_{k=3}^{10} Q_k^{jr} C_k(\mu), \tag{1.28}$$

$r \in \{d, s\}$ distinguishes between $\bar{b} \to \bar{d}$ and $\bar{b} \to \bar{s}$ transitions, and

$$\phi_q = \begin{cases} +2\beta & (q = d) \\ -2\delta\gamma & (q = s) \end{cases} \tag{1.29}$$

is the weak B_q^0–$\overline{B_q^0}$ mixing phase which is related to the phase of M_{12}, Eq. (1.17). In general, the observable $\xi_f^{(q)}$ suffers from hadronic uncertainties, which are introduced by the hadronic matrix elements in Eq. (1.27). However, if the decay $B_q \to f$ is dominated by a single CKM amplitude, the corresponding matrix elements cancel, and $\xi_f^{(q)}$ takes the simple form

$$\xi_f^{(q)} = \mp \exp\left[-i\left(\phi_q - \phi_{\rm D}^{(f)}\right)\right], \tag{1.30}$$

where $\phi_{\rm D}^{(f)}$ is a weak decay phase, which is given as follows:

$$\phi_{\rm D}^{(f)} = \begin{cases} -2\gamma & \text{for dominant } \bar{b} \to \bar{u}\,u\,\bar{r} \text{ CKM amplitudes,} \\ 0 & \text{for dominant } \bar{b} \to \bar{c}\,c\,\bar{r} \text{ CKM amplitudes.} \end{cases} \tag{1.31}$$

This simple formalism has several interesting applications, probably the most important one is the extraction of the CKM angle β from CP-violating effects in the "gold-plated" mode $B_d \to J/\psi\, K_{\rm S}$. In addition to the CP-violating effects in neutral B decays into CP eigenstates discussed above, also certain modes into non-CP eigenstates, for example $B_d \to D^{(*)\pm}\pi^{\mp}$ and $B_s \to D_s^{\pm} K^{\mp}$, play an outstanding rôle to extract CKM phases. These decays will be discussed in more detail in Secs. 3.4 and 3.5.

1.1.6 The "El Dorado" for the LHC: the B_s System

The e^+e^- B factories operating at the $\Upsilon(4S)$ resonance will not be in a position to explore the B_s system. Since it is, moreover, very desirable to have large data samples available to study B_s decays, they are of particular interest for hadron machines and were one of the central targets of this workshop. There are important differences between the B_d and B_s systems:

- Within the SM, a large B_s^0–$\overline{B_s^0}$ mixing parameter $x_s \equiv \Delta M_s/\Gamma_s = \mathcal{O}(20)$ is expected, whereas the mixing phase $\phi_s = -2\lambda^2\eta$ is expected to be very small.
- There may be a sizeable width difference $\Delta\Gamma_s/\Gamma_s = \mathcal{O}(15\%)$, whereas $\Delta\Gamma_d$ is negligible.

The mass difference ΔM_s plays an important rôle to constrain the apex of the unitarity triangle shown in Fig. 1(a), and the non-vanishing width difference $\Delta\Gamma_s$ may allow studies of CP-violating effects in "untagged" B_s rates, [25]–[28], which are defined as follows:

$$\Gamma_s[f(t)] \equiv \Gamma(B_s^0(t) \to f) + \Gamma(\overline{B_s^0}(t) \to f) = \text{PhSp} \times \left[R_{\rm H}\, e^{-\Gamma_{\rm H}^{(s)} t} + R_{\rm L}\, e^{-\Gamma_{\rm L}^{(s)} t}\right], \tag{1.32}$$

where "PhSp" denotes an appropriate, straightforwardly calculable phase-space factor. Interestingly, there are no rapid oscillatory $\Delta M_s t$ terms present in this expression. Although it should be no problem to resolve these B_s^0–$\overline{B_s^0}$ oscillations at the LHC, studies of such untagged rates, which allow the extraction of the observable $\mathcal{A}_{\Delta\Gamma}$ introduced in (1.25) as

$$\mathcal{A}_{\Delta\Gamma} = \frac{R_{\rm H} - R_{\rm L}}{R_{\rm H} + R_{\rm L}}, \tag{1.33}$$

are interesting in terms of efficiency, acceptance and purity.

1.1.7 CP Violation in Charged B Decays

Since there are no mixing effects present in the charged B meson system, non-vanishing CP asymmetries of type

$$\mathcal{A}_{\rm CP}(B^+ \to \overline{f}) \equiv \frac{\Gamma(B^+ \to \overline{f}) - \Gamma(B^- \to f)}{\Gamma(B^+ \to \overline{f}) + \Gamma(B^- \to f)} \tag{1.34}$$

would give us unambiguous evidence for "direct" CP violation in the B system, which has recently been demonstrated in the kaon system by the new experimental results of the KTeV (Fermilab) and NA48 (CERN) collaborations for $\text{Re}(\varepsilon'/\varepsilon)$ [29].

The CP asymmetries (1.34) arise from the interference between decay amplitudes with both different CP-violating weak and different CP-conserving strong phases. In the SM, the weak phases are related to the phases of the CKM matrix elements, whereas the strong phases are induced by final-state-interaction (FSI) processes. In general, the strong phases introduce severe theoretical uncertainties into the calculation of $\mathcal{A}_{\rm CP}(B^+ \to \overline{f})$, thereby destroying the clean relation to the CP-violating weak phases. However, there is an important tool to overcome these problems, which is provided by *amplitude relations* between certain non-leptonic B decays. There are two types of such relations:

- Exact relations, which involve $B \to DK$ decays (pioneered by Gronau and Wyler [30]).
- Approximate relations, which rely on the flavour-symmetries of strong interactions and certain plausible dynamical assumptions, and involve $B \to \pi K$, $\pi\pi$, $K\overline{K}$ decays (pioneered by Gronau, Hernández, London and Rosner [31, 32]).

Unfortunately, the $B \to DK$ approach, which allows a *theoretically clean* determination of γ, makes use of certain amplitude-triangles that are expected to be rather squashed. Moreover, there are additional experimental problems [33], so that this approach is very challenging from a practical point of view. The flavour-symmetry relations between the $B \to \pi K$, $\pi\pi$, $K\overline{K}$ decay amplitudes have received considerable attention in the literature during the last couple of years and led to interesting strategies to probe the CKM angle γ.

1.1.8 Outline of the CP Violation Part

The outline of the part of this chapter dealing with aspects related to CP violation and the determination of the angles of the unitarity triangles is as follows: after an overview of the experimental aspects in Sec. 2, we have a closer look at the benchmark modes to explore CP violation in Sec. 3, where we will discuss the extraction of β from the "gold-plated" decay $B_d \to J/\psi\, K_{\rm S}$, the prospects to probe α with $B_d \to \pi^+\pi^-$ and $B \to \rho\pi$ modes, as well as extractions of γ from $B_d \to D^{*\pm}\pi^\mp$ and $B_s \to D_s^\pm K^\mp$ decays. Finally, we will also give a discussion of γ determinations from $B \to DK$ modes.

Section 4 is devoted to a detailed analysis of another CP benchmark mode, $B_s \to J/\psi\,\phi$, which is particularly promising for the LHC experiments because of its favourable experimental signature and its rich physics potential, allowing one to extract the B_s^0–$\overline{B_s^0}$ mixing parameters ΔM_s and $\Delta\Gamma_s$, as well as the corresponding CP-violating weak mixing phase ϕ_s. Since the CP-violating effects in $B_s \to J/\psi\,\phi$ are tiny in the SM, this channel offers an important tool to search for new physics.

In Sec. 5, we focus on strategies to extract CKM phases that were not considered for the LHC experiments so far, and on new methods, which were developed during this workshop [34]. We discuss extractions of the angle γ from $B \to \pi K$ decays, which received a lot of attention in the literature during the last couple of years. Moreover, we discuss extractions of γ that are provided by $B_{s(d)} \to J/\psi\, K_{\rm S}$ and $B_{d(s)} \to D^+_{d(s)} D^-_{d(s)}$ decays, and a simultaneous determination of β and γ from a combined analysis of the decays $B_d \to \pi^+\pi^-$ and $B_s \to K^+K^-$.

Systematic error considerations in CP measurements are discussed in Sec. 6, and the reach for the B_s^0–$\overline{B_s^0}$ mixing parameters ΔM_s and $\Delta\Gamma_s$ is presented in Sec. 7.

1.2 Rare B Decays

By rare B decays, one commonly understands heavily Cabibbo-suppressed $b \to u$ transitions or flavour-changing neutral currents (FCNC) $b \to s$ or $b \to d$ that in the SM are forbidden at tree-level. Rare decays are an important testing ground of the SM and offer a strategy in the search for new physics complementary to that of direct searches by probing the indirect effects of new interactions in higher order processes. Assuming the validity of the SM, rare FCNC decays allow the measurement of the CKM matrix elements $|V_{ts}|$ and $|V_{td}|$ and thus complement their determination from B^0–$\bar{B}^0$ mixing. Any significant deviation between these two determinations would hint at new physics. With the large statistics available at the LHC, also decay spectra will be accessible, which will allow a direct measurement of virtual new physics effects: in some contrast to the investigation of CP violation, we are in the lucky situation that the impact of new physics on FCNC processes can be defined in a *model-independent* way[3]: at quark-level, $b \to q$, $q = (d, s)$, transitions can be described in terms of an effective Hamiltonian obtained by integrating out virtual effects of heavy particles (top quark and W boson in the SM):

$$\mathcal{H}_{\rm eff}(b \to q) = -4\,\frac{G_F}{\sqrt{2}}\,V_{tb}V_{tq}^*\sum_{i=1}^{10} C_i(\mu)O_i(\mu). \tag{1.35}$$

The relevant operators will be specified in Sec. 8; here we would like to stress that the short-distance coefficients $C_i(\mu)$ encode both perturbative QCD evolution between the hadronic scale $\mu \sim O(m_b)$ and the scale of heavy particles M_H and information on the physics at that scale itself, contained in $C_i(M_H)$. A measurement of these coefficients that significantly deviates from the SM expectation thus would constitute immediate and unambiguous evidence for new physics beyond the SM.

In this report, we concentrate on decays that have a favourable experimental signature at the LHC and for which experimental studies exist at the time of writing: the exclusive decays $B_{d,s} \to \mu^+\mu^-$, $B_d \to K^*\gamma$ and $B_d \to K^*\mu^+\mu^-$. Although it is generally believed that theoretical uncertainties due

[3] Barring the possibility that new physics induces new operators not present in the SM, like e.g. in a left-right symmetric model.

to non-perturbative QCD effects are larger for exclusive than for inclusive decays, the experimental environment of a hadronic machine renders it exceedingly difficult to perform inclusive measurements. There has, however, been recent progress in the calculation of exclusive hadronic matrix elements [35], which narrows down the theoretical uncertainty, and as we shall elaborate on in Sec. 8, one can define experimental observables in which a large fraction of theoretical uncertainties cancels.

1.3 Other B Physics Topics

The B physics potential of the LHC is by far not exhausted by the programme sketched above. Possible further lines of investigation include physics with b flavoured baryons (lifetime measurements, spectra, decay dynamics etc.), physics of b flavoured mesons other than $B_{u,d,s}$ (radial and orbital excitations, B_c), and the study of purely leptonic or semileptonic decays, $B_q \to e\nu$, $B_q \to Me\nu$, where M stands for a meson. From the theory point of view, one major topic whose relevance goes beyond the LHC is the calculation of non-leptonic decay amplitudes from first principles: whereas the discussion in Secs. 3 to 5 promotes a very pragmatic approach which aims at eliminating ("controlling") the effects of strong interactions by measuring a large number of observables that are related by certain approximate symmetry principles, it remains a challenge for theory to provide *predictions* for non-leptonic decay amplitudes, both in factorization approximation and beyond.

Only a limited number of such topics were discussed during the workshop, and so we restrict ourselves to the presentation of selected aspects and review the present status of the theory of non-leptonic decays in Sec. 9, relevant for the prediction of decay rates in general and the extraction of weak phases from CP asymmetries in theoretically "dirty" channels in particular; in Sec. 10, we give an overview of the physics opportunities and predicted decay rates in B_c decays.

2 EXPERIMENTAL OVERVIEW[4]

The LHC will represent a unique opportunity for B physics studies. At a centre-of-mass energy of $\sqrt{s} = 14$ TeV the production cross-section for $b\overline{b}$ pairs will be very high. While current theoretical predictions of the absolute value are rather uncertain, it is expected that it will be about a factor of five higher than the one obtainable at the Tevatron, running at $\sqrt{s} = 2$ TeV. Naturally, therefore, B physics has been an important consideration in the optimization of the LHC experimental programme. The two multi-purpose experiments, ATLAS [36, 37] and CMS [38], have the capabilities to realize a rich and competitive programme and a dedicated experiment, LHCb [39], will have the sole task of exploiting as wide a range of B physics topics as possible.

2.1 Introduction

The ATLAS and CMS detectors (see Fig. 3) have been designed primarily to search for new particles, such as the Higgs boson. The detectors therefore should be able to operate at the highest LHC luminosity and be sensitive to the highest mass scale. However, specific features required for B hadron reconstruction have been accommodated in the design. Both experiments have also put strong emphasis on 'b tagging' (discrimination between b jets and jets from light quarks, which is used in a variety of physics analyses), but this is not discussed in this chapter.

Both the ATLAS and CMS detectors cover the central region of the pp interaction point and have forward-backward and azimuthal symmetry. Inside a super-conducting solenoid (generating a 2 T magnetic field in ATLAS and a 4 T field in CMS, parallel to the beam line), a multi-layer tracking system (ATLAS [40], CMS [41]) covering the $|\eta| < 2.5$ region is located. The system has higher granularity detector layers at small radii (silicon pixel and micro-strip detectors) for good impact parameter resolution and track separation and extends to large radii to improve the transverse momentum resolution

[4]Section coordinator: G.F. Tartarelli, with help from Y. Lemoigne and C. Shepherd-Themistocleous.

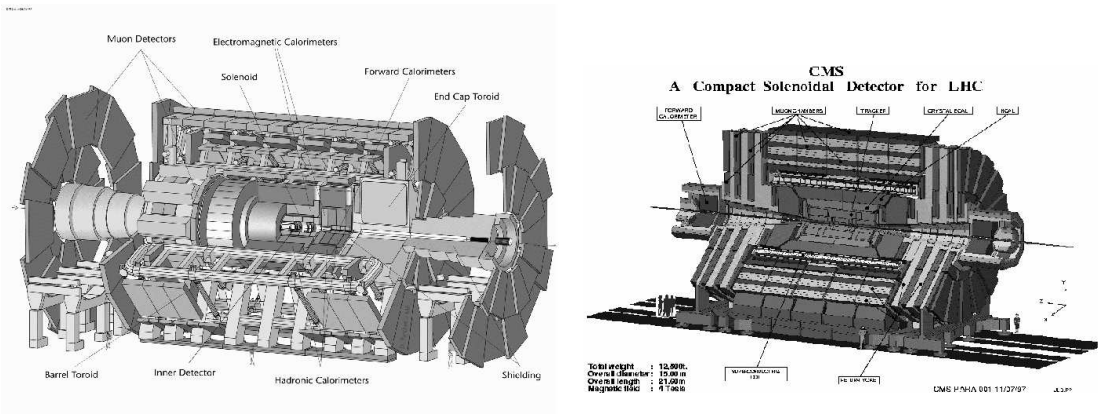

Fig. 3: Pictorial 3D-views of the two central multi-purpose LHC detectors: ATLAS (left) and CMS (right).

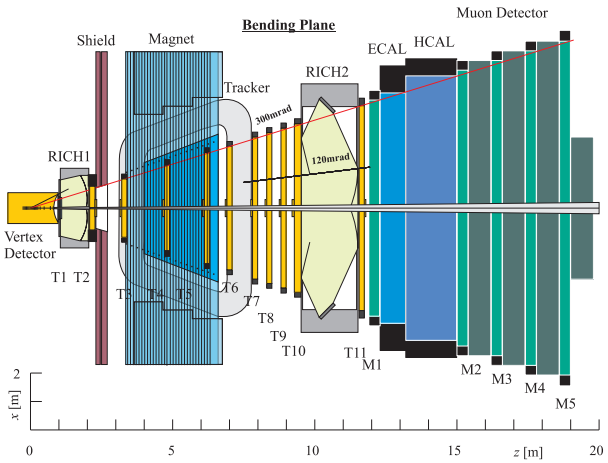

Fig. 4: Schematic 2D view of the LHCb detector in the bending plane. The interaction point is at $z = 0$.

(in ATLAS the tracking system has also additional electron/pion separation as explained Sec. 2.5). In both experiments, the tracking system is surrounded by electromagnetic and hadronic calorimeters (ATLAS [42], CMS [43]) which extend up to about $|\eta| = 5.0$. Finally, outside the calorimeters there are high-precision muon chambers (in the region $|\eta| < 2.7$ in ATLAS [44] and $|\eta| < 2.4$ in CMS [45]) and muon trigger chambers in a smaller pseudo-rapidity range ($|\eta| < 2.4$ in both ATLAS and CMS).

The LHCb detector is a single-arm spectrometer covering the forward region of the pp interactions. A schematic view is shown in Fig. 4. The detector covers the angular region from 10 mrad up to 300 mrad in the horizontal plane (the *bending plane*) and from 10 mrad up to 250 mrad in the vertical plane (the *non-bending plane*), corresponding to the approximate range $2.1 < \eta < 5.3$ in terms of pseudo-rapidity. Starting from the interaction point, it consists of a silicon vertex detector, a RICH detector and a tracking system; the tracking system is followed by a second RICH detector, electromagnetic and hadron calorimeters and by muon detectors. The vertex detector, which is located inside the beam pipe, also includes a pile-up veto counter to reject events with multiple pp interactions. The tracking system is partly included in a dipole magnet field with a maximum value of 1.1 T in the vertical direction. The calorimetry system extends from 30 mrad to 300 (250) mrad in the horizontal (vertical) direction. Muon coverage is assured in the angular range 25 (15) mrad to 294 (245) mrad in the horizontal (vertical) direction.

2.2 Luminosity

The LHC is being built to run at a design luminosity of $10^{34}\,\mathrm{cm}^{-2}\,\mathrm{s}^{-1}$ to maximize the potential for discovering new, heavy particles. From the point of view of B hadron reconstruction, multiple interactions and pile-up effects in the detectors are a complication both at trigger level and in the reconstruction of relatively low-p_T particles. Moreover, the high luminosity will deteriorate the performance (both in terms of radiation damage and occupancy) of the innermost tracking layer when the reconstruction of the B meson vertex position is needed.

It is expected, however, that the LHC will reach design luminosity only gradually in time, starting at $10^{33}\,\mathrm{cm}^{-2}\,\mathrm{s}^{-1}$ and taking three years to reach $10^{34}\,\mathrm{cm}^{-2}\,\mathrm{s}^{-1}$. ATLAS and CMS will take advantage of this so-called *low-luminosity* period in order to carry out most of their B physics programme. At this luminosity, each crossing will have an average of 2 to 3 pile-up events in the tracking detectors which, however, have been shown not to affect significantly the detector performances. It is under current investigation if it is possible to continue certain studies at higher luminosity: for some critical channels, like very rare decays (see Sec. 8), this has been already demonstrated to be feasible (both at trigger and reconstruction level).

In order to have a clean environment, well suited to B physics, the luminosity at LHCb will be locally controlled to have a mean value of $2 \times 10^{32}\,\mathrm{cm}^{-2}\,\mathrm{s}^{-1}$, even when the machine is operating at design luminosity. This value is chosen to optimize the number of single interaction bunch crossings, which will make up $\sim 75\%$ of crossings within an interaction, and to ensure that radiation damage and occupancy problems are not too severe.

In this report we will present estimates of the b physics potential of the three experiments at various integrated luminosities. When a simple comparison is needed, the results will be normalized to one year of running: this corresponds to $2 \times 10^3\,\mathrm{pb}^{-1}$ for LHCb and to $10^4\,\mathrm{pb}^{-1}$ for ATLAS and CMS running at low luminosity. More often the full potential of each experiment is presented: here we take 5 years of running for LHCb and 3 years at low luminosity for ATLAS and CMS (unless the study can be extended into the high-luminosity running period). Whenever possible, the results of the three experiments have been statistically combined to estimate the *ultimate* LHC potential.

2.3 Monte Carlo Generators, Simulation Methods and Assumed Cross-Sections

For the performance studies presented in this chapter, large samples of B hadron events have been produced using the PYTHIA 5.7/JETSET 7.4 [46] event generator. In the ATLAS Monte Carlo (MC), flavour-creation, flavour-excitation and gluon-splitting production processes were included. In CMS, flavour-creation and gluon-splitting were included (see also discussion in the "Bottom production" Chapter of this report [47]). The LHCb MC production was based on flavour-creation and flavour-excitation processes, with additional samples including gluon-splitting. The CTEQ2L [48] set of parton-distribution functions has been used. The Peterson function (with $\epsilon_b = 0.007$) has been used to fragment b quarks to B hadrons. The other PYTHIA physics parameters have been set to their default values. The agreement between PYTHIA predictions and theoretical calculations is discussed elsewhere in this report.

The response of the detectors to the generated particles is simulated with programs based on the GEANT [49] package. Then the event is reconstructed in the sub-detectors relevant to each particular analysis; event reconstruction includes full pattern recognition in the tracking detectors, vertexing and particle identification (muons and electrons and π/K separation, if available).

The procedure detailed above is called *full simulation* and has been used for the majority of the analyses presented. In some cases, a *fast simulation* which does not use GEANT, but a simple parametrization of the detector response has been used.

The results have been normalized assuming a total inelastic cross-section of $80\,\mathrm{mb}$ and a $b\overline{b}$ cross-section of $500\,\mu\mathrm{b}$.

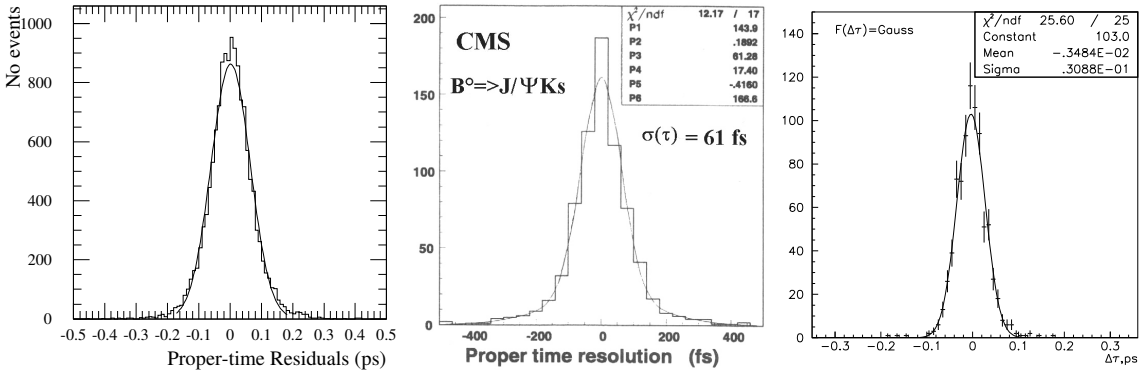

Fig. 5: Typical proper time residual distributions for ATLAS (left), CMS (centre) and LHCb (right). The plots refer to reconstructed $B_s^0 \to J/\psi\phi$ (ATLAS, LHCb) and $B_d^0 \to J/\psi K_S^0$ (CMS) decays.

2.4 Proper Time Resolution

Different detector layouts used by the three experiments lead to differences in the impact parameter and proper decay-time resolutions.

In LHCb the impact parameter is measured in the R–z plane: the resolution increases with transverse momentum and reaches an asymptotic value of about 40 μm already for tracks with transverse momenta $p_T > 3\,\text{GeV}$ [39]. Particles coming from B decays are mostly above this threshold and so LHCb can achieve a proper time resolution (for fully reconstructed exclusive decays) of about $0.031\,\text{ps}$ (see Fig.5).

The ATLAS and CMS experiments measure precisely the projection of the track impact parameter in the R–ϕ plane [37, 38]. The plateau value (for high-p_T tracks) of the transverse impact parameter resolution is about 11 μm (for comparison, the asymptotic value for the impact parameter in the R–z plane is about 90 μm); however, most of the tracks from B decays concentrate in the low-p_T region where the resolution degrades due to multiple scattering. The proper time resolutions in ATLAS and CMS for typical fully reconstructed B decays are characterized by a Gaussian distribution with a width of about $0.060\,\text{ps}$ (see Fig.5).

The proper time resolution estimates summarized in this section refer either to the $B_s^0 \to J/\psi\phi$ decay analysis discussed in Sec. 4 or to the $B_d^0 \to J/\psi K_s^0$ sample (see Sec. 3.1). Slightly different values are estimated according to the B decay channel under study.

2.5 Particle Identification

Particle identification is a very important tool in many B physics channels. In particular, π/K separation plays a key rôle in hadronic B decays (see Secs. 3 and 5), allowing the separation of the decays of interest from similar, and indeed identical, topologies that would otherwise have overlapping (and in some cases overwhelming) spectra. Moreover, π/K separation is crucial for one of the techniques (*kaon* tagging) used to identify the flavour of the b hadron at production (see Sec. 2.7 for a short review of flavour tagging methods).

For this purpose, the LHCb detector has a dedicated system composed of two RICH detectors. The first system, RICH1, located upstream of the magnet, uses silica aerogel and C_4F_{10} as radiators: this detector is intended to identify low-momentum particles over the full angular acceptance. The RICH2 detector, which uses CF_4, is located downstream of the magnet and covers a smaller solid angle. The purpose of this detector is to complement RICH1 by covering the high-end of the momentum spectrum. The performance of LHCb's RICH is shown in Fig. 8. Pions and kaons can be cleanly separated with a significance of more than $10\,\sigma$ in most of the momentum range $1\,\text{GeV} < p < 150\,\text{GeV}$. Efficiencies and purities are expected to be in excess of 90%.

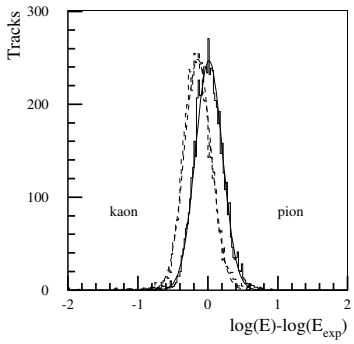

Fig. 6: Logarithm of the energy deposited in the ATLAS straw tracker normalized to the expected energy deposit of a pion, for $p_T = 5\,\text{GeV}$ pions (solid line) and kaons (dashed line).

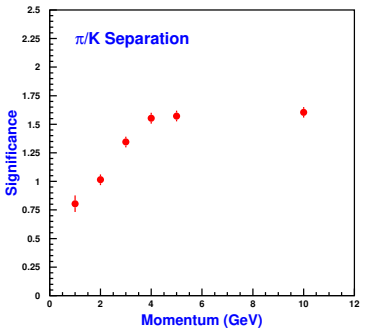

Fig. 7: CMS dE/dx pion/kaon separation, plotted in units of σ versus track momentum.

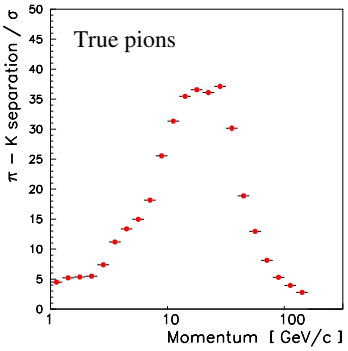

Fig. 8: LHCb RICH pion/kaon separation, after pattern recognition, plotted in units of σ against momentum for true pions.

In the absence of dedicated detectors for particle identification, ATLAS and CMS have studied other methods for obtaining some level of pion/kaon separation, although with reduced performance. The CMS silicon tracker has analogue read-out electronics so that the pulse-height information is preserved and can be used to estimate dE/dx. Preliminary results have been obtained [50] using a full GEANT simulation of the CMS tracker system described in [41]. This study estimates the asymptotic performance of the detector: a number of effects that can influence the dE/dx resolution have not been simulated and will be the subject of future investigations when test-beam data will be available. The estimated π/K separation, shown in Fig. 7 as a function of the particle momentum, has been used to obtain some of the CMS results presented in Sec. 3.

The ATLAS outer tracking system, which uses drift tubes (or *straws*) to provide an average of 36 hits per track, has electron/pion separation capability. The space between the straws is filled with radiator material, and transition-radiation photons, created by crossing electrons, are detected by using a Xenon-based gas mixture in the straws and a double-threshold read-out electronics. This detector can provide some π/K separation using dE/dx, although the pulse-height is not measured [37]. Information about the deposited energy is extracted from the offset and accuracy of the measured drift distance, the fraction of high-threshold hits and the fraction of missing low-threshold hits. A preliminary study has concluded that, by combining all this information, a π/K separation of $0.8\,\sigma$ for tracks with $p_T \sim 5\,\text{GeV}$ can be obtained. The expected performance of this method is shown in Fig. 6. The separation is not good enough to identify individual pions and kaons, but can be used on a statistical basis. A more recent study, incorporating some changes to the readout format of the straw-tracker data, which provide a measurement of time-over-threshold for low-threshold hits, improves the separation significantly.

2.6 Triggers

Triggering is the key-issue for B physics studies at the LHC. Careful trigger-strategies are needed to extract interesting channels from inelastic collisions and the trigger-strategies used by ATLAS [51] and CMS [52] will be different from those used by LHCb, whose trigger is entirely dedicated to B decays. For robustness and flexibility, all three experiments will use multi-level trigger systems with the ATLAS and CMS triggers being divided into three and the LHCb trigger into four levels.

The lowest trigger level of ATLAS [53] and CMS [54], called level-1, which operates at the 40 MHz machine bunch-crossing frequency, uses reduced-granularity data from the muon trigger chambers and from the calorimeters. B physics is accommodated in these triggers by pushing the lepton transverse-momentum thresholds down to the minimum possible, still keeping the output trigger rate

compatible with the acceptance rate of the next trigger level, level-2. In ATLAS this is achieved by requiring a single muon with $p_T > 6$ GeV in $|\eta| < 2.4$. The possibility of using a level-1 dimuon trigger with η-dependent thresholds is under study as a means of increasing statistics. However, all ATLAS studies reported in this chapter have been obtained requiring at least one muon with $p_T > 6$ GeV. In CMS, lower transverse momentum thresholds can be achieved, by adding to the single lepton trigger ($p_T > 7$ GeV for muons and $p_T > 12$ GeV for electrons) also double-lepton triggers ($\mu\mu$, μe and ee) with thresholds which vary with pseudo-rapidity and can go down to 2 or 4 GeV for the two-muon case and to 5 GeV for the two-electron case.

The lowest trigger level in LHCb, called level-0, works at 40 MHz and is based on the identification of single leptons, hadrons and photons with high-p_T in calorimeters and muon chambers. Because of the forward geometry, and high output rate, the 'high'-p_T threshold can be as low as 1 GeV. The hadron trigger allows the collection of large event samples in rare decay channels without leptons. The level-0 trigger is combined with the pile-up veto to reject bunch crossings likely to contain more than one pp interaction. After the pile-up veto, the rate is reduced to about 9 MHz already, so that the high-p_T trigger has to provide only an additional reduction factor of about 10 to match the design level-0 output rate of about 1 MHz. The allocation of bandwidth between the trigger components and the assignment of thresholds is adjustable to match running conditions and physics requirements. At present the nominal thresholds for the single particle triggers are 1 GeV for muons, 2.3 GeV for electrons, 2.4 GeV for hadrons and 4 GeV for photons.

In ATLAS, the level-2 trigger [55] uses full-granularity data from the muon system, the calorimeters and from the tracking system. The level-2 trigger will confirm and refine the level-1 information and then look for specific final states according to the physics channel to be studied. Fast algorithms will be used to reconstruct tracks in the tracking system to allow p_T and mass-cuts. The second-muon trigger threshold will be set to $p_T = 3$ GeV. The dimuon trigger covers both some rare B decays and channels with J/ψ's in the final state. Triggers with $J/\psi \to ee$, with the p_T threshold on the two electrons as low as 0.5 GeV, will also be available. Hadronic triggers will be available for selected channels. The maximum total level-2 output rate is limited to about 1 kHz. CMS will follow a similar strategy.

In LHCb, the next trigger-level after level-0, called level-1, uses information from the *vertex* detector. This trigger is meant to complement the level-0 information by exploiting the displacement of b decay vertices. The vertex trigger will first reconstruct the event primary vertex and then look for track pairs with significant impact parameters with respect to the primary vertex, which are close in space. This signature provides high efficiency in all B decay modes. The total output rate is about 40 kHz. Successively, the level-2 trigger will refine the vertex trigger by adding momentum information to the tracks forming the secondary vertices and reduce the data rate to 5 kHz.

In all three experiments, the final trigger decision will be taken by a level-3 trigger which feeds full event data from all detectors to an offline-like algorithm to reconstruct specific final states. Selected events will be stored for offline analysis.

The trigger performance of the experiments will be summarized elsewhere in this report, for certain important decay modes. It will become clear that the enormous rate of B production at the LHC can indeed be properly exploited.

2.7 Flavour Tagging

An important issue of many CP-violation and B^0 mixing studies is the determination of the flavour of a b hadron at production. The LHC experiments have already successfully investigated several tagging strategies, but the studies are not yet completed (ATLAS [56], CMS [57], LHCB [39]).

Tagging algorithms can be divided into two broad categories: *Opposite Side* (OS) and *Same Side* (SS) algorithms, according to whether one studies the b or the $\overline{b}$ quark in the event. The nomenclature, OS and SS, used to distinguish between the b and $\overline{b}$ quarks, is used for historical reasons (it is derived from

the LEP experiments), but it does not imply that the two quarks be produced in separate hemispheres. Indeed, for the LHCb experiment there is *no* other side and both the b and the $\overline{b}$ quarks are produced predominantly in the same forward-cone. Moreover, for the LHC experiments, the importance of the gluon-splitting mechanism for producing $b\overline{b}$ pairs implies that the two quarks be not always on opposite sides. We will thus include in the OS category all algorithms that try to deduce the initial flavour of the B meson under study by identifying the flavour of the other b hadron in the event. In the SS category we include all algorithms that look directly at the particles accompanying the B meson which has decayed in the channel under investigation (also called *signal* B in the following).

It can be shown that the statistical error of an asymmetry measurement is inversely proportional to the quantity $(1-2\omega)\sqrt{\epsilon N}$, where N is the total (untagged) number of events, ϵ is the tagging efficiency and ω is the wrong-tag fraction. For this reason, tagger-cuts are chosen in order to maximize the *quality factor* $Q = \epsilon D^2$, where $D = 1-2\omega$ is called tagger-*dilution*. Approximate numbers for efficiencies and dilutions for the algorithms described below are listed in Tab. 1. Further developments and cut optimization might be needed to improve the performance of the tagging algorithms already studied and to bring all of them at the same level of understanding. The majority of the presented results refers to the $B^0_d \to J/\psi K^0_s$ sample (see Sec. 3.1). Variations from sample to sample have been observed. Because of this and because of differences in the simulation details, trigger-selections and analysis-cuts, a direct comparison between tagger potentials (and experimental performance) is not straightforward.

2.7.1 Opposite Side Tagging

The OS techniques which have been studied up to now by the LHC experiments are: lepton (muon or electron) tagging, kaon tagging (LHCb only) and jet-charge tagging.

In the lepton-tagging method, one looks for a lepton in the event coming from the semileptonic decay of the other b quark in the event: $b \to l$. This method has a low efficiency (due to the relatively low b semileptonic branching ratio of about 10%), but good purity, which is further enhanced by the fact that all three experiments use leptons also for triggering. The main contributions to the mistag rate are due to flavour mixing of the neutral B mesons and to cascade decays $b \to c \to l$. Wrong tags from cascade decays can be reduced by increasing the lepton p_T threshold. It has also been shown [56] that the mistag rate increases with increasing p_T of the signal B for a fixed lepton-tag transverse-momentum threshold. For the studies presented in this chapter, the threshold has been set to 5 GeV for both electrons and muons in the ATLAS analysis, to 2 (2.5) GeV for muons (electrons) in CMS and to 1.5 GeV for both muons and electrons in LHCb.

Kaon tagging exploits the decay chain $b \to c \to s$ to identify the flavour of the b quark from the charge of the kaon produced in the cascade decay. This method can be only used by LHCb as it requires the particle identification capability of the RICH detector. Candidate kaons are searched for down to a p_T of 0.4 GeV and are required to have impact parameter significance incompatible with the reconstructed primary vertex at the 3σ level. For kaon tagging (as well as for lepton tagging), if more than one candidate survives all cuts, the one with the highest p_T is chosen.

Jet-charge tagging deduces the flavour of the other b quark in the event by looking at the total charge of the tracks which belong to the b fragmentation. At LEP, where this algorithm was first developed, the identification of the opposite-side jet in $Z \to b\overline{b}$ events was almost straightforward. At the LHC, the other b jet may escape the detector-acceptance and can be identified only by dedicated jet-clustering algorithms. These algorithms are usually based on track clustering possibly seeded by displaced tracks. Once the jet has been found, the jet total charge, Q_{jet}, is defined by an average of the tracks' charge in the cluster, weighted by a function of their momenta. The right (wrong) sign events are then defined as those with $Q_{jet} > +c$ ($Q_{jet} < -c$), where c is a tunable cut. Although investigated in the past, OS jet charge is not used in the ATLAS analyses presented in this report. The LHCb numbers for this tagging method, which are calculated for events where no other type of tag has been found, are preliminary and are not used for the results presented in this chapter.

2.7.2 *Same Side Tagging*

The SS techniques presented in this section exploits production and fragmentation properties of the B meson to deduce its flavour. These techniques are not affected by mistags due to mixing. Moreover, as they apply to the same B meson whose decay is under investigation, there is no loss of efficiency due to the identification of the other b jet in the event.

During the process of a $\overline{b}$ quark fragmentation to produce a B_d^0 meson, pions which are charge-correlated to the flavour of the B meson, can be produced by two mechanisms [58]. The $\overline{b}$ quark can pick up a d quark from the quark sea to form a B_d^0, thus making available a $\overline{d}$ quark to form a π^+. Another mechanism proceeds through production of orbitally excited states of B mesons, called B^{**}, which then decay to B_d^0: $B^{**} \to B^{(*)0}\pi^+$. If a B^{*0} is produced, it decays radiatively as $B^{*0} \to B^0\gamma$.

The B–π *correlation* method, studied by ATLAS, exploits these correlations by searching for low-p_T pions, compatible with coming from the primary vertex, in proximity of the decayed B meson. Tracks belonging to the B decay products are excluded and what it is called *pion* is actually a generic charged track, as no π/K separation is used. In this method, both production mechanisms described above contribute correlated pions and no attempt is made to separate these two contributions.

The CMS experiment prefers to concentrate on the explicit reconstruction of the B^{**} resonance (B^{**} *method*). In the MC, these resonances have been modelled according to [59]. In this method, pions with $p_T > 1$ GeV are combined with a B_d^0 to give a B^{**} meson with a mass between 5.6 and 5.9 GeV. As above, the charge sign of the associated pion gives the tag. No attempt is made to reconstruct the low-p_T photon which is present when a B^{*0} is produced in the cascade and to resolve the different peaks which superimpose in the B^{**} mass spectrum. It would also be possible to study the mistag rate from the data itself by looking at the *side-bands* of the mass resonance, so that one need not rely only on the MC modelling of the process.

Similar to the B–π correlation method, the B_s^0 tagging method, which is under investigation by LHCb, consists in looking for a primary kaon in the vicinity of the B_s^0 meson. Efficiency and dilution for this tagger, which is not used for the results presented in this chapter, are preliminary.

In a different approach, it is possible to use jet-charge tagging also on the *same side*. In this case, similarly to the OS jet-charge tagging, the jet charge is a weighted average of the charge of the tracks in the jet, but the tracks belonging to the B meson decay products are excluded from the sum. The weights are functions of the momentum of the track and are often written in the form $w(p)^k$, where $w(p)$ can be chosen as the transverse momentum, the projection of the momentum along the B direction or a more complicated function of them. The parameter k controls the relative weights of soft and hard tracks in the total charge.

2.7.3 *Combined Tagging*

The *best* tagging strategy would combine all taggers, weighted by their dilutions, simultaneously on both sides on an event-by-event basis. This requires, however, a full understanding of tagger correlations. The CMS experiment has performed a preliminary study of these correlations for four of the tagger algorithms described above (lepton tag, B^{**}, SS jet charge and OS jet charge). The results are summarized in Tab. 2, where, for pairs of algorithms, the combined efficiency is shown, taking into account overlaps. Correlations are sizeable (e.g. between B^{**} and SS jet charge tags, as expected) and need to be properly taken into account in combining taggers.

In a simplified approach, overlaps can be avoided by applying taggers one after the other, i.e. by applying the second tagger on the sample not tagged by the first one (and so on). The LHCb experiment combines lepton and kaon tagging: if more than one tag is present in one event, the *best* tag is chosen in the following order: muon, electron and kaon. The combined efficiency and dilution of this algorithm is reported in Tab. 1. In ATLAS, only lepton tagging and B–π tagging have been statistically combined so far. Lepton tagging (which has the highest purity) is applied first and then, on the remaining events,

Tagging Method			ATLAS		CMS		LHCb	
			ϵ	D	ϵ	D	ϵ	D
OS	Lepton Tag	e	0.016	0.46	0.027	0.44	0.40	0.40
		μ	0.025	0.52	0.034	0.44		
	Kaon Tag		n/a		n/a			
	Jet Charge		n/a		0.70	0.18	0.60	0.16
SS	B–π		0.82	0.16	n/a		n/a	
	B^{**}		n/a		0.22	0.32	n/a	
	Jet Charge		0.62	0.23	0.50	0.23	n/a	
	B_s^0 tag		n/a		n/a		0.11	0.34

Table 1: Efficiencies (ϵ) and dilutions (D) for the flavour-tagging algorithms described in the text. The shorthand "n/a" (*not available*) means that one tagger either cannot be used or has not yet been fully studied by a particular experiment. The LHCb numbers for lepton and kaon tagging refer to the combined algorithm described in the text.

A	B	$\epsilon(A)$	$\epsilon(B)$	$\epsilon(A)+\epsilon(B)$	$\epsilon(A\cup B)$
Lepton Tag	B^{**}	0.06	0.215	0.275	0.26
Lepton Tag	SS Jet Charge	0.06	0.5	0.56	0.53
Lepton Tag	OS Jet Charge	0.06	0.7	0.76	0.72
B^{**}	SS Jet Charge	0.215	0.5	0.715	0.56
B^{**}	OS Jet Charge	0.215	0.7	0.915	0.76
SS Jet Charge	OS Jet Charge	0.5	0.7	1.2	0.845

Table 2: Combined tagging efficiencies from CMS MC. The last column shows the combined efficiency of algorithms A and B when the overlap has been subtracted: $\epsilon(A\cup B)=\epsilon(A)+\epsilon(B)-\epsilon(A\cap B)$.

tagging pions are searched for. Similarly, CMS combines four algorithms in the following order (of decreasing dilution): lepton tagging, B^{**}, SS jet charge and OS jet charge. Each tagger is applied, with its own dilution, on the sample not tagged by the previous one; in the end, the total number of selected events is four times as large as the initial lepton tagged sample.

3 BENCHMARK CP MODES[5]

This section deals with the use of benchmark B decays to explore CP violation and to extract the angles of the unitarity triangles. By 'benchmark' we mean modes that are well established in the literature. Some, but by no means all, of these channels will be probed by other experiments before the LHC starts to operate. To be specific, we will discuss the extraction of β from mixing-induced CP violation in the "gold-plated" decay $B_d \to J/\psi\, K_{\rm S}$, the prospects to probe α with $B_d \to \pi^+\pi^-$ and $B \to \rho\pi$ modes, as well as extractions of γ from $B_d \to D^{*\pm}\pi^{\mp}$ and $B_s \to D_s^{\pm}K^{\mp}$ decays. Finally, we will also give a discussion of the determination of γ from $B \to DK$ decays. Since $B_s \to J/\psi\,\phi$ – another benchmark CP mode – is of particular interest for the LHC, we have devoted a separate section to the discussion of the physics potential of this "gold-plated" mode for the LHC experiments: Sec. 4.

3.1 Extracting β from $B_d \to J/\psi\, K_{\rm S}$[6]

Probably the most important application of the formalism discussed in Sec. 1.1.5 is the decay $B_d \to J/\psi\, K_{\rm S}$ [60], which is a transition into a CP eigenstate with eigenvalue -1 and originates from $\bar{b} \to \bar{c}\,c\,\bar{s}$ quark-level decays.

[5] Section coordinators: R. Fleischer and G. Wilkinson.

[6] With help from P. Colrain, Y. Lemoigne and G.F. Tartarelli.

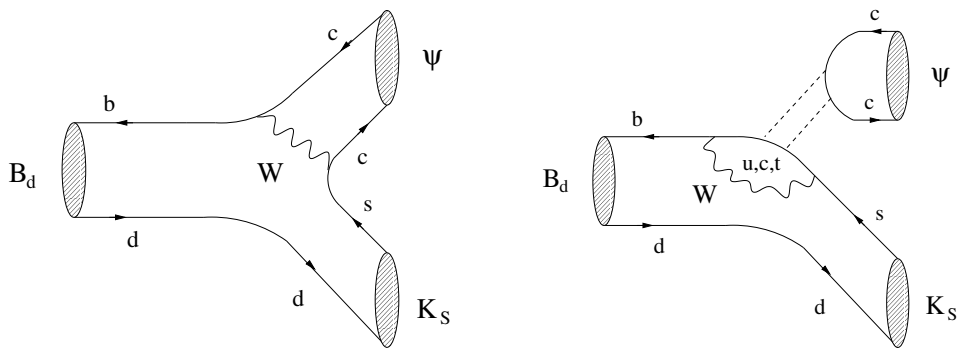

Fig. 9: Feynman diagrams contributing to $B_d \to J/\psi\, K_{\rm S}$, consisting of colour-suppressed tree-diagram-like and penguin topologies. The dashed lines in the penguin topology represent a colour-singlet exchange.

3.1.1 Theoretical Aspects

In the case of $B_d \to J/\psi\, K_{\rm S}$, we have to consider both current–current, i.e. tree-diagram-like, and penguin contributions, as depicted in Fig. 9. The corresponding transition amplitude can be written as follows [61]:

$$A(B_d^0 \to J/\psi\, K_{\rm S}) = \lambda_c^{(s)} \left(A_{\rm cc}^{c'} + A_{\rm pen}^{c'}\right) + \lambda_u^{(s)} A_{\rm pen}^{u'} + \lambda_t^{(s)} A_{\rm pen}^{t'}\,, \tag{3.1}$$

where $A_{\rm cc}^{c'}$ denotes the current–current contributions, i.e. the "tree" processes in Fig. 9, and the amplitudes $A_{\rm pen}^{q'}$ describe the contributions from penguin topologies with internal q quarks ($q \in \{u, c, t\}$). These penguin amplitudes take into account both QCD and electroweak penguin contributions. The primes in (3.1) remind us that we are dealing with a $\bar{b} \to \bar{s}$ transition, and the $\lambda_q^{(s)} \equiv V_{qs} V_{qb}^*$ are CKM factors. Making use of the unitarity of the CKM matrix and applying the generalized Wolfenstein parametrization, including non-leading terms in λ, we obtain

$$A(B_d^0 \to J/\psi\, K_{\rm S}) = \left(1 - \frac{\lambda^2}{2}\right) \mathcal{A}' \left[1 + \left(\frac{\lambda^2}{1-\lambda^2}\right) a' e^{i\theta'} e^{i\gamma}\right], \tag{3.2}$$

where

$$\mathcal{A}' \equiv \lambda^2 A \left(A_{\rm cc}^{c'} + A_{\rm pen}^{ct'}\right) \;\text{ and }\; a' e^{i\theta'} \equiv R_b \left(\frac{A_{\rm pen}^{ut'}}{A_{\rm cc}^{c'} + A_{\rm pen}^{ct'}}\right) \tag{3.3}$$

with $A_{\rm pen}^{ct'} \equiv A_{\rm pen}^{c'} - A_{\rm pen}^{t'}$. The quantity $A_{\rm pen}^{ut'}$ is defined in analogy to $A_{\rm pen}^{ct'}$, and the CKM factor A is given as follows:

$$A \equiv \frac{1}{\lambda^2} |V_{cb}| = 0.81 \pm 0.06\,; \tag{3.4}$$

the definition of $R_b = 0.41 \pm 0.07$ can be found in (1.9).

It is very difficult to calculate the "penguin" parameter $a' e^{i\theta'}$, which introduces the CP-violating phase factor $e^{i\gamma}$ into the $B_d^0 \to J/\psi\, K_{\rm S}$ decay amplitude and represents – sloppily speaking – the ratio of the penguin to tree contributions. However, this parameter, and therefore also $e^{i\gamma}$, enters in (3.2) in a doubly Cabibbo-suppressed way. Consequently, to a very good approximation, $B_d^0 \to J/\psi\, K_{\rm S}$ is dominated by only *one* CKM amplitude, so that, from (1.24) and (1.30):

$$\mathcal{A}_{\rm CP}^{\rm mix}(B_d \to J/\psi\, K_{\rm S}) = +\sin[-(\phi_d - 0)] = -\sin(2\beta)\,. \tag{3.5}$$

Since Eq. (1.30) applies with excellent accuracy to $B_d \to J/\psi\, K_{\rm S}$, as penguins enter essentially with the same weak phase as the leading tree contribution, it is referred to as the "gold-plated" mode to determine the B_d^0–$\overline{B_d^0}$ mixing phase [60]. Strictly speaking, mixing-induced CP violation in $B_d \to J/\psi\, K_{\rm S}$ probes $\sin(\phi_d + \phi_K)$, where ϕ_K is related to the CP-violating weak K^0–$\overline{K^0}$ mixing phase. Similar modifications must also be performed for other final-state configurations containing $K_{\rm S}$ or $K_{\rm L}$ mesons. However, ϕ_K

Selection stage	ATLAS		CMS		LHCb	
	$\mu^+\mu^-$	e^+e^-	$\mu^+\mu^-$	e^+e^-	$\mu^+\mu^-$	e^+e^-
First trigger level	733k	48.9k	3485k	893k	818k	425k
Second trigger level	536k	16.8k	1394k	353k	116k	60k
B_d^0 reconstruction	160k	4.8k	384k	49k	73k	15k
Signal/Background	31	16	8	2	7	2

Table 3: $B_d^0 \to J/\psi\, K_S^0$ event yields at different stages of the selection procedure and S/B ratio for one year's data. The events are untagged apart from the ATLAS $J/\psi \to e^+e^-$ sample which is automatically tagged by the level-1 trigger muon. The ATLAS level-2 trigger numbers also include the J/ψ-reconstruction offline-cuts.

is negligible in the SM, and – owing to the small value of the CP-violating parameter ε_K of the neutral kaon system – can only be affected by very contrived models of new physics [62].

First measurements of $\sin(2\beta)$ from the CP asymmetry (3.5) have recently been reported by the OPAL, CDF and ALEPH collaborations [63]:

$$\sin(2\beta) = \begin{cases} 3.2^{+1.8}_{-2.0} \pm 0.5 & \text{(OPAL Collaboration)} \\ 0.79^{+0.41}_{-0.44} & \text{(CDF Collaboration)} \\ 0.93^{+0.64+0.36}_{-0.88-0.24} & \text{(ALEPH Collaboration).} \end{cases} \tag{3.6}$$

Although the experimental uncertainties are very large, it is interesting to note that these results favour the SM expectation of a *positive* value of $\sin(2\beta)$. In the B factory era, an experimental uncertainty of $\Delta \sin(2\beta)|_{\rm exp} = 0.05$ appears to be achievable, whereas the experimental uncertainty at the LHC is expected to be one order of magnitude smaller, as discussed on page 22.

In addition to (3.5), one more important implication of the SM is

$$\mathcal{A}_{\rm CP}^{\rm dir}(B_d \to J/\psi\, K_{\rm S}) \approx 0 \approx \mathcal{A}_{\rm CP}(B^+ \to J/\psi\, K^+), \tag{3.7}$$

which is interesting for the search of new physics. An observation of these direct CP asymmetries at the level of 10% would be a strong indication for physics beyond the SM.

In view of the tremendous experimental accuracy that can be achieved in the LHC era, it is an important issue to investigate the theoretical accuracy of (3.5) and (3.7), which is a very challenging theoretical task. An interesting channel in this respect is $B_s \to J/\psi\, K_{\rm S}$ [61], allowing one to control the (presumably very small) penguin uncertainties in the determination of β from CP-violating effects in $B_d \to J/\psi\, K_{\rm S}$, and to extract the angle γ. We shall come back to this strategy in Sec. 5.2.

3.1.2 Experimental Studies

As well as being theoretically "gold-plated", the decay $B_d^0 \to J/\psi\, K_S^0$, with $J/\psi \to \mu^+\mu^-$ or $J/\psi \to e^+e^-$ is experimentally clean, and can be reconstructed with relatively low background. The $B_d^0 \to J/\psi K_S^0$ branching ratio is measured to be $(8.9 \pm 1.2) \times 10^{-4}$ [64], yielding a visible branching ratio $B(B_d^0 \to J/\psi[\to \mu^+\mu^-$ or $e^+e^-]\, K_S^0[\to \pi^+\pi^-])$ of 1.8×10^{-5}. For a complete account of each of the analyses described below, see Refs. [56, 57, 39].

Selection

In each experiment, the event samples were generated using PYTHIA and the full detector response was simulated using the GEANT program. For the ATLAS analysis, electron and muon identification efficiencies are parametrized as a function of p_T and η using separate samples of fully simulated calorimeter and muon chamber data and then applied to the $B_d^0 \to J/\psi\, K_S^0$ sample.

The trigger strategies for the three experiments are summarized in Sec. 2.6: here the triggers relevant for the $B_d^0 \to J/\psi\, K_S^0$ analysis are briefly recalled. In the ATLAS analysis, a single muon

	ATLAS		CMS		LHCb	
	$\mu^+\mu^-$	e^+e^-	$\mu^+\mu^-$	e^+e^-	$\mu^+\mu^-$	e^+e^-
Mass resolution [MeV/c^2]	18	24	16	22	7	20
Proper time resolution [ps]	73	73	61	61	36	44

Table 4: Mass and proper time resolution of the reconstructed B_d^0 meson after all offline selection-cuts for each experiment.

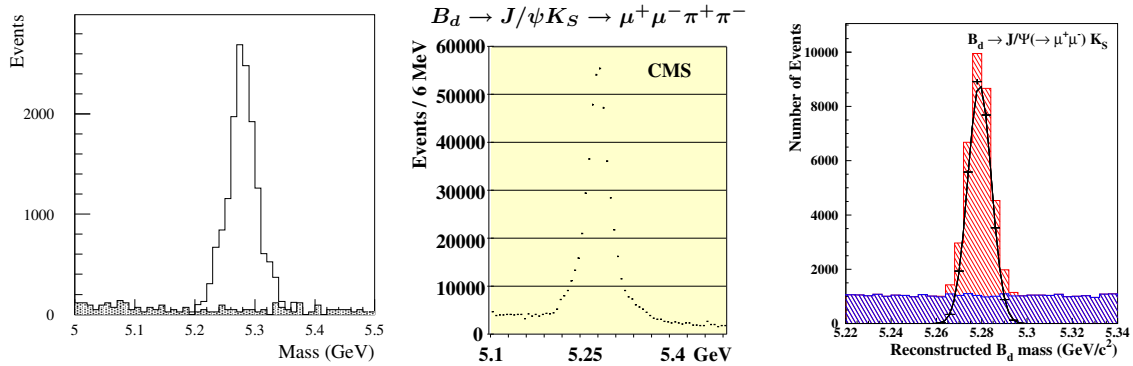

(a) ATLAS (b) CMS (c) LHCb

Fig. 10: Examples for reconstructed $B_d^0 \to J/\psi\, K_S^0$ mass peaks (signal and background) for the three LHC experiments: (a) ATLAS $J/\psi \to e^+e^-$ sample after 3 years of data; (b) CMS $J/\psi \to \mu^+\mu^-$ sample after 1 year of data; (c) LHCb $J/\psi \to \mu^+\mu^-$ sample after 1 year of data.

with $p_T > 6\,\text{GeV}$ and $|\eta| < 2.4$ is required at level-1. To increase statistics, a dimuon trigger (with η–dependent thresholds) is under study. At level-2, the trigger requires either a second muon with $p_T > 3\,\text{GeV}$ and an electron with $p_T > 5$ GeV or a e^+e^- pair, with electron p_T thresholds of 0.5 GeV. In CMS, the following level-1 triggers are available: one muon with $p_T > 7$ GeV, two muons with $p_T > 2$ or 4 GeV (depending on η), one electron with $p_T > 12$ GeV, two electrons with $p_T > 5$ GeV or an electron-muon pair with $p_T(e) > 4.5$ GeV and $p_T(\mu) > 2$ or 4 GeV.

The first step in reconstructing $B_d^0 \to J/\psi\, K_S^0$ decays is the selection of oppositely charged lepton pairs originating from a common vertex and with a mass close to the J/ψ mass. Next, K_S^0 candidates are selected and combined with the J/ψ candidates to form B_d^0 candidates. In ATLAS, the same lepton trigger p_T-cuts are applied in the offline selection. In CMS and LHCb, no offline-cuts are applied to the lepton-p_T after pattern-recognition.

For the $J/\psi \to e^+e^-$ selection, both ATLAS and CMS use an asymmetric window for the reconstructed J/ψ mass in order to account for bremsstrahlung energy-losses which produce a long tail at small invariant masses. Cuts on the J/ψ decay-length remove the prompt-J/ψ background. In LHCb, to guarantee a good vertex resolution, the tracks are required to have hits in the vertex detector.

In ATLAS and CMS, the K_S^0 candidates are reconstructed from all oppositely charged track pairs originating from a common vertex and with a mass close to that of the kaon. In LHCb, the charged tracks are required to be identified as pions in the RICH system. To reduce combinatorial background, the K_S^0 candidate vertices are required to be well separated from the primary vertex. The leptons and pions from the surviving J/ψ and K_S^0 candidates are then used to reconstruct candidate $B_d^0 \to J/\psi\, K_S^0$ decays using a three-dimensional kinematic fit to the four tracks and applying vertex and mass constraints on both the lepton-lepton and $\pi^+\pi^-$ system. Finally, the fully reconstructed B_d^0 is required to point to the reconstructed primary vertex. Table 3 gives the (untagged) event yields at various stages of the selection procedure. The final B_d^0 mass and proper time resolutions are shown in Tab. 4.

In each experiment, the dominant source of background arises from the combination of a true J/ψ from B decay and any other K_S^0 within the event, which can originate from fragmentation or from other B decays or be a fake K_S^0. In LHCb, thanks to the π/K separation available in the RICH, the fake

Tagging method	ATLAS		CMS		LHCb	
	efficiency	dilution	efficiency	dilution	efficiency	dilution
electron	0.012/–	0.46/–	0.024/0.035	0.44	n/a	n/a
muon	0.025/1.	0.52/0.57	0.033/0.035	0.44	n/a	n/a
B–π (or B^{**})	0.82/0.80	0.16/0.14	0.21	0.32	n/a	n/a
jet charge (SS)	0.64/0.71	0.17/0.12	0.5	0.23	n/a	n/a
jet charge (OS)	n/a	n/a	0.70	0.18	n/a	n/a
lepton and kaon	n/a	n/a	n/a	n/a	0.40	0.40

Table 5: Tagging efficiencies and dilution factors for each of the tagging methods used by the three collaborations in the $B_d^0 \to J/\psi\, K_S^0$ analysis. Numbers before and after the slash (/) are for the $J/\psi \to \mu^+\mu^-$ and $J/\psi \to e^+e^-$ samples, respectively. ATLAS uses B–π and CMS uses B^{**} tagging (see Sec. 2.7). The shorthand "n/a" means *not available* or *not applied* in this analysis by a particular experiment.

K_S^0 contribution is reduced and the only significant background is due to real J/ψ from B combined with a real K_S^0. However, this background is rather large due to the large number of K_S^0 mesons from fragmentation produced in the forward direction within the LHCb acceptance. ATLAS used fast simulation programs (after careful comparison with full simulation results) to generate large samples of all backgrounds, whereas LHCb used smaller samples of fully simulated events and extrapolated to higher statistics. CMS used a combination of the two approaches. The signal/background ratios obtained in the three experiments after all offline selection-cuts and before any flavour tagging (except for the ATLAS $J/\psi \to e^+e^-$ sample, where the flavour is tagged automatically by the level-1 trigger muon) are summarized in Table 3. Figure 10 shows examples for B_d^0 mass peaks (signal and background) after all offline-cuts: the background levels are low in all cases.

Tagging

Some of the flavour tagging strategies introduced in Sec. 2.7 have been studied in particular detail for the $B_d^0 \to J/\psi\, K_S^0$ channel. All three experiments use the lepton from the semileptonic decay of the other b hadron in the event (the opposite side b) to tag the flavour of the B_d^0 at production. In the ATLAS $J/\psi \to e^+e^-$ sample, the level-1 trigger muon provides a 100% efficient tag. Using the π–K separation provided by its RICH detector, LHCb can also use kaons to tag the flavour of the opposite-side b quark. In addition to the lepton tag, ATLAS and CMS studied jet-charge tagging (both on the opposite and same side) and B–π correlation tagging. The same-side jet-charge tags and the B–π tags are highly correlated. For this reason, ATLAS chose to use only the higher purity B–π tag. It has not yet been demonstrated that the same side B–π tag method will work in LHCb, since the track densities encountered there are large. All three experiments plan to combine all tagging information in each event in order to obtain optimal statistical precision. The efficiencies and mistag rates of all tagging methods are shown in Tab. 5. For the LHCb study, the overall tagging efficiency and dilution of the combined lepton and kaon tagging method (see Sec. 2.7.3) have been used.

Sensitivity to β

The CKM parameter β is extracted from a fit to the measured time-dependent asymmetry with a function of the form:

$$\mathcal{A}_{CP}(B_d^0 \to J/\psi K_S^0) = D \sin(2\beta) \sin \Delta m t, \tag{3.8}$$

where D is the overall dilution factor due to both tagging and background. Here any direct CP violation is neglected, and the only free parameter in the fit is $\sin 2\beta$. The background is assumed to have no asymmetry. Figure 11 shows an example of a fit to the LHCb time-dependent CP asymmetry distribution after one year of data taking.

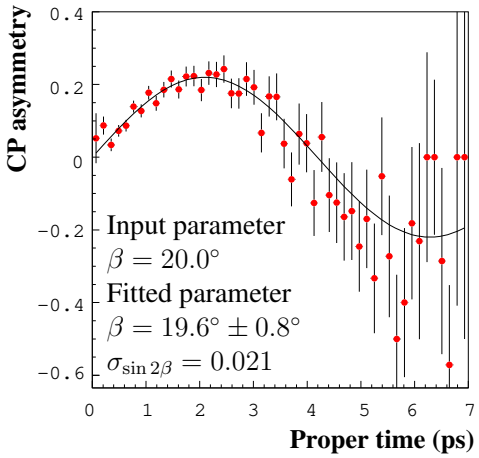

Fig. 11: Example for a LHCb fit of the time-dependent asymmetry Eq. (3.8) with one year's data.

Tagging method	ATLAS		CMS		LHCb	
	$\mu^+\mu^-$	e^+e^-	$\mu^+\mu^-$	e^+e^-	$\mu^+\mu^-$	e^+e^-
Lepton	0.039	0.031	0.031		n/a	n/a
B–π	0.026	n/a	0.023		n/a	n/a
SS Jet charge	n/a	n/a	0.021		n/a	n/a
OS Jet charge	n/a	n/a	0.023		n/a	n/a
Lepton and kaon	n/a	n/a	n/a		0.023	0.051
Total	0.017		0.015		0.021	

Table 6: Sensitivity to $\sin 2\beta$ after one year of data taking at the LHC. For the ATLAS $J/\psi \to \mu^+\mu^-$ sample, lepton tags have been removed from the B–π tagged sample. The four partial CMS results are correlated, but in the total sensitivity overlaps have been subtracted. The shorthand "n/a" means *not available* or *not applied* in this analysis by a particular experiment.

Table 6 summarizes the sensitivity of the three experiments to $\sin 2\beta$ using the different tagging methods studied by each experiment. The ATLAS lepton-tagged events have been removed from the B–π tagged sample to yield two statistically independent samples. The four separate CMS results are statistically correlated. However, to obtain the final precision for $\sin 2\beta$, the analysis was performed using only those events not tagged by another method, as explained in Sec. 2.7.3.

All experiments estimate a statistical error on $\sin 2\beta$ which is independent of the input value for β. Combining the statistical precision achievable after 3 years of running at ATLAS and CMS with 5 years of running at LHCb, a total statistical precision for $\sin 2\beta$ of 0.005 can be obtained. This precision is one order of magnitude better than the expected statistical precision at the e^+e^- B factories. With this sensitivity, the experiments can also probe the direct CP violating contribution $\mathcal{A}_{CP}^{\rm dir}(\mathrm{B}^0_{\rm d} \to \mathrm{J}/\psi \mathrm{K}^0_{\rm S})$ to the asymmetry. Fitting an additional term to account for such a contribution degrades the precision on $\sin 2\beta$ by $\sim 30\%$ and gives a similarly small uncertainty on $\mathcal{A}_{CP}^{\rm dir}(\mathrm{B}^0_{\rm d} \to \mathrm{J}/\psi \mathrm{K}^0_{\rm S})$.

Systematic Uncertainties

In order not to compromise the excellent statistical precision obtainable for the determination of $\sin 2\beta$, a similar or better control of the systematic uncertainties must be achieved.

A detailed discussion of systematic errors on CP-violation measurements and strategies for their control are presented in Sec. 6. As theoretical uncertainties are expected to be very small, the main contribution to the systematic error comes from the initial-state production-asymmetry and from experimental factors. The latter ones include tagging uncertainties and uncertainties from background.

ATLAS have performed a preliminary estimate of such uncertainties using $B^+ \to J/\psi(\mu\mu)K^+$

and $B_d^0 \to J/\psi(\mu\mu)K^{\star 0}$ control samples [56]. It is estimated that for a statistical error of $\sin 2\beta = 0.010\,(\text{stat.})$, achievable after 3 years running, a corresponding systematic error of $\sin 2\beta = 0.005\,(\text{sys.})$, coming from the limited size of the control channels, can be obtained.

3.2 Probing α with $B_d \to \pi^+\pi^-$[7]

Another benchmark CP mode is $B_d \to \pi^+\pi^-$, which allows one to probe the CKM angle α. Unfortunately, penguin topologies render the interpretation of the CP-violating $B_d \to \pi^+\pi^-$ observables in terms of α difficult.

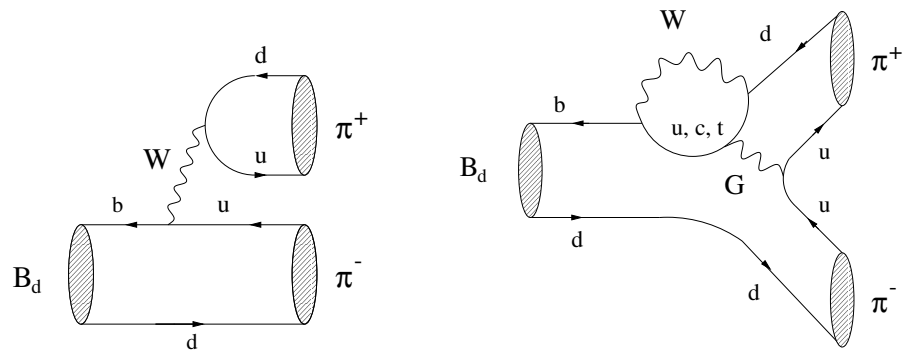

Fig. 12: Feynman diagrams contributing to $B_d^0 \to \pi^+\pi^-$.

3.2.1 Theoretical Aspects

The decay $B_d^0 \to \pi^+\pi^-$ is described by the Feynman diagrams shown in Fig. 12, and in analogy to (3.1), the corresponding decay amplitude can be expressed as

$$A(B_d^0 \to \pi^+\pi^-) = \lambda_u^{(d)}\left(A_{\text{cc}}^u + A_{\text{pen}}^u\right) + \lambda_c^{(d)} A_{\text{pen}}^c + \lambda_t^{(d)} A_{\text{pen}}^t\,. \tag{3.9}$$

If this mode did not comprise penguin contributions, its mixing-induced CP asymmetry would allow a measurement of $\sin 2\alpha$, in complete analogy to $B_d \to J/\psi K_S$:

$$\mathcal{A}_{\text{CP}}^{\text{mix}}(B_d \to \pi^+\pi^-) = -\sin[-(2\beta + 2\gamma)] = -\sin 2\alpha. \tag{3.10}$$

However, this relation is strongly affected by penguin effects, which were analysed by many authors [65, 66]. Various methods for controlling the corresponding hadronic uncertainties have been proposed; unfortunately, these strategies are usually rather challenging from an experimental point of view.

The best-known approach was proposed by Gronau and London [67]. It makes use of the SU(2) isospin relation

$$\sqrt{2}\,A(B^+ \to \pi^+\pi^0) = A(B_d^0 \to \pi^+\pi^-) + \sqrt{2}\,A(B_d^0 \to \pi^0\pi^0), \tag{3.11}$$

and of its CP-conjugate, which form two triangles in the complex plane. The sides of these triangles can be determined through the corresponding branching ratios, while their relative orientation can be fixed by measuring the CP-violating observable $\mathcal{A}_{\text{CP}}^{\text{mix}}(B_d \to \pi^+\pi^-)$. Following these lines, it is in principle possible to take into account the QCD penguin effects in the extraction of α. It should be noted that electroweak penguins cannot be controlled with the help of this isospin strategy. However, their effect is expected to be rather small, and – as was pointed out recently [68, 69] – can be included through additional theory input. Unfortunately, the Gronau–London approach suffers from an experimental problem,

[7] With help from J. Charles, D. Rousseau and A. Starodumov.

since the measurement of $B(B_d \to \pi^0\pi^0)$, which is expected to be of $\mathcal{O}(10^{-6})$ or smaller, is very difficult. However, upper bounds on the CP-averaged $B_d \to \pi^0\pi^0$ branching ratio may already be useful to put upper bounds on the QCD penguin uncertainty that affects the determination of α [66, 70].

Alternative methods for controlling penguin uncertainties are very desirable. One of them is provided by $B \to \rho\,\pi$ modes [71, 72], and will be discussed in more detail in the following subsection. As we shall see in Sec. 5.4, another interesting strategy is to use the CP-violating observables of $B_s \to K^+K^-$ *together* with those of $B_d \to \pi^+\pi^-$, which allows a simultaneous determination of β and γ *without* any assumptions about penguin topologies.

The observation of $B_d \to \pi^+\pi^-$ was announced by the CLEO collaboration in the summer of 1999 [73], with a branching ratio of

$$B(B_d \to \pi^+\pi^-) = \left(0.47^{+0.18}_{-0.15} \pm 0.13\right) \times 10^{-5}. \tag{3.12}$$

Other CLEO results on $B \to \pi K$ modes indicate that QCD penguins play in fact an important rôle and definitely do affect the extraction of α from $B_d \to \pi^+\pi^-$ [74]. In order to discuss penguin effects in a quantitative way, we use once more the unitarity of the CKM matrix, and rewrite (3.9) as follows:

$$A(B_d^0 \to \pi^+\pi^-) = e^{i\gamma}\,T + e^{-i\beta}\,P\,, \tag{3.13}$$

where the complex quantities

$$T \equiv -|\lambda_u^d|\left[A_{\rm cc}^u + A_{\rm pen}^u - A_{\rm pen}^c\right], \qquad P \equiv -|\lambda_t^d|\left[A_{\rm pen}^t - A_{\rm pen}^c\right], \tag{3.14}$$

denote the $B_d^0 \to \pi^+\pi^-$ "tree" and "penguin" amplitudes, respectively. The CP-conjugate amplitude can be obtained straightforwardly from (3.13) by replacing β by $-\beta$ and γ by $-\gamma$. For the following considerations, also the CP-conserving strong phase $\delta \equiv {\rm Arg}(PT^*)$ plays an important rôle. Since the B_d^0–$\overline{B_d^0}$ mixing phase is given by 2β in the SM, the unitarity relation $\alpha + \beta + \gamma = 180^\circ$ allows one to express the CP-violating observables $\mathcal{A}_{\rm CP}^{\rm dir}(B_d^0 \to \pi^+\pi^-)$ and $\mathcal{A}_{\rm CP}^{\rm mix}(B_d^0 \to \pi^+\pi^-)$ as functions of the CKM angle α, and the hadronic parameters $|P|/|T|$ and δ. Consequently, we have at our disposal two observables that depend on three "unknowns". Eliminating the CP-conserving strong phase δ, one obtains [66]:

$$\mathcal{A}_{\rm CP}^{\rm mix}(B_d^0 \to \pi^+\pi^-) = -\sqrt{1 - \mathcal{A}_{\rm CP}^{\rm dir\,2}}\ \sin 2\alpha_{\rm eff}\,, \tag{3.15}$$

where

$$\cos(2\alpha - 2\alpha_{\rm eff}) = \frac{1}{\sqrt{1 - \mathcal{A}_{\rm CP}^{\rm dir\,2}}}\left[1 - \left(1 - \sqrt{1 - \mathcal{A}_{\rm CP}^{\rm dir\,2}}\right)\left|\frac{P}{T}\right|^2\right] \tag{3.16}$$

with $2\alpha_{\rm eff} \equiv {\rm Arg}\left[-\xi^{(d)}_{\pi^+\pi^-}\right]$. $\xi_f^{(q)}$ was defined in Eq. (1.27). The quantity $2\alpha_{\rm eff}$ reduces to 2α if penguin topologies are neglected. Once the time-dependent CP-asymmetry (1.22) has been measured, Eqs. (3.15) and (3.16) allow one to fix contours in the $(|P|/|T|, 2\alpha)$ plane. This plot constitutes a model-independent representation of the experimental data in terms of the SM parameters. In order to simplify the following experimental discussion, we keep only leading order terms in $|P|/|T|$, which yields [75]

$$\begin{aligned}
\mathcal{A}_{\rm CP}^{\rm dir}(B_d \to \pi^+\pi^-) &= 2\left|\frac{P}{T}\right|\sin\delta\sin\alpha + \mathcal{O}((|P|/|T|)^2), \\
\mathcal{A}_{\rm CP}^{\rm mix}(B_d \to \pi^+\pi^-) &= -\sin(2\alpha) - 2\left|\frac{P}{T}\right|\cos\delta\,\cos(2\alpha)\sin\alpha + \mathcal{O}((|P|/|T|)^2),
\end{aligned} \tag{3.17}$$

and leave the analysis of the exact results given in [66] for further studies. Unfortunately, a theoretically reliable prediction for the "penguin" to "tree" ratio $|P|/|T|$, which would allow the extraction of α, is very challenging. An interesting new approach in this context was recently proposed in Ref. [76]. We shall come back to it in Sec. 9. Let us finally note that any QCD-based approach to calculate $|P|/|T|$ requires also knowledge of $|V_{td}/V_{ub}|$. This input can be avoided, if all CP-violating weak phases are expressed in terms of the Wolfenstein parameters $\overline{\rho}$ and $\overline{\eta}$, allowing one to fix contours in the $\overline{\rho}$–$\overline{\eta}$ plane [66].

Selection stage	ATLAS	CMS	LHCb
First trigger level	46k	52k	149.9k
Second trigger level	4.2k	4.3k	67.5k
Two-body selection	2.3k	1.6k	14.5k
$\pi^+\pi^-$ selection	2.3k	0.9k	4.9k
		(2.6k)	

Table 7: Event yields in $\mathrm{B_d^0} \to \pi^+\pi^-$ at various stages of the selection procedure for one year's operation. The final yields are for flavour-tagged events (an alternative yield is given for CMS, in brackets, for a selection assuming no dE/dx information).

	ATLAS	CMS	LHCb
Mass resolution [MeV/c^2]	70	27	17
Proper time resolution [ps]	0.065	0.060	0.04
Signal / two-body background	0.19	1.6	15
		(0.33)	
Signal / other background	1.6	5	>1
Tagging dilution	0.56	0.56	0.40

Table 8: Attributes of the $\mathrm{B_d^0} \to \pi^+\pi^-$ samples for the three experiments (an alternative signal/two-body background number is given for CMS, in brackets, assuming no dE/dx information). Note that ATLAS performs a fit to all events passing its two-body selection; the background levels shown here are for illustration, imposing a 1 σ mass window.

3.2.2 Experimental Studies

Low branching ratio and lack of any sub-mass constraints make the reconstruction of $\mathrm{B_d^0} \to \pi^+\pi^-$ a very demanding task. Isolating the signal from other two-body topologies, like $\mathrm{B_d^0} \to \mathrm{K^\pm\pi^\mp}$, $\mathrm{B_s^0} \to \mathrm{K^+K^-}$, $\mathrm{B_s^0} \to \mathrm{K^\pm\pi^\mp}$, $\Lambda_\mathrm{b} \to \mathrm{p\pi^-}$ and $\Lambda_\mathrm{b} \to \mathrm{pK^-}$, poses additional problems. Despite these challenges, extensive simulation studies have demonstrated the substantial potential of the LHC experiments in this mode. Following recent measurements [73], these studies have assumed branching ratios of 0.5×10^{-5} for $\mathrm{B_d^0} \to \pi^+\pi^-$ and $\mathrm{B_s^0} \to \mathrm{K^\pm\pi^\mp}$, 1.9×10^{-5} for $\mathrm{B_d^0} \to \mathrm{K^\pm\pi^\mp}$ and $\mathrm{B_s^0} \to \mathrm{K^+K^-}$ and 8×10^{-5} for $\Lambda_\mathrm{b} \to \mathrm{p\pi^-}$ and $\Lambda_\mathrm{b} \to \mathrm{pK^-}$. Note that much of the following discussion is also relevant for the topics dealt with in Secs. 5.1 and 5.4.

Selection

The expected event-yields passing the early trigger levels are shown in Tab. 7. In this mode LHCb in particular benefits from the high efficiency of its hadron trigger. For ATLAS and CMS, the triggering muon will be used to flavour-tag the events, whereas for LHCb lepton and kaon tags will be used.

The higher level trigger and reconstruction-cuts are optimized to fight combinatorial background from other $b\bar{b}$ events and select genuine two-body B decays. In these, the requirements on the secondary vertex are the most powerful, but isolation and kinematic cuts also play a rôle. The details of the selection are discussed in Refs. [37, 38, 39]. The event yields after two-body selection are shown in Tab. 7.

In order to reject non-$\pi^+\pi^-$ two-body background, LHCb exploits its powerful RICH system, demanding that both tracks be identified as a pion or lighter particle. This requirement and a window of $\pm 30\,\mathrm{MeV/c^2}$ around the $\mathrm{B_d^0}$ mass reduce the contamination by such decays to 7%. As explained in Sec. 2, CMS will achieve a certain level of π–K separation from the dE/dx information available from the tracker, and the numbers and fit results presented here rely on this assumption, although Tabs. 7 and 8 contain alternative numbers for a hadron-blind selection. The requirements that both particles have an ionization within $^{+\infty}_{-0.75\sigma}$ of the expected pion energy loss, and an invariant mass within $^{+54}_{-40}$ MeV/c^2 of the nominal $\mathrm{B_d^0}$ mass, are expected to yield a final contamination of 40%. ATLAS chooses to make no further cuts, but rather exploit the remaining discriminant information in a multi-parameter fit, in

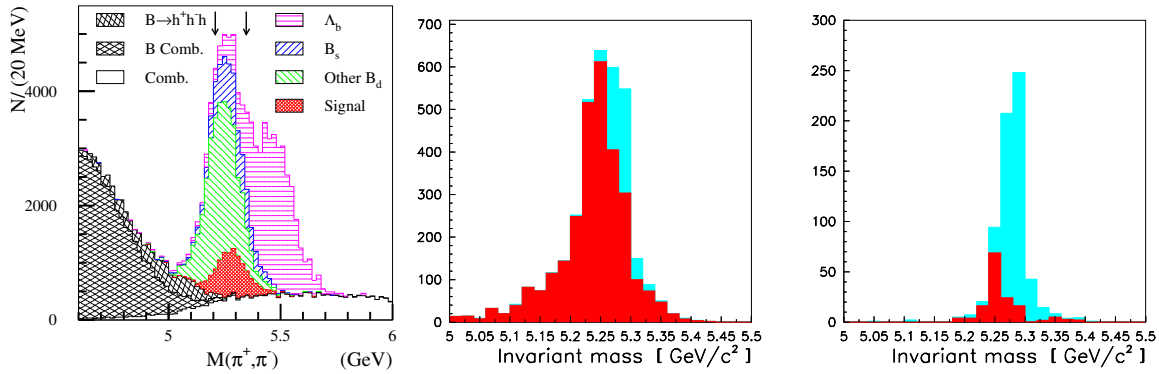

(a) ATLAS (b) LHCb before RICH (c) LHCb after RICH

Fig. 13: $\pi^+\pi^-$ invariant mass peaks as simulated by ATLAS and LHCb. The LHCb plots show the spectra before and after the application of RICH information, with signal indicated by the light shading. The ATLAS plot also contains Λ_b decays and combinatorial background.

particular the limited dE/dx information discussed in Sec. 2. At present, only ATLAS and the CMS hadron-blind analysis have considered the background contribution from $\Lambda_{\rm b}$ decays.

In addition to two-body contamination, there will be some residual combinatorial background passing the final cuts, which is expected to be dominated by events with a false vertex being faked by two unrelated high impact parameter tracks. The low branching ratio of the signal-process makes is very difficult to estimate the level of combinatorial background. ATLAS and CMS have used a combination of fast and full simulation techniques, whereas LHCb has extrapolated from a large sample of fully GEANT-simulated events. All experiments conclude that the combinatorial background should be smaller than the signal.

Some attributes of the final selected samples are given in Tab. 8, and examples for mass peaks are shown in Fig. 13.

Fitting the CP Asymmetry

Assuming the performance figures presented above, the experiments have used MC techniques to estimate their expected sensitivity to the CP asymmetries $\mathcal{A}^{\rm mix}_{\pi^+\pi^-}$ and $\mathcal{A}^{\rm dir}_{\pi^+\pi^-}$ from time-dependent fits, where these are defined in the usual manner:

$$\mathcal{A}_{\rm CP}(\mathrm{B}^0_{\rm d} \to \pi^+\pi^-)(\mathrm{t}) \;=\; \mathcal{A}^{\rm dir}_{\pi^+\pi^-}\cos\Delta mt \,+\, \mathcal{A}^{\rm mix}_{\pi^+\pi^-}\sin\Delta mt. \tag{3.18}$$

For the present study, LHCb has considered two-parameter fits of $\mathcal{A}^{\rm mix}_{\pi^+\pi^-}$ and $\mathcal{A}^{\rm dir}_{\pi^+\pi^-}$ to $\mathrm{B}^0_{\rm d} \to \pi^+\pi^-$ candidates passing tight cuts. Any CP asymmetry in the background has been neglected, assuming that these effects can be controlled with sufficient precision through a study of separate samples isolated by the RICH system. The CMS sensitivity with the dE/dx selection has been evaluated, also assuming any background-asymmetry to be known. The uncertainties obtainable with one year's statistics are shown in Tab. 9: they are found to be independent of the values of the true CP asymmetries, symmetric and Gaussian. The low frequency of the oscillations means that there is a significant correlation between $\mathcal{A}^{\rm mix}_{\pi^+\pi^-}$ and $\mathcal{A}^{\rm dir}_{\pi^+\pi^-}$.

ATLAS have developed a sophisticated method for extracting the $\mathrm{B}^0_{\rm d} \to \pi^+\pi^-$ asymmetries, whereby they are determined from an unbinned maximum-likelihood fit, simultaneously with the asymmetries of the other two-body classes. Considering the allowed $\pi\pi$, πK and KK modes, $\Lambda_{\rm b} \to {\rm p}\pi^-$, pK^- decays and the combinatorial background give nine coefficients. The likelihood of a given decay-hypothesis is computed using the event fraction, the proper time, the invariant mass of the two tracks under the hypothesis, the measured specific ionization and the flavour at production and decay-time. It

	ATLAS	CMS	LHCb
$\mathcal{A}^{\rm dir}_{\pi^+\pi^-}$	0.16	0.11	0.09
$\mathcal{A}^{\rm mix}_{\pi^+\pi^-}$	0.21	0.14	0.07
Correlation coefficient	–0.25	–0.51	–0.49

Table 9: Expected sensitivities for the $\mathrm{B}^0_{\rm d} \to \pi^+\pi^-$ CP asymmetry coefficients $\mathcal{A}^{\rm dir}_{\pi^+\pi^-}$ and $\mathcal{A}^{\rm mix}_{\pi^+\pi^-}$ with one year of data, and correlation between the fitted parameters (the CMS numbers assume a selection exploiting dE/dx information).

is assumed that the branching ratios will be known with fractional errors of 5% and a possible CP asymmetry of the background is neglected. The uncertainties on the $\mathrm{B}^0_{\rm d} \to \pi^+\pi^-$ coefficients with one year's statistics are shown in Tab. 9. Without the $0.8\,\sigma$ π/K separation provided by the ionization information, the sensitivity is about 20% worse.

Sensitivity to α

Present studies to estimate the combined LHC precision for α rely on the sensitivities given in Tab. 9 and Eqs. (3.17); they are presently extended to include the full expression (3.16). The simpler expression gives rise to 'singularities' in the precision for α for certain parameter values [75] which are not likely to occur with the full treatment.

Simulated measurements have shown that the sensitivities to the CP asymmetry coefficients quoted in Tab. 9, estimated from the χ^2 parabolic approximation, describe correctly the spread of experimental results. Also, the sensitivities do not depend on the actual values of the asymmetries, so that the numbers in Tab. 9 *with correlations* are sufficient to summarize the experimental precision of the measurements.

In contrast, the sensitivity to the parameters α and δ depends on the chosen set of parameters α, δ, $|P/T|$ and on the theoretical uncertainty of $|P/T|$, so that the sensitivity to α can only be given for specific scenarios. Also, Eqs. (3.17) entail a four-fold discrete ambiguity in α. Here sensitivities are given under the assumption that this ambiguity can be correctly resolved.

Figure 14(a) shows the expected sensitivity to α as a function of α and δ for a given $|P/T|=0.2\pm0.02$, after extended LHC running (3 years of low luminosity running of ATLAS and CMS combined with 5 years of LHCb). The sensitivity is around 2° in the larger part of the plane, except around the lines corresponding to $\delta = 90^\circ$ and 270° and $\alpha = 45^\circ$ and 135°. For these values of δ and α, the leading-order term in $|P/T|$ of the mixing-induced CP asymmetry $\mathcal{A}^{\rm mix}_{\rm CP}(B_d \to \pi^+\pi^-)$ vanishes, as can be seen in (3.17).

Figure 14(b) shows the expected sensitivity to α as a function of α for the fixed values $\delta = 30^\circ$, $|P/T| = 0.2$ and different values of the uncertainty on $|P/T|$ and the integrated luminosities. It appears that for values of α around 90°, the sensitivity to α is already limited after one year if the uncertainty on $|P/T|$ is not better than 10%. The effect of the uncertainty on $|P/T|$ is less dramatic for values of α around 0° or 180°, which are disfavoured by current SM fits.

3.2.3 Conclusions

At the LHC it should be possible to measure the $\mathrm{B}^0_{\rm d} \to \pi^+\pi^-$ CP-violating observables with high precision. Interpreting these observables in terms of the angle α, however, requires external information on the strength of the penguin contributions. This information has to be rather precise if one is to fully exploit LHC's powerful reach. Although exact conclusions depend on the particular parameter-set, it appears more promising to analyse the observables of $\mathrm{B}^0_{\rm d} \to \pi^+\pi^-$ and other two-body decays in the context of the approach discussed in Sec. 5.4.

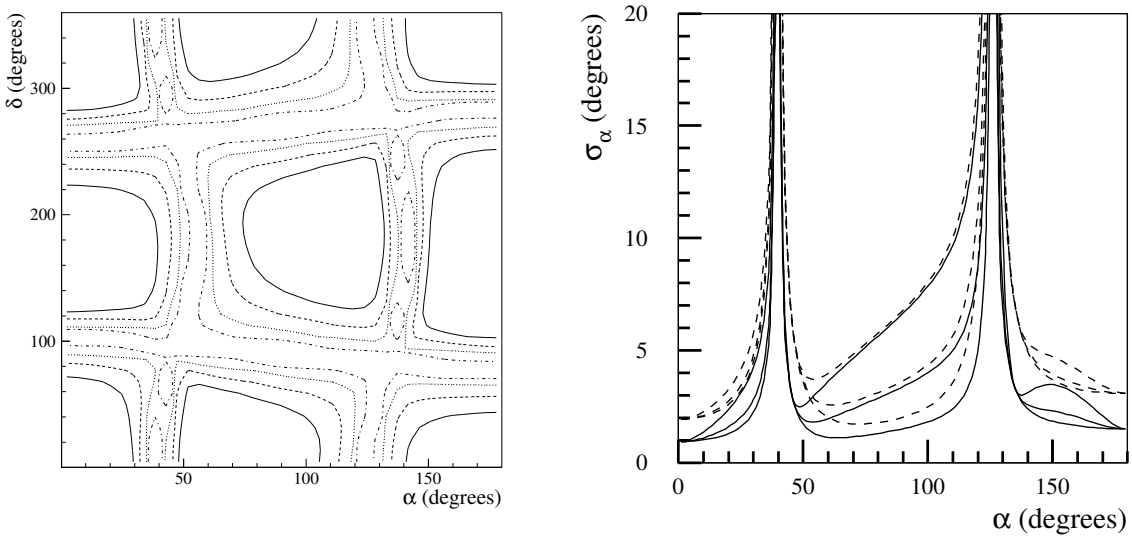

Fig. 14: Combined LHC sensitivity to α: (a) Sensitivity to α as a function of α and δ for a given $|P/T| = 0.2 \pm 0.02$, for extended running at the LHC. The contour lines correspond to a sensitivity of 2° (solid), 3° (dashed), 5° (dotted) and 10° (dashed-dotted). (b) Sensitivity to α as a function of α, for $\delta = 30^\circ$, $|P/T|$ = 0.2 after one year (dashed lines) and 5 years (solid lines). In both cases, the curves are given from bottom to top for an uncertainty of $|P/T|$ of 0.02, 0.05 and 0.1.

3.3 Extracting α from $B \to \rho\pi$ Modes[8]

3.3.1 Theoretical Introduction

The analysis of the decays $B_d \to \rho^\pm\pi^\mp$ allows, in principle, the extraction of α [77]. However, the simplest approach, where the ρ meson is considered as stable particle, is plagued by both high order discrete ambiguities and penguin pollution, like in $B_d^0 \to \pi^+\pi^-$. To solve either problem, Snyder and Quinn [72] proposed a full three-body analysis of the decay $B_d^0 \to \pi^+\pi^-\pi^0$ in the ρ resonance region, taking into account interference effects between vector mesons of different charges. The knowledge of the strong decay $\rho \to \pi\pi$, parametrized as a Breit-Wigner amplitude, allows the extraction of all parameters that describe both the tree and penguin contributions to $B_d \to \rho\pi$, including α, from a multi-dimensional likelihood-fit.

The two-body $B_d \to \rho\pi$ amplitudes can be written as:

$$A^{\pm\mp}(B_d^0 \to \rho^\pm\pi^\mp) = e^{-i\alpha}\,T^{\pm\mp} + P^{\pm\mp}\,, \qquad A^{00}(B_d^0 \to \rho^0\pi^0) = e^{-i\alpha}\,T^{00} + P^{00}. \tag{3.19}$$

The CP-conjugate amplitudes $\overline{A}^{ij} \equiv A(\overline{B_d^0} \to \rho^i\pi^j)$ are obtained by changing the sign of the weak phases. The full three-body $B_d \to \pi^+\pi^-\pi^0$ amplitude takes the form:

$$A(B_d \to \pi^+\pi^-\pi^0) = A^{+-}f_+ + A^{-+}f_- + A^{00}f_0\,, \tag{3.20}$$

when ρ-dominance is assumed. Here f_i stands for the Breit-Wigner amplitude for the decay of the ρ^i, and is a function of the two independent variables of the three-pion Dalitz-plot, which are chosen as the invariant masses $s^\pm = (p_{\pi^\pm} + p_{\pi^0})^2$. The Breit-Wigner parametrization is not unique; in the following we take:

$$f_+ \propto \frac{\cos\theta^*}{s^+ - m_\rho^2 + im_\rho\Gamma_\rho}\,, \tag{3.21}$$

where θ^* is the helicity angle of the ρ decay which is given in terms of (s^+, s^-) by the standard formulae. This dependence enhances the number of events in the corners of the Dalitz-plot, where interferences are maximal.

[8] With help from J. Charles, A. Jacholkowska and J. Libby.

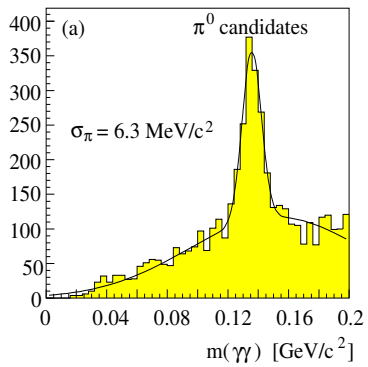

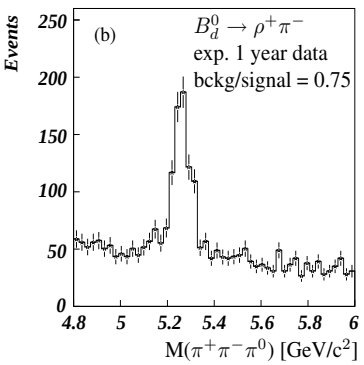

Fig. 15: The invariant mass for (a) π^0 candidates in $B_d^0 \to \pi^+\pi^-\pi^0$ events; (b) $B_d^0 \to \rho\pi$ candidates reconstructed in LHCb. The combinatorial background comes mainly from inclusive $b\bar{b}$ events.

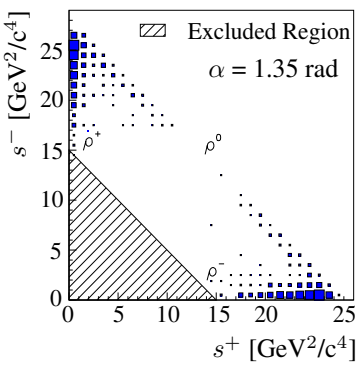

Fig. 16: The Dalitz-plot for $B_d^0 \to \pi^+\pi^-\pi^0$ decays after acceptance-cuts for events generated using the stand-alone simulation.

The time-dependent analysis of the event distribution in the Dalitz-plot allows one to extract $|A(B_d^0 \to \pi^+\pi^-\pi^0)|$, $|\overline{A}(\overline{B_d^0} \to \pi^+\pi^-\pi^0)|$ and Im$[\frac{q}{p}\overline{A}A^*]$ as functions of (s^+, s^-). Using (3.20) and (3.21), it is straightforward to show that the magnitudes and the relative phases of the two-body amplitudes A^{ij} and $\overline{A}^{ij}$ can be obtained [72]; this amounts to determining 11 independent parameters, taking into account that one overall phase is irrelevant, and including the overall normalization. In addition, assuming isospin symmetry and neglecting electroweak penguins, the relation [71]

$$P^{00} = -\frac{1}{2}(P^{+-} + P^{-+}) \tag{3.22}$$

allows a further reduction in the number of independent parameters that describe A^{ij} and $\overline{A}^{ij}$. These parameters can be chosen as α and the complex amplitudes T^{-+}, T^{00}, P^{+-} and P^{-+}. It is important to note that A^{ij} and $\overline{A}^{ij}$ are determined without discrete ambiguity in the general case, such that both $\cos 2\alpha$ and $\sin 2\alpha$ (and thus α in $[0, \pi]$) are accessible [72]. This resolves in particular the ambiguity between α and $\pi/2 - \alpha$.

3.3.2 Experimental Studies

Selection

The LHCb collaboration has performed full simulation studies on the selection of the $B_d^0 \to \pi^+\pi^-\pi^0$ channel. The charged pions are reconstructed in the tracking devices and are identified in the RICH detectors. At present, only π^0s built from two resolved photons are used in the analysis. Figure 15(a) shows the two-photon invariant-mass in $B_d^0 \to \pi^+\pi^-\pi^0$ events, for photons with energy above 2 GeV. The resolution of the π^0 mass varies between 5 and 7 MeV, depending on the π^0 production angle. The overall efficiency for π^0 reconstruction is 25%, with a signal to combinatorial background ratio of approximately 1. The measured π^0 mass is used in further B_d^0 mass reconstruction.

The background comes from combinatorials and from inclusive $b\bar{b}$ events. For its suppression, the following qualitative selection-cuts have been applied:

- a pre-selection for charged pions and photons which required the momentum or energy to exceed a value depending on the polar angle of the candidate. For charged pions, the momentum-cut varied between 1 and 2 GeV and for photons the energy-cut varied between 2 and 6 GeV;
- selection of signal-like events based on a discriminant variable built from kinematic variables of π, ρ and B_d^0;
- selection based on the reconstructed secondary vertex for a $\pi^+\pi^-$ combination;

- Dalitz-plot cuts to eliminate low energy π^0 combinatorial background due to particles from the primary vertex.

These selection criteria result in a combinatorial background-suppression factor of the order of 10^7 and give an acceptance for triggered and tagged events of 1%. Figure 15(b) shows the expected $\pi^+\pi^-\pi^0$ invariant mass distribution after one year of data taking. The measured B^0_d width is 50 MeV/c^2. The annual event-yields for triggered, fully reconstructed and tagged events are given in Tab. 10.

Channel	$B^0 \to \rho^+\pi^-$	$B^0 \to \rho^-\pi^+$	$B^0 \to \rho^0\pi^0$
B	44×10^{-6}	10×10^{-6}	1×10^{-6}
Event Yield	1000	200	100

Table 10: Annual event-yields for $B \to \rho\pi$ decays. The branching fractions are crude estimates used in BABAR's study of these decays [6].

Figure 16 shows the Dalitz-plot for the $B^0_d \to \pi^+\pi^-\pi^0$ channel after acceptance-cuts. Helicity effects enhance the population in the interference regions, in particular in the most critical $\rho^{\pm}$–ρ^0 regions, where the sensitivity to the α parameter is highest. The ρ^+–ρ^- interference region is not accessible due to the dominance of combinatorial background in the corresponding area of the Dalitz-space.

Sensitivity to α

A stand-alone simulation which introduces the weak phase α as well as the relative tree and penguin amplitudes was used to generate events for the fitting studies. Cuts in the Dalitz-space have been made to eliminate the ρ^-–ρ^+ interference region. Furthermore, cuts are applied to the invariant mass of a ρ candidate to select only resonant decays. However, the full LHCb acceptance has not yet been simulated and backgrounds have not been considered.

The amplitudes used for these studies contain a large penguin contribution and are identical to those studied by Babar [6]. Their values are given Tab. 11. Samples of 10^5 events were generated for each value of α. An unbinned maximum-likelihood fit was used to extract the parameters. The form of the used likelihood is:

$$-2\ln\mathcal{L} \;=\; -2\sum_{i=1}^{N_{\mathrm{B^0_d}}} \ln\left(\frac{|A(s_i^+, s_i^-, t_i;\alpha)|^2}{\mathcal{N}(\alpha)}\right) - 2\sum_{j=1}^{N_{\overline{\mathrm{B^0_d}}}} \ln\left(\frac{|\bar{A}(s_j^+, s_j^-, t_j;\alpha)|^2}{\mathcal{N}(\alpha)}\right),$$

where $N_{\mathrm{B^0_d}}$ and $N_{\overline{\mathrm{B^0_d}}}$ are the number of $\mathrm{B^0_d}$ and $\overline{\mathrm{B^0_d}}$ events, respectively, and $\mathcal{N}$ is the normalization. It is given by $(|A|^2 + |\bar{A}|^2)$, integrated over the Dalitz-plot acceptance, and was calculated numerically using a sub-sample of 20000 simulated events. The fit was performed on 75 sub-samples of 1000 events, to simulate approximately 1 year data taking, and 15 samples of 5000 events to simulate 5 years data taking. The mean fitted value of α and the mean error are given in Tab. 12. The error varies with the true value of α as expected [72], and the fitted values are unbiased for $\alpha = 0.9$ and 1.35 radians. The bias of $\sim$0.15 radians for $\alpha = 1.95$ radians was not observed when fits were made to samples where no Dalitz-plot selection was made. Therefore, this bias appears to be related to the exclusion of the ρ^+–ρ^- interference region and needs further investigation. Correction for this bias will be required to extract α from the final data sample and will introduce systematic uncertainties which may be of a magnitude similar to the statistical precision.

In Fig. 17 an example of a likelihood-scan curve is given for 1000 fitted events generated with $\alpha = 1.35$ radians. The fake mirror solution at $\frac{\pi}{2} - \alpha$ gives a local minimum in the likelihood-curve. The difference in the likelihood, expressed as χ^2 $(= -2\ln\mathcal{L})$, between the true and the mirror solution for the 75 one year data samples is displayed in Fig. 18(a). In approximately 10% of all cases, the mirror solution is the global minimum or is separated by less than 1 σ from the true solution. The same quantity

Parameter	Value
α	0.9, 1.35 or 1.95 radians
T^{+-}	1.00
T^{-+}	0.47
T^{00}	0.14
P^{+-}	$-0.20\,e^{-0.5\mathrm{i}}$
P^{-+}	$0.15\,e^{2.0\mathrm{i}}$

Table 11: The three values of α and the amplitudes used in the generation of the studied samples.

	1 year		5 years	
α (°)	$\langle\alpha\rangle$ (°)	$\langle\sigma_\alpha\rangle$ (°)	$\langle\alpha\rangle$ (°)	$\langle\sigma_\alpha\rangle$ (°)
51.6	51.6	4.9	51.0	2.1
77.3	76.2	2.5	76.2	1.1
111.7	102.6	4.3	102.0	1.8

Table 12: The mean fitted values of α, $\langle\alpha\rangle$, and the mean error on α, $\langle\sigma_\alpha\rangle$, for samples approximating 1 or 5 years data taking for LHCb at α = 0.90, 1.35 and 1.95 radians ($51.6^\circ, 77.3^\circ$ and 111.7°).

for the 15 five year data samples is shown in Fig. 18(b). The mirror and true solution minima are now well separated.

3.3.3 Conclusions

From the theoretical point of view, the main advantage of the isospin analysis of the decay $B_d \to \pi^+\pi^-\pi^0$ in the ρ-dominance assumption, with respect to its analogue in the two-pion channel, is the determination of the penguin amplitudes and the resolution of discrete ambiguities. From the experimental side, it benefits from larger branching ratios [73] and from interference, which entails that the sensitivity of the analysis is directly proportional to the colour-suppressed channel $B \to \rho^0\pi^0$. This can be compared to the Gronau-London branching ratio construction [67] in $B_d \to \pi\pi$, which has a sensitivity proportional to the amplitude squared of $B_d \to \pi^0\pi^0$.

Preliminary studies for LHCb have shown that $\mathrm{B^0_d} \to \pi^+\pi^+\pi^0$ events can be reconstructed and selected in sufficient numbers, so that an unambiguous value for α can be extracted without the problems that afflict the $\mathrm{B^0_d} \to \pi^+\pi^-$ channel. It should be stressed that the fitting studies are preliminary and also optimistic in the sense that the exact LHCb acceptance has not been used and backgrounds have not been included. Also, the observed biases are likely to introduce significant systematic uncertainties. Furthermore, several important issues remain to be considered, which already have been studied in the specific context of e^+e^- B factories [78, 79, 80]. One may cite, among others, various points: the influence of higher resonances (ρ', $\rho^3\ldots$), the influence of the exact parametrization of the Breit-Wigner amplitude, the existence of bounds on the penguin-induced error on α, when the $\rho^0\pi^0$ channel is too scarce to achieve the full analysis, and the rôle of electroweak penguins. All these issues will be further investigated in the future.

There are also some topics, yet to be investigated, which should enhance the precision on α: the determination of the branching fractions from e^+e^- experiments provide additional constraints on the fit and the untagged sample can be used to determine parameters other than α. It is to be expected that after several years of data taking at e^+e^- experiments and/or at the LHC era, the above issues will be much better understood.

3.4 Extracting $2\beta + \gamma$ from $B_d \to D^{(*)\pm}\pi^\mp$ decays[9]

So far, we have put a strong emphasis on neutral B decays into final CP eigenstates. However, in order to extract CKM phases, there are also interesting decays of $B_{d,s}$ mesons into final states that are *not* eigenstates of the CP operator. An important example is provided by the decays $B_d \to D^{(*)\pm}\pi^\mp$, which receive only contributions from tree-diagram-like topologies, and are the topic of this subsection.

[9] With help from J. Rademacker.

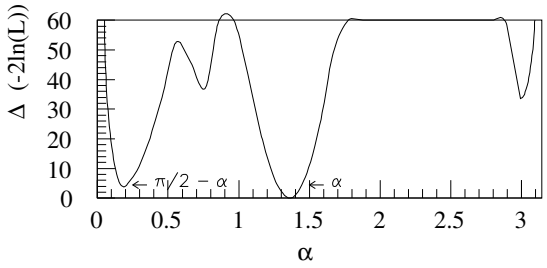

Fig. 17: Example of a likelihood-scan curve for 1000 fitted LHCb events, generated with $\alpha = 1.35$. α was fixed to 40 values between 0 and π radians and the negative likelihood was minimized with respect to the other 8 parameters.

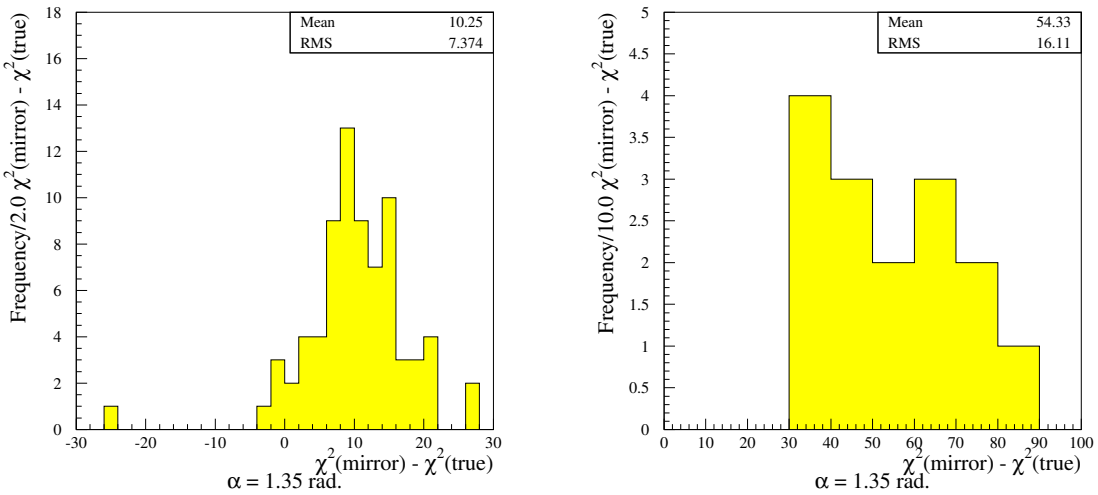

(a) LHCb 1 year data samples

(b) LHCb 5 year data samples

Fig. 18: The difference in $-2\ln\mathcal{L}$ between the true and mirror solution minima.

3.4.1 Theoretical Aspects

As can be seen in Fig. 19, B^0_d- and $\overline{B^0_d}$ mesons may both decay into $D^{(*)+}\pi^-$, thereby leading to interference effects between B^0_d–$\overline{B^0_d}$ mixing and decay processes. Consequently, the time-dependent decay rates for initially, i.e. at time $t = 0$, present B^0_d- or $\overline{B^0_d}$ mesons decaying into the final state $f \equiv D^{(*)+}\pi^-$ allow one to determine the observable [17]

$$\xi_f^{(d)} = -\,e^{-i\phi_d}\frac{A(\overline{B^0_d} \to f)}{A(B^0_d \to f)} = -\,e^{-i(\phi_d+\gamma)}\left(\frac{1-\lambda^2}{\lambda^2 R_b}\right)\frac{\overline{M}_f}{M_{\overline{f}}}, \tag{3.23}$$

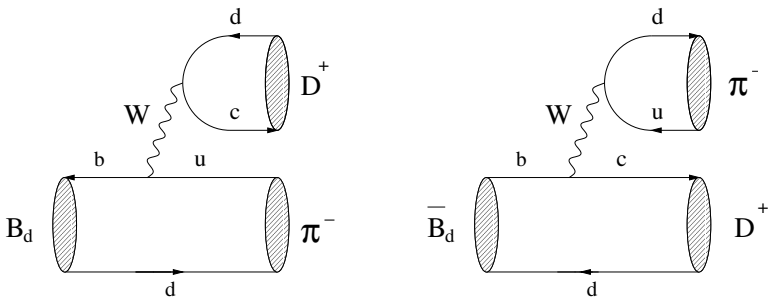

Fig. 19: Feynman diagrams contributing to $B^0_d, \overline{B^0_d} \to D^{(*)+}\pi^-$.

whereas those corresponding to $\bar{f} \equiv D^{(*)-}\pi^+$ allow one to extract

$$\xi_{\bar{f}}^{(d)} = -\,e^{-i\phi_d}\frac{A(\overline{B_d^0}\to\bar{f})}{A(B_d^0\to\bar{f})} = -\,e^{-i(\phi_d+\gamma)}\left(\frac{\lambda^2 R_b}{1-\lambda^2}\right)\frac{M_{\overline{f}}}{\overline{M}_f}. \tag{3.24}$$

Here, R_b is the usual CKM factor (see (3.4)), and

$$\overline{M}_f \equiv \left\langle f\middle|\overline{O}_1(\mu)\mathcal{C}_1(\mu)+\overline{O}_2(\mu)\mathcal{C}_2(\mu)\middle|\overline{B_d^0}\right\rangle, \quad M_{\overline{f}} \equiv \left\langle \overline{f}\middle|O_1(\mu)\mathcal{C}_1(\mu)+O_2(\mu)\mathcal{C}_2(\mu)\middle|\overline{B_d^0}\right\rangle \tag{3.25}$$

are hadronic matrix elements of the following current–current operators:

$$\begin{array}{rclcrcl} \overline{O}_1 &=& (\bar{d}_\alpha u_\beta)_{\text{V-A}}\,(\bar{c}_\beta b_\alpha)_{\text{V-A}}\,, & & \overline{O}_2 &=& (\bar{d}_\alpha u_\alpha)_{\text{V-A}}\,(\bar{c}_\beta b_\beta)_{\text{V-A}}\,, \\ O_1 &=& (\bar{d}_\alpha c_\beta)_{\text{V-A}}\,(\bar{u}_\beta b_\alpha)_{\text{V-A}}\,, & & O_2 &=& (\bar{d}_\alpha c_\alpha)_{\text{V-A}}\,(\bar{u}_\beta b_\beta)_{\text{V-A}}\,, \end{array} \tag{3.26}$$

where α and β denote colour indices, and V–A refers to the Lorentz structures $\gamma_\mu(1-\gamma_5)$. The observables $\xi_f^{(d)}$ and $\xi_{\bar{f}}^{(d)}$ allow a *theoretically clean* extraction of the weak phase $\phi_d+\gamma$ [81], as the hadronic matrix elements $\overline{M}_f$ and $M_{\overline{f}}$ cancel in the following combination:

$$\xi_f^{(d)} \times \xi_{\bar{f}}^{(d)} = e^{-2i(\phi_d+\gamma)}. \tag{3.27}$$

Since the B_d^0–$\overline{B_d^0}$ mixing phase ϕ_d, i.e. 2β, can be determined rather straightforwardly with the help of the "gold-plated" mode $B_d \to J/\psi\, K_S$ (see Sec. 3.1), one may extract the CKM angle γ from (3.27). As the $\bar{b}\to\bar{u}$ quark-level transition in Fig. 19 is doubly Cabibbo-suppressed by $\lambda^2 R_b \approx 0.02$ with respect to the $b\to c$ transition, the interference effects are tiny. However, the branching ratios are large, i.e. of order 10^{-3}, and the $D^{(*)\pm}\pi^\mp$ states can be reconstructed with a good efficiency and modest background. Consequently, $B_d \to D^{(*)\pm}\pi^\mp$ decays offer an interesting strategy to determine γ, as we will discuss in the following.

3.4.2 Experimental Studies

LHCb have investigated the potential of measuring γ through $B_d^0 \to D^{*\mp}\pi^\pm$ with the D^* decaying strongly to a D^0 meson. As interference effects are tiny, a very large data sample is necessary to extract γ with an interesting precision. Two methods have been studied: first a conventional exclusive reconstruction with $\overline{D^0}\to K^+\pi^-$ and second a partial reconstruction approach in order to boost statistics. The reconstruction study has also been extended to $B_d^0 \to D^{*\mp}a_1^\pm$ decays, but such events have not yet been considered for the extraction of CKM phases.

Exclusive Reconstruction

Loose RICH criteria were used to select the candidate $\overline{D^0}$ decay products. To identify D^{*-}, the difference between the reconstruced D^{*-} and $\overline{D^0}$ masses was required to lie within a 3 MeV wide window around its nominal value of 144 MeV, just above the pion mass. Figure 20(a) shows the signal-peak ($\sigma = 1$ MeV) with the background superimposed in arbitray units. The usual B^0 cuts (high p_T and detached vertex) were applied to the pion coming from the B^0. The final B^0 mass peak has a width of 13 MeV. Selecting events within a window of ± 30 MeV results in 84k selected events (triggered & tagged) per year with a S/B of ~ 12.

Partial Reconstruction

Instead of reconstructing the full decay chain, one can obtain all necessary information from the pion coming directly from the B^0 (the 'fast pion', π_f) and the pion coming from the D^{*-} (the 'slow pion', π_s). As shown below, one can reconstruct the full B^0 momentum from the momenta of π_f and π_s and

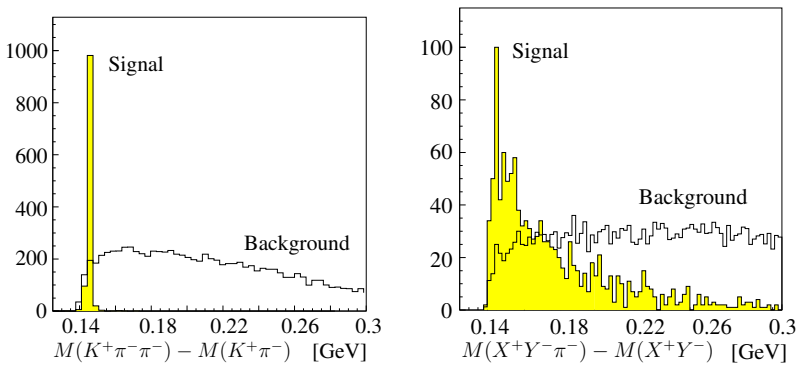

Fig. 20: The difference between reconstructed D^{*-} and $\overline{D^0}$ masses for the exclusive and inclusive reconstruction. The background is superimposed with arbitrary normalization. For the exclusive reconstruction, $\Delta m \in [143.5\,\text{MeV}, 146.5\,\text{MeV}]$, for the inclusive reconstruction, $\Delta m \in [144\,\text{MeV}, 160\,\text{MeV}]$.

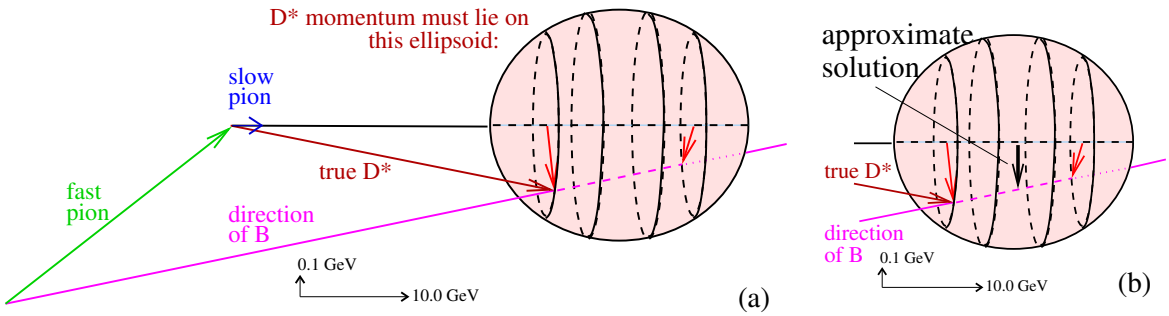

Fig. 21: Sketch of the kinematics in the $B^0_d \to D^{*\mp}\pi^{\pm}$ decay, showing in (a) the two possible solutions and in (b) the approximation that is actually used in the analysis.

the direction of the B^0. This direction can be inferred from the position of the primary vertex and the decay vertex of the B^0, the latter being defined by the crossing point of fast and slow pion.

To reconstruct the D^* (and then B^0) momentum from this limited information, we use the fact that, if the π_s momentum is known, the possible D^* momenta are restricted to lie on a two-dimensional surface. This surface is shown schematically in Fig. 21(a). Kinematics allows two possible solutions, but in practice they lie very close, and it suffices to approximate the true solution by the minimal distance between the slow pion and the B^0 vector as shown in Fig. 21(b). In order to suppress background, a probability distribution is cut on, which exploits the allowed ranges and expected correlations between the parameters in this reconstruction.

To further reduce background, one can use a cut similar to that on the mass difference between the D^{*-} and the $\overline{D^0}$ as applied in the exclusive case. Instead of fully reconstructing the $\overline{D^0}$, one tries to identify two charged decay products of the $\overline{D^0}$ (X^+, Y^-) and cuts on the difference Δm between the pseudo masses:

$$\Delta m = M(X^+Y^-\pi^-) - M(X^+Y^-). \tag{3.28}$$

Δm would be the mass difference between the D^* and the D^0 if X^+ and Y^- were the only decay products of the D^0. In general, though, there will be some missing momentum. Fortunately the missing momentum cancels to some extent in Eq. (3.28), so that even for the partially reconstructed $\overline{D^0}$ this remains a powerful cut as shown in Fig. 20(b).

After all cuts, 260k reconstructed, triggered and tagged events per year are expected inside the mass window of $\pm 200\,\text{MeV}$ with a S/B ~ 3. The reconstruction returns a mass peak of width $200\,\text{MeV}$.

$B_d^0 \to D^{*\mp} a_1^{\pm}$

The same inclusive analysis was performed for the channel $B_d^0 \to D^{*\mp} a_1^{\pm}$, with $a_1^{\pm} \to \rho^0 \pi^{\pm}$, which has a branching ratio that is about three times larger than that of $B_d^0 \to D^{*\mp}\pi^{\pm}$. As expected, the efficiency for this channel is lower, as more particles need to be reconstructed, while the mass resolution is slightly improved ($\sigma \approx 180\,\text{MeV}$), due to better reconstruction of the B^0 decay vertex from 4 instead of only 2 particles. 360k reconstructed, triggered and tagged events are expected within a $\pm 200\,\text{MeV}$ mass window per year, with a S/B of ~ 4.

The yield in all analyses is summarized in Tab. 13, with a total that assumes negligible correlations between the selections.

Sensitivity to γ

For $B_d^0 \to D^{*\mp}\pi^{\pm}$ decays the parameters $\xi_f^{(d)}$ and $\xi_{\bar{f}}^{(d)}$ can in principle be completely determined by fitting the two time-dependent asymmetries

$$\begin{aligned} A_{D^{*-}}(\tau) &= \frac{\Gamma_\tau\left(B_d^0 \to D^{*-}\pi^+\right) - \Gamma_\tau\left(\overline{B_d^0} \to D^{*-}\pi^+\right)}{\Gamma_\tau\left(B_d^0 \to D^{*-}\pi^+\right) + \Gamma_\tau\left(\overline{B_d^0} \to D^{*-}\pi^+\right)} \\ &= \frac{\left(1 - \left|\xi_{\bar{f}}^{(d)}\right|^2\right)\cos(\Delta m\tau) - 2\left|\xi_{\bar{f}}^{(d)}\right|\sin\left(-\left(\phi_d+\gamma\right)+\Delta_S\right)\sin(\Delta m\tau)}{1+\left|\xi_{\bar{f}}^{(d)}\right|^2}, \quad (3.29) \\ A_{D^{*+}}(\tau) &= \frac{\Gamma_\tau\left(\overline{B_d^0} \to D^{*+}\pi^-\right) - \Gamma_\tau\left(B_d^0 \to D^{*+}\pi^-\right)}{\Gamma_\tau\left(\overline{B_d^0} \to D^{*+}\pi^-\right) + \Gamma_\tau\left(B_d^0 \to D^{*+}\pi^-\right)} \\ &= \frac{\left(1 - \left|\xi_f^{(d)}\right|^2\right)\cos(\Delta m\tau) - 2\left|\xi_f^{(d)}\right|\sin\left(+\left(\phi_d+\gamma\right)+\Delta_S\right)\sin(\Delta m\tau)}{1+\left|\xi_f^{(d)}\right|^2}, \quad (3.30) \end{aligned}$$

where Δ_S is a possible strong phase shift entering $\xi_f^{(d)}$ via $\overline{M}_f/M_{\overline{f}}$.

Acceptance-effects cancel in each of the two asymmetries. In practice, as the interference effect is so tiny, $|\xi_{\bar{f}}^{(d)}| = 1/|\xi_f^{(d)}|$ needs to be constrained. Therefore, fits have been performed assuming this parameter be known with a relative precision of $\epsilon_{|\xi|}$. This uncertainty translates directly into a relative uncertainty on $\sin(\Delta_S \pm \{\phi_d + \gamma\})$. Throughout, a plausible true value of $|\xi_{\bar{f}}^{(d)}| = 0.016$ has been assumed; the final resolution on γ turns out to be directly proportional to this value (if $\epsilon_{|\xi|} = 0$), i.e. $\sigma_\gamma \propto 1/|\xi_{\bar{f}}^{(d)}|$.

Using a stand-alone MC simulation and feeding it with the parameters, event yields (340k) and S/B ratios (~ 3) for $B_d^0 \to D^{*\mp}\pi^{\pm}$ as discussed above, the statistical error on $\sin(\Delta_S \pm \{\phi_d + \gamma\})$ is found to be (for $\epsilon_{|\xi|} = 0$):

$$\sigma_{\sin} = \frac{0.26}{\sqrt{\text{no. of years}}}, \quad (3.31)$$

independent of the input values for $(\phi_d + \gamma)$ and Δ_S. Translating this into γ–Δ_S space, the resolution now does depend on the input values; an uncertainty in $|\xi_{\bar{f}}^{(d)}|$ also introduces a dependence on $\sin(\Delta_S \pm \{\phi_d + \gamma\})$. Figure 22 shows the error on $(\phi_d + \gamma)$ as a function of $(\phi_d + \gamma)$ for $\Delta_S = 0$, after 1 and after 5 years of LHCb data taking, for the cases that $|\xi_{\bar{f}}^{(d)}|$ is known exactly (broken lines) and that the uncertainty in $|\xi_{\bar{f}}^{(d)}|$ is 10% (solid lines). Assuming that ϕ_d can be fixed with negligible uncertainty from $\mathrm{B_d^0} \to \mathrm{J/\psi K_S^0}$ decays, this error will apply to γ itself.

Channel	S/B	Yield
$B_d^0 \to D^{*\mp}\pi^{\pm}$ (excl.)	12	83k
$B_d^0 \to D^{*\mp}\pi^{\pm}$ (incl.)	3	260k
$B_d^0 \to D^{*\mp}a_1^{\pm}$ (incl.)	4	360k
Total		703k

Table 13: Expected S/B and yields in reconstructed, triggered and tagged events in one year of LHCb data taking.

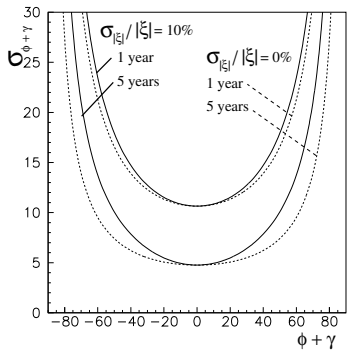

Fig. 22: Error on $\phi_d + \gamma$ as a function of $\phi_d + \gamma$ for $\Delta_S = 0$, after 1 and 5 years of data taking, assuming that $|\xi_{\bar{f}}^{(d)}|$ is known perfectly or up to 10%.

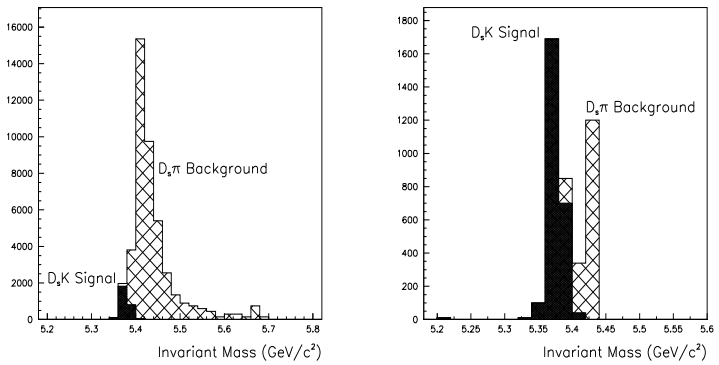

(a) No RICH (b) With RICH

Fig. 23: LHCb reconstruction of $B_s \to D_s^{\pm}K^{\mp}$, with the contribution of $B_s \to D_s^{\pm}\pi^{\mp}$ background before (a) and after (b) including the RICH information.

Presumably the large yield in $B_d^0 \to D^{*\mp}a_1^{\pm}$ events can also be exploited to obtain additional sensitivity to γ. However the presence of two spin-1 particles in the decay complicates the extraction, and in order to disentangle the final-state configurations, an angular analysis has to be performed (see [27] for the discussion of an analogous problem). This study has not yet been performed.

3.4.3 Conclusions

We have seen that the large statistics at the LHC offers the possibility of measuring γ with very interesting precision from $B_d^0 \to D^{*\mp}\pi(a_1)^{\pm}$ decays, despite the expected smallness of interference effects.

3.5 Extracting $\gamma - 2\delta\gamma$ from $B_s \to D_s^{\pm}K^{\mp}$ Decays

3.5.1 Theoretical Aspects

The decays $B_s \to D_s^{\pm}K^{\mp}$ receive only contributions from tree-diagram-like topologies and are the B_s counterparts of the $B_d \to D^{(*)\pm}\pi^{\mp}$ modes discussed in Sec. 3.4. They probe the CKM combination $\gamma - 2\delta\gamma$ instead of $\gamma + 2\beta$ in a *theoretically clean* way [82].[10] Since one decay path in $B_s^0, \overline{B_s^0} \to D_s^+K^-$ is only suppressed by $R_b \approx 0.41$, and not doubly Cabibbo-suppressed by $\lambda^2 R_b$, as in the case of $B_d \to D^{(*)\pm}\pi^{\mp}$, the interference effects in $B_s \to D_s^{\pm}K^{\mp}$ are much larger. A similar strategy to determine $\gamma - 2\delta\gamma$ is also provided by the colour-suppressed decays $B_s \to D\phi$ [83]. In Ref. [25], untagged data samples of these decays were considered to extract CKM phases, and angular distributions of untagged decays of the kind $B_s \to D^{*\pm}K^{*\mp}$, $B_s \to D^*\phi$ were considered in [27].

[10]The CP-violating weak B_s^0–$\overline{B_s^0}$ mixing phase $\phi_s = -2\delta\gamma$ can be extracted with the help of the decay $B_s \to J/\psi\,\phi$, see Sec. 4.

3.5.2 Experimental Studies

LHCb have investigated the expected event yields in $B_s \to D_s^{\pm} K^{\mp}$ and the resulting sensitivity to γ–$2\delta\gamma$ [39]. The selection of this mode is experimentally challenging, as $B_s \to D_s^{\pm}\pi^{\mp}$ events which come with a 20 times larger branching ratio need to be rejected. Figure 23 shows the event sample before and after including the information from the RICH detector. It can be seen that with the RICH's π–K discrimination the $B_s \to D_s^{\pm}\pi^{\mp}$ contamination can be adequately suppressed. 2.4k reconstructed and tagged events are expected in one year, with a low background.

The CKM phase γ–$2\delta\gamma$ can be determined from a fit to such a sample, in a manner directly analogous to that described in Sec. 3.4. Here, however, the intrinsic sensitivity is higher as the interference effects are larger. As always, the precision on the CKM phase depends on the value of the input parameters, which include $\Delta\Gamma_s/\Gamma_s$ and Δm_s. After one year's operation, the precision is typically 8° (mean) $\pm\, 2^\circ$(rms) for scenarios with $\Delta m_s = 15\,\mathrm{ps}^{-1}$, and degrades to $\sim 12^\circ$ for $\Delta m_s = 45\,\mathrm{ps}^{-1}$. Full tables can be found in [39]. Assuming that $2\delta\gamma$ can be constrained from $\mathrm{B_s} \to \mathrm{J}/\psi\phi$ decays, $B_s \to D_s^{\pm} K^{\mp}$ will provide a very clean and competitive measurement of the angle γ.

3.6 Extracting γ from $B \to DK$ Decays

During the recent years, relations among amplitudes of non-leptonic B decays have been very popular to develop strategies for extracting the angles of the unitarity triangles, in particular γ. The prototype of this approach involves charged $B^{\pm} \to DK^{\pm}$ decays [30].

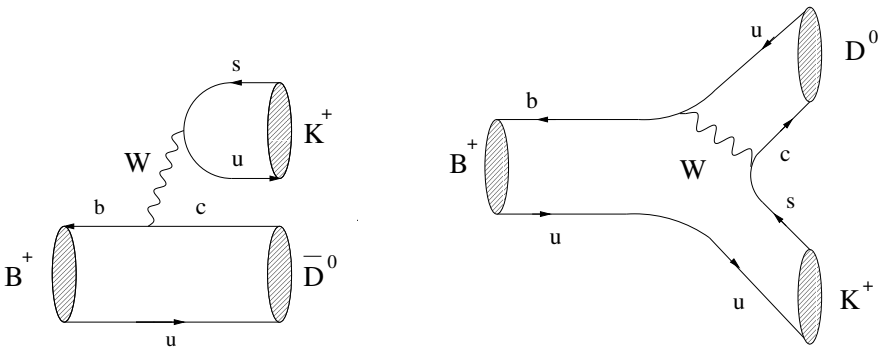

Fig. 24: Feynman diagrams contributing to the decays $B^+ \to \overline{D^0}K^+$ and $B^+ \to D^0K^+$.

3.6.1 Theoretical Aspects

The decays $B^+ \to \overline{D^0}K^+$ and $B^+ \to D^0K^+$, which are pure "tree" decays, as can be seen in Fig. 24, provide an interesting strategy to extract γ, if we make in addition use of the transition $B^+ \to D_+^0 K^+$. Here, D_+^0 denotes the CP eigenstate of the neutral D meson system with CP eigenvalue $+1$, given by

$$\left|D_+^0\right\rangle = \frac{1}{\sqrt{2}}\left(\left|D^0\right\rangle + \left|\overline{D^0}\right\rangle\right), \tag{3.32}$$

and leads to the following amplitude relations:

$$\sqrt{2}A(B^+ \to D_+^0 K^+) = A(B^+ \to D^0 K^+) + A(B^+ \to \overline{D^0}K^+), \tag{3.33}$$
$$\sqrt{2}A(B^- \to D_+^0 K^-) = A(B^- \to \overline{D^0}K^-) + A(B^- \to D^0 K^-). \tag{3.34}$$

Since we are dealing with pure "tree" decays that are caused by $\bar{b} \to \bar{c}\,u\,\bar{s}$, $\bar{u}\,c\,\bar{s}$ quark-level transitions, we have

$$a \equiv A(B^+ \to D^0 K^+) = A(B^- \to \overline{D^0}K^-) \times e^{2i\gamma}, \tag{3.35}$$
$$A \equiv A(B^+ \to \overline{D^0}K^+) = A(B^- \to D^0 K^-), \tag{3.36}$$

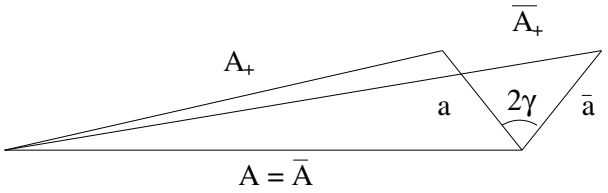

Fig. 25: Triangle relations between charged $B^\pm \to DK^\pm$ decay amplitudes.

allowing a *theoretically clean* determination of γ with the help of the triangle construction shown in Fig. 25. Unfortunately, we have to deal with rather squashed triangles, since $a \equiv A(B^+ \to D^0 K^+)$ is colour-suppressed with respect to $A \equiv A(B^+ \to \overline{D^0} K^+)$:

$$\frac{|a|}{|A|} = \frac{|\overline{a}|}{|\overline{A}|} \approx \frac{1}{\lambda} \frac{|V_{ub}|}{|V_{cb}|} \times \frac{a_2}{a_1} \approx 0.41 \times \frac{a_2}{a_1} \approx 0.1\,, \tag{3.37}$$

where a_1 and a_2 are the usual phenomenological colour factors.

In 1998, the CLEO collaboration has reported the observation of $B^+ \to \overline{D^0} K^+$ [84]:

$$B(B^+ \to \overline{D^0} K^+) = (0.257 \pm 0.065 \pm 0.032) \times 10^{-3}. \tag{3.38}$$

Using arguments based on "colour suppression", we expect

$$B(B^+ \to D^0 K^+) \approx 10^{-2} \times B(B^+ \to \overline{D^0} K^+). \tag{3.39}$$

While the branching ratio $B(B^+ \to \overline{D^0} K^+)$ can be measured using conventional methods, the measurement of $B(B^+ \to D^0 K^+)$ suffers from considerable experimental problems [33]:

- If the branching ratio of $B^+ \to D^0 K^+$ is measured through hadronic decays of the D^0 meson, e.g. through $B^+ \to D^0[\to K^-\pi^+]\, K^+$, we have large interference effects of $\mathcal{O}(1)$ with the decay chain $B^+ \to \overline{D^0}[\to K^-\pi^+]\, K^+$ (note that the $\overline{D^0}$ decay is doubly Cabibbo-suppressed).
- All possible hadronic tags of the D^0 in $B^+ \to D^0 K^+$ will be affected by such interference effects.
- Such problems can in principle be avoided by using semi-leptonic tags $D^0 \to l^+ \nu_l X_s$. However, here there will be large backgrounds due to $B^+ \to l^+ \nu_l X_c$, which may be difficult to control.

Moreover, decays of neutral D mesons into CP eigenstates, such as $D^0_+ \to \pi^+\pi^-, K^+K^-$, are experimentally challenging. Consequently, the original method proposed by Gronau and Wyler [30] will unfortunately be very difficult in practice. A variant of this approach was proposed by Atwood, Dunietz and Soni in [33]. In order to overcome the problems discussed above, the following decay chains can be considered:

$$B^+ \to \overline{D^0}\,[\to f_i]\, K^+, \quad B^+ \to D^0\,[\to f_i]\, K^+, \tag{3.40}$$

where f_i denotes doubly Cabibbo-suppressed (Cabibbo-favoured) non-CP modes of the $\overline{D^0}$ (D^0), for instance, $f_i = K^-\pi^+$, $K^-\pi^+\pi^0$. In order to extract γ, at least two different final states f_i have to be considered. In this method, one makes use of the large interference effects, which spoil the hadronic tag of the D^0 in the original Gronau–Wyler method. In contrast to the case of $B^+ \to D^0_+ K^+$ discussed above, here both contributing decay amplitudes should be of comparable size, thereby leading to potentially large CP-violating effects. Furthermore, the branching ratio $B(B^+ \to D^0 K^+)$, which is difficult to measure, is not required, but can rather be determined as a by-product. Unfortunately, this approach is also challenging, since many channels are involved, with total branching ratios of $\mathcal{O}(10^{-7})$ or even smaller. An accurate determination of the relevant D branching ratios $B(D^0 \to f_i)$ and $B(\overline{D^0} \to f_i)$ is also essential for this method.

So far, we have only considered charged $B^\pm \to DK^\pm$ decays. However, also neutral decays of the kind $B^0_d \to DK^{*0}$, which are shown in Fig. 26, allow one to extract γ [85]. As these modes are

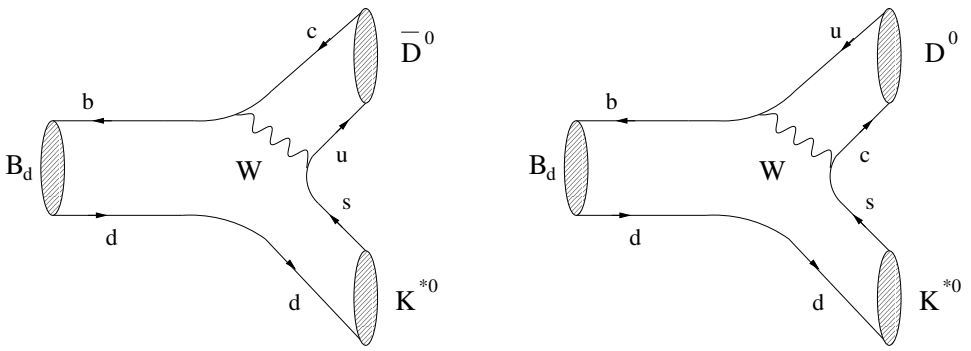

Fig. 26: Feynman diagrams contributing to the decays $B^0_d \to \overline{D^0} K^{*0}$ and $B^0_d \to D^0 K^{*0}$.

"self-tagging" through $K^{*0} \to K^+\pi^-$, no time-dependent measurements are required in this case. If we make again use of the CP eigenstate D^0_+ of the neutral D meson system, we obtain the following amplitude relations:

$$\sqrt{2}A(B^0_d \to D^0_+ K^{*0}) = A(B^0_d \to \overline{D^0} K^{*0}) + A(B^0_d \to D^0 K^{*0}), \tag{3.41}$$

$$\sqrt{2}A(\overline{B^0_d} \to D^0_+ \overline{K^{*0}}) = A(\overline{B^0_d} \to D^0 \overline{K^{*0}}) + A(\overline{B^0_d} \to \overline{D^0}\,\overline{K^{*0}}). \tag{3.42}$$

Moreover, we have

$$b \equiv A(B^0_d \to D^0 K^{*0}) = A(\overline{B^0_d} \to \overline{D^0}\,\overline{K^{*0}}) \times e^{2i\gamma}, \tag{3.43}$$

$$B \equiv A(B^0_d \to \overline{D^0} K^{*0}) = A(\overline{B^0_d} \to D^0 \overline{K^{*0}}), \tag{3.44}$$

allowing one to extract γ from the triangle construction shown in Fig. 27, which is completely analogous to the $B^\pm \to DK^\pm$ case. However, there is an important difference, which is due to the fact that both decays $B^0_d \to \overline{D^0} K^{*0}$ and $B^0_d \to D^0 K^{*0}$ are "colour-suppressed", as can be seen in Fig. 26:

$$\frac{|A(B^0_d \to D^0 K^{*0})|}{|A(B^0_d \to \overline{D^0} K^{*0})|} \approx \frac{1}{\lambda}\frac{|V_{ub}|}{|V_{cb}|}\frac{a_2}{a_2} \approx 0.41\,. \tag{3.45}$$

Consequently, the triangles are expected to be not as squashed as for $B^\pm \to DK^\pm$. The corresponding branching ratios are expected to be of $\mathcal{O}(10^{-5})$. However, the detection of the neutral D meson CP eigenstate D^0_+ also poses considerable difficulties.

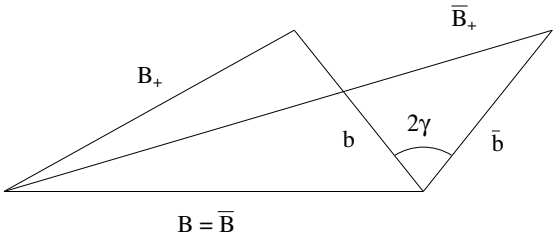

Fig. 27: Triangle relations between neutral $B_d \to DK^*$ decay amplitudes.

3.6.2 Experimental Studies

Both ATLAS [37] and LHCb [39] have investigated the possibility of determining γ through amplitude relations in the family of $B^0_d \to DK^{*0}$ decays. Both experiments have demonstrated that it will be possible to reconstruct samples of such events, with LHCb in particular benefiting from its hadron trigger. However, with the branching ratios that have been assumed, the yields are still low, with only a few 10's of events expected in the $D_1 K^{*0}$ and $D_1 \overline{K^{*0}}$ modes. At this level, several years are required to integrate sufficient statistics for a meaningful measurement. The experiments will continue to investigate this, and associated B → DK measurements, and search for possible improvement.

4 THE "GOLD-PLATED" DECAY $B_s \to J/\psi\,\phi$[11]

The decay $\mathrm{B}_s^0 \to \mathrm{J}/\psi\phi$ shown in Fig. 28 is the B_s counterpart to the "gold-plated" mode $\mathrm{B}_d \to J/\psi\, K_\mathrm{S}$ and is particularly interesting because of its rich physics potential. A complete analysis of this decay appears feasible at the LHC, because of the large statistics and good proper time resolution of the experiments.

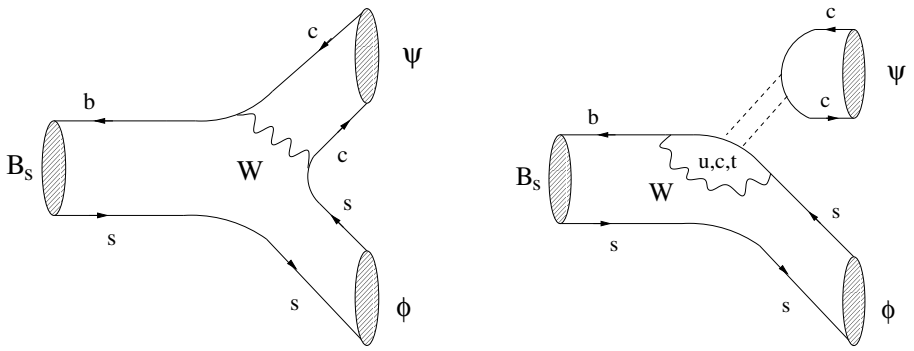

Fig. 28: Feynman diagrams contributing to $\mathrm{B}_s^0 \to J/\psi\,\phi$. The dashed lines represent a colour-singlet exchange.

4.1 Theoretical Aspects

In the case of $\mathrm{B}_s^0 \to J/\psi\,\phi$, the final state is an admixture of different CP eigenstates. In order to disentangle them, an angular analysis of the decay products of $\mathrm{B_s} \to \mathrm{J}/\psi(\mathrm{l^+l^-})\,\phi(\mathrm{K^+K^-})$ has to be performed [87, 88]. In addition to interesting strategies to extract the B_s^0–$\overline{B_s^0}$ mixing parameters $\Delta\Gamma_s$ and ΔM_s, we may also probe the weak mixing phase $\phi_s = -2\delta\gamma = -2\lambda^2\eta$, thereby allowing one to measure the Wolfenstein parameter η [26, 88]. A particularly interesting feature of $\mathrm{B}_s^0 \to \mathrm{J}/\psi\phi$ decays is that they exhibit tiny CP-violating effects within the SM. Consequently, they represent a sensitive probe for CP-violating contributions from physics beyond the SM [62, 89]. Since new-physics contributions have to compete with SM tree-diagram-like topologies, the natural place for any manifestation of new physics is in CP asymmetries induced by B_s mixing. Illustrations of the new-physics effects in $\mathrm{B}_s^0 \to \mathrm{J}/\psi\phi$ for specific scenarios of new physics can be found in [90, 91] and are discussed in more detail below.

4.1.1 General Structure of the Decay Probability Functions

For an initially, i.e. at time $t = 0$, present B_s^0 meson, the time-dependent angular distribution of the decay chain $\mathrm{B_s} \to \mathrm{J}/\psi(\mathrm{l^+l^-})\,\phi(\mathrm{K^+K^-})$ can be written generically as follows:

$$f(\Theta', \Theta'', \chi; t) = \sum_k \mathcal{O}^{(k)}(t)\, g^{(k)}(\Theta', \Theta'', \chi), \tag{4.1}$$

where we have denoted the angles describing the kinematics of the decay products of $J/\psi \to l^+l^-$ and $\phi \to K^+K^-$ by Θ', Θ'' and χ. The functions $\mathcal{O}^{(k)}(t)$ describe the time-evolution of the angular distribution (4.1), and can be expressed in terms of real or imaginary parts of bilinear combinations of decay amplitudes. In the case of decays into two vector mesons, such as $\mathrm{B}_s^0 \to J/\psi\,\phi$, it is convenient to introduce linear polarization amplitudes $A_0(t)$, $A_\parallel(t)$ and $A_\perp(t)$ [92]. Whereas $A_\perp(t)$ describes a CP-odd final-state configuration, both $A_0(t)$ and $A_\parallel(t)$ correspond to CP-even final-state configurations, i.e. to the CP eigenvalues -1 and $+1$, respectively. The $\mathcal{O}^{(k)}(t)$ of the corresponding angular distribution are given by

$$|A_f(t)|^2 \quad \text{with} \quad f \in \{0, \parallel, \perp\}, \tag{4.2}$$

[11] Section coordinators: R. Fleischer and M. Smizanska, with help from A. Dighe, P. Galumian and N. Zaitsev.

as well as by the interference terms

$$\mathrm{Re}\{A_0^*(t)A_\parallel(t)\} \quad \text{and} \quad \mathrm{Im}\{A_f^*(t)A_\perp(t)\} \quad \text{with} \quad f \in \{0,\parallel\}. \tag{4.3}$$

These quantities are governed by

$$\xi_{\psi\phi}^{(s)} \propto e^{-i\phi_s}\left[\frac{\lambda_u^{(s)*}A_{\rm pen}^{ut'} + \lambda_c^{(s)*}\left(A_{\rm cc}^{c'} + A_{\rm pen}^{ct'}\right)}{\lambda_u^{(s)}A_{\rm pen}^{ut'} + \lambda_c^{(s)}\left(A_{\rm cc}^{c'} + A_{\rm pen}^{ct'}\right)}\right], \tag{4.4}$$

where we have used the unitarity of the CKM matrix, the $\lambda_q^{(s)}$ are given by $V_{qs}V_{qb}^*$, and $A_{\rm pen}^{ut'}$ and $A_{\rm pen}^{ct'}$ denote the differences of penguin topologies with internal up- and top-quark and charm- and top-quark exchanges, respectively. The $A_{\rm pen}^{ut'}$ pieces are strongly CKM-suppressed by $|\lambda_u^{(s)}/\lambda_c^{(s)}| \approx 0.02$; the penguin amplitudes are suppressed even further because of their loop and colour structure. Yet, the "current–current" amplitudes are "colour-suppressed", and we may well have

$$\frac{\left|\lambda_u^{(s)}A_{\rm pen}^{ut}\right|}{\left|\lambda_c^{(s)}\left(A_{\rm cc}^{c} + A_{\rm pen}^{ct}\right)\right|} = \mathcal{O}(10^{-3}), \tag{4.5}$$

yielding

$$\xi_{\psi\phi}^{(s)} \propto e^{-i\phi_s}\left[1 - 2\,i\,\sin\gamma \times \mathcal{O}(10^{-3})\right]. \tag{4.6}$$

Since ϕ_s is of $\mathcal{O}(0.03)$ in the SM, there may well be hadronic uncertainties as large as $\mathcal{O}(10\%)$ in the extraction of ϕ_s. These hadronic uncertainties, which are an important issue for the LHC, can be controlled with the help of the decay $\mathrm{B}_d \to J/\psi\,\rho^0$ [93]. Moreover, the angular distribution of this decay allows one to determine both $\sin\phi_d$ and $\cos\phi_d$, i.e. to fix ϕ_d *unambiguously*, and to extract γ, if penguin effects in $\mathrm{B}_d \to J/\psi\,\rho^0$ are sizeable. An unambiguous determination of the B_d^0–$\overline{B_d^0}$ mixing phase ϕ_d is also possible by combining the $\mathrm{B}_s^0 \to \mathrm{J}/\psi\phi$ observables with those of the decay $\mathrm{B}_d \to J/\psi(l^+l^-)\,K^{*0}(\pi^0 K_{\rm S})$ [94]; other alternatives can be found in [95]. For simplicity, we assume $\xi_{\psi\phi}^{(s)} \propto e^{-i\phi_s}$ in the following discussion, i.e. that the $\mathrm{B}_s^0 \to J/\psi\,\phi$ decay amplitudes do not involve a CP-violating weak phase, which implies vanishing direct CP violation; the question of the hadronic uncertainties affecting (4.6) is left for further studies.

4.1.2 Time-Evolution of the Decay Probability Functions

For our considerations, the time-evolution of the decay probability functions specified in (4.2) and (4.3) plays a central rôle. In the case of (4.2), we obtain (see also [89])

$$|A_0(t)|^2 = \frac{|A_0(0)|^2}{2}\left[(1+\cos\phi_s)\,e^{-\Gamma_{\rm L}^{(s)}t} + (1-\cos\phi_s)\,e^{-\Gamma_{\rm H}^{(s)}t} + 2e^{-\Gamma_s t}\sin(\Delta M_s t)\sin\phi_s\right], \tag{4.7}$$

$$|A_\parallel(t)|^2 = \frac{|A_\parallel(0)|^2}{2}\left[(1+\cos\phi_s)\,e^{-\Gamma_{\rm L}^{(s)}t} + (1-\cos\phi_s)\,e^{-\Gamma_{\rm H}^{(s)}t} + 2e^{-\Gamma_s t}\sin(\Delta M_s t)\sin\phi_s\right], \tag{4.8}$$

$$|A_\perp(t)|^2 = \frac{|A_\perp(0)|^2}{2}\left[(1-\cos\phi_s)\,e^{-\Gamma_{\rm L}^{(s)}t} + (1+\cos\phi_s)\,e^{-\Gamma_{\rm H}^{(s)}t} - 2e^{-\Gamma_s t}\sin(\Delta M_s t)\sin\phi_s\right], \tag{4.9}$$

whereas we have in the case of the interference terms (4.3):

$$\begin{aligned}\mathrm{Re}\{A_0^*(t)A_\parallel(t)\} &= \frac{1}{2}|A_0(0)||A_\parallel(0)|\cos(\delta_2-\delta_1)\\ &\quad\times\left[(1+\cos\phi_s)\,e^{-\Gamma_{\rm L}^{(s)}t} + (1-\cos\phi_s)\,e^{-\Gamma_{\rm H}^{(s)}t} + 2e^{-\Gamma_s t}\sin(\Delta M_s t)\sin\phi_s\right]\end{aligned} \tag{4.10}$$

$$\mathrm{Im}\{A_\parallel^*(t)A_\perp(t)\} = |A_\parallel(0)||A_\perp(0)|\Big[e^{-\Gamma_s t}\left\{\sin\delta_1\cos(\Delta M_s t) - \cos\delta_1\sin(\Delta M_s t)\cos\phi_s\right\}$$

$$-\frac{1}{2}\left(e^{-\Gamma_{\rm H}^{(s)}t}-e^{-\Gamma_{\rm L}^{(s)}t}\right)\cos\delta_1\sin\phi_s\Big], \tag{4.11}$$

$$\begin{aligned}\mathrm{Im}\{A_0^*(t)A_\perp(t)\} \;=\; & |A_0(0)||A_\perp(0)|\Big[e^{-\Gamma_s t}\left\{\sin\delta_2\cos(\Delta M_s t)-\cos\delta_2\sin(\Delta M_s t)\cos\phi_s\right\}\\ & -\frac{1}{2}\left(e^{-\Gamma_{\rm H}^{(s)}t}-e^{-\Gamma_{\rm L}^{(s)}t}\right)\cos\delta_2\sin\phi_s\Big].\end{aligned} \tag{4.12}$$

Here the CP-conserving strong phases δ_1 and δ_2 are defined as follows [88]:

$$\delta_1 \equiv \arg\Big\{A_\parallel(0)^* A_\perp(0)\Big\}, \quad \delta_2 \equiv \arg\Big\{A_0(0)^* A_\perp(0)\Big\}. \tag{4.13}$$

The time-evolutions (4.7)–(4.12) generalize those given in [88] to the case of a sizeable B_s^0–$\overline{\mathrm{B}_s^0}$ mixing phase ϕ_s, thereby allowing one to include also new-physics effects [89]; an even more generalized formalism, taking into account also penguin contributions, can be found in [93]. It should be noted that new physics is expected to manifest itself only in the decay probability functions $\mathcal{O}^{(k)}(t)$ and that the form of the $g^{(k)}(\Theta^{'},\Theta^{''},\chi)$ is not affected.

Since the meson content of the $J/\psi\,\phi$ final states is independent of the flavour of the initial meson, B_s^0 or $\overline{\mathrm{B}_s^0}$, we may use the same angles $\Theta^{'}$, $\Theta^{''}$ and χ to describe the kinematics of the decay products of the CP-conjugate transition $\overline{\mathrm{B}_s^0} \to J/\psi\,\phi$. Consequently, we have

$$\overline{f}(\Theta^{'},\Theta^{''},\chi;t) = \sum_k \overline{\mathcal{O}}^{(k)}(t)\, g^{(k)}(\Theta^{'},\Theta^{''},\chi). \tag{4.14}$$

Within this formalism, CP transformations relating $\mathrm{B}_s^0 \to [J/\psi\,\phi]_f$ to $\overline{\mathrm{B}_s^0} \to [J/\psi\,\phi]_f$ ($f \in \{0,\parallel,\perp\}$) are taken into account in the expressions for the $\mathcal{O}^{(k)}(t)$ and $\overline{\mathcal{O}}^{(k)}(t)$, and do not affect the form of the $g^{(k)}(\Theta^{'},\Theta^{''},\chi)$. Therefore the same functions $g^{(k)}(\Theta^{'},\Theta^{''},\chi)$ are present in (4.1) and (4.14) (see also [26]). The CP-conjugate functions $\overline{\mathcal{O}}^{(k)}(t)$ take the following form:

$$|\overline{A}_0(t)|^2 \;=\; \frac{|A_0(0)|^2}{2}\left[(1+\cos\phi_s)\,e^{-\Gamma_{\rm L}^{(s)}t}+(1-\cos\phi_s)\,e^{-\Gamma_{\rm H}^{(s)}t}-2e^{-\Gamma_s t}\sin(\Delta M_s t)\sin\phi_s\right], \tag{4.15}$$

$$|\overline{A}_\parallel(t)|^2 \;=\; \frac{|A_\parallel(0)|^2}{2}\left[(1+\cos\phi_s)\,e^{-\Gamma_{\rm L}^{(s)}t}+(1-\cos\phi_s)\,e^{-\Gamma_{\rm H}^{(s)}t}-2e^{-\Gamma_s t}\sin(\Delta M_s t)\sin\phi_s\right], \tag{4.16}$$

$$|\overline{A}_\perp(t)|^2 \;=\; \frac{|A_\perp(0)|^2}{2}\left[(1-\cos\phi_s)\,e^{-\Gamma_{\rm L}^{(s)}t}+(1+\cos\phi_s)\,e^{-\Gamma_{\rm H}^{(s)}t}+2e^{-\Gamma_s t}\sin(\Delta M_s t)\sin\phi_s\right], \tag{4.17}$$

$$\begin{aligned}\mathrm{Re}\{\overline{A}_0^*(t)\overline{A}_\parallel(t)\} \;=\; & \frac{1}{2}|A_0(0)||A_\parallel(0)|\cos(\delta_2-\delta_1)\\ & \times\left[(1+\cos\phi_s)\,e^{-\Gamma_{\rm L}^{(s)}t}+(1-\cos\phi_s)\,e^{-\Gamma_{\rm H}^{(s)}t}-2e^{-\Gamma_s t}\sin(\Delta M_s t)\sin\phi_s\right],\end{aligned} \tag{4.18}$$

$$\begin{aligned}\mathrm{Im}\{\overline{A}_\parallel^*(t)\overline{A}_\perp(t)\} \;=\; & -|A_\parallel(0)||A_\perp(0)|\Big[e^{-\Gamma_s t}\left\{\sin\delta_1\cos(\Delta M_s t)-\cos\delta_1\sin(\Delta M_s t)\cos\phi_s\right\}\\ & +\frac{1}{2}\left(e^{-\Gamma_{\rm H}^{(s)}t}-e^{-\Gamma_{\rm L}^{(s)}t}\right)\cos\delta_1\sin\phi_s\Big],\end{aligned} \tag{4.19}$$

$$\begin{aligned}\mathrm{Im}\{\overline{A}_0^*(t)\overline{A}_\perp(t)\} \;=\; & -|A_0(0)||A_\perp(0)|\Big[e^{-\Gamma_s t}\left\{\sin\delta_2\cos(\Delta M_s t)-\cos\delta_2\sin(\Delta M_s t)\cos\phi_s\right\}\\ & +\frac{1}{2}\left(e^{-\Gamma_{\rm H}^{(s)}t}-e^{-\Gamma_{\rm L}^{(s)}t}\right)\cos\delta_2\sin\phi_s\Big].\end{aligned} \tag{4.20}$$

4.1.3 Angular Distributions

The full angular distribution of $\mathrm{B_s} \to \mathrm{J}/\psi(\mathrm{l}^+\mathrm{l}^-)\;\phi(\mathrm{K}^+\mathrm{K}^-)$ involves three physical angles. The convention used is as follows (see Fig. 29): the $z^{'}(z^{''})$-axis is defined to be the direction of $p_{J/\psi}(p_\phi)$ in the rest

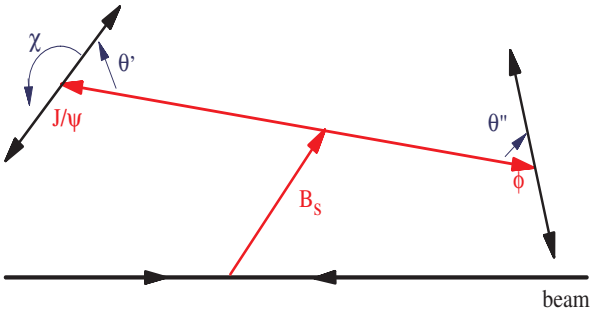

Fig. 29: Angular conventions for the decay $\mathrm{B_s^0} \to \mathrm{J}/\psi\,\phi$.

frame of the B_s^0. Let the $x'(x'')$-axis be any arbitrarily fixed direction in the plane normal to the $z'(z'')$ axis. The $y'(y'')$-axis is then fixed uniquely. Let (Θ', φ') specify the direction of the ℓ^+ in the J/ψ rest frame, and let (Θ'', φ'') be the direction of the K^+ in the ϕ rest frame. Since the orientation of the x' and x'' axes is a matter of convention, only the combination $\chi \equiv \varphi' + \varphi''$ of the two azimuthal angles is physical. The full angular distribution in terms of the three physical angles $(\Theta', \Theta'', \chi)$ (normalized such that $\Gamma = |A_0(t)|^2 + |A_\parallel(t)|^2 + |A_\perp(t)|^2$) is given by

$$
\begin{aligned}
W^+(\Omega, t) \;=\; \frac{d^3\Gamma}{d\cos\Theta'\, d\cos\Theta''\, d\chi} = \frac{9}{64\pi} \Big\{ & 4|A_0(t)|^2 \sin^2\Theta' \cos^2\Theta'' \\
& + |A_\parallel(t)|^2 [(1+\cos^2\Theta')\sin^2\Theta'' - \sin^2\Theta' \sin^2\Theta'' \cos 2\chi] \\
& + |A_\perp(t)|^2 [(1+\cos^2\Theta')\sin^2\Theta'' + \sin^2\Theta' \sin^2\Theta'' \cos 2\chi] \\
& + 2\mathrm{Im}(A_\parallel(t)^* A_\perp(t)) \sin^2\Theta' \sin^2\Theta'' \sin 2\chi - \sqrt{2}\mathrm{Re}(A_0^*(t) A_\parallel(t)) \sin 2\Theta' \sin 2\Theta'' \cos\chi \\
& + \sqrt{2}\mathrm{Im}(A_0^*(t) A_\perp(t)) \sin 2\Theta' \sin 2\Theta'' \sin\chi \Big\}\,, \qquad (4.21)
\end{aligned}
$$

where the bilinear combinations of the complex functions $A_0(t)$, $A_\parallel(t)$ and $A_\perp(t)$ are defined in (4.7) to (4.12). The angular distribution $W^-(\Omega, t)$ of the CP-conjugate transition $\overline{\mathrm{B_s^0}} \to J/\psi\,\phi$ is analogous to (4.21), using the bilinear combinations of $\overline{A}_0(t)$, $\overline{A}_\parallel(t)$ and $\overline{A}_\perp(t)$ defined in Eqs. (4.15) to (4.20).

4.1.4 An Illustration of New-Physics Effects

As we have already noted, a very important feature of $B_s \to J/\psi\,\phi$ decays is that they represent a sensitive probe for CP-violating contributions to B_s^0–$\overline{B_s^0}$ mixing from physics beyond the SM. Let us illustrate these effects in this subsection, where we shall follow closely Ref. [91], for a particular scenario of new physics, the symmetrical $\mathrm{SU_L(2) \times SU_R(2) \times U(1)}$ model with spontaneous CP violation (SB–LR) [96, 97]. Needless to note that there are also other scenarios for physics beyond the SM which are interesting in this respect, for example models allowing mixing to a new isosinglet down quark, as in $\mathrm{E_6}$ [90].

In a recent paper [98], the SB–LR model has been investigated in the light of current experimental constraints from K- and B decay observables. In a large region of parameter space, the model mainly affects neutral-meson mixing, but does not introduce sizeable "direct" CP violation. The sensitive observables constraining the model are thus the meson mass difference in the kaon sector ΔM_K, those in the B sector ΔM_d, ΔM_s, the "indirect" CP-violating parameter ϵ_K of the neutral kaon system, and the mixing-induced CP asymmetry $\mathcal{A}_{\mathrm{CP}}^{\mathrm{mix}}(B_d \to J/\psi\, K_\mathrm{S})$. In particular, it was found that, for a set of fixed CKM parameters and quark masses, the model predicts a small value for $|\mathcal{A}_{\mathrm{CP}}^{\mathrm{mix}}(B_d \to J/\psi\, K_\mathrm{S})|$ below 10%, which is in agreement at the 2σ level with the CDF measurement $0.79^{+0.41}_{-0.44}$, but at variance with the SM expectation 0.73 ± 0.21 [99].

As was pointed out in [91], the SB–LR model predicts also values for the mixing-induced CP

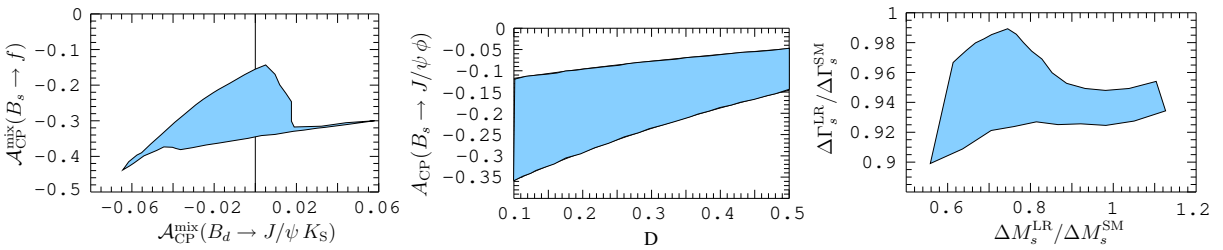

(a) Allowed values for $\mathcal{A}_{\rm CP}^{\rm mix}(B_d \to J/\psi K_{\rm S})$ and $\mathcal{A}_{\rm CP}^{\rm mix}(B_s \to f)$, with $f = D_s^+ D_s^-, J/\psi\,\eta^{(\prime)}$.

(b) $A_{\rm CP}(B_s \to J/\psi\phi)$ as a function of the hadronic parameter D.

(c) Correlation between ΔM_s and $\Delta\Gamma_s$, normalized to their SM values.

Fig. 30: Predictions of the left-right symmetric model for several CP observables.

asymmetries of $B_s \to J/\psi\,\phi$ – and similar modes, such as $B_s \to D_s^+ D_s^-$ and $J/\psi\,\eta^{(\prime)}$ – that largely deviate from the SM expectation of very small CP-violating effects. In the case of the latter modes, which are decays into CP eigenstates with CP eigenvalue $+1$, we simply have

$$\mathcal{A}_{\rm CP}^{\rm mix}(B_s \to f) = \sin\phi_s, \text{ where } \phi_s \equiv \phi_s^{\rm SM} + \phi_s^{\rm NP} = -2\lambda^2\eta + \phi_s^{\rm NP}, \tag{4.22}$$

with $\phi_s^{\rm NP}$ originating from new physics. In Fig. 30(a), we show the allowed region for $\mathcal{A}_{\rm CP}^{\rm mix}(B_s \to f) = \sin\phi_s$ and $\mathcal{A}_{\rm CP}^{\rm mix}(B_d \to J/\psi\, K_{\rm S})$ in the SB–LR model; the corresponding direct CP asymmetries remain very small, since new contributions to the decay amplitudes are strongly suppressed. The figure illustrates nicely that CP asymmetries as large as $\mathcal{O}(40\%)$ may arise in the B_s channels, whereas the SB–LR model favours a small CP asymmetry in $B_d \to J/\psi\, K_{\rm S}$.

In order to simplify the discussion of $B_s \to J/\psi\,\phi$, let us consider the CP asymmetry

$$\mathcal{A}_{\rm CP}(B_s(t) \to J/\psi\,\phi) \equiv \frac{\Gamma(t) - \overline{\Gamma}(t)}{\Gamma(t) + \overline{\Gamma}(t)} = \left[\frac{1-D}{F_+(t) + DF_-(t)}\right] \sin(\Delta M_s t)\, \sin\phi_s, \tag{4.23}$$

where $\Gamma(t)$ and $\overline{\Gamma}(t)$ denote the time-dependent rates for decays of initially, i.e. at $t = 0$, present B_s^0- and $\overline{B_s^0}$ mesons into $J/\psi\,\phi$ final states, respectively. The remaining quantities are defined as

$$D \equiv \frac{|A_\perp(0)|^2}{|A_0(0)|^2 + |A_\parallel(0)|^2} \text{ and } F_\pm(t) \equiv \frac{1}{2}\left[(1 \pm \cos\phi_s)\, e^{+\Delta\Gamma_s t/2} + (1 \mp \cos\phi_s)\, e^{-\Delta\Gamma_s t/2}\right]. \tag{4.24}$$

Note that we have $F_+(t) = F_-(t) = 1$ for a negligible width difference $\Delta\Gamma_s$. Obviously, the advantage of the "integrated" observable (4.23) is that it can be measured *without* performing an angular analysis. The disadvantage is of course that it also depends on the hadronic quantity D, which precludes a theoretically clean extraction of ϕ_s from (4.23). However, this feature does not limit the power of this CP asymmetry to search for indications of new physics, which would be provided by a measured sizeable value of (4.23). Model calculations of D, making use of the factorization-hypothesis, typically give $D = 0.1 \ldots 0.5$ [88], which is also in agreement with a recent analysis of the $B_s \to J/\psi\,\phi$ polarization amplitudes performed by the CDF collaboration [86]. In order to extract ϕ_s from CP-violating effects in the decay $B_s \to J/\psi\,\phi$ in a theoretically clean way, an angular analysis has to be performed, as is discussed in detail above.

Although the B_s^0–$\overline{B_s^0}$ oscillations are very rapid, it should be possible to resolve them at the LHC (see Sec. 7). The first extremal value of the time-dependent CP asymmetry (4.23), corresponding to $\Delta M_s t = \pi/2$, is given to a very good approximation by

$$A_{\rm CP}(B_s \to J/\psi\,\phi) = \left(\frac{1-D}{1+D}\right) \sin\phi_s, \tag{4.25}$$

which would also fix the magnitude of (4.23) in the case of a negligible width difference $\Delta\Gamma_s$. In Fig. 30(b), we show the prediction of the SB–LR model for (4.25) as a function of the hadronic parameter D. For a value of $D = 0.3$, this CP asymmetry may be as large as –25%. The dilution through the hadronic parameter D is not effective in the case of the CP-violating observables of the $B_s \to J/\psi[\to l^+l^-]\,\phi[\to K^+K^-]$ angular distribution, which allow one to probe $\sin\phi_s$ directly (see Sec. 4.1.2). Predictions for other B_s decays in the SB–LR model have been discussed in [100].

Let us finally note that new physics affects also the B_s^0–$\overline{B_s^0}$ mass and width differences. In the latter case, we have [101]

$$\Delta\Gamma_s = \Delta\Gamma_s^{\rm SM}\cos\phi_s, \tag{4.26}$$

where $\Delta\Gamma_s^{\rm SM} = \mathcal{O}(-15\%)$ is the SM width difference [23, 24]. In Fig. 30(c), we show the correlation between ΔM_s and $\Delta\Gamma_s$ in the SB–LR model. The reduction of $\Delta\Gamma_s$ through new-physics effects, which is described by (4.26), is fortunately not very effective in this case, whereas the mass difference ΔM_s may be reduced significantly.

4.2 Experimental Studies

The prospective performance of ATLAS, CMS and LHCb in analysing $\mathrm{B}_s^0 \to \mathrm{J}/\psi(\mu^+\mu^-)\phi(\mathrm{K}^+\mathrm{K}^-)$ has been studied in [37, 103, 104, 102].

4.2.1 Expected Data Characteristics

Despite different strategies, all three experiments expect a large number of events in this channel. With present studies the highest yield is expected in CMS, where a dimuon trigger is used. At higher trigger-level the identification of two muons is essential for $\mathrm{J}/\psi \to \mu^+\mu^-$ online selection in all three experiments. The reconstruction is completed in tracking and vertex detectors by fitting muon candidate trajectories into a common vertex. For reconstructing ϕ mesons, pairs of oppositely charged particles are fitted into a common vertex and their invariant mass is calculated assuming they are kaons. In LHCb, the RICHes are used to separate charged K mesons from π mesons, allowing a reduction of the backgrounds to $\mathrm{B}_s^0 \to \mathrm{J}/\psi\phi$. As explained in Sec. 2.5, there is a limited possibility of charged hadron identification in both ATLAS and CMS; however this has not been exploited in the present studies. The stronger solenoidal field in CMS leads to better B_s^0 invariant mass resolution and lower $\mathrm{B}_s^0 \to \mathrm{J}/\psi\phi$ background than in ATLAS. For this channel, the most significant difference between the performance of the three experiments lies in the superior proper time resolution of LHCb. The expected data and background-characteristics in $\mathrm{B}_s^0 \to \mathrm{J}/\psi(\mu^+\mu^-)\phi(\mathrm{K}^+\mathrm{K}^-)$, as presented in the workshop, are summarized in Tab. 14. It is possible that the inclusion of low-threshold dimuon-triggers may also boost the final event yields in ATLAS and LHCb, as has been demonstrated to be the case in CMS.

Flavour tagging is important to properly explore the physics of $\mathrm{B}_s^0 \to \mathrm{J}/\psi\phi$ decays. This study considers only lepton and charged K mesons tags for LHCb and a jet charge method for ATLAS and CMS (see Sec. 2.7). CMS are presently extending their study to include other tags. The efficiencies and the wrong tag fractions in this channel are summarized in Tab. 14.

The studies presented here do not exhaust the whole potential of the three experiments. Future studies can be extended in trigger and offline selections as well as in tagging methods.

4.2.2 Modelling $\mathrm{B}_s^0 \to \mathrm{J}/\psi\phi$ Decays

The distribution (4.21) contains eight unknown independent parameters. These are the amplitudes $|A_{||}(0)|$, $|A_\perp(0)|$, the relative strong phases δ_1 and δ_2, the decay rate difference, $\Delta\Gamma_{\rm s} = \Gamma_{\rm H} - \Gamma_{\rm L}$, and mean decay rate $\Gamma_s = (\Gamma_{\rm H} + \Gamma_{\rm L})/2$ of the mass eigenstates B_H^0 and B_L^0 , their mass difference $\Delta M_s = x_{\rm s}\,/\Gamma_s$ and the weak phase ϕ_s. These parameters can be determined from the measured three decay angles and lifetimes. In the workshop two strategies were studied: the method of moments approach [104] and a maximum-likelihood fit.

	ATLAS	CMS	LHCb
Event yields	300,000	600,000	370,000
Proper time resolution	0.063 ps	0.063 ps	0.031 ps
Background	$\sim$ 15% dominated by $B_d^0 \to J/\psi K^*$, $J/\psi K^+\pi^-$	$\sim$ 10% dominated by $B_d^0 \to J/\psi K^*$, $J/\psi K^+\pi^-$	$\sim$ 3% combinatorial
Tagging	jet charge tag $\epsilon \sim 63\%$ wrong 38%	jet charge tag $\epsilon \sim 32\%$ wrong 33% lepton tag $\epsilon \sim 6.1\%$ wrong 28%	lepton tag + charged K tag $\epsilon \sim 40\%$ wrong 30%

Table 14: Summary of performance parameters for $B_s^0 \to J/\psi(\mu^+\mu^-)\phi(K^+K^-)$. The proper time resolutions have been determined by a single Gaussian fit. The event yields assume 3 years operation for ATLAS & CMS, and 5 years for LHCb.

Parameter	$\left\|\frac{A_{\|\|}(0)}{A_0(0)}\right\|^2$	$\left\|\frac{A_\perp(0)}{A_0(0)}\right\|^2$	δ_1	δ_2	$\Delta\Gamma_s$	$1/\Gamma_s$	x_s	ϕ_s
Value	0.64	0.14	0	π	$0.15 \times \Gamma_s$	1.54 ps	20–40	0.04–0.8

Table 15: Input values of theory parameters used in simulating $B_s^0 \to J/\psi\phi$.

	ATLAS	CMS	LHCb
$\Delta\Gamma_s$	12%	8%	9%
Γ_s	0.7%	0.5%	0.6%
$A_{\|\|}$	0.8%	0.6%	0.7%
$A_\perp$	3%	2%	2%
ϕ_s ($x_s = 20$)	0.03	0.014	0.02
ϕ_s ($x_s = 40$)	0.05	0.03	0.03

Table 16: Expected statistical uncertainties on $B_s^0 \to J/\psi\phi$ parameters for each experiment under the assumptions given in the text. Apart from ϕ_s, the errors are relative.

In the method of moments approach [88], the terms bilinear in A in (4.21) are determined from the data using an appropriate set of weighting functions, which separate out the terms with different angular dependences. The question of information-content loss in the angular moments analysis was investigated in [105]. For the results presented in this report, the likelihood-approach is adopted.

We define a likelihood-function by

$$L = \prod_{i=1}^{N} \int_0^\infty \frac{(\epsilon_1 W^+(t_i,\Omega_i) + \epsilon_2 W^-(t_i,\Omega_i) + b\, e^{-\Gamma_0 t_i})\rho(t-t_i)\,dt}{\int_{t_{\min}}^\infty (\int_0^\infty (\epsilon_1 W^+(t,\Omega) + \epsilon_2 W^-(t,\Omega) + b\, e^{-\Gamma_0 t})\rho(t'-t)\,dt')\,dt}\,, \tag{4.27}$$

where $\epsilon_1 = \epsilon_2 = 0.5$ for untagged events, $\epsilon_1 = 1-w$, $\epsilon_2 = w$ if the B_s^0 is tagged as a particle, and $\epsilon_1 = w$, $\epsilon_2 = 1-w$ if the B_s^0 is tagged as an anti-particle, b is the level of background and Γ_0 is the average decay-rate of the background as determined from simulation. The time resolution function $\rho(t-t_i)$ was approximated by a Gaussian of width $\sigma = 0.063$ ps and $\sigma = 0.031$ ps for ATLAS/CMS and LHCb respectively. The index i runs over all N events. Finally, $t_{\min}$ is the minimum proper lifetime allowed in the event selection.

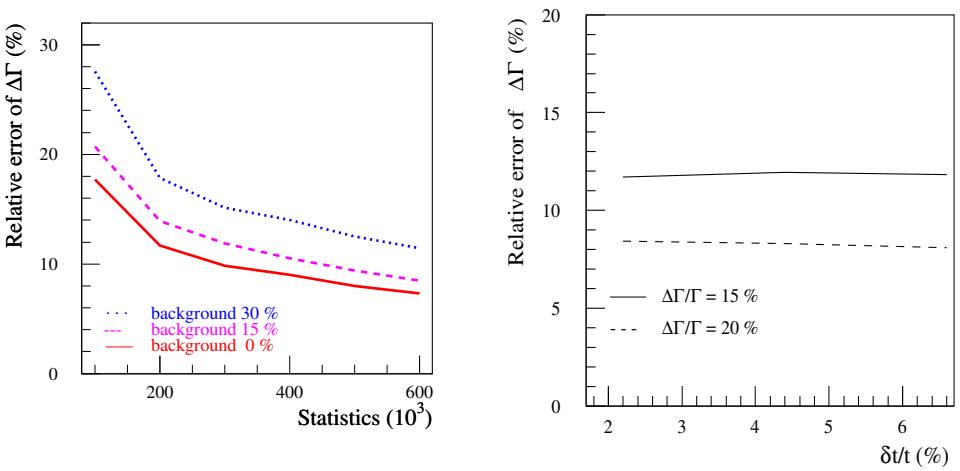

Fig. 31: Expected relative error on $\Delta\Gamma_s$ from $B_s^0 \to J/\psi\phi$. (a) Estimate of the relative error of $\Delta\Gamma_s$ as a function of signal-statistics for several values of background. The background is expected to be between 4% and 15%. (b) Relative error of $\Delta\Gamma_s$ as a function of the relative precision of the lifetime measurement $\delta t/t$ for two values of $\Delta\Gamma_s$ /Γ_s. LHCb expects $\delta t/t = 2.2\%$, ATLAS/CMS 4.4%. A background of 15% and statistics of 300,000 events is assumed.

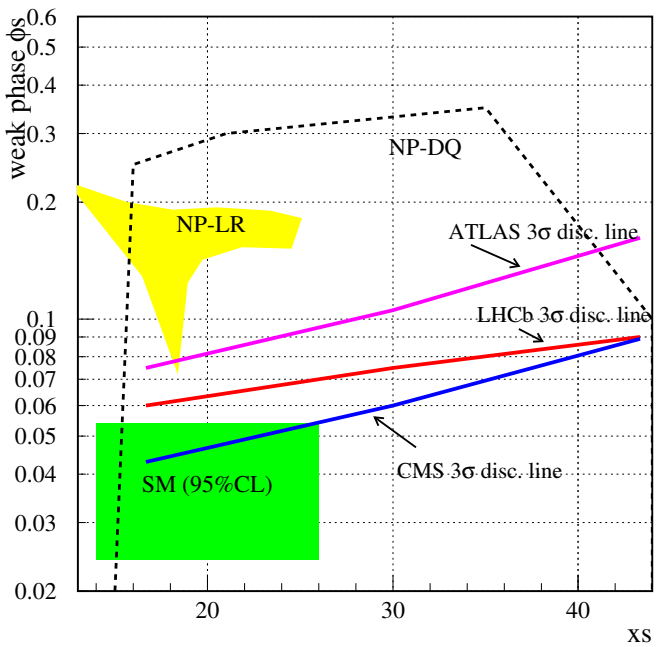

Fig. 32: The x_s–ϕ_s region allowed in the SM, the left-right symmetric model with spontaneous CP violation (NP-LR) and the iso-singlet down quark mixing model (NP-DQ). Also shown is the region of experimental sensitivity of ATLAS and CMS, corresponding to 63 fs, and of LHCb with 31 fs. The NP–LR allowed region appears smaller than that of the SM, because it does not include all theory uncertainties.

4.2.3 *Parameter Determination and Estimate of Precision*

The expected experimental precision is not sufficient to allow a simultaneous determination of eight unknown parameters. Besides the limited statistics, the correlations between different parameters pose a problem: while in (4.21) the eight parameters are independent, simulations with the maximum-likelihood approach showed that in the experimental data some of the parameters have obvious correlations. There is a strong correlation between the two phases δ_1 and δ_2, which precludes a simultaneous measurement of both of them with this method. Also a second pair of parameters, ΔM_s and the weak phase ϕ_s, shows certain correlations that depend on the values of ΔM_s and the time resolution. Consequently, the reduced set of parameters: $\Delta\Gamma_s$, Γ_s, $|A_{||}(0)|$, $|A_{\perp}(0)|$ and ϕ_s were determined in the fit and the other parameters were fixed. For the strong phases the values $\delta_1 = 0$ and $\delta_2 = \pi$ were used as suggested in Ref. [106].[12] ΔM_s is assumed to be determined from other channels, for instance $\mathrm{B}_s^0 \to D_s\pi$, although it should be stressed that also $\mathrm{B}_s^0 \to \mathrm{J}/\psi\phi$ is a very suitable channel for such a measurement.

The choice of input values of the unknown parameters, both fixed and free, based on the experimental results [107, 86, 64] and theoretical considerations [88, 106, 108] is summarized in Tab. 15.

The main results of the study are summarized in Tab. 16 for each experiment. With this method, the rate difference $\Delta\Gamma_s$ can be determined with a relative statistical error which for LHCb, CMS and ATLAS varies between 8 and 12% for $\Delta\Gamma_s\,/\Gamma_s = 0.15$, Fig. 31(a). The differences between the experiments are small, mainly because the error is not sensitive to the different proper time precision of each experiment, Fig. 31(b). The statistical errors of Γ_s, $|A_{||}(0)|$ and $|A_{\perp}(0)|$ are typically a few percent. The precision to which the weak phase ϕ_s can be measured depends strongly on the proper time resolution and x_{s} (Fig. 32). There is a sensitivity to the SM range of ϕ_s, and a clear potential for probing models of new physics, such as for instance the left-right symmetric model [91] or the isosinglet down quark model [90]. If penguin contributions are non-negligible, the number of parameters will increase, which will necessitate simultaneous analyses of $\mathrm{B}_s^0 \to \mathrm{J}/\psi\phi$ and SU(3) related channels as indicated earlier in the theoretical discussion. The combined LHC sensitivity to these parameters will be even better, but this study has not yet been performed.

Studies with the method of moments approach gave results broadly in agreement with the likelihood-fits, but with certain differences which are yet to be resolved. In particular, the moments analysis indicated that the strong phases can be extracted simultaneously with the other parameters through the separation of different angular terms [104]. Future work will resolve these issues.

4.3 Conclusions

A rich variety of physics can be studied through the decay $\mathrm{B}_s^0 \to \mathrm{J}/\psi\phi$ and all three LHC experiments will be able to perform powerful and interesting measurements. More work is encouraged to further extend the experimental potential, in particular by improving the sensitivity to the weak mixing phase ϕ_s, and to establish the optimum approach for analysing the data.

5 NEW STRATEGIES TO EXTRACT CKM PHASES[13]

In addition to the refined studies of the usual benchmark CP modes described above, an important goal of the workshop was to explore strategies for the extraction of CKM phases that had not been considered for ATLAS, CMS and LHCb before, and to search for new strategies. In this section, we will discuss extractions of γ from $B \to \pi K$ decays, which received a lot of attention in the literature over the last couple of years [109], and new techniques [34, 61, 93, 110], which were developed during this workshop and make use of certain U-spin related B decays, where all down and strange quarks are interchanged

[12] Note that this suggestion is based on the factorization approximation and not expected to hold once non-factorizable contributions are taken into account.

[13] Section coordinators: R. Fleischer and G. Wilkinson.

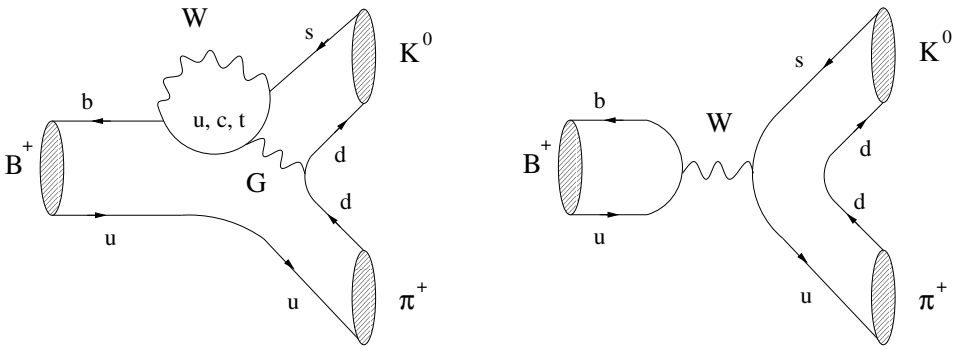

Fig. 33: Feynman diagrams contributing to $B^+ \to \pi^+ K^0$.

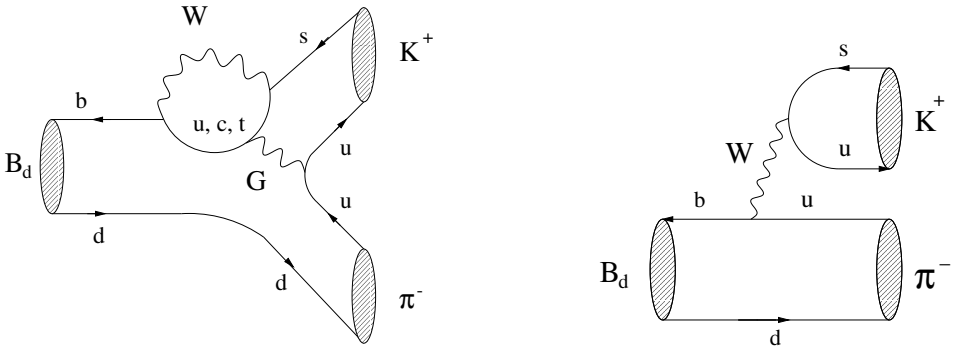

Fig. 34: Feynman diagrams contributing to $B_d^0 \to \pi^- K^+$.

with each other [111]. For the "prehistory" of the use of U-spin arguments to relate non-leptonic B decays, the reader is referred to [111]–[116].

5.1 Extracting γ from $B \to \pi K$ Decays[14]

In order to obtain direct information on γ, $B \to \pi K$ decays are very interesting. These modes are not just an "unwanted" background for $B \to \pi\pi$, but have a very interesting physics potential. Experimental data for these modes start to become available: since 1997, when the first results on $B^\pm \to \pi^\pm K$ and $B_d \to \pi^\mp K^\pm$ were reported by the CLEO collaboration, there were several updated results for CP-averaged $B \to \pi K$ branching ratios at the 10^{-5} level [117]. Interestingly, these CP-averaged branching ratios may already lead to highly non-trivial constraints on γ [118, 119]. Unfortunately, the present experimental uncertainties are too large to decide how effective these bounds actually are. The new results of the e^+e^- B factories will certainly improve this situation, so that we should have a much better picture by the time the LHC starts running. In 1999, also the first preliminary results for CP-violating asymmetries in charmless hadronic B meson decays were reported by the CLEO collaboration [117], which do not yet indicate CP violation in such transitions. So far, to probe γ, the following three combinations of $B \to \pi K$ decays were considered in the literature: $B^\pm \to \pi^\pm K$ and $B_d \to \pi^\mp K^\pm$ [118, 120, 121], $B^\pm \to \pi^\pm K$ and $B^\pm \to \pi^0 K^\pm$ [31, 119, 122, 68], as well as the combination of the neutral decays $B_d \to \pi^0 K_{\rm S}$ and $B_d \to \pi^\mp K^\pm$ [68]. Since the first combination does not involve a neutral pion, it is particularly promising for the LHC from an experimental point of view, although the other two combinations would have certain advantages from a theoretical point of view. The experimental feasibility studies therefore put a strong emphasis on that approach. Let us note, before having a closer look at this strategy, that $B \to \pi K$ decays play not only an important rôle to probe γ, but also to obtain insights into the world of electroweak penguins. This interesting aspect is discussed in more detail in

[14]With help from C. Shepherd-Themistocleous.

Refs. [17, 120, 68, 123].

5.1.1 The $B^\pm \to \pi^\pm K$, $B_d \to \pi^\mp K^\pm$ Strategy

Within the framework of the SM, the decays $B^+ \to \pi^+ K^0$ and $B_d^0 \to \pi^- K^+$ receive contributions from Feynman diagrams of the type shown in Figs. 33 and 34, respectively. Because of the tiny ratio $|V_{us}V_{ub}^*|/|V_{ts}V_{tb}^*| \approx 0.02$, the QCD penguins play the dominant rôle in these decays, despite their loop-suppression. Using the SU(2) isospin symmetry of strong interactions to relate QCD penguin topologies, we may derive the following amplitude relations [114]:

$$A(B^+ \to \pi^+ K^0) \equiv P, \quad A(B_d^0 \to \pi^- K^+) = -\left[P + T + P_{\rm ew}^{\rm C}\right], \tag{5.1}$$

where

$$T \equiv |T| e^{i\delta_T} e^{i\gamma} \quad \text{and} \quad P_{\rm ew}^{\rm C} \equiv -\left|P_{\rm ew}^{\rm C}\right| e^{i\delta_{\rm ew}^{\rm C}} \tag{5.2}$$

are due to tree-diagram-like topologies and EW penguins, respectively. The label "C" reminds us that only "colour-suppressed" EW penguin topologies contribute to $P_{\rm ew}^{\rm C}$. Making use of the unitarity of the CKM matrix and applying the generalized Wolfenstein parametrization, including non-leading terms in λ, we obtain [114]

$$A(B^+ \to \pi^+ K^0) = -\left(1 - \frac{\lambda^2}{2}\right) \lambda^2 A \left[1 + \rho\, e^{i\theta} e^{i\gamma}\right] \mathcal{P}_{tc}\,, \tag{5.3}$$

where

$$\rho\, e^{i\theta} = \left(\frac{\lambda^2 R_b}{1-\lambda^2}\right)\left[1 - \left(\frac{\mathcal{P}_{uc} + \mathcal{A}}{\mathcal{P}_{tc}}\right)\right]. \tag{5.4}$$

Here $\mathcal{P}_{tc} \equiv |\mathcal{P}_{tc}| e^{i\delta_{tc}}$ and $\mathcal{P}_{uc}$ describe differences of penguin topologies with internal top- and charm-quark and up- and charm-quark exchanges, respectively, and $\mathcal{A}$ is due to the annihilation topology in Fig. 33. It is important to note that ρ is strongly CKM-suppressed by $\lambda^2 R_b \approx 0.02$. For the parametrization of $B^\pm \to \pi^\pm K$ and $B_d \to \pi^\mp K^\pm$ observables, it is convenient to introduce

$$r \equiv \frac{|T|}{\sqrt{\langle |P|^2 \rangle}}, \quad \epsilon_{\rm C} \equiv \frac{|P_{\rm ew}^{\rm C}|}{\sqrt{\langle |P|^2 \rangle}} \;\text{ with }\; \langle |P|^2 \rangle \equiv \frac{1}{2}\left(|P|^2 + |\overline{P}|^2\right), \tag{5.5}$$

as well as the strong phase differences

$$\delta \equiv \delta_T - \delta_{tc}\,, \quad \Delta_{\rm C} \equiv \delta_{\rm ew}^{\rm C} - \delta_{tc}\,. \tag{5.6}$$

In addition to the ratio

$$R \equiv \frac{B(B_d^0 \to \pi^- K^+) + B(\overline{B_d^0} \to \pi^+ K^-)}{B(B^+ \to \pi^+ K^0) + B(B^- \to \pi^- \overline{K^0})} \tag{5.7}$$

of CP-averaged branching ratios, also the "pseudo-asymmetry"

$$A_0 \equiv \frac{B(B_d^0 \to \pi^- K^+) - B(\overline{B_d^0} \to \pi^+ K^-)}{B(B^+ \to \pi^+ K^0) + B(B^- \to \pi^- \overline{K^0})} \tag{5.8}$$

plays an important rôle in probing γ. Here, we have neglected tiny phase-space effects, which can, however, be taken into account in a straightforward way (see [118]). Explicit expressions for R and A_0 in terms of the parameters specified above are given in [114]. Using the presently available experimental results from the CLEO collaboration [117], we obtain

$$R = 1.0 \pm 0.3, \quad A_0 = 0.04 \pm 0.18. \tag{5.9}$$

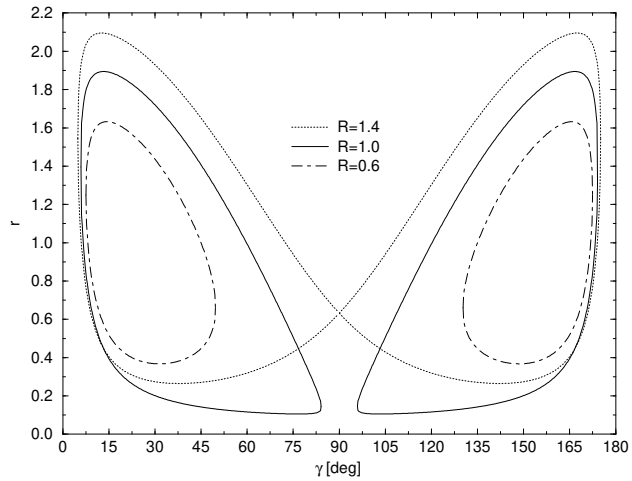

Fig. 35: The contours in the γ–r plane for $|A_0| = 0.2$ ($\rho = \epsilon_{\rm C} = 0$).

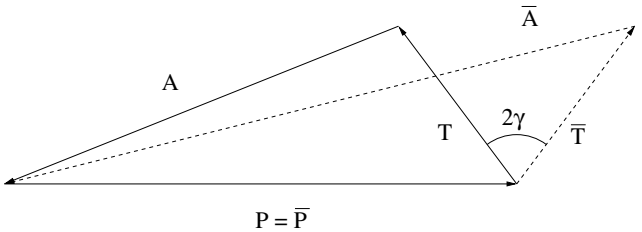

Fig. 36: Triangle construction to determine γ from the $B_d \to \pi^{\mp}K^{\pm}$, $B^{\pm} \to \pi^{\pm}K$ system in the case of $\rho = \epsilon_{\rm C} = 0$. Here we have $A \equiv A(B^0_d \to \pi^- K^+)$ and $\overline{A} \equiv A(\overline{B^0_d} \to \pi^+ K^-)$; note that $\rho = 0$ implies $P = \overline{P} \equiv A(B^- \to \pi^- \overline{K^0})$.

The pseudo-asymmetry A_0 allows one to eliminate the strong phase δ in the expression for R, and to fix contours in the $\gamma - r$ plane [114]. These contours, which are illustrated in Fig. 35, correspond to the mathematical implementation of a simple triangle construction [120], which is related to the amplitude relation (5.1), and is shown in Fig. 36. In order to determine γ, the quantity r, i.e. the magnitude of the "tree" amplitude T, has to be fixed. At this stage, a certain model dependence enters. An approximate way to fix this amplitude is to neglect "colour-suppressed" current–current operator contributions to $B^+ \to \pi^+\pi^0$, and to use SU(3) flavour-symmetry to relate the "colour-allowed" current–current amplitude of that decay to T:

$$|T| \approx \lambda \frac{f_K}{f_\pi} \sqrt{2} |A(B^+ \to \pi^+ \pi^0)| \,. \tag{5.10}$$

Another approach to obtain information on $|T|$ is to use "factorization" [124], leading to

$$|T|_{\rm fact} = \frac{G_{\rm F}}{\sqrt{2}} \, \lambda \, |V_{ub}| \, a_1 \, \left(M^2_{B_d} - M^2_\pi \right) \, f_K \, F_{B\pi}(M^2_K; 0^+) \,, \tag{5.11}$$

where $F_{B\pi}$ is a quark–current form factor and $a_1 \approx 1$ the usual phenomenological colour factor. Using the form factor $F_{B\pi}(M^2_K; 0^+) = 0.3$, as obtained e.g. from QCD sum rules on the light-cone [125, 126], one finds

$$|T|_{\rm fact} = a_1 \times \left[\frac{|V_{ub}|}{3.2 \times 10^{-3}} \right] \times 7.8 \times 10^{-9} \, {\rm GeV} \,. \tag{5.12}$$

As was pointed out in [121], also semileptonic $B^0 \to \pi^- l^+ \nu_l$ decays may play an important rôle to fix $|T|$ with the help of arguments based on "factorization". Using (5.11), one finds [118]

$$r_{\rm fact} = 0.18 \times a_1 \times \left[\frac{|V_{ub}|}{3.2 \times 10^{-3}} \right] \sqrt{\left[\frac{1.8 \times 10^{-5}}{B(B^{\pm} \to \pi^{\pm} K)} \right] \times \left[\frac{\tau_{B_u}}{1.6 \, {\rm ps}} \right]} \,. \tag{5.13}$$

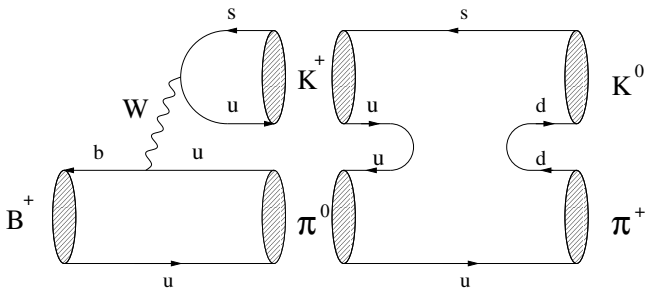

Fig. 37: Rescattering process contributing to $B^+ \to \pi^+ K^0$.

Making use of such arguments based on "factorization", present data give $r = 0.18 \pm 0.05$. Although the factorization-hypothesis [124] may work reasonably well for "colour-allowed" tree-diagram-like topologies [127], T may be shifted from its "factorized" value, as the properly defined amplitude T does not only receive contributions from such "tree" topologies, but also from penguin and annihilation processes [114, 113], which are strongly related to rescattering processes [113, 128, 129]. In an interesting recent paper by Beneke, Buchalla, Neubert and Sachrajda [76], it was pointed out that there is a heavy-quark expansion for non-leptonic B decays into two light mesons, and that non-factorizable corrections, as well as rescattering processes, are suppressed by $\Lambda_{\rm QCD}/m_b$. This approach may turn out to be useful to fix the parameter r, which is required in order to determine γ from $B_d \to \pi^\mp K^\pm$, $B^\pm \to \pi^\pm K$ decays.

Interestingly, it is possible to derive bounds on γ that do *not* depend on r at all [118]. To this end, we eliminate δ in R through A_0. If we now treat r as a "free" variable, we find that R takes the minimal value [114]

$$R_{\rm min} = \kappa \, \sin^2\gamma \, + \, \frac{1}{\kappa}\left(\frac{A_0}{2\,\sin\gamma}\right)^2 \geq \kappa \, \sin^2\gamma, \tag{5.14}$$

where

$$\kappa = \frac{1}{w^2}\left[1 + 2\,(\epsilon_{\rm C}\,w)\cos\Delta_C + (\epsilon_{\rm C}\,w)^2\right] \;\text{with}\; w = \sqrt{1 + 2\,\rho\,\cos\theta\cos\gamma + \rho^2}. \tag{5.15}$$

The inequality in (5.14) arises if we keep both r and δ as free parameters [118]. $R_{\rm min}$ restricts the allowed range for γ, since values of γ implying $R_{\rm exp} < R_{\rm min}$ are excluded. In particular, $A_0 \neq 0$ would allow one to exclude a certain range of γ around 0° or 180°, whereas a measured value of $R < 1$ would exclude a certain range around 90°, which would be of great phenomenological importance. The first results reported by CLEO in 1997 gave $R = 0.65 \pm 0.40$ and led to great excitement, whereas the most recent update is the one given in (5.9). If the parameter r is fixed, significantly stronger constraints on γ can be obtained from the observable R [68, 69]. In particular, these constraints require only $R \neq 1$ and are also effective for $R > 1$.

The theoretical accuracy of the strategies to probe γ through the $B^\pm \to \pi^\pm K$, $B_d \to \pi^\mp K^\pm$ system is limited both by rescattering processes of the kind $B^+ \to \{\pi^0 K^+, \pi^0 K^{*+}, \ldots\} \to \pi^+ K^0$ [128, 129], which are illustrated in Fig. 37, and by the "colour-suppressed" EW penguin contributions described by the amplitude $P_{\rm ew}^{\rm C}$ [121, 129]. In (5.14), these effects are described by the parameter κ. If they are neglected, we have $\kappa = 1$. The rescattering effects – it cannot be excluded that they may lead to values of ρ as large as $\mathcal{O}(0.1)$ – can be controlled in the contours in the γ–r plane and can be included in the constraints on γ related to (5.14) through experimental data on $B^\pm \to K^\pm K$ decays, which are the U-spin counterparts of $B^\pm \to \pi^\pm K$ [114, 115]. Another important indicator for large rescattering effects are the $B_d \to K^+K^-$ modes, for which there already exist strong experimental constraints [130].

An improved description of the EW penguins is possible if we use the general expressions for the corresponding four-quark operators and perform appropriate Fierz transformations [114, 120, 129]. Following these lines, we obtain

$$q_{\rm C}\, e^{i\omega_{\rm C}} \equiv \frac{\epsilon_{\rm C}}{r}\, e^{i(\Delta_{\rm C} - \delta)} = 0.66 \times \left[\frac{0.41}{R_b}\right] \times a_{\rm C}\, e^{i\omega_{\rm C}}, \tag{5.16}$$

where $a_{\rm C}\, e^{i\omega_{\rm C}} = a_2^{\rm eff}/a_1^{\rm eff}$ is the ratio of certain generalized "colour factors". Experimental data on $B \to D^{(*)}\pi$ decays imply $a_2/a_1 = \mathcal{O}(0.25)$. A first step to fix the hadronic parameter $a_{\rm C}\, e^{i\omega_{\rm C}}$ experimentally is provided by the mode $B^+ \to \pi^+\pi^0$ [114]; interesting constraints were derived in [69]. For a detailed discussion of the impact of rescattering and EW penguin effects on the strategies to probe γ with $B^\pm \to \pi^\pm K$ and $B_d \to \pi^\mp K^\pm$ decays, the reader is referred to [114, 115, 68, 131]. In order to control these hadronic uncertainties – in addition to the full experimental picture of all $B \to \pi K$, $K\overline{K}$ decays – also the theoretical approach for dealing with non-leptonic B decays into two light mesons developed recently in Ref. [76] may play an important rôle.

5.1.2 The Charged $B^\pm \to \pi^\pm K$, $B^\pm \to \pi^0 K^\pm$ Strategy

Several years ago, Gronau, Rosner and London proposed an SU(3) strategy to determine γ from the charged decays $B^\pm \to \pi^\pm K$, $\pi^0 K^\pm$, $\pi^0\pi^\pm$ [31]. However, as was pointed out by Deshpande and He [132], this elegant approach is unfortunately spoiled by EW penguins [133], which play an important rôle in several non-leptonic B meson decays because of the large top-quark mass [15, 16]. Recently, this approach was resurrected by Neubert and Rosner [119, 122], who pointed out that in this case the EW penguin contributions can be controlled by using only the general expressions for the corresponding four-quark operators, appropriate Fierz transformations, and the SU(3) flavour-symmetry of strong interactions (see also [120]).

In the case of $B^+ \to \pi^+ K^0$, $\pi^0 K^+$, SU(2) isospin symmetry implies

$$A(B^+ \to \pi^+ K^0) \,+\, \sqrt{2}\, A(B^+ \to \pi^0 K^+) = -\,[(T + C) \,+\, P_{\rm ew}]\,. \tag{5.17}$$

The phase structure of this relation is completely analogous to $B^+ \to \pi^+ K^0$, $B_d^0 \to \pi^- K^+$, as can be seen by comparing with (5.1) and (5.2):

$$T + C = |T + C|\, e^{i\delta_{T+C}}\, e^{i\gamma}, \quad P_{\rm ew} = -\,|P_{\rm ew}| e^{i\delta_{\rm ew}}\,. \tag{5.18}$$

In order to probe γ, it is useful to introduce the following observables [68]:

$$R_{\rm c} \equiv 2\left[\frac{B(B^+ \to \pi^0 K^+) + B(B^- \to \pi^0 K^-)}{B(B^+ \to \pi^+ K^0) + B(B^- \to \pi^- \overline{K^0})}\right], \tag{5.19}$$

$$A_0^{\rm c} \equiv 2\left[\frac{B(B^+ \to \pi^0 K^+) - B(B^- \to \pi^0 K^-)}{B(B^+ \to \pi^+ K^0) + B(B^- \to \pi^- \overline{K^0})}\right], \tag{5.20}$$

which correspond to R and A_0; general expressions can be obtained from those for R and A_0 by the following replacements:

$$r \to r_{\rm c} \equiv \frac{|T + C|}{\sqrt{\langle |P|^2\rangle}}, \quad \delta \to \delta_{\rm c} \equiv \delta_{T+C} - \delta_{tc}\,, \quad P_{\rm ew}^{\rm C} \to P_{\rm ew}. \tag{5.21}$$

Using the presently available experimental results from the CLEO collaboration [117], one finds

$$R_{\rm c} = 1.3 \pm 0.5, \quad A_0^{\rm c} = 0.35 \pm 0.34. \tag{5.22}$$

The observables $R_{\rm c}$ and $A_0^{\rm c}$ allow one to fix contours in the γ–r_c plane, in complete analogy to the $B^\pm \to \pi^\pm K$, $B_d \to \pi^\mp K^\pm$ strategy. However, the charged $B \to \pi K$ approach has certain advantages from a theoretical point of view:

- SU(3) flavour-symmetry allows one to fix the parameter $r_c \propto |T + C|$ as follows [31]:

$$T + C \approx -\,\sqrt{2}\,\frac{V_{us}}{V_{ud}}\,\frac{f_K}{f_\pi}\, A(B^+ \to \pi^+\pi^0)\,, \tag{5.23}$$

  where r_c thus determined is – in contrast to r – not affected by rescattering effects; present data give $r_c = 0.21 \pm 0.06$. The factor f_K/f_π takes into account factorizable SU(3) breaking.

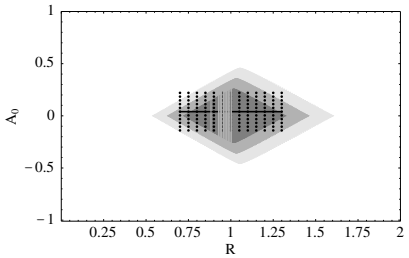

Fig. 38: Allowed region in the R–A_0 plane, characterizing $B^\pm \to \pi^\pm K$, $B_d \to \pi^\mp K^\pm$ in the SM. $0.13 \leq r \leq 0.23$, $q_{\rm C} = 0.17$. FSIs are neglected.

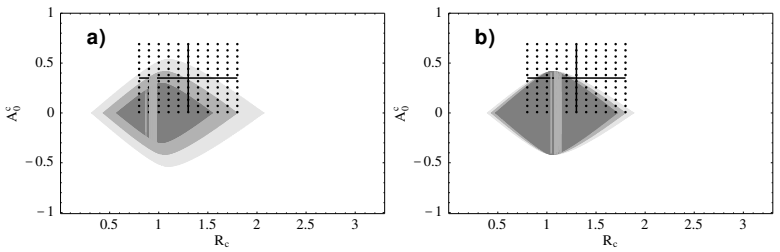

(a) $0.15 \leq r_{\rm c} \leq 0.27$, $q = 0.63$. (b) $r_{\rm c} = 0.21$, $0.48 \leq q \leq 0.78$.

Fig. 39: Allowed region in the $R_{\rm c}$–$A_0^{\rm c}$ plane, characterizing $B^\pm \to \pi^\pm K$, $\pi^0 K^\pm$ in the SM. FSIs are neglected.

- In the strict SU(3) limit, we have [119]

$$q\, e^{i\omega} \equiv \left|\frac{P_{\rm ew}}{T+C}\right| e^{i(\delta_{\rm ew}-\delta_{T+C})} = 0.66 \times \left[\frac{0.41}{R_b}\right], \tag{5.24}$$

  which does – in contrast to (5.16) – not involve a hadronic parameter. Taking into account factorizable SU(3) breaking and using present data gives $q = 0.63 \pm 0.15$.

The contours in the γ–r_c plane may be affected – in analogy to the $B^\pm \to \pi^\pm K$, $B_d \to \pi^\mp K^\pm$ case – by rescattering effects [68]. They can be taken into account with the help of additional experimental data [114, 115, 134], and if we use the observable

$$B_0^{\rm c} \equiv A_0^{\rm c} - \left[\frac{B(B^+ \to \pi^+ K^0) - B(B^- \to \pi^- \overline{K^0})}{B(B^+ \to \pi^+ K^0) + B(B^- \to \pi^- \overline{K^0})}\right] \tag{5.25}$$

instead of $A_0^{\rm c}$, the terms of $\mathcal{O}(\rho)$, which describe the rescattering effects, are suppressed by $r_{\rm c}$ [131]. The major theoretical advantage of the $B^+ \to \pi^+ K^0$, $\pi^0 K^+$ strategy with respect to $B^\pm \to \pi^\pm K$, $B_d \to \pi^\mp K^\pm$ is that r_c and $P_{\rm ew}/(T+C)$ can be fixed by using *only* SU(3) arguments, i.e. no additional dynamical arguments have to be employed. Consequently, the theoretical accuracy is mainly limited by non-factorizable SU(3) breaking effects. The approach developed recently in [76] may help to reduce these uncertainties.

Let us finally note that the observable $R_{\rm c}$ may also imply interesting constraints on γ [119]. These bounds, which are conceptually quite similar to [118], are related to the extremal values of $R_{\rm c}$ that arise if we keep only the strong phase $\delta_{\rm c}$ as an "unknown" free parameter. As the resulting general expression is rather complicated [68, 131], let us expand it in r_c [119]. If we keep only the leading-order terms and make use of the SU(3) relation (5.24), we obtain

$$R_c^{\rm ext}\Big|_{\delta_{\rm c}}^{\rm LO} = 1 \,\pm\, 2\, r_c\, |\cos\gamma - q|. \tag{5.26}$$

Interestingly, there are no terms of $\mathcal{O}(\rho)$ present in this expression, i.e. rescattering effects do not enter at this level [119, 122]. However, FSI processes may still have a sizeable impact on the associated bounds on γ. Several strategies to control these uncertainties were considered in the recent literature [68, 131, 134], and also the approach of Ref. [76] may shed light on these issues.

Unfortunately, the neutral pions appearing in $B^\pm \to \pi^0 K^\pm$ rener the charged approach challenging from the experimental point of view. The strategy using the neutral decays $B_d \to \pi^0 K_{\rm S}$ and $B_d \to \pi^\mp K^\pm$ to extract γ, which was proposed in [68], is even worse in this respect, and we will not discuss it here in more detail, although it would have an interesting theoretical advantage concerning the impact of rescattering effects.

5.1.3 Some Remarks about New Physics

Since B_q^0–$\overline{B_q^0}$ mixing ($q \in \{d, s\}$) is a "rare" flavour-changing neutral-current (FCNC) process, it is very likely that it is significantly affected by new physics, which may act upon the mixing parameters ΔM_q and $\Delta\Gamma_q$ as well as on the CP-violating mixing phase ϕ_q. Important examples for such scenarios of new physics are non-minimal SUSY models, left–right-symmetric models, models with extended Higgs sectors, four generations, or Z-mediated FCNCs [10]. Since $B_d \to J/\psi\, K_{\rm S}$ and $B_s \to J/\psi\, \phi$ – the benchmark modes to measure ϕ_d and ϕ_s – are governed by current–current, i.e. "tree", processes, new physics is expected to affect their *decay amplitudes* only in a minor way. Consequently, these modes still measure ϕ_d and ϕ_s.

In the clean strategies to measure γ with the help of pure "tree" decays, such as $B \to DK$, $B_d \to D^{(*)\pm}\pi^{\mp}$ or $B_s \to D_s^{\pm}K^{\mp}$, new physics is also expected to play a very minor rôle. These strategies therefore provide a "reference" value for γ. Since, on the other hand, the $B \to \pi K$ strategies to determine γ rely on the interference between tree and penguin contributions, discrepancies with the "reference" value for γ may well show up in the presence of new physics [135, 136]. If we are lucky, we may even get immediate indications for new physics from $B \to \pi K$ decays [137], as the SM predicts interesting correlations between the corresponding observables as shown in Figs. 38 and 39. Here the dotted regions correspond to the CLEO results that were reported in 1999 [117].

If future measurements should yields results significantly outside the allowed regions shown in these figures, we would have an indication for new physics. On the other hand, if we should find values lying inside these regions, this would not automatically imply a confirmation of the SM. In this case, we would be in a position to extract a value for γ by following the strategies described above, which may well lead to discrepancies with the "reference" values for γ that are implied by the theoretically clean "tree" strategies, or with the usual fits of the unitarity triangle. In a recent paper [136], several specific models were employed to explore the impact of new physics on $B \to \pi K$ decays. For example, in models with an extra Z' boson or in SUSY models with broken R-parity, the resulting electroweak penguin coefficients can be much larger than in the SM, since they arise already at tree level.

Interestingly, the present experimental range coincides perfectly with the SM region in Fig. 38. This feature should be compared with the situation in Fig. 39. Unfortunately, the present experimental uncertainties are too large to speculate on new-physics effects. However, the experimental situation should improve considerably in the years before the start of the LHC. The strategies discussed in the following subsections are also well suited to search for new physics.

5.1.4 Experimental Studies

Preliminary studies for the determination of γ using the Kπ decay modes of B mesons have been performed for the LHCb experiment. As explained above, γ may be determined using a number of strategies that involve the final states $\mathrm{K}^+\pi^-$, $\mathrm{K}^0\pi^+$, $\mathrm{K}^+\pi^0$ and $\mathrm{K}^0\pi^0$. Experimentally it is easiest to reconstruct final states which contain charged particles and have reconstructible decay vertices. Clearly, therefore, the strategy involving $\mathrm{K}^+\pi^-$ and $\mathrm{K}^0\pi^+$ final states provides the cleanest experimental channel and has been studied first. Future work will involve a study of the feasibility of reconstructing the $\mathrm{K}^+\pi^0$ mode. A clean reconstruction of the $\mathrm{K}^0\pi^0$ mode is unlikely to be possible at LHCb.

The experimental values to be determined are the ratios R and A_0 given in (5.7) and (5.8) with differing final states in numerator and denominator. This means that the ratio of trigger and reconstruction efficiencies must be known for these final states. This is in contrast to most CP violation measurements where these quantities cancel and will be an additional source of systematic error which has yet to be investigated.

The principal features of the Kπ decays used for reconstruction are well separated vertices and large impact parameters. The particle identification provided by the RICH detectors is vital for the $\mathrm{K}^+\pi^-$ mode and very helpful for the $\mathrm{K}^0\pi^+$ mode. The overall trigger efficiencies for the two channels

are around 30% each, relative to events decaying in the acceptance. The net trigger and reconstruction efficiency is about 0.02 for the $K^+\pi^-$ channel and 0.01 for $K^0\pi^+$. The difference is mainly due to the detector acceptance. With the latest CLEO branching ratio measurements of $(18.2 \pm 5) \times 10^{-6}$ for $K^0\pi^+$ and $(18.8 \pm 3) \times 10^{-6}$ for $K^+\pi^-$ [73], these efficiencies result in about 90,000 events in the $K^0\pi^+$ and 175,000 events in the $K^+\pi^-$ channel per year. These numbers are rather preliminary since the background studies are still in an early stage, and it may prove necessary to tighten the reconstruction-cuts.

Translating these numbers into final CP sensitivities is however not trivial. The measured values of the ratios R and A_0 define contours in the r–γ plane such as those in Fig. 35. A value for γ can only be extracted once r is known whose value must be determined from theory. Experimental results indicating large rescattering effects which would imply large errors in r are, for example, large CP violation in the $B^+ \to K^0\pi^+$ channel or branching ratios for $B^+ \to K^+K^0$ and $B^0 \to K^+K^-$, which are larger than expected. The precise value of r will have a large effect on the expected errors. There is also a four-fold ambiguity for the value of γ. Figure 40 illustrates the errors that might be expected assuming a value for r of $0.18 \pm 10\%$, for two of the possible solutions. For one of these solutions the error is $\sim 2^\circ$, whereas for the other it is $\sim 7^\circ$. These uncertainties are mirrored in the remaining two solutions.

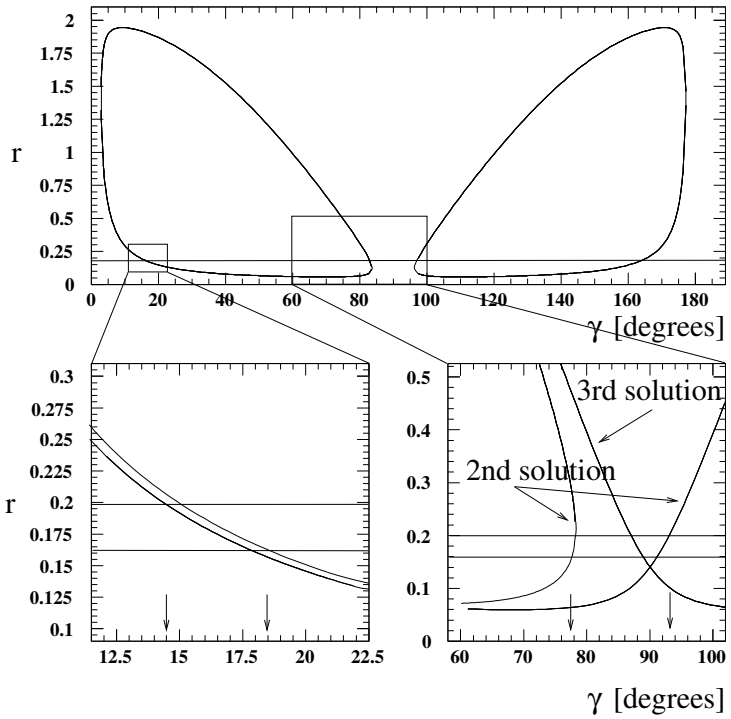

Fig. 40: An experimental study of the contours in the γ–r plane (see also Fig. 35): the top plot corresponds to $R = 1.0$, $A_0 = 0.1$ and $r = 0.18$; in the blow-up plots, the bands indicate the spread of the central contour from correlated errors on R and A_0 of 3%, and $\pm 10\%$ on r; arrows indicate the allowed range for γ. The error on γ from the first solution is $\pm 2^\circ$; the second solution yields $77^\circ < \gamma < 93^\circ$. Note that for our specific choice of input parameters the allowed band for the second solution partially overlaps with that of the third one, starting at 88°.

In summary, from this preliminary study, it is expected that LHCb will be able to provide determinations of the ratios A_0 and R for the strategy involving $K^0\pi^+$ and $K^+\pi^-$ final states with errors around 3%. As explained above this cannot simply be translated into a CP sensitivity. Work on these promising decays is still underway and will be extended to include a study of the $K^+\pi^0$ channel.

5.2 Extracting γ from $B_{s(d)} \to J/\psi\, K_{\rm S}$ Decays[15]

As we have already discussed in Sec. 3.1, the "gold-plated" mode $B_d \to J/\psi\, K_{\rm S}$ plays an outstanding rôle in the determination of the B^0_d–$\overline{B^0_d}$ mixing phase ϕ_d, i.e. of the CKM angle β. In this subsection, we will have a closer look at the decay $B_s \to J/\psi\, K_{\rm S}$ [61] (see also [111]), which is related to $B_d \to J/\psi\, K_{\rm S}$ by interchanging all down and strange quarks (see Fig. 9), and may allow an interesting extraction of the CKM angle γ.

5.2.1 Theoretical Aspects

In analogy to (3.2), the $B_s \to J/\psi\, K_{\rm S}$ decay amplitude can be expressed as follows:

$$A(B^0_s \to J/\psi\, K_{\rm S}) = -\lambda\, \mathcal{A}\left[1 - a\, e^{i\theta} e^{i\gamma}\right], \tag{5.27}$$

where

$$\mathcal{A} \equiv \lambda^2 A \left(A^c_{\rm cc} + A^{ct}_{\rm pen}\right) \text{ and } a\, e^{i\theta} \equiv R_b \left(\frac{A^{ut}_{\rm pen}}{A^c_{\rm cc} + A^{ct}_{\rm pen}}\right) \tag{5.28}$$

correspond to (3.3). It should be emphasized that (3.2) and (5.27) rely only on the unitarity of the CKM matrix. In particular, these SM parametrizations of the $B^0_{d(s)} \to J/\psi\, K_{\rm S}$ decay amplitudes also take into account FSI effects, which can be considered as long-distance penguin topologies with internal up- and charm-quark exchanges [113].

Comparing (3.2) with (5.27), we observe that the "penguin parameter" $a' e^{i\theta'}$ is doubly Cabibbo-suppressed in the $B^0_d \to J/\psi\, K_{\rm S}$ decay amplitude (3.2), whereas $a\, e^{i\theta}$ enters (5.27) in a Cabibbo-allowed way. Consequently, there may be sizeable CP-violating effects in $B_s \to J/\psi\, K_{\rm S}$, which provide *two* independent observables, $\mathcal{A}^{\rm dir}_{\rm CP}(B_s \to J/\psi\, K_{\rm S})$ and $\mathcal{A}^{\rm mix}_{\rm CP}(B_s \to J/\psi\, K_{\rm S})$, depending on the *three* "unknowns" a, θ and γ, as well as on the B^0_s–$\overline{B^0_s}$ mixing phase ϕ_s. Consequently, in order to determine these "unknowns", we need an additional observable, which is provided by

$$H \equiv \left(\frac{1-\lambda^2}{\lambda^2}\right)\left(\frac{|\mathcal{A}'|}{|\mathcal{A}|}\right)^2 \frac{\langle\Gamma(B_s \to J/\psi\, K_{\rm S})\rangle}{\langle\Gamma(B_d \to J/\psi\, K_{\rm S})\rangle}, \tag{5.29}$$

where the CP-averaged decay rates $\langle\Gamma(B_s \to J/\psi\, K_{\rm S})\rangle$ and $\langle\Gamma(B_d \to J/\psi\, K_{\rm S})\rangle$ can be determined from the "untagged" rates introduced in (1.32) through

$$\langle\Gamma(B_q \to f)\rangle \equiv \frac{\Gamma_q[f(0)]}{2}. \tag{5.30}$$

In (5.29), we have neglected tiny phase-space effects, which can be included straightforwardly [61].

Since the U-spin flavour-symmetry of strong interactions implies

$$|\mathcal{A}'| = |\mathcal{A}| \text{ and } a' = a, \quad \theta' = \theta, \tag{5.31}$$

we can determine a, θ and γ as a function of the B^0_s–$\overline{B^0_s}$ mixing phase ϕ_s by combining H with $\mathcal{A}^{\rm dir}_{\rm CP}(B_s \to J/\psi\, K_{\rm S})$ and $\mathcal{A}^{\rm mix}_{\rm CP}(B_s \to J/\psi\, K_{\rm S})$ or $\mathcal{A}_{\Delta\Gamma}(B_s \to J/\psi\, K_{\rm S})$. In contrast to certain isospin relations, electroweak penguins do not lead to any problems in these U-spin relations. As we have already noted, the B^0_s–$\overline{B^0_s}$ mixing phase $\phi_s = -2\delta\gamma$ is expected to be negligible in the SM. It can be probed with the help of $B_s \to J/\psi\, \phi$, Sec. 4. Strictly speaking, in the case of $B_s \to J/\psi\, K_{\rm S}$, we have $\phi_s \to -2\delta\gamma - \phi_K$, where ϕ_K is related to the K^0–$\overline{K^0}$ mixing phase and is negligible in the SM (see also the comment in Sec. 3.1). Since the value of the CP-violating parameter ε_K of the neutral kaon system is very small, ϕ_K can only be affected by very contrived models of new physics [62].

[15] With help from P. Colrain.

Interestingly, the strategy to extract γ from $B_{s(d)} \to J/\psi\, K_{\rm S}$ does not require a non-trivial CP-conserving strong phase θ. However, its experimental feasibility depends strongly on the value of the quantity a introduced in (5.28). It is very difficult to estimate a theoretically. In contrast to the "usual" QCD penguin topologies, the QCD penguins contributing to $B_{s(d)} \to J/\psi\, K_{\rm S}$ require a colour-singlet exchange, as indicated in Fig. 9 through the dashed lines, and are "Zweig-suppressed". Such a comment does not apply to the electroweak penguins, which contribute in "colour-allowed" form. The current–current amplitude $A_{\rm cc}^{c}$ is due to "colour-suppressed" topologies, and the ratio $A_{\rm pen}^{ut}/(A_{\rm cc}^{c} + A_{\rm pen}^{ct})$, which governs a, may be sizeable. It is interesting to note that the measured branching ratio $B(B_d^0 \to J/\psi\, K^0) = 2\, B(B_d^0 \to J/\psi\, K_{\rm S}) = (8.9 \pm 1.2) \times 10^{-4}$ [64] probes only the combination $\mathcal{A}' \propto \left(A_{\rm cc}^{c'} + A_{\rm pen}^{ct'}\right)$ of current–current and penguin amplitudes, and obviously does not allow their separation. It would be very important to have a better theoretical understanding of the quantity $a\, e^{i\theta}$. However, such analyses are beyond the scope of this workshop, and are left for further studies. Let us note that the measured $B_d^0 \to J/\psi\, K_{\rm S}$ branching ratio implies, if we use U-spin arguments, a $B_s \to J/\psi\, K_{\rm S}$ branching ratio at the level of 2×10^{-5}.

The general formalism to extract γ from $B_{s(d)} \to J/\psi\, K_{\rm S}$ decays can be found in [61]. Although the corresponding formulae are quite complicated, the basic idea is very simple: if ϕ_s is used as input, the CP-violating asymmetries $\mathcal{A}_{\rm CP}^{\rm dir}(B_s \to J/\psi\, K_{\rm S})$ and $\mathcal{A}_{\rm CP}^{\rm mix}(B_s \to J/\psi\, K_{\rm S})$ allow one to fix a contour in the γ–a plane in a *theoretically clean* way. Another contour can be fixed with the help of the U-spin relations (5.31) by combining the observable H with $\mathcal{A}_{\rm CP}^{\rm mix}(B_s \to J/\psi\, K_{\rm S})$. Alternatively, we may combine H with $\mathcal{A}_{\Delta\Gamma}(B_s \to J/\psi\, K_{\rm S})$ to fix a third contour in the γ–a plane. The intersection of these contours then gives γ and a. The general formulae simplify considerably, if we keep only terms linear in a. Within this approximation, we obtain

$$\tan\gamma \approx \frac{\sin\phi_s + \mathcal{A}_{\rm CP}^{\rm mix}(B_s \to J/\psi\, K_{\rm S})}{(1-H)\cos\phi_s}\,. \tag{5.32}$$

Let us illustrate this approach by considering a simple example. Assuming a negligible B_s^0–$\overline{B_s^0}$ mixing phase, i.e. $\phi_s = 0$, and $\gamma = 76^\circ$, which lies within the presently allowed "indirect" range for this angle, as well as $a = a' = 0.2$ and $\theta = \theta' = 30^\circ$, we obtain the following $B_{s(d)} \to J/\psi\, K_{\rm S}$ observables:

$$\begin{aligned} &\mathcal{A}_{\rm CP}^{\rm dir}(B_s \to J/\psi\, K_{\rm S}) = 0.20,\ \mathcal{A}_{\rm CP}^{\rm mix}(B_s \to J/\psi\, K_{\rm S}) = 0.33,\\ &\mathcal{A}_{\Delta\Gamma}(B_s \to J/\psi\, K_{\rm S}) = 0.92,\ H = 0.95. \end{aligned} \tag{5.33}$$

The corresponding contours in the γ–a plane are shown in Fig. 41. Interestingly, in the case of these contours, we would not have to deal with "physical" discrete ambiguities for γ, since values of a larger than 1 would simply appear unrealistic. If it should become possible to measure $\mathcal{A}_{\Delta\Gamma}$ with the help of the widths difference $\Delta\Gamma_s$, the dotted line could be fixed. In this example, the approximate expression (5.32) yields $\gamma \approx 82^\circ$, which deviates from the "true" value of $\gamma = 76^\circ$ by only 8%. It is also interesting to note that we have $\mathcal{A}_{\rm CP}^{\rm dir}(B_d \to J/\psi\, K_{\rm S}) = -0.98\%$ in our example.

An important by-product of the strategy described above is that the quantities a' and θ' allow one to take into account the penguin contributions in the determination of ϕ_d from $B_d \to J/\psi\, K_{\rm S}$, which are presumably very small because of the strong Cabibbo suppression in (3.2). However, as we have already noted in Sec. 3.1, these uncertainties are an important issue for the LHC because of the tremendously small experimental uncertainty for the CP-violating $B_d \to J/\psi\, K_{\rm S}$ observables. Using (5.31), we obtain an interesting relation between the direct CP asymmetries arising in the modes $B_d \to J/\psi\, K_{\rm S}$ and $B_s \to J/\psi\, K_{\rm S}$ and their CP-averaged rates:

$$\frac{\mathcal{A}_{\rm CP}^{\rm dir}(B_d \to J/\psi\, K_{\rm S})}{\mathcal{A}_{\rm CP}^{\rm dir}(B_s \to J/\psi\, K_{\rm S})} \approx -\frac{B(B_s \to J/\psi\, K_{\rm S})}{B(B_d \to J/\psi\, K_{\rm S})}\,. \tag{5.34}$$

Let us note that an analogous relation holds also between the CP-violating asymmetries in the decays $B^\pm \to \pi^\pm K$ and $B^\pm \to K^\pm K$ [113, 114].

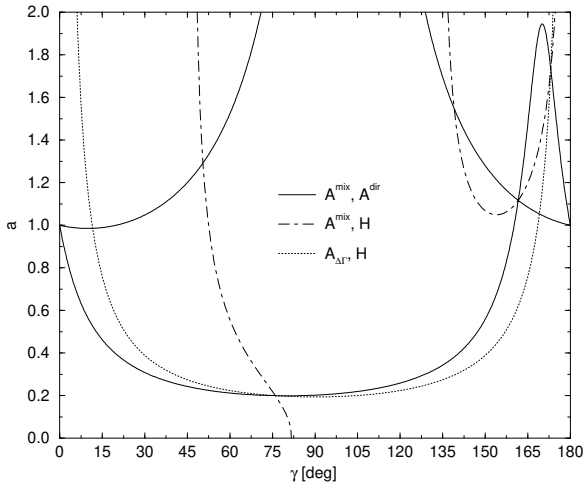

Fig. 41: Contours in the γ–a plane fixed through the $B_{s(d)} \to J/\psi\, K_{\rm S}$ observables for an example discussed in the text.

Before turning to the experimental feasibility studies, let us say a few words on the SU(3) breaking corrections. Whereas the solid curves in Fig. 41 are *theoretically clean*, the dot-dashed and dotted lines are affected by U-spin breaking corrections. Because of the suppression of $a' e^{i\theta'}$ in (3.2) through λ^2, these contours are essentially unaffected by possible corrections to (5.31), and rely predominantly on the U-spin relation $|\mathcal{A}'| = |\mathcal{A}|$. In the "factorization" approximation, we have

$$\left.\frac{|\mathcal{A}'|}{|\mathcal{A}|}\right|_{\rm fact} = \frac{F_{B_d^0 K^0}(M^2_{J/\psi}; 1^-)}{F_{B_s^0 \overline{K^0}}(M^2_{J/\psi}; 1^-)}\,, \tag{5.35}$$

where the form factors $F_{B_d^0 K^0}(M^2_{J/\psi}; 1^-)$ and $F_{B_s^0 \overline{K^0}}(M^2_{J/\psi}; 1^-)$ parametrize the quark–current matrix elements $\langle K^0|(\bar{b}s)_{\rm V-A}|B_d^0\rangle$ and $\langle \overline{K^0}|(\bar{b}d)_{\rm V-A}|B_s^0\rangle$, respectively [106]. We are not aware of quantitative studies of (5.35), which could be performed, for instance, with the help of sum rule or lattice techniques. In the light-cone sum-rule approach, sizeable SU(3) breaking effects were found for $B_{d,s} \to K^*$ form factors [35]. It should be emphasized that also non-factorizable corrections, which are not included in (5.35), may play an important rôle. We are optimistic that SU(3) breaking will be under better control by the time the $B_s \to J/\psi\, K_{\rm S}$ measurements can be performed in practice.

5.2.2 Experimental Studies

Both CMS and LHCb have performed preliminary studies of the feasibility to extract the CKM angle γ from a measurement of the time-dependent CP asymmetry in the decay $B_s \to J/\psi\, K_S$. From these, and the results presented in Sec. 3.1, the potential of ATLAS may also be gauged.

The $B_s \to J/\psi\, K_S$ branching ratio is expected to be at the level of 2.0×10^{-5}, see Sec. 5.2.1, compared to $(4.45 \pm 0.6) \times 10^{-4}$ [64] for $B_d \to J/\psi\, K_S$. The B_s production rate is 30% of the B_d^0 rate. Assuming the same selection procedure as used in the $B_d \to J/\psi\, K_S$ analysis, the $B_s \to J/\psi\, K_S$ event yield will therefore be 1/74 that of the B_d^0 yield. Experimentally the isolation of these events is challenging, due to the large combinatorial background and the close B_d^0 peak, only 90 $\mathrm{MeV/c^2}$ away.

CMS have developed a selection tailored to $B_s \to J/\psi\, K_S$ decays. The combinatorial background can be heavily suppressed with a lower p_T-cut of 1.5 $\mathrm{GeV/c}$ on the pions from the $\mathrm{K_S^0}$ decays, A S/B ratio of $\approx$ 0.5 can be achieved, with an event yield of 4100 events per year. The mass resolution is better than $< 20\,\mathrm{MeV/c^2}$ and thus sufficient to separate the events from B_d^0 decays. The reconstructed mass peaks can be seen in Fig. 42(a).

LHCb have not yet investigated cuts specific to $B_s \to J/\psi\, K_S$. As can be seen from Fig. 42(b), the standard $B_d \to J/\psi\, K_S$ selection results in a combinatorial background which is an order of mag-

nitude above the $B_s \to J/\psi\, K_S$ signal. Further work will improve the selection to suppress this contamination. The invariant mass resolution is better than $10\,\mathrm{MeV/c^2}$, so that the $\mathrm{B_d^0}$ and $\mathrm{B_s^0}$ peaks are cleanly separated.

These studies indicate that a measurement of the CP asymmetry in $B_s \to J/\psi\, K_S$ is feasible at the LHC, so that γ can be extracted from that decay. For the parameter-set considered in Sec. 5.2.1, CMS estimate that a precision of $\sim 9^\circ$ is achievable in 3 years operation.

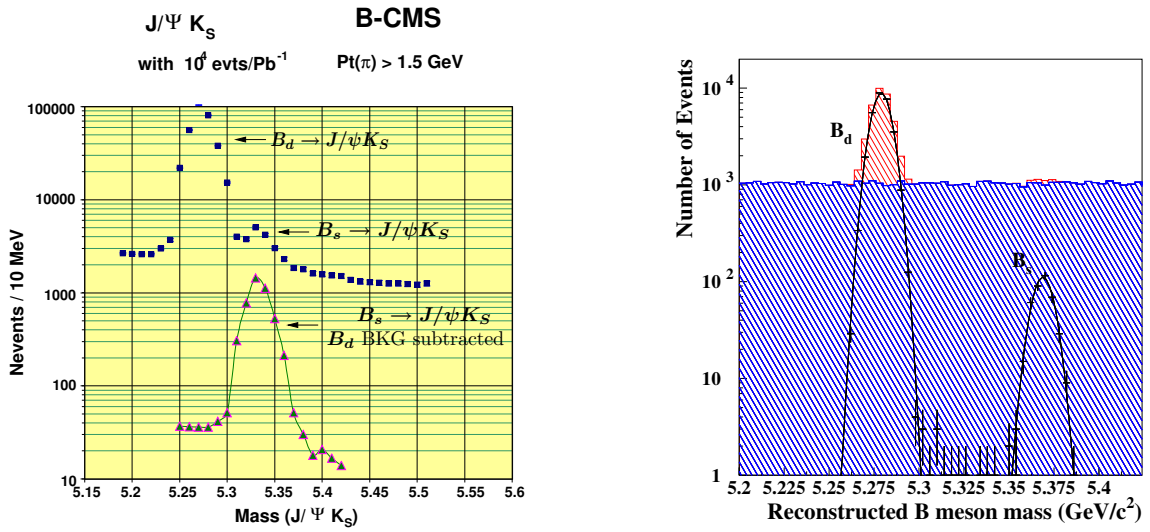

(a) CMS (b) LHCb

Fig. 42: $B_d \to J/\psi(\to \mu^+\mu^-)\, K_S$ and $B_s \to J/\psi(\to \mu^+\mu^-)\, K_S$ mass peaks.

5.3 Extracting γ from $B_{d(s)} \to D^+_{d(s)} D^-_{d(s)}$ Decays [16]

Usually, $B_d \to D_d^+ D_d^-$ decays appear in the literature as a tool to probe the B_d^0–$\overline{B_d^0}$ mixing phase ϕ_d [4, 5, 6]. In fact, if penguins played a negligible rôle in these modes, $\phi_d = 2\beta$ could be determined from the corresponding mixing-induced CP-violating effects. However, penguin topologies, which contain also important contributions from FSI effects, may well be sizeable, although it is very difficult to calculate them in a reliable way. The strategy discussed in this subsection makes use of the penguin topologies [61], allowing one to determine γ, if the overall $B_d \to D_d^+ D_d^-$ normalization is fixed through the CP-averaged, i.e. "untagged" $B_s \to D_s^+ D_s^-$ rate, and if the B_d^0–$\overline{B_d^0}$ mixing phase ϕ_d is determined separately, for instance with the help of the "gold-plated" decay $B_d \to J/\psi\, K_S$. It should be emphasized that no $\Delta M_s t$ oscillations have to be resolved to measure the untagged $B_s \to D_s^+ D_s^-$ rate.

5.3.1 Theoretical Aspects

The decays $B^0_{d(s)} \to D^+_{d(s)}\, D^-_{d(s)}$ are transitions into a CP eigenstate with eigenvalue $+1$ and originate from $\bar{b} \to \bar{c}\, c\, \bar{d}\,(\bar{s})$ quark-level decays. We have to deal with both current–current and penguin contributions, as can be seen in Fig. 43. In analogy to (3.2) and (5.27), the corresponding transition amplitudes can be written as follows:

$$A(B_s^0 \to D_s^+ D_s^-) = \left(1 - \frac{\lambda^2}{2}\right) \tilde{\mathcal{A}}' \left[1 + \left(\frac{\lambda^2}{1-\lambda^2}\right) \tilde{a}' e^{i\tilde{\theta}'} e^{i\gamma}\right], \tag{5.36}$$

$$A(B_d^0 \to D_d^+ D_d^-) = -\lambda\, \tilde{\mathcal{A}} \left[1 - \tilde{a}\, e^{i\tilde{\theta}} e^{i\gamma}\right], \tag{5.37}$$

[16] With help from V. Gibson.

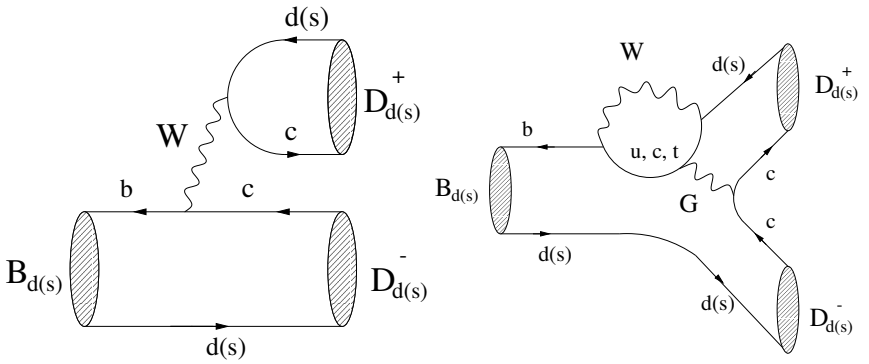

Fig. 43: Feynman diagrams contributing to $B^0_{d(s)} \to D^+_{d(s)}\, D^-_{d(s)}$.

where the quantities $\tilde{\mathcal{A}}$, $\tilde{\mathcal{A}}'$ and $\tilde{a}\, e^{i\tilde{\theta}}$, $\tilde{a}'\, e^{i\tilde{\theta}'}$ take the same form as for $B_{s(d)} \to J/\psi\, K_{\rm S}$. In contrast to the decays $B_{s(d)} \to J/\psi\, K_{\rm S}$, there are "colour-allowed" current–current contributions to $B_{d(s)} \to D^+_{d(s)}\, D^-_{d(s)}$, as well as contributions from "exchange" topologies, and the QCD penguins do not require a colour-singlet exchange, i.e. they are not "Zweig-suppressed".

Since the phase structures of the $B^0_d \to D^+_d D^-_d$ and $B^0_s \to D^+_s D^-_s$ decay amplitudes are completely analogous to those of $B^0_s \to J/\psi\, K_{\rm S}$ and $B^0_d \to J/\psi\, K_{\rm S}$, respectively, the approach discussed in the previous subsection can be applied after a straightforward replacements of variables. Neglecting tiny phase-space effects, which can be taken into account straightforwardly (see [61]), we have

$$\tilde{H} = \left(\frac{1-\lambda^2}{\lambda^2}\right)\left(\frac{|\tilde{\mathcal{A}}'|}{|\tilde{\mathcal{A}}|}\right)^2 \frac{\langle\Gamma(B_d \to D^+_d D^-_d)\rangle}{\langle\Gamma(B_s \to D^+_s D^-_s)\rangle}\,, \tag{5.38}$$

where the CP-averaged rates can be determined with the help of (5.30). The $B_{d(s)} \to D^+_{d(s)} D^-_{d(s)}$ counterpart to (5.32) takes the following form:

$$\tan\gamma \approx \frac{\sin\phi_d - \mathcal{A}^{\rm mix}_{\rm CP}(B_d \to D^+_d D^-_d)}{(1-\tilde{H})\cos\phi_d}\,, \tag{5.39}$$

where the different sign of the mixing-induced CP asymmetry results from the different CP eigenvalues of the $B_d \to D^+_d D^-_d$ and $B_s \to J/\psi\, K_{\rm S}$ final states.

Let us illustrate the strategy to determine γ, again by considering a simple example. Assuming $\tilde{a} = \tilde{a}' = 0.1$, $\tilde{\theta} = \tilde{\theta}' = 210^\circ$, $\gamma = 76^\circ$ and a B^0_d–$\overline{B^0_d}$ mixing phase of $\phi_d = 2\beta = 53^\circ$, we obtain the following observables:

$$\mathcal{A}^{\rm dir}_{\rm CP}(B_d \to D^+_d D^-_d) = -0.092, \quad \mathcal{A}^{\rm mix}_{\rm CP}(B_d \to D^+_d D^-_d) = 0.88 \quad \text{and} \quad \tilde{H} = 1.05. \tag{5.40}$$

In this case, studies of CP violation in $B_d \to J/\psi\, K_{\rm S}$ would yield $\sin(2\beta) = 0.8$, which is the central value of the most recent CDF analysis [63], implying $2\beta = 53^\circ$ or $2\beta = 180^\circ - 53^\circ = 127^\circ$. This twofold ambiguity can be resolved experimentally, for example, by combining $B_s \to J/\psi\,\phi$ with $B_d \to J/\psi\,\rho^0$ [93] (for alternatives, see [95]), as noted in Sec. 4. In this example, we obtain the contours in the γ–$\tilde{a}$ plane shown in Fig. 44. Since values of $\tilde{a} = \mathcal{O}(1)$ appear unrealistic, we would obtain a single "physical" solution of 76° in this case. The approximate expression (5.39) gives $\gamma \approx 70^\circ$.

As in the $B_{s(d)} \to J/\psi\, K_{\rm S}$ case, only the contours involving the observable $\tilde{H}$, i.e. the dot-dashed lines in Fig. 44, are affected by SU(3) breaking corrections, which are essentially due to the U-spin breaking corrections to $|\tilde{\mathcal{A}}'| = |\tilde{\mathcal{A}}|$. Within the "factorization" approximation, we have

$$\left.\frac{|\tilde{\mathcal{A}}'|}{|\tilde{\mathcal{A}}|}\right|_{\rm fact} \approx \frac{(M_{B_s} - M_{D_s})\,\sqrt{M_{B_s} M_{D_s}}\,(w_s+1)}{(M_{B_d} - M_{D_d})\,\sqrt{M_{B_d} M_{D_d}}\,(w_d+1)}\,\frac{f_{D_s}\,\xi_s(w_s)}{f_{D_d}\,\xi_d(w_d)}\,, \tag{5.41}$$

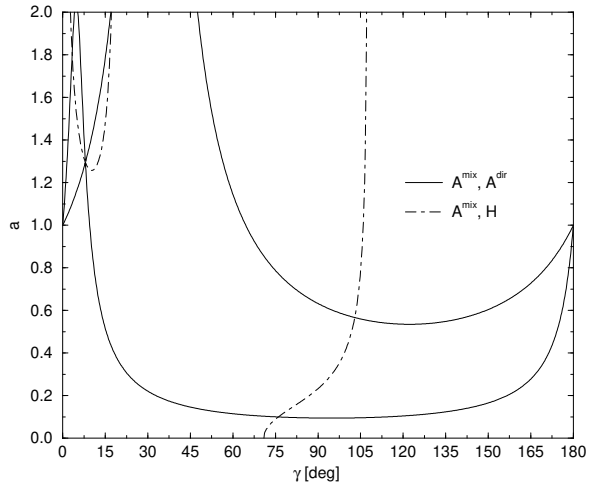

Fig. 44: Contours in the γ–$\tilde{a}$ plane fixed through the $B_{d(s)} \to D^+_{d(s)}\, D^-_{d(s)}$ observables for an example discussed in the text.

where the restrictions from heavy-quark effective theory on the $B_q \to D_q$ form factors have been taken into account by introducing appropriate Isgur–Wise functions $\xi_q(w_q)$ with $w_q = M_{B_q}/(2M_{D_q})$ [138]. Studies of the light-quark dependence of the Isgur–Wise function were performed within heavy-meson chiral perturbation theory, indicating an enhancement of ξ_s/ξ_d at the level of 5% [139]. Applying the same formalism to f_{D_s}/f_D gives values at the 1.2 level [140], which is of the same order of magnitude as the results of recent lattice calculations [141]. Further studies are needed to get a better picture of the SU(3) breaking corrections to the ratio $|\tilde{\mathcal{A}}'|/|\tilde{\mathcal{A}}|$. Since "factorization" may work reasonably well for $B_q \to D_q^+ D_q^-$, the leading corrections are expected to be due to (5.41).

The experimental feasibility of the strategy to extract γ from $B_{d(s)} \to D^+_{d(s)}\, D^-_{d(s)}$ decays depends strongly on the size of the penguin parameter $\tilde{a}$, which is difficult to predict theoretically. The branching ratio for $B^0_d \to D^+_d D^-_d$ is expected to be around 4×10^{-4} level [138]; the one for $B^0_s \to D^+_s D^-_s$ is enhanced by $1/\lambda^2 \approx 20$, and correspondingly is expected at the 8×10^{-3} level.

5.3.2 Experimental Studies

LHCb have conducted a preliminary feasibility study of this analysis, considering the modes where the D decays to $K\pi\pi$ and the D_s to $KK\pi$. For the $B_s \to D_s D_s$ decay, only the total rate is required, which is advantageous experimentally as it is neither necessary to resolve the rapid oscillations, nor does flavour tagging reduce the already suppressed yield in B_s events. The observables $\mathcal{A}^{\rm mix}_{\rm CP}$ and $\mathcal{A}^{\rm dir}_{\rm CP}$ are extracted from a fit to the time-dependent CP asymmetry for $B \to DD$ decays. For this channel it is therefore necessary to obtain the decay-time of the event and to flavour tag the decays. This analysis thus relies on all the fortes of the LHCb detector, namely the specialized trigger, the particle identification capability and the precise vertexing.

The final states for both decays consist of six hadrons, so that the hadron trigger is vital and must be efficient for the low values of p_T, which result from the large final-state multiplicity. The vertex trigger is particularly efficient for these channels as there are two vertices containing three tracks (D vertices) to be triggered on in each decay. The particle identification information from the RICH detectors is important for background-suppression and to eliminate reflections from $KK\pi$ to $K\pi\pi$ and vice versa.

The analysis is at a preliminary level and still underway, but the first results look promising. The trigger efficiencies for both channels are found to be around 25% for events decaying within the acceptance. The reconstruction relies principally on requiring well separated secondary vertices, appropriate invariant masses and p_T-cuts. Reconstruction efficiencies for the B and B_s of about 30% have been

found. Using product branching ratios $B(B \to X) \times B(X \to Y)$ of 3.6×10^{-5} for $B \to DD$ and 3.2×10^{-4} for $B_s \to D_s D_s$ gives about 3×10^5 events per year for $B \to DD$, after flavour tagging, and 1.9×10^5 events per year for $B_s \to D_s D_s$. These estimates have been obtained by studying signal MC simulations only. A study of the effect of backgrounds is currently underway. The errors achievable on γ depend on the specific values of γ and β. For $\gamma = 75^\circ$ and $\beta = 50^\circ$, an error of about 1° is expected. It should be emphasized that these numbers are preliminary, but it seems that the potential of LHCb in this promising channel is good.

5.4 A Simultaneous Determination of β and γ from $B_d \to \pi^+\pi^-$ and $B_s \to K^+K^-$[17]

In this subsection, we combine the CP-violating observables of the decay $B_d \to \pi^+\pi^-$ with those of the transition $B_s \to K^+K^-$, which is the U-spin counterpart of $B_d \to \pi^+\pi^-$. Following these lines, a simultaneous determination of $\phi_d = 2\beta$ and γ becomes possible [110]. This approach is not affected by any penguin topologies – it rather makes use of them – and does not rely on certain "plausible" dynamical or model-dependent assumptions. Moreover, FSI effects, which led to considerable attention in the recent literature in the context of the determination of γ from $B \to \pi K$ decays (see Sec. 5.1), do not lead to any problems, and the theoretical accuracy is only limited by U-spin breaking effects. This strategy, which is furthermore very promising with regard to the search for indications of new physics [137], is conceptually quite similar to the extractions of γ with the help of the decays $B_{s(d)} \to J/\psi\, K_{\rm S}$ and $B_{d(s)} \to D^+_{d(s)} D^-_{d(s)}$ discussed in Secs. 5.2 and 5.3, respectively (see also [111]).

5.4.1 Theoretical Aspects

As can be seen from Fig. 12, $B_d \to \pi^+\pi^-$ and $B_s \to K^+K^-$ are related to each other by interchanging all down and strange quarks, i.e. they are U-spin counterparts. If we make use of the unitarity of the CKM matrix and apply the generalized Wolfenstein parametrization, including non-leading terms in λ, the $B^0_d \to \pi^+\pi^-$ decay amplitude can be expressed as follows [110]:

$$A(B^0_d \to \pi^+\pi^-) = e^{i\gamma}\,\mathcal{C}\left[1 - d\,e^{i\theta}e^{-i\gamma}\right], \tag{5.42}$$

where

$$\mathcal{C} \equiv \lambda^3 A\, R_b \left(A^u_{\rm cc} + A^{ut}_{\rm pen}\right), \quad d\,e^{i\theta} \equiv \frac{1}{R_b}\left(\frac{A^{ct}_{\rm pen}}{A^u_{\rm cc} + A^{ut}_{\rm pen}}\right) \tag{5.43}$$

with $A^{ut}_{\rm pen} \equiv A^u_{\rm pen} - A^t_{\rm pen}$. In analogy to (5.42), we obtain for the $B^0_s \to K^+K^-$ decay amplitude

$$A(B^0_s \to K^+K^-) = e^{i\gamma}\lambda\,\mathcal{C}'\left[1 + \left(\frac{1-\lambda^2}{\lambda^2}\right) d' e^{i\theta'} e^{-i\gamma}\right], \tag{5.44}$$

where

$$\mathcal{C}' \equiv \left(\frac{\lambda^3 A\, R_b}{1-\lambda^2/2}\right)\left(A^{u'}_{\rm cc} + A^{ut'}_{\rm pen}\right) \text{ and } d' e^{i\theta'} \equiv \frac{1}{R_b}\left(\frac{A^{ct'}_{\rm pen}}{A^{u'}_{\rm cc} + A^{ut'}_{\rm pen}}\right) \tag{5.45}$$

correspond to (5.43). The general expressions for the $B_d \to \pi^+\pi^-$ and $B_s \to K^+K^-$ observables (1.24) and (1.25) in terms of the parameters specified above can be found in [110].

Since $B_d \to \pi^+\pi^-$ and $B_s \to K^+K^-$ are related to each other by interchanging all down and strange quarks, the U-spin flavour-symmetry of strong interactions implies

$$d' = d \quad \text{and} \quad \theta' = \theta. \tag{5.46}$$

If we assume that the B^0_s–$\overline{B^0_s}$ mixing phase ϕ_s is negligible, or that it is fixed through $B_s \to J/\psi\,\phi$, the four CP-violating observables provided by $B_d \to \pi^+\pi^-$ and $B_s \to K^+K^-$ depend – in the strict

[17] With help from D. Rousseau and A. Starodumov.

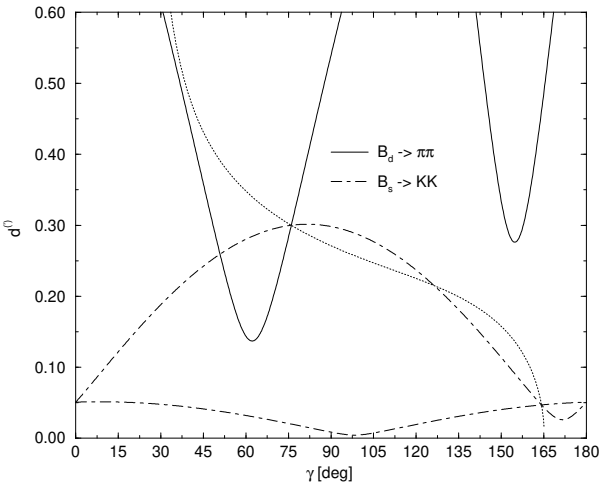

Fig. 45: The contours in the γ–$d^{(\prime)}$ planes fixed through the CP-violating $B_d \to \pi^+\pi^-$ and $B_s \to K^+K^-$ observables for a specific example discussed in the text.

U-spin limit – on the four "unknowns" d, θ, $\phi_d = 2\beta$ and γ. We have therefore sufficient observables at our disposal to extract these quantities simultaneously. In order to determine γ, it suffices to consider $\mathcal{A}_{\rm CP}^{\rm mix}(B_s \to K^+K^-)$ and the direct CP asymmetries $\mathcal{A}_{\rm CP}^{\rm dir}(B_s \to K^+K^-)$, $\mathcal{A}_{\rm CP}^{\rm dir}(B_d \to \pi^+\pi^-)$. If we make use, in addition, of $\mathcal{A}_{\rm CP}^{\rm mix}(B_d \to \pi^+\pi^-)$, ϕ_d can be determined as well. The full formulae needed to implement this approach can be found in [110].

The use of the U-spin flavour-symmetry to extract γ can be minimized, if we use not only ϕ_s, but also the B_d^0–$\overline{B_d^0}$ mixing phase ϕ_d as an input. Then, the CP-violating observables $\mathcal{A}_{\rm CP}^{\rm dir}(B_d \to \pi^+\pi^-)$, $\mathcal{A}_{\rm CP}^{\rm mix}(B_d \to \pi^+\pi^-)$ and $\mathcal{A}_{\rm CP}^{\rm dir}(B_s \to K^+K^-)$, $\mathcal{A}_{\rm CP}^{\rm mix}(B_s \to K^+K^-)$ allow one to fix contours in the γ–d and γ–d' planes in a *theoretically clean* way. In order to extract γ and the hadronic parameters d, θ, θ' with the help of these contours, the U-spin relation $d' = d$ is sufficient. Let us illustrate this approach for a specific example:

$$\begin{array}{ll} \mathcal{A}_{\rm CP}^{\rm dir}(B_d \to \pi^+\pi^-) = +24\%, & \mathcal{A}_{\rm CP}^{\rm mix}(B_d \to \pi^+\pi^-) = +4.4\%, \\ \mathcal{A}_{\rm CP}^{\rm dir}(B_s \to K^+K^-) = -17\%, & \mathcal{A}_{\rm CP}^{\rm mix}(B_s \to K^+K^-) = -28\%, \end{array} \tag{5.47}$$

corresponding to the input parameters $d = d' = 0.3$, $\theta = \theta' = 210^\circ$, $\phi_s = 0$, $\phi_d = 53^\circ$ and $\gamma = 76^\circ$. In Fig. 45, the corresponding contours in the γ–d and γ–d' planes are represented by the solid and dot-dashed lines, respectively. Their intersection yields a twofold solution for γ, given by 51° and our input value of 76°. The dotted line is related to

$$K \equiv -\left(\frac{1-\lambda^2}{\lambda^2}\right)\left[\frac{\mathcal{A}_{\rm CP}^{\rm dir}(B_d \to \pi^+\pi^-)}{\mathcal{A}_{\rm CP}^{\rm dir}(B_s \to K^+K^-)}\right], \tag{5.48}$$

which can be combined with the mixing-induced CP asymmetry $\mathcal{A}_{\rm CP}^{\rm mix}(B_s \to K^+K^-)$ through the U-spin relation (5.46) to fix another contour in the γ–d plane. Combining all contours in Fig. 45 with one another, we obtain a single solution for γ in this example, which is given by the "true" value of 76°.

It should be emphasized that the theoretical accuracy of γ and of the hadronic parameters d, θ and θ' is only limited by U-spin breaking effects. In particular, it is not affected by any FSI or penguin effects. A first consistency check is provided by $\theta = \theta'$. Moreover, we may determine the normalization factors $\mathcal{C}$ and $\mathcal{C}'$ of the $B_d^0 \to \pi^+\pi^-$ and $B_s^0 \to K^+K^-$ decay amplitudes (see (5.42) and (5.44)) with the help of the corresponding CP-averaged branching ratios. Comparing them with the "factorized" result

$$\left|\frac{\mathcal{C}'}{\mathcal{C}}\right|_{\rm fact} = \frac{f_K}{f_\pi}\frac{F_{B_sK}(M_K^2;0^+)}{F_{B_d\pi}(M_\pi^2;0^+)}\left(\frac{M_{B_s}^2 - M_K^2}{M_{B_d}^2 - M_\pi^2}\right), \tag{5.49}$$

we have another interesting probe for U-spin breaking effects. Interestingly, the relation

$$d' e^{i\theta'} = d\, e^{i\theta} \tag{5.50}$$

is not affected by U-spin breaking corrections within a certain model-dependent approach (a modernized version [15, 142] of the "Bander–Silverman–Soni mechanism" [143]), which relies on the factorization approximation to estimate the relevant hadronic matrix elements [110]. Although this approach appears rather simple and may be affected by non-factorizable effects, it strengthens our confidence into the U-spin relations used for the extraction of β and γ from the decays $B_d \to \pi^+\pi^-$ and $B_s \to K^+K^-$. Further theoretical studies along the lines of Ref. [76] to investigate the U-spin breaking effects in the $B_d \to \pi^+\pi^-$, $B_s \to K^+K^-$ system would be very interesting. In order to obtain further experimental insights, the $B_d \to \rho^+\rho^-$, $B_s \to K^{*+}\,K^{*-}$ system would be of particular interest, allowing one to determine γ together with the mixing phases ϕ_d and ϕ_s, and tests of several interesting U-spin relations [93].

Since penguin processes play an important rôle in the decays $B_s \to K^+K^-$ and $B_d \to \pi^+\pi^-$, they may well be affected by new physics – which likewise applies to the determination of γ, where furthermore the unitarity of the CKM matrix is employed. Interestingly, the SM implies a rather restricted region in the space of the CP-violating observables of the $B_s \to K^+K^-$, $B_d \to \pi^+\pi^-$ system [137], which is shown in Fig. 46. A future measurement of observables lying significantly outside of the allowed region shown in this figure would be an indication for new physics. Such a discrepancy could either be due to CP-violating new-physics contributions to B_s^0–$\overline{B_s^0}$ mixing, or to $B_d \to \pi^+\pi^-$, $B_s \to K^+K^-$ decay amplitudes. The former case would also be indicated simultaneously by large CP-violating effects in the mode $B_s \to J/\psi\,\phi$, which would allow us to extract the B_s^0–$\overline{B_s^0}$ mixing phase ϕ_s (see Sec. 4). A discrepancy between the measured $B_d \to \pi^+\pi^-$, $B_s \to K^+K^-$ observables and the region corresponding to the value of ϕ_s from $B_s \to J/\psi\phi$ would then signal new-physics contributions to the $B_d \to \pi^+\pi^-$, $B_s \to K^+K^-$ decay amplitudes. On the other hand, if $B_s \to J/\psi\,\phi$ should exhibit negligible CP-violating effects, any discrepancy between the $B_d \to \pi^+\pi^-$, $B_s \to K^+K^-$ observables and the volume shown in Fig. 46 would indicate new-physics contributions to the corresponding decay amplitudes. If, however, the observables should lie within the region predicted by the SM, we can extract a value for the CKM angle γ by following the strategy discussed above, which may well be in disagreement with those implied by theoretically clean strategies making use of pure "tree" decays, thereby also indicating the presence of new physics.

5.4.2 Experimental Studies

It was demonstrated in Sec. 3.2.2 that the LHC experiments can expect large event yields in the two-body decay $\mathrm{B_d^0} \to \pi^+\pi^-$. With an appropriately modified selection, similarly high statistics can be accumulated in $\mathrm{B_s^0} \to \mathrm{K^+K^-}$. The excellent proper time resolution of the experiments then allows $\mathrm{B_s^0}$ oscillations to be distinguished, and the CP asymmetry coefficients to be measured. By using the relations presented above, the $\mathrm{B_d^0} \to \pi^+\pi^-$ and $\mathrm{B_s^0} \to \mathrm{K^+K^-}$ observables can be used to cleanly extract CP phases, most interestingly the angle γ. The potential of this approach has been investigated by all three experiments.

Event Yields and Asymmetry Sensitivity

Apart from the final requirements on the best particle-hypothesis and the invariant mass of the two candidate tracks, the CMS and LHCb isolation of $\mathrm{B_s^0} \to \mathrm{K^+K^-}$ events is identical to the $\mathrm{B_d^0} \to \pi^+\pi^-$ selection described in Sec. 3.2.2. After flavour tagging, LHCb expects an annual yield of 4.6 events, with a contamination from other two-body modes of 15%. The equivalent numbers for CMS are 960 and 540 respectively, assuming the dE/dx based selection. As explained previously, ATLAS favours an approach where the asymmetry of all selected two-body events is fitted simultaneously. In this sample, 1.4k $\mathrm{B_s^0} \to \mathrm{K^+K^-}$ events are expected within the one σ mass window.

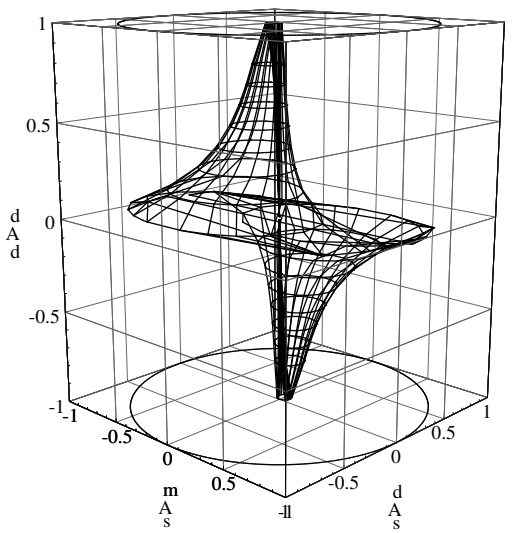

Fig. 46: The allowed region in the space of $A_s^{\rm d} \equiv \mathcal{A}_{\rm CP}^{\rm dir}(B_s \to K^+K^-)$, $A_s^{\rm m} \equiv \mathcal{A}_{\rm CP}^{\rm mix}(B_s \to K^+K^-)$ and $A_d^{\rm d} \equiv \mathcal{A}_{\rm CP}^{\rm dir}(B_d \to \pi^+\pi^-)$, characterizing $B_s \to K^+K^-$ and $B_d \to \pi^+\pi^-$ in the SM ($\phi_s = 0$).

$\Delta m_s\,[\mathrm{ps}^{-1}]$	ATLAS	CMS	LHCb
15	0.09	0.10	0.034
20	0.13	0.13	0.047
30	/	0.33	0.068

Table 17: Expected sensitivities for the $\mathrm{B_s^0} \to \mathrm{K^+K^-}$ CP asymmetry coefficients $\mathcal{A}_{\mathrm{K^+K^-}}^{\rm mix}$ and $\mathcal{A}_{\mathrm{K^+K^-}}^{\rm dir}$ for 3 (ATLAS/CMS) and 5 (LHCb) years' data taking, for different values of Δm_s and $\Delta\Gamma_s = 0$.

$\Delta m_s\,[\mathrm{ps}^{-1}]$	1 year	Extended running
15	3.7°	1.9°
20	4.8°	2.4°
30	7.4°	3.4°

Table 18: Expected sensitivities for the unitarity triangle angle γ for the $\mathrm{B_d^0} \to \pi^+\pi^-$/$\mathrm{B_s^0} \to \mathrm{K^+K^-}$ analysis for LHC running after one year and 3 (ATLAS/CMS) / 5 (LHCb) years, as a function of Δm_s and for the parameter-set specified in the text.

The precision of the fitted the $\mathrm{B_s^0} \to \mathrm{K^+K^-}$ CP parameters $\mathcal{A}_{\mathrm{K^+K^-}}^{\rm mix}$ and $\mathcal{A}_{\mathrm{K^+K^-}}^{\rm dir}$ depends not only on the event yields, but also on the value of Δm_s, which governs the rapidity of the $\mathrm{B_s^0}$–$\overline{B_s^0}$ oscillations. Table 17 shows the precision expected for three different values of Δm_s after an extended period of running. The uncertainties for one year's running scale in the expected statistical manner, except that ATLAS and CMS retain no sensitivity for $\Delta m_s = 30\,\mathrm{ps}^{-1}$ with the smaller data-set.

Sensitivity to the CP Violating Phases

The sensitivity to which γ can be determined has been studied by all three experiments, assuming that the $\mathrm{B_s^0} \to \mathrm{K^+K^-}$ and $\mathrm{B_d^0} \to \pi^+\pi^-$ asymmetries be known to the precision given in Tabs. 17 and 9, respectively. With the scenario given in the previous subsection ($d = d' = 0.3$, $\theta = \theta' = 210°$, $\phi_s = 0$, $\phi_d = 53°$, $\gamma = 76°$ and $\Delta m_s = 15\,\mathrm{ps}^{-1}$, $\Delta\Gamma_s = 0$ and assuming an uncertainty of 1% on $\sin(2\beta) = \sin(\phi_d)$), the sensitivity after one year at LHC is $\sigma_\gamma = 3.7°$, if the constraints $d = d'$ and $\theta = \theta'$ are applied. It improves to $\sigma_\gamma = 1.9°$ after 5 years. Table 18 shows how these uncertainties increase with Δm_s. In the considered range of parameters, the sensitivity is clearly impressive.

To give an indication on how the sensitivity depends on the scenario, Fig. 47 shows the ultimate sensitivity for 5 years of LHC, in the scenario given above but as a function of the true value of γ and $\theta = \theta'$. For most values of γ and θ, the sensitivity to γ is better than $4°$, except in regions around $\gamma = 90°$ and $\gamma = 20°$. The sensitivity depends significantly on the assumed value of $d = d'$: it decreases (increases) by a factor of two if $d = d' \simeq 0$ ($d = d' = 0.5$).

The number of the degrees of freedom is large enough to allow one to relax one of the two constraints $d = d'$ and $\theta = \theta'$. This approximately doubles the uncertainty on γ, but allow one to check the

U-spin flavour-symmetry relations $d = d'$ and $\theta = \theta'$. Figure 47 shows that a typical precision of 15° on $\theta - \theta'$ and 0.1 on $d - d'$ can be reached, but in regions that are largely disjoint in θ. These numbers also indicate the level to which U-spin symmetry must hold in order to improve the estimate of γ without biasing it.

5.5 Conclusions

Thanks to their high yield in two-body decays and good proper time resolution, the LHC experiments are well suited to performing a combined analysis of $\mathrm{B}^0_\mathrm{d} \to \pi^+\pi^-$ and $\mathrm{B}^0_\mathrm{s} \to \mathrm{K}^+\mathrm{K}^-$. This analysis offers a powerful and precise way to determine the angle γ in a manner sensitive to new-physics contributions.

6 SYSTEMATIC ERROR CONSIDERATIONS IN CP MEASUREMENTS[18]

6.1 Introduction

The excellent statistical precision expected in many CP-violation measurements at the LHC demands that there be good control of systematic uncertainties. The challenges posed by hadronic effects in interpreting certain observables are discussed elsewhere in this chapter; here, biases from experimental factors and initial state asymmetries will be considered, and possible control strategies examined.

6.2 Sources and Categories of Systematic Bias

CP measurements require the reconstruction of a final state, and frequently the tagging of the initial state flavour. Time-dependent rates, or branching ratios, are then combined into asymmetries from which CKM phases can be extracted. These measurements are inherently robust, in that to first order experimental unknowns will cancel or can be assumed to be the same for all processes under consideration. However, certain charge- and flavour-dependent effects may exist, which can indeed bias the measurement:

- **Production asymmetries**
  As explained in the Chapter on b production [47], the initial fraction of b and $\bar{b}$ hadrons at the LHC is not expected to be identical. A production asymmetry will exist, and this asymmetry will vary as a function of rapidity and p_T, reaching values of several percent. Furthermore, this asymmetry can be different for each hadron species. In this section, the fractions of B^0_d, $\overline{\mathrm{B}^0_\mathrm{d}}$, B^0_s, $\overline{\mathrm{B}^0_\mathrm{s}}$, B^+ and B^- mesons per event are denoted by f_0, $\overline{f_0}$, f_s, $\overline{f_s}$, f_+ and f_-.
- **Tagging efficiency**
  All methods of flavour tagging rely on measuring the charge of one or more selected tracks. If the track reconstruction efficiency, or particle assignment (for lepton or kaon tags), has a charge-dependence, then a difference in the tagging efficiency for b and $\bar{b}$ hadrons will result. Such a dependence is certainly possible, for instance in LHCb where positive and negative tracks are preferentially swept by the dipole to different areas of the detector. Furthermore, an asymmetric tagging efficiency can develop from effects such as a difference in interaction cross-sections for K^+ and K^-. The tagging efficiency for B and $\bar{\mathrm{B}}$ mesons will be denoted by ϵ and $\overline{\epsilon}$.
- **Mistag rate**
  Assuming a flavour tag has been performed, the probability of that tag being correct can also have a flavour-dependence. For instance in a lepton tag, different reconstructed momentum spectra for l^+ and l^- are conceivable. These will result not only in different efficiencies, but also in different $\mathrm{B} \to \mathrm{l}$ purities for the two samples. The mistag rates for B and $\bar{\mathrm{B}}$ mesons will be represented by ω and $\overline{\omega}$.
- **Final state acceptance**
  Clearly, in any measurement where different final states are being compared, the relative trigger

[18] Section coordinators: R. Fleischer and G. Wilkinson.

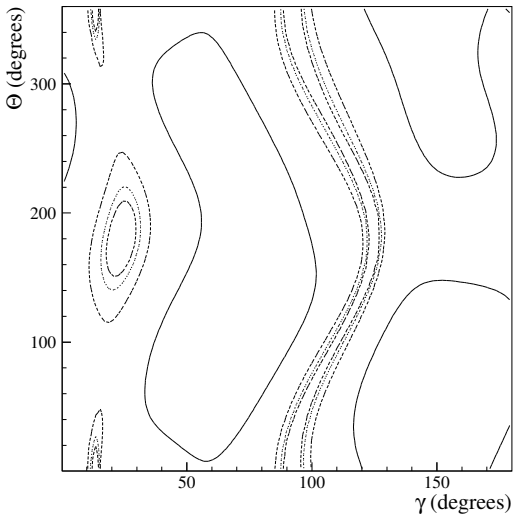

(a) Sensitivity to γ for 5 years of LHC, with the constraints $\phi_s = 0$, $d = d'$ and $\theta = \theta'$ assuming an uncertainty of 1% on $\sin(2\beta)$, and with input values $d = d' = 0.3$, and $\phi_d = 53^\circ$, $\Delta m_s = 15\,\mathrm{ps}^{-1}$ and $\Delta\Gamma_s = 0$. The contour lines correspond to sensitivities of 2° (solid), 4° (dashed), 6° (dotted) and 8° (dotted-dashed).

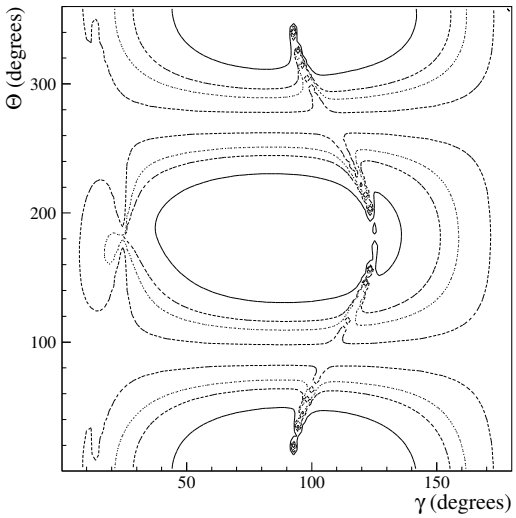

(b) Sensitivity to $\theta - \theta'$ for the same fit as in (a) except the relaxed $\theta = \theta'$ constraint. The contour lines correspond to sensitivities of 10° (solid), 15° (dashed), 20° (dotted) and 50° (dotted-dashed).

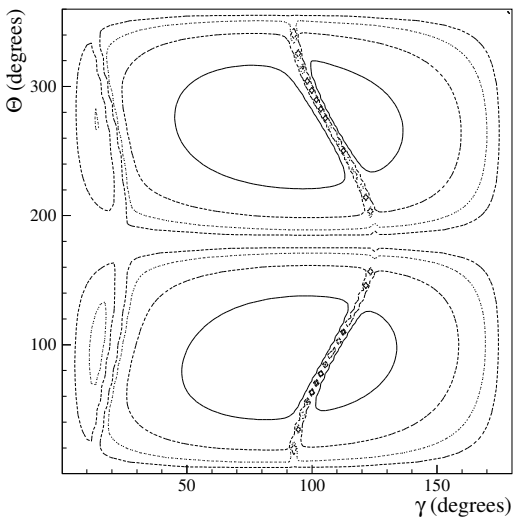

(c) Sensitivity to $d - d'$ for the same fit as in (a) except the relaxed $d = d'$ constraint. The contour lines correspond to sensitivities of 0.05 (solid), 0.1 (dashed), 0.2 (dotted) and 0.4 (dotted-dashed).

Fig. 47: Sensitivity of fits to the LHC combined $\mathrm{B}^0_\mathrm{d} \to \pi^+\pi^-$ and $\mathrm{B}^0_\mathrm{s} \to \mathrm{K}^+\mathrm{K}^-$ samples.

Channel	ATLAS	CMS	LHCb
$B^{\pm} \to J/\psi K^{\pm}$	1700k	5100k	880k
$B^0_d \to J/\psi K^{0*}$	880k	2900k	800k
$B^0_s \to D_s \pi$	3.5k	4.5k	86k

Table 19: Untagged annual event yields in selected control channels. The ATLAS numbers assume a level-2 trigger muon threshold of 3 GeV [56].

and reconstruction efficiencies can be different. However, even if the asymmetry involves a single topology in the final state, the efficiency may differ for the charge-conjugate case, for the same charge acceptance reasons as explained above.

Background is obviously an additional source of possible bias, and will require careful attention. However, this is a problem common to most physics measurements, and therefore is not considered here.

These effects will have different consequences for each category of measurement. The present discussion focuses on measurements involving decays into CP eigenstates, such as $B^0_d \to J/\psi K^0_S$. Here the observed asymmetry $\mathcal{A}^{\rm obs}(t)$ is constructed from the number of flavour-tagged B^0 and $\overline{B^0}$ decays into $J/\psi K^0_S$, as a function of proper time. Allowing for the factors considered above, $\mathcal{A}^{\rm obs}(t)$ is related to the true decay distributions $R^{\rm true}_{B^0,\overline{B^0}\to J/\psi K^0_S}$ as follows:

$$\mathcal{A}^{\rm obs}(t) = \frac{(1-2\omega)R^{\rm true}_{B^0_d\to J/\psi K^0_S}(t) \; - \; \frac{\overline{f_0}\,\overline{\epsilon}}{f_0\epsilon}(1-2\overline{\omega})R^{\rm true}_{\overline{B^0_d}\to J/\psi K^0_S}(t)}{R^{\rm true}_{B^0_d\to J/\psi K^0_S}(t) \; + \; \frac{\overline{f_0}\,\overline{\epsilon}}{f_0\epsilon}\,R^{\rm true}_{\overline{B^0_d}\to J/\psi K^0_S}(t)}\,. \tag{6.1}$$

Assuming that the flavour-dependent effects in tagging and production are small, $\mathcal{A}^{\rm obs}(t)$ is related to the true physics asymmetry

$$A^{\rm phy}(t) = \frac{R^{\rm true}_{B^0_d\to J/\psi K^0_S}(t) - R^{\rm true}_{\overline{B^0_d}\to J/\psi K^0_S}(t)}{R^{\rm true}_{B^0_d\to J/\psi K^0_S}(t) + R^{\rm true}_{\overline{B^0_d}\to J/\psi K^0_S}(t)}$$

as follows:

$$\mathcal{A}^{\rm obs}(t) \approx (1-2\omega)\left[A^{\rm phy}(t) \; - \; \frac{1}{2}\left(\frac{\overline{f_0}\,\overline{\epsilon}}{f_0\epsilon} - 1\right)(1 - A^{\rm phy}(t)^2) \; - \; \left(\frac{\omega-\overline{\omega}}{1-2\omega}\right)(1 - A^{\rm phy}(t))\right]. \tag{6.2}$$

In the absence of production or tagging asymmetries, this reduces to the well known expression $\mathcal{A}^{\rm obs}(t) = (1-2\omega)\,\mathcal{A}^{\rm phy}(t)$. Even here, therefore, the extraction of $\mathcal{A}^{\rm phy}(t)$ requires that the mistag rate ω be known. In the more general case it is also necessary to know $\overline{f_0}/f_0$, $\overline{\epsilon}/\epsilon$ and $\omega - \overline{\omega}$. Note because there is only a single final state involved, there is no dependence on any acceptance. In the following, we consider strategies to determine the tagging and production factors.

6.3 Use of Control Channels

6.3.1 Introduction and Event Yields

Several channels are useful for controlling systematic biases of the type considered above. Three which are discussed here are $B^{\pm} \to J/\psi K^{\pm}$, $B^0_d \to J/\psi K^{0*}$ and $B^0_s \to D_s\pi$. The LHC experiments expect significant event yields in these modes, as is shown in Tab. 19, with background-levels well under control. Sample invariant mass distributions for $B^{\pm} \to J/\psi K^{\pm}$and $B^0_d \to J/\psi K^{0*}$ are shown in Fig. 48.

Here an approach is presented which shows how any flavour-dependent tagging-effects and production asymmetries may be determined from these channels alone. This is to demonstrate the power of the available constraints. In practice it is envisaged that a combination of these channels, MC, and detailed detector cross-checks will be used. An example of the latter is the intention of LHCb to take data-sets with swapped dipole polarity, thereby constraining any charge-acceptance systematics.

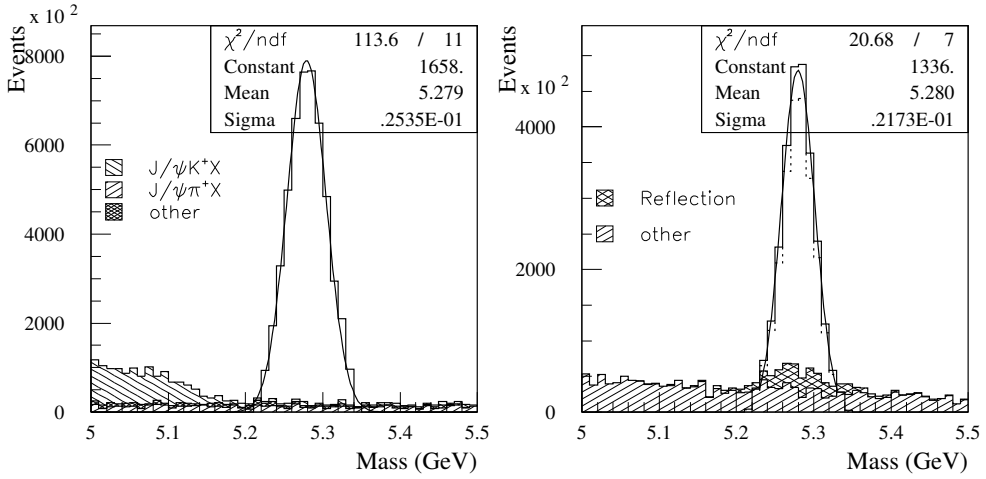

Fig. 48: Invariant mass distributions (open histograms) for $\mathrm{B}^{\pm} \to \mathrm{J}/\psi\mathrm{K}^{\pm}$ (left) and $\mathrm{B}^0_\mathrm{d} \to \mathrm{J}/\psi\mathrm{K}^{0*}$ (right) with superimposed estimated background contributions (shaded histograms) at ATLAS after 3 years of running.

6.3.2 $\mathrm{B}^{\pm} \to \mathrm{J}/\psi\mathrm{K}^{\pm}$

By reconstructing and flavour tagging $\mathrm{B}^{\pm} \to \mathrm{J}/\psi\mathrm{K}^{\pm}$ decays, the tagging efficiencies and mistag rates ϵ, $\overline{\epsilon}$, ω and $\overline{\omega}$ may be directly measured. The expected event yields enable this to be done with annual relative precision of a few 10^{-3} per experiment, which is certainly adequate for the CP asymmetry measurements. These factors can be determined in bins of tag-method, trigger-category, p, p_T and rapidity, in order to account for correlations.

Comparing the number of untagged $\mathrm{J}/\psi\mathrm{K}^+$ and $\mathrm{J}/\psi\mathrm{K}^-$ events gives sensitivity to the $\mathrm{B}^+/\mathrm{B}^-$ production fractions f^+/f^-. However, what is generally of interest are the B^0_d and B^0_s quantities, $f^0_d/\overline{f^0_d}$ and $f^0_s/\overline{f^0_s}$. More importantly, any observed asymmetry may well receive contributions from direct CP violation and detector effects, and the decoupling of these factors will be very difficult. This motivates the use of other control channels.

6.3.3 $\mathrm{B}^0_\mathrm{d} \to \mathrm{J}/\psi\mathrm{K}^{0*}$

The final state of the family of modes B^0, $\overline{\mathrm{B}^0} \to \mathrm{J}/\psi\mathrm{K}^{0*}$, $\mathrm{J}/\psi\overline{\mathrm{K}^{0*}}$ is flavour specific to the meson at decay, therefore enabling these events to be used in a similar manner to $\mathrm{B}^{\pm} \to \mathrm{J}/\psi\mathrm{K}^{\pm}$. However, the oscillation of the mesons before decay provides additional observables which may be usefully exploited.

Consider the four decay rates $R^{\mathrm{B}^0,\overline{\mathrm{B}^0}\to\mathrm{B}^0,\overline{\mathrm{B}^0}}(t)$ of genuine B^0 and $\overline{\mathrm{B}^0}$ mesons into reconstructed B^0 and $\overline{\mathrm{B}^0}$ final states:

$$R^{\mathrm{B}^0\to\mathrm{B}^0}(t) \;\propto\; f_0\,|A|^2\,a(t)\,(1+\cos\Delta mt)\,e^{-\Gamma t}\,; \quad R^{\overline{\mathrm{B}^0}\to\overline{\mathrm{B}^0}}(t) \;\propto\; \overline{f_0}\,|\overline{A}|^2\,\overline{a}(t)\,(1+\cos\Delta mt)\,e^{-\Gamma t};$$
$$R^{\mathrm{B}^0\to\overline{\mathrm{B}^0}}(t) \;\propto\; f_0\,|\overline{A}|^2\,\overline{a}(t)\,(1-\cos\Delta mt)\,e^{-\Gamma t}\,; \quad R^{\overline{\mathrm{B}^0}\to\mathrm{B}^0}(t) \;\propto\; \overline{f_0}\,|A|^2\,a(t)\,(1-\cos\Delta mt)\,e^{-\Gamma t},$$

where $|A|$ and $|\overline{A}|$ represent the absolute rates of the decays, which may be different because of direct CP violation, and $a(t)$ and $\overline{a}(t)$ are acceptance factors for the two final states. Then the observed untagged decay distribution into B^0 events, $R^{\mathrm{X}\to\mathrm{B}^0}(t)$, is:

$$R^{\mathrm{X}\to\mathrm{B}^0}(t) \;=\; |A|^2 a(t)\,(f_0+\overline{f_0})\,\left[1 \;+\; \frac{f_0-\overline{f_0}}{f_0+\overline{f_0}}\,\cos\Delta mt\right]\,e^{-\Gamma t}, \tag{6.3}$$

with the conjugated expression for $R^{\mathrm{X}\to\overline{\mathrm{B}^0}}(t)$. Therefore evidence of any oscillation term in the untagged rates signifies an initial state production asymmetry, independent of CP violation and detector effects. Fitting this term enables the ratio $f_0/\overline{f_0}$ to be determined.

Information on the flavour-dependence of the tagging efficiency can also be obtained. The observed decay distribution for B^0 mesons of initial state flavour tagged B^0 *and* $\overline{\mathrm{B}^0}$ events is $R^{\mathrm{X}_{\mathrm{tag}}\to\mathrm{B}^0}(t)$, where:

$$R^{\mathrm{X}_{\mathrm{tag}}\to\mathrm{B}^0}(t) \,=\, |A|^2 a(t)\,(f_0\epsilon + \overline{f_0}\overline{\epsilon})\,\left[1 \,+\, \frac{f_0\epsilon - \overline{f_0}\overline{\epsilon}}{f_0\epsilon + \overline{f_0}\overline{\epsilon}}\,\cos\Delta m t\right]\,e^{-\Gamma t}. \tag{6.4}$$

Thus here, and in the charge conjugated case, fitting an oscillation amplitude to the decay distribution enables the ratio $\overline{f_0}\overline{\epsilon}\,/\,f_0\epsilon$ to be determined.

Finally, there are four decay distributions for initial state tagged B^0, $\overline{\mathrm{B}^0}$ mesons decaying as B^0, $\overline{\mathrm{B}^0}$, denoted by $R^{\mathrm{B}^0,\overline{\mathrm{B}^0}_{\mathrm{tag}}\to\mathrm{B}^0\overline{\mathrm{B}^0}}(t)$ with

$$R^{\mathrm{B}^0_{\mathrm{tag}}\to\mathrm{B}^0}(t) = |A|^2 a(t)\,(f_0\epsilon(1-\omega) \,+\, \overline{f_0}\overline{\epsilon\omega})\,\left[1 \,+\, \frac{f_0\epsilon(1-\omega) \,-\, \overline{f_0}\overline{\epsilon\omega}}{f_0\epsilon(1-\omega) \,+\, \overline{f_0}\overline{\epsilon\omega}}\,\cos\Delta m t\right]\,e^{-\Gamma t}. \tag{6.5}$$

Fitting the oscillation amplitude for $R^{\mathrm{B}^0_{\mathrm{tag}}\to\mathrm{B}^0}(t)$ and $R^{\mathrm{B}^0_{\mathrm{tag}}\to\overline{\mathrm{B}^0}}(t)$ and using the previous results enables $\overline{\omega}/(1-\omega)$ to be determined. The other two distributions do the same for $\omega/(1-\overline{\omega})$. From these results ω and $\overline{\omega}$ can be fixed.

These expressions show how the necessary correction factors can be extracted from data. However, the arguments presented so far do not account for any proper time-dependence in the acceptance, which is certainly not realistic. If the time-dependence is identical for $a(t)$ and $\overline{a}(t)$, then the extractions are still possible, as it will cancel in the ratios of say, $R^{\mathrm{X}\to\mathrm{B}^0}(t)$ and $R^{\mathrm{X}\to\overline{\mathrm{B}^0}}(t)$.

A still more general approach is possible, which dispenses with any assumption on the proper time and flavour-dependence of the acceptance. Consider the ratio

$$\frac{R^{\mathrm{B}^0_{\mathrm{tag}}\to\mathrm{B}^0}(t)/R^{\overline{\mathrm{B}^0_{\mathrm{tag}}}\to\mathrm{B}^0}(t)}{R^{\mathrm{B}^0_{\mathrm{tag}}\to\overline{\mathrm{B}^0}}(t)/R^{\overline{\mathrm{B}^0_{\mathrm{tag}}}\to\overline{\mathrm{B}^0}}(t)} = \frac{\left[1+\frac{1-\overline{\eta}}{1+\overline{\eta}}\cos\Delta m t\right]\left[1+\frac{1-\eta}{1+\eta}\cos\Delta m t\right]}{\left[1-\frac{1-\eta}{1+\eta}\cos\Delta m t\right]\left[1-\frac{1-\overline{\eta}}{1+\overline{\eta}}\cos\Delta m t\right]}, \tag{6.6}$$

where η is given as $\epsilon\omega f_0/\overline{\epsilon}(1-\overline{\omega})\overline{f_0}$, and $\overline{\eta}$ is the conjugated expression. These factors may be simultaneously fitted and combined with the $\mathrm{B}^\pm \to \mathrm{J}/\psi\mathrm{K}^\pm$ results to extract $f_0/\overline{f_0}$. Alternatively, they may be used directly to extract $\sin 2\beta$ from the $\mathrm{B}^0_{\mathrm{d}} \to \mathrm{J}/\psi\mathrm{K}^0_{\mathrm{S}}$ decay rates. Rather than constructing the conventional CP asymmetry, the ratio of the B^0 tagged and $\overline{\mathrm{B}^0}$ tagged decays may be formed:

$$\frac{R^{\mathrm{B}^0_{\mathrm{tag}}\to\mathrm{J}/\psi\mathrm{K}^{\mathrm{s}}_0}(t)}{R^{\overline{\mathrm{B}^0_{\mathrm{tag}}}\to\mathrm{J}/\psi\mathrm{K}^{\mathrm{s}}_0}(t)} = K\left[\frac{1-(\frac{1-\overline{\eta}}{1+\overline{\eta}})\sin 2\beta\sin\Delta m t}{1+(\frac{1-\eta}{1+\eta})\sin 2\beta\sin\Delta m t}\right],$$

where K is a normalization factor and $\eta, \overline{\eta}$ are the factors determined from (6.6). With this method, $\sin 2\beta$ can be cleanly determined, although the need to also fit K reduces the statistical precision with respect to the conventional approach.

6.3.4 $\mathrm{B}^0_{\mathrm{s}} \to \mathrm{D}_{\mathrm{s}}\pi$

In controlling tagging systematics in $\mathrm{B}^0_{\mathrm{s}}$ measurements, the values of ϵ, $\overline{\epsilon}$, ω and $\overline{\omega}$ measured in the $\mathrm{B}^0_{\mathrm{d}}$ channels may be used. However, constraints are required on the production ratio $f_s/\overline{f_s}$. Here it is impracticable to use $\mathrm{J}/\psi\mathrm{K}$ channels, as these are suppressed with respect to the $\mathrm{B}^0_{\mathrm{d}}$ case. Rather it is preferable to use the decay $\mathrm{B}^0_{\mathrm{s}} \to \mathrm{D}_{\mathrm{s}}\pi$, where no CP violation is expected. Attention must be given to detector acceptance effects in the final state, but it should prove possible to control these to the level required by the precision of $\mathrm{B}^0_{\mathrm{s}}$ measurements.

Measurement	$\mathrm{B}^{\pm} \to \mathrm{J}/\psi\mathrm{K}^{\pm}$	$\mathrm{B}^0_\mathrm{d} \to \mathrm{J}/\psi\mathrm{K}^{0*}$
$\delta[(f_0 - \overline{f_0})/(f_0 + \overline{f_0})]$	0.05%	0.07%
$\delta D/D$ (Lepton Tagging)	0.0038	0.0047
$\delta D/D$ (B–π Tagging)	0.0030	0.0039

Table 20: Estimated ATLAS uncertainties on the determination of the production asymmetry, $(f_0 - \overline{f_0})/(f_0 + \overline{f_0})$, and of the dilution, $D = 1 - 2\omega$, for lepton tagging and B–π tagging using $\mathrm{B}^{\pm} \to \mathrm{J}/\psi\mathrm{K}^{\pm}$ and $\mathrm{B}^0_\mathrm{d} \to \mathrm{J}/\psi\mathrm{K}^{0*}$ control samples, after 3 years of running.

6.4 Application to the $\mathrm{B_d} \to \mathrm{J}/\psi\mathrm{K}^0_\mathrm{S}$ Sample

To give a quantitative impression of the precision expected from the control channels, Tab. 20 shows the results of an ATLAS study into the expected uncertainties after 3 years operation on the $B^0_d - \overline{B}^0_d$ production asymmetry, $(f_0 - \overline{f_0})/(f_0 + \overline{f_0})$, and the tagging dilution, $D = 1 - 2\omega$. D has been evaluated separately for lepton tagging and B–π correlation tagging (see Sec. 2.7) [56]. Uncertainties have been calculated with both the $\mathrm{B}^{\pm} \to \mathrm{J}/\psi\mathrm{K}^{\pm}$ and the $\mathrm{B}^0_\mathrm{d} \to \mathrm{J}/\psi\mathrm{K}^{0*}$ samples. The study has been done in the context of the $B^0_d \to J/\psi K^0_S$ analysis (leading to the estimate of the systematic uncertainty on the $\sin 2\beta$ measurement given in Sec. 3.1), but the results are more general. The errors are small compared to the expected statistical uncertainty of $\sin 2\beta$.

6.5 Other Measurements and Conclusions

The discussion so far has focused on $\mathrm{B}^0_\mathrm{d} \to \mathrm{J}/\psi\mathrm{K}^0_\mathrm{S}$, since this is a very important measurement, with an excellent statistical precision expected. However there are other classes of measurement planned for the LHC:

- **Asymmetries involving decays to non-CP eigenstates**
  Measurements such as the determination of γ from $\mathrm{B}^0_\mathrm{d} \to \overline{\mathrm{D}}^{*-}\pi^+$ involve the comparison of four different decay rates, as explained in Sec. 3.4.2. Although there are two final states which may have different acceptances, due to detector-charge effects, the asymmetries which are formed to extract the physics unknowns do not compare these states. Therefore charge acceptance effects will not bias the measurement. Information on tagging factors and production asymmetries is obtained from the usual control channels.
- **Branching ratio comparisons**
  Methods such as the $\mathrm{B}^0_\mathrm{d} \to \pi\mathrm{K}$ strategies to determine γ, described in Sec. 5.1.4, rely on the comparison of several branching ratios. Here it is necessary to know well the relative reconstruction efficiencies, in particular the contribution of the trigger. Although challenging, this should prove possible at a level which will be adequate alongside the statistical and theoretical uncertainties.

It can be concluded that there is no a priori reason why tagging related biases, production asymmetries or detector effects should prevent the experiments from properly exploiting the enormous B statistics at the LHC.

7 B–$\bar{\mathrm{B}}$ MIXING[19]

The physics of B–$\bar{\mathrm{B}}$ mixing is of prime importance for the study of flavour dynamics. Today, the experimental information on B_d and B_s mixing, i.e. the mass differences ΔM_d and ΔM_s, implies already significant constraints on the unitarity triangle. A precise measurement of ΔM_s, for which only a lower limit exists so far, will be an invaluable piece of information on the flavour sector of either the SM or its possible extension. Even if ΔM_s is measured before, LHC's B physics capabilities are likely to remain

[19]Section coordinators: G. Buchalla, L. Lellouch and P. Vikas with help from V. Ghete, O. Schneider and A. Starodumov.

indispensable to fully exploit the potential of B–$\bar{\text{B}}$ mixing. In addition to ΔM_s, also the lifetime difference $\Delta\Gamma_s$ provides us with interesting opportunities. The measurement of this quantity is likewise very difficult and will be a suitable goal for the LHC B physics programme.

The main theory input needed is, on the one hand, perturbative QCD corrections and, on the other hand, hadronic matrix elements of four-quark operators, schematically

$$\langle B_q \mid (\bar{q}\Gamma b)(\bar{q}\Gamma' b) \mid \bar{B}_q \rangle,$$

where Γ, Γ' stand for the relevant combinations of Dirac matrices and $q \in \{s, d\}$. Whereas the perturbative terms are known to NLO in QCD [144, 23], hadronic matrix elements can be obtained from first principles using lattice QCD and we start this section by an overview of the relevant lattice results. We then discuss specifically the mass and width difference ΔM_q and $\Delta\Gamma_q$ of the B_q system and give predictions for the expected ranges of ΔM_s and $\Delta\Gamma_s$ in the SM. The section concludes with experimental considerations on the measurement of B_s^0 oscillations at the LHC.

The numerical results presented in this section are obtained using the following input parameters:

$$m_b = 4.8\,\text{GeV}, \quad \bar{m}_b(m_b) = 4.4\,\text{GeV}, \quad \bar{m}_s(m_b) = 0.1\,\text{GeV}, \quad \bar{m}_t(m_t) = 167\,\text{GeV}, \tag{7.1}$$

$$M_B = 5.28\,\text{GeV}, \quad M_{B_s} = 5.37\,\text{GeV}, \quad B(B_s \to Xe\nu) = 0.104\,,$$

and the two-loop expression for α_s with $\Lambda^{(5)}_{\overline{\text{MS}}} = 225\,\text{MeV}$. Above, m_b is the pole mass and the barred masses refer to the $\overline{\text{MS}}$ scheme.

7.1 Hadronic Matrix Elements from Lattice Calculations

The matrix elements relevant for B mixing are

$$\langle B_q \mid (\bar{q}b)_{V-A}(\bar{q}b)_{V-A} \mid \bar{B}_q \rangle \equiv \frac{8}{3} B_{B_q}(\mu) f_{B_q}^2 M_{B_q}^2\,, \tag{7.2}$$

$$\langle B_s \mid (\bar{q}b)_{S+P}(\bar{q}b)_{S+P} \mid \bar{B}_s \rangle = -\frac{5}{3}\,\frac{M_{B_s}^2 B_S(\mu)}{(\bar{m}_b(\mu) + \bar{m}_s(\mu))^2}\, f_{B_s}^2 M_{B_s}^2, \tag{7.3}$$

$$\langle 0 \mid \bar{q}\gamma_\mu\gamma_5 b \mid \bar{B}_q \rangle = i f_{B_q} p_\mu, \tag{7.4}$$

which are parametrized in terms of the leptonic decay constants f_{B_q} and the B-parameters $B_{(B_q,S)}(\mu)$. Instead of the scale- and scheme-dependent parameter B_{B_q}, one usually introduces the renormalization-group invariant parameter $\hat{B}_{B_q}$, which to NLO in QCD is given by [144, 18]

$$\hat{B}_{B_q}^{\text{nlo}} = B_{B_q}(\mu)[\alpha_s(\mu)]^{-6/23}\left[1 + \frac{\alpha_s(\mu)}{4\pi} J_5\right], \quad J_5 = \frac{5165}{3174} \quad \text{(NDR scheme)}. \tag{7.5}$$

While the matrix elements (7.2) and (7.3) can be determined as such on the lattice, the dimensionless quantities B_{B_q} and $M_{B_s}^2 B_S/(\bar{m}_b + \bar{m}_s)^2$ are obtained from ratios of Euclidean correlation functions in which many statistical and systematic uncertainties are expected to cancel. Thus, it is advantageous to get the matrix elements from an independent determination of the above quantities and f_{B_q}, combined with the experimental value of M_{B_q}.

Because the b quark with mass $m_b \sim 5\,\text{GeV}$ has a Compton-wavelength that is not large compared to typical (quenched) lattice spacings, $a \sim (2-4)\,\text{GeV}^{-1}$, it cannot be simulated directly as a relativistic quark on present day lattices. This has led to a variety of approaches for studying hadrons composed of a heavy quark and light degrees of freedom. In the *relativistic* approach, calculations are performed with a discretization of the relativistic Dirac action, for heavy quarks with masses around that of the charm and extrapolated in mass up to m_b, using heavy quark effective theory as a guide. There are also effective theory approaches, in which QCD is expanded in inverse powers of the b quark mass. Of these, there is

Quantity	$N_f = 0$	$N_f = 2$
f_B (MeV)	175 ± 20	200 ± 30
f_{B_s} (MeV)	200 ± 20	230 ± 30
f_{B_s}/f_B	1.14 ± 0.05	1.15 ± 0.07

Table 21: Summary of the results for leptonic decay constants of B mesons from lattice QCD in the quenched ($N_f = 0$) approximation and with two flavours of sea quarks ($N_f = 2$). It is evident that the values for f_{B_q} are sensitive to quenching effects, whereas their ratio is not.

the *static-quark* approach, in which the heavy quark is treated as an infinite-mass, spin-1/2, static source of colour; a variant of this approach, in which a number of leading $1/m_b$ corrections to the static limit are included in the action, goes under the name of *non-relativistic QCD* or *NRQCD*. Finally, there is a *hybrid* approach in which results, calculated at m_b with a relativistic action, are given a non-relativistic interpretation. While we favour the *relativistic* approach, which does not suffer from the typical ills of effective theories (operator proliferation and power divergences when higher-order corrections are taken into account), the different approaches should be viewed as complementary and any significant disagreement amongst them should be understood.

An important source of uncertainty in many present day lattice calculations is the quenched approximation ($N_f = 0$), in which the feedback of quarks on the gauge fields is neglected. More and more, though, groups are doing away with this approximation and are performing full QCD calculations with two flavours of sea quarks ($N_f = 2$), usually with masses around that of the strange quark. Even then, there is some way to go to reach our physical world where there are $N_f = 3$ light sea quarks: the two very light up and down quarks, and the more massive strange quark.

Because this is not the place for a full-fledged review, we will only very rarely quote individual results and rather give summary numbers, which are meant to reflect the present state of lattice calculations. The results taken into account are those obtained as of January 2000, most of which are referenced in one of the reviews in Ref. [145].

7.1.1 Leptonic Decay Constants

Lattice calculations of the leptonic decay constants f_{B_q} have a long history and results obtained in the quenched approximation with the different approaches to heavy quarks described above are gradually converging. The dominant systematic errors (quenching aside) depend on the approach used, but they are typically of the order of 10%.

In the past year or two, a number of groups have begun studying the effect of unquenching on decay constants by performing $N_f = 2$ calculations with a variety of approaches to heavy quarks. While these calculations are still in rather early stages, and should therefore be given time to mature, they nevertheless suggest an $\mathcal{O}(10-20\%)$ increase in f_{B_q}. f_{B_s}/f_B, however, appears to change very little, indicating that theoretical uncertainties, including the effects of quenching, cancel in such SU(3)-breaking ratios. Because systematic errors depend on the approach and parameters used, it is difficult to combine systematically results from different groups. We therefore choose to give, in Tab. 21, summary numbers for the quenched and unquenched decay constants which are meant to reflect the present situation.

Because a final number is needed for phenomenological purposes, we provide the following summary of the summaries, taking into account the fact that the unquenched results are still rather preliminary and correspond to $N_f = 2$:

$$f_B = (200 \pm 40)\,\text{MeV}, \quad f_{B_s} = (230 \pm 40)\,\text{MeV} \quad \text{and} \quad \frac{f_{B_s}}{f_B} = 1.15 \pm 0.07\,. \tag{7.6}$$

These are the values of the decay constants to be used for numerical estimates in the subsequent subsections. The errors will certainly come down significantly once the unquenched calculations mature.

7.1.2 B-Parameters for ΔM

The lattice calculation of these B-parameters is less mature than that of leptonic decay constants. Nonetheless, there have been a number of calculations over the years.

Agreement amongst calculations using the relativistic approach is good, and recent work at different values of the lattice spacing [146, 141] indicates that discretization errors are small in this approach. Agreement with the NRQCD calculation of Ref. [147] is less good. However, in matching the lattice results to $\overline{\rm MS}$, the authors use the one-loop static instead of NRQCD coefficients, thereby inducing large systematic uncertainties. Thus, until the NRQCD results are finalized, we choose to use the relativistic results to establish our summary numbers for B-parameters. In any case, all methods predict that B_{B_s}/B_B is very close to one.

An effect that has not yet been addressed in B-parameter calculations is the error associated with the quenched approximation: there exist no unquenched calculations of B_{B_q} to date. However, because these parameters correspond to ratios of rather similar matrix elements, their errors are expected to be smaller than those of decay constants.

Compiling the relativistic results, we give for the B-parameters:

$$B_{B_q}(m_b) = 0.91 \pm 0.06, \quad \hat{B}^{\rm nlo}_{B_q} = 1.40 \pm 0.09 \qquad \text{and} \qquad \frac{B_{B_s}}{B_B} = 1.00(3)\ , \tag{7.7}$$

where we do not distinguish $q = d$ from $q = s$. The renormalization group invariant parameter $\hat{B}^{\rm nlo}_{B_q}$ is obtained from $B_{B_q}(m_b)$ using (7.5) with the input parameters of (7.1).

The theoretical determination $\Delta M_s/\Delta M_d$ requires calculation of the non-perturbative parameter R_{sd} (or ξ), defined as

$$\frac{\Delta M_s}{\Delta M_d} = \left|\frac{V_{ts}}{V_{td}}\right|^2 R_{sd} = \left|\frac{V_{ts}}{V_{td}}\right|^2 \left(\frac{M_{B_s}}{M_{B_d}}\right) \xi^2\ . \tag{7.8}$$

While there are at least two possible ways of obtaining R_{sd} from the lattice, the most accurate and most reliable, at present, is via:

$$R_{sd} \equiv \left(\frac{M_{B_s}}{M_B}\right) \left(\frac{f_{B_s}}{f_B}\right)^2 \left(\frac{B_{B_s}}{B_B}\right)\ , \tag{7.9}$$

with (f_{B_s}/f_B) and (B_{B_s}/B_B) determined on the lattice and (M_{B_s}/M_B) measured experimentally. The different approaches have been explored using relativistic quarks by two groups [146, 141].

Because the results obtained by these groups are fully compatible with the value of R_{sd} obtained using the results (7.6) and (7.7), we quote the latter value as our summary number:

$$R_{sd} = 1.35(17) \qquad \text{or} \qquad \xi \equiv \sqrt{R_{sd}\left(\frac{M_B}{M_{B_s}}\right)} = 1.15(7)\ . \tag{7.10}$$

7.1.3 B-Parameter for $\Delta\Gamma_s$

No complete calculation of $m^2_{B_s} B_S/(\bar{m}_b + \bar{m}_s)^2$ in (7.3) exists to date. There has been one calculation performed within the relativistic approach, but with only a single heavy quark whose mass is close to that of the charm [148]. There is also an NRQCD calculation, but where the matching of the lattice to $\overline{\rm MS}$ is performed using the one-loop static instead of NRQCD coefficients [24]. Both are quenched.

The two results are, respectively:

$$\frac{M^2_{B_s} B_S(m_b)}{(\bar{m}_b(m_b) + \bar{m}_s(m_b))^2} = 1.07(1) \quad \text{and} \quad 1.54(3)(24)\ , \tag{7.11}$$

where the first was obtained from [148] using the conversion of [23] and the masses in (7.1). Both these numbers should be considered preliminary, though the second does include an estimate of systematic

errors. So, for the moment, we take

$$\frac{M_{B_s}^2 B_S(m_b)}{(\bar{m}_b(m_b)+\bar{m}_s(m_b))^2} = 1.4(4). \tag{7.12}$$

The near future, however, should bring new results.

7.2 The Mass Difference ΔM

In the SM the B_q mass difference, calculated from box diagrams with virtual top exchange, is given by

$$\Delta M_q = \frac{G_F^2 M_W^2}{6\pi^2}\,\eta_B S_0(x_t)\, M_{B_q}\hat{B}_{B_q} f_{B_q}^2\,|V_{tq}|^2. \tag{7.13}$$

Here $S_0(x_t)$, where $x_t = \bar{m}_t^2/M_W^2$, is the top-quark mass dependent Inami-Lim function for B–$\bar{\text{B}}$ mixing. To an accuracy of better than 1%, $S_0(x_t) \simeq 0.784 x_t^{0.76}$. η_B is a correction factor describing short-distance QCD effects. It has been calculated at next-to-leading order in [144]. With the definition of $\hat{B}_{B_q}$ in (7.5), and employing the running mass $\bar{m}_t(m_t)$ in $S_0(x_t)$, the numerical value is $\eta_B = 0.55$ (with negligible uncertainty). Note that η_B, being a short-distance quantity, is independent of the flavour content of the B meson: it is identical for B_d and B_s. The dependence on the light-quark flavour $q = d$, s belongs to the non-perturbative, long-distance effects, which are isolated in the matrix element (7.2) [144, 18].

Experimentally, ΔM_q can be measured from flavour oscillations of neutral B_q mesons. The current world average is given by [149]

$$\Delta M_d = (0.476 \pm 0.016)\,\text{ps}^{-1}, \quad \Delta M_s > 14.3\,\text{ps}^{-1}\ @\,95\%\,\text{CL}. \tag{7.14}$$

The measurement of ΔM_d can be used to constrain $|V_{td}|$ via (7.13). While the short-distance quantity $\eta_B S_0(x_t)$ is known very precisely, large uncertainties are still present in the hadronic matrix element $B_{B_q} f_{B_q}^2$. Numerically,

$$|V_{td}| = 7.36\times 10^{-3}\left[\frac{167\,\text{GeV}}{\bar{m}_t(m_t)}\right]^{0.76}\left[\frac{237\,\text{MeV}}{f_{B_d}\sqrt{\hat{B}_{B_d}^{\text{nlo}}}}\right]\left[\frac{\Delta M_d}{0.476\,\text{ps}^{-1}}\right]^{0.5}. \tag{7.15}$$

The theoretical uncertainties are reduced considerably in the ratio $\Delta M_s/\Delta M_d$, as given in (7.8). With the results (7.14), an upper limit on $|V_{td}/V_{ts}|$ can be inferred from (7.8). This limit already represents a very interesting CKM constraint, which disfavours negative values of the Wolfenstein parameter ϱ. A future precision measurement of ΔM_s will be a crucial input for the phenomenology of quark mixing. Using $|V_{td}/V_{ts}| > 0.17$ [5] and Eqs. (7.8), (7.10), (7.14), we find a SM prediction of

$$\Delta M_s = (14.3 - 26)\,\text{ps}^{-1}. \tag{7.16}$$

7.3 The Width Difference $\Delta\Gamma$

$(\Delta\Gamma/\Gamma)_{B_s}$ is expected to be one of the largest rate differences in the b hadron sector,[20] with typical size of (10–20)% [19, 108]. The measurement of a substantial $(\Delta\Gamma/\Gamma)_{B_s}$ would open new possibilities for CP violation studies with untagged B_s mesons [25, 27, 26]. Numerically, one has, using NLO coefficients [23]:

$$\left(\frac{|\Delta\Gamma|}{\Gamma}\right)_{B_s} = \left(\frac{f_{B_s}}{230\,\text{MeV}}\right)^2\left[0.007\,B(m_b) + 0.132\,\frac{M_{B_s}^2 B_S(m_b)}{(\bar{m}_b(m_b)+\bar{m}_s(m_b))^2} - 0.078\right] = 0.11(7) \tag{7.17}$$

[20] The width difference in the B_d system is Cabibbo suppressed. We thus only consider the B_s sector.

with the B-parameters as discussed in Sec. 7.1. Note that the B-parameters are to be taken in the NDR scheme as defined in [23]. The last term in (7.17), –0.078, represents $1/m_b$ corrections [108] and has a relative uncertainty of at least 20%. An additional 30% scale-ambiguity from perturbation theory has not been displayed in (7.17).

7.4 Measurement of B_s^0 Oscillations

The probability density to observe an initial B_s^0 meson decaying as a $\overline{B_s^0}$ meson at time t after its creation is given by:

$$P_{B_s^0 \to \overline{B_s^0}}(t) = \frac{\Gamma_s^2 - (\Delta\Gamma_s/2)^2}{2\Gamma_s} e^{-\Gamma_s t} \left[\cosh \frac{\Delta\Gamma_s t}{2} + \mu \cos(\Delta M_s t) \right], \tag{7.18}$$

where $\mu = -1$, $\Delta\Gamma_s = \Gamma_H - \Gamma_L$ and $\Gamma_s = (\Gamma_H + \Gamma_L)/2$. If the initial B_s^0 meson decays as a B_s^0 at time t, the probability density $P_{B_s^0 \to B_s^0}$ is given by the above expression with $\mu = +1$. Experimentally, ΔM_s can be determined by measuring the following time-dependent asymmetry:

$$A(t) = \frac{P_{B_s^0 \to B_s^0}(t) - P_{B_s^0 \to \overline{B_s^0}}(t)}{P_{B_s^0 \to B_s^0}(t) + P_{B_s^0 \to \overline{B_s^0}}(t)} = \frac{\cos(\Delta M_s t)}{\cosh \frac{\Delta\Gamma_s t}{2}}. \tag{7.19}$$

The mass difference ΔM_s is 2π times the oscillation frequency. Within the SM, one has, using the formulae of [23] and the matrix elements of Sec. 7.1,[21] suppressing a 30% renormalization-scale uncertainty,

$$\frac{|\Delta\Gamma_s|}{\Delta M_s} = (4.3 \pm 2.0) \times 10^{-3}, \tag{7.20}$$

which is independent of uncertainties due to CKM matrix elements. It has mainly hadronic uncertainties which are expected to decrease in the future. Therefore, within the SM, ΔM_s can in principle be inferred from a direct measurement of $\Delta\Gamma_s$, although with a large error. Small values of $\Delta\Gamma_s$ and large values of ΔM_s are difficult to measure. However, Eq. (7.20) implies that the smaller $\Delta\Gamma_s$ is, the easier it should be to measure ΔM_s, and, inversely, the larger ΔM_s is, the easier it should be to measure $\Delta\Gamma_s$.

The effect of $\Delta\Gamma_s$ being non-zero is to damp the B_s^0 oscillations with a time-dependent factor. Figure 49 shows the proper time distributions of $B_s^0 \to D_s^- \pi^+$ candidates generated with two different values of $\Delta\Gamma_s$ [39]. The curves display the result of a maximum-likelihood fit to the total sample. The damping of the B_s^0 oscillations due to $\Delta\Gamma_s/\Gamma_s$ is not significant at the expected value of 16%, but could be important if $\Delta\Gamma_s$ turns out to be unexpectedly large. The B_s^0 decay-width difference can be obtained by fitting proper time distributions of untagged samples of events simultaneously for the mean B_s^0 lifetime $\tau_{B_s} = 1/\Gamma_s$ and $\Delta\Gamma_s/\Gamma_s$. All three experiments will use their $B_s^0 \to J/\psi\phi$ events for this measurement as described in Sec. 4.2. In addition, LHCb will have an untagged sample of $B_s^0 \to D_s^- X$ events thanks to their low-level hadronic triggers. LHCb expect to directly observe and measure $\Delta\Gamma_s/\Gamma_s$ after one year of data-taking with their untagged $B_s \to D_s^- \pi^+$ sample, if $\Delta\Gamma_s/\Gamma_s$ is at least 20% [39].

The B meson flavour at production and decay-time and the B_s^0 proper time with good resolution are the ingredients needed to measure ΔM_s. The best channels to make this measurement are B_s^0 decays to exclusive, flavour specific states like $B_s^0 \to D_s^- \pi^+$. The flavour of the B_s^0 at its decay is unambiguously tagged by the sign of the D_s^-. The B_s^0 flavour at production can be determined from the sign of the decay product(s) of the other b hadron in the event. The factors which affect the sensitivity of an experiment to measure ΔM_s are the wrong tag fraction, ω_{tag}, the presence of background and the proper time resolution, σ_t. The corresponding dilution factors for the time-dependent asymmetry are $D_{tag} = 1 - 2\omega_{tag}$, $D_{bkg} \approx N_{signal}/(N_{signal} + N_{bkg})$ and $D_{time} \approx \exp\left(-(\Delta M_s \sigma_t)^2/2\right)$. Here, N_{signal} and N_{bkg} are the number of signal- and background-events, respectively. The measured asymmetry is given by

$$A_{meas}(t) = A(t) \cdot D_{tag} \cdot D_{bkg} \cdot D_{time}. \tag{7.21}$$

[21] Note that according to the sign convention used in this report, (1.15), $\Delta\Gamma_s$ is negative in the SM.

	ATLAS	CMS	LHCb
Channels used:			
B_s^0 decay channels	$D_s^-\pi^+$ $D_s^- a_1^+$	$D_s^-\pi^+$	$D_s^-\pi^+$
D_s^- decay channels	$\phi\pi^-$	$\phi\pi^-$ $K^{*0}K^-$	$\phi\pi^-$ (see text)
ϕ decay channel	K^+K^-	K^+K^-	K^+K^-
a_1^+ decay channel	$\rho^0\pi^+$		
K^{*0} decay channel		$K^+\pi^-$	
Assumptions:			
$B(\bar{b} \to B_s^0)$	0.105	0.105	0.12
$B(B_s^0 \to D_s^-\pi^+)$	3.0×10^{-3}	3.0×10^{-3}	3.0×10^{-3}
$B(B_s^0 \to D_s^- a_1^+)$	6.0×10^{-3}	–	–
$B(D_s^- \to \phi\pi^-)$	0.036	0.036	
$B(D_s^- \to K^{*0}K^-)$	–	0.033	–
$B(D_s^- \to K^+K^-\pi^-)$	–	–	0.04
B_s^0 lifetime	1.54 ps	1.61 ps	1.57 ps
Analysis performance:			
Reconstructed signal-events per year	3457	4500	86000
Rec. and tagged signal-events per year	3457	4500	34500
B_s^0 purity of tagged sample	0.38	0.5	0.95
Wrong tag probability	0.22	0.22	0.30
Proper time resolution(Gaussian function(s))	50 fs (60.5%) 93 fs (39.5%)	65 fs	43 fs
ΔM_s reach after one year of running:			
Measurable values of ΔM_s up to	$30\,\text{ps}^{-1}$	$26\,\text{ps}^{-1}$	$48\,\text{ps}^{-1}$
95% CL excl. of ΔM_s values up to	–	$29\,\text{ps}^{-1}$	$58\,\text{ps}^{-1}$
$\sigma(\Delta m_s)$ for $\Delta m_s = 20\,\text{ps}^{-1}$	0.11	–	0.011
x_s reach after one year of running:			
Measurable values of x_s up to	46	42	75
95% CL excl. of x_s values up to	–	47	91

Table 22: Summary of the analyses and results for B_s^0 oscillation frequency measurements by the LHC experiments.

The amplitude fit method [150] has been used to determine the experimental reach for a ΔM_s measurement from the time-dependent asymmetry. In this method, $\cos(\Delta M_s t)$ is multiplied by an amplitude parameter A. The value of the parameter and its error σ_A are determined for each ΔM_s value by a maximum-likelihood fit. For a measurement of ΔM_s in a region well inside the sensitivity of an experiment, the standard maximum-likelihood method is foreseen.

ATLAS [37], CMS [151, 152] and LHCb [39] have determined their sensitivities to ΔM_s using events generated by PYTHIA [46] and then passed through detailed detector simulation. Table 22 summarizes the channels used, assumptions, performance and results of the three analyses. All three have used $B_s^0 \to D_s^-\pi^+$ and ATLAS has also used $B_s^0 \to D_s^- a_1^+$ followed by $a_1^+ \to \rho^0\pi^+$. The D_s^- is reconstructed via its decay into $\phi\pi^-$ followed by $\phi \to K^+K^-$ by all three experiments and also $D_s^- \to K^{*0}K^-$ followed by $K^+\pi^-$ by CMS. CMS has assumed a 50% efficiency of the higher level triggers for calculating the final yield of reconstructed B_s^0 mesons. ATLAS also reconstructed $D_s^- \to K^{*0}K^-$, but did not include it in their final analysis since after applying the cuts needed to obtain a reasonable rate of the level-2 trigger, the addition of this mode did not improve their limit. D_s^- decay modes other than $\phi\pi^-$ contributing to the $K^+K^-\pi^-$ final state will also be reconstructed by LHCb; for the yield presented in Tab. 22, an effective $D_s^- \to K^+K^-\pi^-$ branching ratio of 4% is assumed, with the same efficiency and purity as for $D_s^- \to \phi\pi^-$. For flavour tagging at production, ATLAS and CMS have used the trigger muon, which primarily comes from the semileptonic decay of

the other b hadron in the event. LHCb use identified muons, electrons and kaons from the decay of the other b hadron. Other tagging techniques will be developed in the future.

Figures 50 and 51 from ATLAS illustrate the sensitivity of ΔM_s measurements as a function of the integrated luminosity and the signal-content of the sample. 1000 experiments were performed at each ΔM_s point and a ΔM_s value was considered "reachable" if 95% of the experiments gave a value within 2σ of the input value. CMS and LHCb have defined two kinds of reaches — one for a measurement and the other one for 95% CL exclusion. Figure 52 shows the result for ΔM_s reach from CMS using the amplitude method. The amplitude, A, together with its error, σ_A, is shown for different x_s, where $x_s \equiv \Delta M_s/\Gamma_s$. x_s values below the intersection point of the $1.645\,\sigma_A$ curve and the line $A = 1$ are excluded at 95% CL. CMS determined their reach by a method similar to that used by ATLAS, but an experiment was considered "successful" if the x_s value corresponded to the highest peak in the amplitude spectrum and was in the vicinity of x_s^{true} within the natural width ($\pm$ 1.5 in x_s) of the amplitude distribution. The two methods yielded the same results. Figure 53 shows the statistical significance $S = 1/\sigma_A$ of the B_s^0 oscillation signal as a function of ΔM_s from LHCb. The LHCb reach for ΔM_s quoted in Tab. 22 is for $S = 5$ (5σ measurement) and $S = 1.645$ (95% CL exclusion). According to these studies, ΔM_s can be measured up to $30\,\text{ps}^{-1}$ (ATLAS), $26\,\text{ps}^{-1}$ (CMS) and $48\,\text{ps}^{-1}$ (LHCb) with one year of data. The addition of more channels is likely to improve the reach. Thus, each of the three experiments will be able to fully explore the ΔM_s range allowed in the SM, Eq. (7.16), after one year of data-taking. In addition, the likely precision on ΔM_s will be such that the extraction of $|V_{ts}/V_{td}|^2$ will be limited by the theoretical uncertainty on R_{sd} (see expressions (7.8) to (7.10)).

8 RARE DECAYS[22]

Flavour-changing neutral current decays involving $b \to s$ or $b \to d$ transitions occur only at loop-level in the SM, come with small exclusive branching ratios $\sim O(10^{-5})$ or smaller and thus provide an excellent probe of indirect effects of new physics and information on the masses and couplings of the virtual SM or beyond-the-SM particles participating. Within the SM, these decays are sensitive to the CKM matrix elements $|V_{ts}|$ and $|V_{td}|$, respectively; a measurement of these parameters or their ratio would be complementary to their determination from B mixing, discussed in Sec. 7.

The effective field theory for $b \to s(d)$ transitions is universal for all the channels discussed here. Due to space-restrictions, we cannot review all important features of that effective theory; for a quick overview we refer to Chapter 9 of the BaBar Physics Book [6], where also references to more detailed reviews can be found. Here we simply state that the effective Hamiltonian governing rare decays can be obtained from the SM Hamiltonian by performing an operator product expansion yielding

$$\mathcal{H}_{\text{eff}}^q = -\frac{4G_F}{\sqrt{2}}\, V_{tb}V_{tq}^* \sum_{i=1}^{11} C_i(\mu)\mathcal{O}_i^q(\mu), \tag{8.1}$$

where the $\mathcal{O}_i^q$ are local renormalized operators and $V_{tb}V_{tq}^*$ are CKM matrix elements with $q = s, d$. The Wilson-coefficients C_i can be calculated in perturbation theory and encode the relevant short-distance physics, in particular any potential new-physics effects. The renormalization-scale μ can be viewed as separating the long- and short-distance regimes. For calculating decay rates with the help of (8.1), the value of μ has to be chosen as $\mu \sim m_b$ in a truncated perturbative expansion. The Hamiltonian (8.1) is suitable to describe physics in the SM as well as in a number of its extensions, for instance the minimal SUSY model. The operator basis in (8.1) is, however, not always complete, and in some models, for instance those exhibiting left-right symmetry, new physics also shows up in the form of new operators. This proviso should be kept in mind when analysing rare B decays for new-physics effects by measuring Wilson-coefficients.

At present, the following channels have been evaluated for LHCb, CMS and ATLAS:

[22] Section coordinators: P. Ball and F. Rizatdinova with help from P. Bartalini, P. Koppenburg, M. Misiak, A. Nikitenko, N. Nikitin and E. Polycarpo.

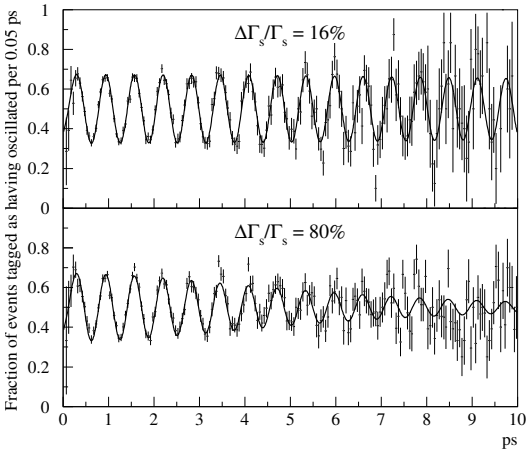

Fig. 49: Fraction of events tagged as having oscillated as a function of proper time for two different values of $\Delta\Gamma_s/\Gamma_s$, for $\Delta M_s = 10$ ps^{-1} [39]. The curves display the result of the maximum-likelihood fit to the total sample.

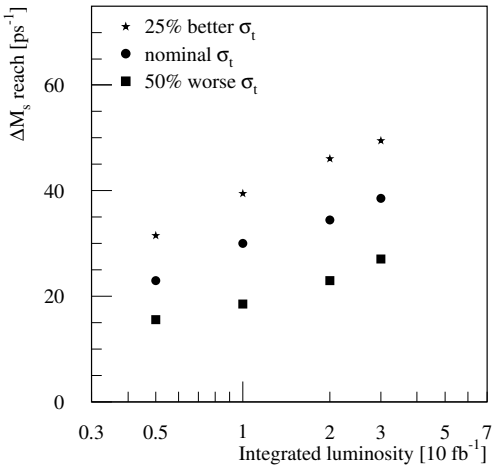

Fig. 50: ΔM_s reach of ATLAS as a function of the integrated luminosity for various proper time resolutions σ_t.

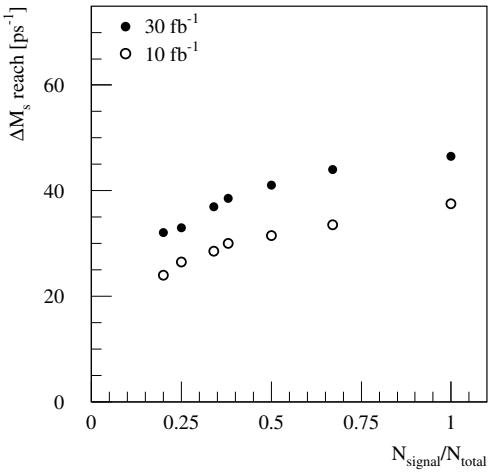

Fig. 51: ΔM_s reach of ATLAS as a function of the signal-content of the sample for nominal proper time resolution and integrated luminosities of 10 fb^{-1} and 30 fb^{-1}.

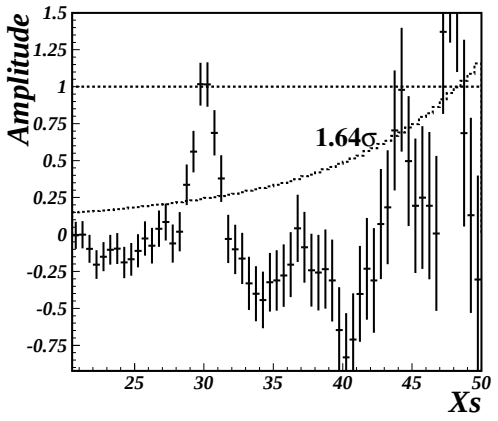

Fig. 52: The amplitude with its error, σ_A, for an input value of $x_s = 30$ from CMS.

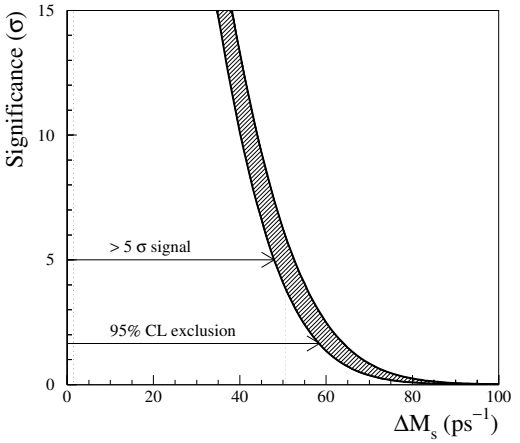

Fig. 53: Statistical significance of the B_s^0 oscillation signal as a function of ΔM_s. The band delimited by the two curves reflects the 1σ statistical uncertainty on the proper-time resolution of $\sigma_t = (43 \pm 2)$fs.

- purely muonic decays $B^0_{d,s} \to \mu^+\mu^-$ (all experiments);
- the radiative decay $B^0_d \to K^{*0}\gamma$ (LHCb only);
- semimuonic decays $B^0_d \to \rho^0\mu^+\mu^-$, $B^0_d \to K^{*0}\mu^+\mu^-$, $B^0_s \to \phi^0\mu^+\mu^-$ (all experiments).

As a reflection of this rather preliminary status of rare B decay studies for the LHC, we confine this section's discussion to channels most of which are in principle accessible at e^+e^- B factories and can also be studied at the Tevatron. This applies in particular to the radiative decay $B \to K^*\gamma$ that has already been measured at CLEO [153] and for which at the time of the first physics runs at the LHC rather accurate measurements should be available. The situation is different for $B \to \mu^+\mu^-$, which will be seen before the start of the LHC only if it is enhanced drastically, i.e. by orders of magnitude, by new-physics effects. Also the measurement of the spectra of $B \to K^*\mu^+\mu^-$ will be reserved to the LHC, although the decay itself should be seen at the B factories before. In general, and in contrast to the exploration of CP violation, the main impact of the LHC on the study of rare decays will be to provide radically increased statistics rather than opening new, alternative channels.

8.1 $B^0 \to \mu^+\mu^-$

This decay is an experimental favourite thanks to its unique signature and at the same time a challenge, as its SM branching ratio is of order 10^{-9}. The motivation for measuring this decay lies mainly in its rôle as indicator for possible new physics which might significantly enhance the branching ratio. The present experimental bounds from Tevatron are in the 10^{-6} range.

8.1.1 Theoretical Framework

The purely muonic neutral B decays are described by only three operators [154]:

$$O^q_P = (\bar{q}\gamma_5 b)(\bar{\mu}\gamma_5\mu), \qquad O^{q'}_P = (\bar{q}\gamma_5 b)(\bar{\mu}\mu), \qquad O^q_A = (\bar{q}\gamma^\alpha\gamma_5 b)(\bar{\mu}\gamma_\alpha\gamma_5\mu),$$

with $q = s, d$. In the SM, these transitions proceed through electroweak penguin diagrams with Z and H^0 exchange as well as W box diagrams. Introducing dimensionless Wilson-coefficients $C^{q,q'}_{P,A}$, the branching ratio is given by

$$B(B_q \to \mu^+\mu^-) = \frac{G_F^2}{8\pi}\,\tau_B f_B^2 m_B^3 \sqrt{1-\frac{4m_\mu^2}{m_B^2}}\left\{\left|C^q_P - \frac{2m_\mu}{m_B}\,C^q_A\right|^2 + \left(1-\frac{4m_\mu^2}{m_B^2}\right)\left|C^{q'}_P\right|^2\right\}. \quad (8.2)$$

In the SM, the coefficients C_P arise from penguin diagrams with physical and unphysical neutral scalar exchange and are suppressed by a factor $(m_b/m_W)^2$ [155]. The decay rate is then determined solely by the coefficient

$$C^q_{A,SM} = \frac{\alpha V_{tb}V^*_{tq}}{\sqrt{8}\pi\sin^2\theta_w}\,Y(x_t), \quad (8.3)$$

where $x_t \equiv m_t^2/m_W^2$, $\sin^2\theta_w$ is the weak mixing angle and the function $Y(x)$ is at leading order in QCD given by [156]

$$Y(x) = \frac{x}{8}\left[\frac{x-4}{x-1} + \frac{3x}{(x-1)^2}\,\ln x\right]. \quad (8.4)$$

The SM branching fractions are then given by (with f_{B_q} from (7.6), $|V_{td}|$ from (7.15) and $m_t = 167\,\text{GeV}$)

$$B(B_d \to \mu^+\mu^-) = (1.0 \pm 0.5)\times 10^{-10}\left[\frac{f_{B_d}}{200\,\text{MeV}}\right]^2\left[\frac{\overline{m}_t(\overline{m}_t)}{167\,\text{GeV}}\right]^{3.12}\left[\frac{|V_{td}|}{0.0074}\right]^2\left(\frac{\tau_{B_d}}{1.56\,\text{ps}}\right), \quad (8.5)$$

$$B(B_s \to \mu^+\mu^-) = (3.7 \pm 1.0)\times 10^{-9}\left[\frac{f_{B_s}}{230\,\text{MeV}}\right]^2\left[\frac{\overline{m}_t(\overline{m}_t)}{167\,\text{GeV}}\right]^{3.12}\left[\frac{|V_{ts}|}{0.040}\right]^2\left(\frac{\tau_{B_s}}{1.54\,\text{ps}}\right). \quad (8.6)$$

Due to these tiny SM branching ratios and the favourable experimental signature, these decay processes are ideal candidates for new physics to be observed, for example flavour-changing neutral Higgses. New-physics scenarios have been investigated e.g. in Refs. [155, 157].

8.1.2 Experimental Considerations

Purely muonic B decays, so-called "self-triggering" channels, have a clear signature that can be used at level-1 trigger in all LHC experiments. Only muon identification is necessary. The expected numbers of events quoted in the following refer to the SM branching ratios $B(B_s^0 \to \mu^+\mu^-) = (3.5 \pm 1.0) \times 10^{-9}$ and $B(B_d^0 \to \mu^+\mu^-) = 1.5 \times 10^{-10}$, i.e. the "optimistic" end of the theory prediction (8.5).

The CMS collaboration has performed a detailed study of the observability of $B_s^0 \to \mu^+\mu^-$ [158] at both low and high luminosity, implementing the complete pattern recognition and track reconstruction procedure. Both the gluon-fusion and the gluon-splitting production mechanisms are included and yield comparable contributions. CMS has tuned the experimental selection criteria to optimize the signal-to-background ratio as follows:

1. Only muon pairs satisfying the requirement $0.4 < \Delta R_{\mu\mu} < 1.2$ were considered as candidates for $B_s^0 \to \mu^+\mu^-$; the transverse momentum of the muon pair must be larger than 12 GeV and p_T of either muon be larger than 4.3 GeV.
2. The effective mass of the dimuon pair was required to be within a 80 MeV mass window around the nominal B_s^0 mass. Only 1.1% of background combinations are retained after this mass-cut.
3. The third set of cuts is based on the secondary vertex reconstruction: the distance between B_s^0 and primary vertex in the transverse plane is required to be larger than $12\sigma_{\rm vtx}$, about 820 μm, where $\sigma_{\rm vtx}$ is the vertex resolution. The angle α between the line joining primary and secondary vertex and transverse momentum vector was required to satisfy $\cos\alpha > 0.9997$. The absolute error of the secondary vertex reconstruction was required to be less than 80 μm. The distance between the two muons, d_2, had to be smaller than 50 μm and the ratio $d_2/\sigma(d_2)$ smaller than 2.
4. Isolation of the dimuon pair in the tracker was required, i.e. no charged particles with $p_T > 0.9$ GeV must be found in the cone $R < 0.5 \times \Delta R_{\mu\mu} + 0.4$ around the dimuon momentum direction. The isolation requirement is important for suppressing the background induced by gluon-splitting. About 50% of the signal- and 3% of the background-events passed through the isolation-cut in the tracker. An additional factor 2.3 of background-suppression was obtained by requiring isolation of the dimuon pair in the calorimeters, i.e. the transverse energy in the electromagnetic and hadron calorimeters was required to be less than 4 GeV in the same tracker cone.

After applying these cuts, the number of expected events detected by CMS after 3 years running at low luminosity is 21 with less than 3 background-events at 90% C.L., assuming the SM branching ratio. CMS will observe this channel even after 1 year running at low luminosity. Taking into account the production ratio $B_d^0/B_s^0 = 0.40/0.11$ and the expected SM branching ratio (8.5), CMS also expects, for three years running at low luminosity, to find 2.2 ± 1.1 $B_d \to \mu^+\mu^-$ events with again essentially no background.

LHCb's sensitivity to the decay $B_s \to \mu^+\mu^-$ has been studied using fully GEANT generated samples of both signal- and background-events. Good quality tracks are combined into a vertex if they are identified as muon tracks with high confidence level and are within 50 μm in space. The secondary vertex must also satisfy quality criteria and be well displaced from the primary vertex. The impact parameter of the reconstructed B_s candidate is required to be smaller than 35 μm and a mass window of 20 MeV around the nominal B_s mass is applied. After all those selection-cuts 11 signal-events per year are expected. Since the initial background-sample was very small compared to the number of events in one year of LHCb operation, pions which are a direct product of B decays were allowed to make pairs with muons, "faking" the background-signature, in order to increase the statistics of the sample. Using this procedure, it was possible to estimate the rejection power of the cuts in the impact parameter and the mass of the B_s candidate, assuming they are uncorrelated and that the mass distribution in a mass window of 200 MeV around the nominal value is flat. The expected background-yield in one year is 3.3 events. Studies with high statistics samples of full GEANT simulation are underway, in order to make the background-estimate more precise. Hence LHCb will observe the decay $B_s \to \mu^+\mu^-$ within 1 year of running.

The ATLAS collaboration has made a detailed study of the decay mode $B_s^0 \to \mu^+\mu^-$, using

Experiment	ATLAS	CMS	LHCb
Signal	27	21	33
Background	93	3	10

Table 23: Expected signal- and background-events for $B_s \to \mu^+\mu^-$ after 3 years running at low luminosity.

Experiment	ATLAS	CMS
$B_s^0 \to \mu^+\mu^-$	92	26
$B_d^0 \to \mu^+\mu^-$	14	4.1
Background	660	< 6.4

Table 24: The expected statistics for purely muonic decays after one year running at high luminosity.

fully simulated samples [37]. To suppress the combinatorial background, cuts on the quality of vertex reconstruction and on the decay length of the reconstructed B meson were applied. Further background-reduction was obtained by imposing cuts on the angle between the line joining primary and secondary vertex and the transverse momentum vector and on the isolation of the dimuon pair formed in the decay of the B meson. The mass resolution obtained after all selection-cuts is $\sigma(M) = 68\,\text{MeV}$. The mass window $^{+2\sigma}_{-1\sigma}$ was taken for estimating the number of signal- and background-events. After applying cuts, the number of expected events detected by ATLAS after 3 years running at low luminosity, assuming the SM branching fraction, is 27 with 93 background-events. For $B_d^0 \to \mu^+\mu^-$, one can expect 4 signal-events with 93 background-events.

Hence, all three experiments will be able to measure the SM branching fraction of $B_s^0 \to \mu^+\mu^-$. The numbers of events expected by the three collaborations after 3 years' data collection are given in Tab. 23.

Both ATLAS and CMS are planning to continue the study of purely muonic decays at high luminosity $10^{34}\text{cm}^{-2}\text{s}^{-1}$. This is made possible by the low dimuon trigger rate which is expected to be around 30 Hz in ATLAS. In both experiments, the number of minimum bias events accepted together with the triggered events is expected to be 10 times larger than at the LHC run at low luminosity. The CMS collaboration estimated the possibility to detect the purely muonic decay using a high luminosity pixel configuration that leads to degradation of the vertex resolution. The ATLAS collaboration assumed that the geometry of the inner detector will be the same as at low luminosity (no degradation in vertex and p_T resolution is expected compared to the low luminosity results). The same analysis-cuts as at low luminosity were applied to the signal- and background-events by both collaborations. The resulting numbers of events expected by the ATLAS and CMS collaborations after 1 year running at high luminosity are given in Tab. 24, assuming the SM branching fraction. The decay $B_s^0 \to \mu^+\mu^-$ can clearly be observed after 1 year running at high luminosity by both collaborations. Concerning $B_d^0 \to \mu^+\mu^-$, the sensitivity of ATLAS to the branching ratio will be at the level of 3×10^{-10}, i.e. roughly a factor 3 above the SM prediction. High luminosity measurements of the purely muonic decays would significantly improve the data to be obtained at low luminosity.

8.2 $B \to K^*\gamma$

In this subsection we discuss the specifics of the radiative FCNC transition $B \to K^*\gamma$ relevant for the LHC, concentrating on non-perturbative QCD effects. For the treatment of perturbative issues, in particular the reduction of renormalization-scale dependence and remaining uncertainties, we refer to [159, 160].

8.2.1 Theoretical Framework

The theoretical description of the $B \to K^*\gamma$ decay is quite involved with regard to both long- and short-distance contributions. In terms of the effective Hamiltonian (8.1), the decay amplitude can be written as

$$\mathcal{A}(\bar{B} \to \bar{K}^*\gamma) = -\frac{4G_F}{\sqrt{2}} V_{tb}V_{ts}^* \langle \bar{K}^*\gamma | C_7 O_7 + i\epsilon^\mu \sum_{i\neq 7} C_i \int d^4x e^{iqx} T\{j_\mu^{em}(x) O_i(0)\} | \bar{B}\rangle \,, \qquad (8.7)$$

where j_μ^{em} is the electromagnetic current and ϵ_μ the polarization vector of the photon. O_7 is the only operator containing the photon field at tree-level:

$$O_7 = \frac{e}{16\pi^2}\, m_b \bar{s}\sigma_{\mu\nu} R b F^{\mu\nu} \tag{8.8}$$

with $R = (1+\gamma_5)/2$. Other operators, the second term in (8.7), contribute mainly closed fermion loops. The first complication is now that the first term in (8.7) depends on the regularization- and renormalization-scheme. For this reason, one usually introduces a scheme-independent linear combination of coefficients, called "effective coefficient" (see [160] and references therein):

$$C_7^{\rm eff}(\mu) = C_7(\mu) + \sum_{i=3}^{6} y_i C_i(\mu), \tag{8.9}$$

where the numerical coefficients y_i are given in [160].

The current-current operators

$$O_1 = (\bar{s}\gamma^\mu L b)(\bar{c}\gamma_\mu L c), \qquad O_2 = (\bar{s}\gamma_\mu L c)(\bar{c}\gamma^\mu L b) \tag{8.10}$$

give vanishing contribution to the perturbative $b \to s\gamma$ amplitude at one loop. Thus, to leading logarithmic accuracy (LLA) in QCD and neglecting long-distance contributions from $O_{1,2}$ to the $b\bar{s}\gamma X$ Green's functions, the $\bar{B} \to \bar{K}^*\gamma$ amplitude is given by

$$\mathcal{A}_{O_7}^{\rm LLA}(\bar{B} \to \bar{K}^*\gamma) = -\frac{4G_F}{\sqrt{2}}\, V_{tb}V_{ts}^* C_7^{(0)\rm eff} \langle \bar{K}^*\gamma | O_7 | \bar{B}\rangle. \tag{8.11}$$

Here, $C_7^{(0)\rm eff}$ denotes the leading logarithmic approximation to $C_7^{\rm eff}$. The above expression is, however, not the end of the story, as the second term in (8.7) also contains long-distance contributions. Some of them can be viewed as the effect of virtual intermediate resonances $\bar{B} \to \bar{K}^* V^* \to \bar{K}^*\gamma$. The main effect comes from $c\bar{c}$ resonances and is contributed by the operators O_1 and O_2 in (8.7). It is governed by the virtuality of V^*, which, for a real photon, is just $-1/m_{V^*}^2 \sim -1/4m_c^2$. The presence of such power-suppressed terms $\sim 1/m_c^2$ has first been derived for inclusive decays in Ref. [161] in a framework based on operator product expansion. The first, and to date only, study for exclusive decays was done in [162]. Technically, one performs an operator product expansion of the correlation function in (8.7), with a soft non-perturbative gluon being attached to the charm-loop, resulting in terms being parametrically suppressed by inverse powers of the charm quark mass. As pointed out in [163], although the power increases for additional soft gluons, it is possible that contributions of additional external hard gluons could remove the power-suppression. This question is also relevant for inclusive decays and deserves further study.

After inclusion of the power-suppressed terms $\sim 1/m_c^2$, the $\bar{B} \to \bar{K}^*\gamma$ amplitude reads

$$\mathcal{A}^{\rm LLA}(B \to \bar{K}^*\gamma) = -\frac{4G_F}{\sqrt{2}}\, V_{tb}V_{ts}^* \langle \bar{K}^*\gamma \mid C_7^{(0)\rm eff} O_7 + \frac{1}{4m_c^2}\, C_2^{(0)} O_F \mid \bar{B}\rangle. \tag{8.12}$$

Here, O_F is the effective quark-quark-gluon operator obtained in [162], which describes the leading non-perturbative corrections. The two hadronic matrix elements can be described in terms of three form factors, T_1, L and $\tilde{L}$:

$$\begin{aligned}
\langle \bar{K}^*(p)\gamma | \bar{s}\sigma_{\mu\nu} q^\nu b | \bar{B}(p_B)\rangle &= i\epsilon_{\mu\nu\rho\sigma}\epsilon_\gamma^{*\mu}\epsilon_{K^*}^{*\nu} p_B^\rho p^\sigma 2T_1(0), \\
\langle \bar{K}^*(p)\gamma | O_F | \bar{B}(p_B)\rangle &= \frac{e}{36\pi^2}\Big[L(0)\epsilon_{\mu\nu\rho\sigma}\epsilon_\gamma^{*\mu}\epsilon_{K^*}^{*\nu} p_B^\rho p^\sigma \\
&\quad + i\tilde{L}(0)\left\{ (\epsilon_{K^*}^* p_B)(\epsilon_\gamma^* p_B) - \frac{1}{2}\,(\epsilon_{K^*}^*\epsilon_\gamma^*)(m_B^2 - m_{K^*}^2)\right\}\Big].
\end{aligned} \tag{8.13}$$

The calculation of the above form factors requires genuinely non-perturbative input. Available methods include, but do not exhaust, lattice calculations and QCD sum rules. Again, a discussion of the respective strengths and weaknesses of these approaches is beyond the scope of this report. Let it suffice to say that – at least at present – lattice cannot reach the point $(p_B - p)^2 = 0$ relevant for $B \to K^*\gamma$, and that QCD sum rules on the light-cone predict [35]

$$T_1(0) = 0.38 \pm 20\% \tag{8.14}$$

at the renormalization scale $\mu = 4.8\,\text{GeV}$. For the other two form factors, QCD sum rules predict [162]

$$L(0) = (0.55 \pm 0.10)\,\text{GeV}^3, \qquad \tilde{L}(0) = (0.7 \pm 0.1)\,\text{GeV}^3. \tag{8.15}$$

Numerically, these corrections increase the decay rate by about 5 to 10%. After their inclusion, one obtains

$$\begin{aligned} B(B \to K^*\gamma) &= \frac{\alpha}{32\pi^4}\, G_F^2 |V_{tb}V_{ts}^*|^2 \left|C_7^{(0)\text{eff}}\right|^2 m_b^2\, \frac{(m_B^2 - m_{K^*}^2)^3}{m_B^3}\, |T_1(0)|^2 \\ &\quad \times \left(1 - \frac{1}{18 m_c^2}\, \frac{C_2^{(0)}}{C_7^{(0)\text{eff}}}\, \frac{1}{m_b}\, \frac{L(0) + \tilde{L}(0)}{T_1(0)}\right) \\ &= 4.4 \times 10^{-5}(1 + 8\%) \end{aligned} \tag{8.16}$$

for the central values of the QCD sum rule results, which agrees with the experimental measurement.

Let us close this subsection with a few remarks on the decay $B \to \rho\gamma$. Although at first glance it might seem that its structure is the same as that of $B \to K^*\gamma$, this is actually not the case. There are additional long-distance contributions to $B \to \rho\gamma$, which are CKM-suppressed for $B \to K^*\gamma$ and have been neglected in the previous discussion; these contributions comprise

- weak annihilation mediated by $O_{1,2}^u$ with non-perturbative photon emission from light quarks; these contributions are discussed in [164] and found to be of order 10% at the amplitude level;
- effects of virtual $u\bar{u}$ resonances (ρ, ω,...); they are often said to be small, but actually have not been studied yet in a genuinely non-perturbative framework, so that statements about their smallness lack proper justification.

For the above reasons it is, at present, premature to aim at an accurate determination of $|V_{ts}|/|V_{td}|$ from a measurement of $B(B \to \rho\gamma)$ and $B(B \to K^*\gamma)$. A very recent discussion of long-distance effects in $B \to V\gamma$ decays can also be found in Ref. [165].

8.2.2 Experimental Considerations

The radiative decay $B_d^0 \to K^{*0}\gamma$ has been studied by the LHCb collaboration at both the particle and the full-simulation level [166]. The event selection and reconstruction can be summarized as follows:

- selection: $X^+X^-\gamma$ combinations; tracks are consistent with K^-- and π^+-hypotheses; $|M(K^-\pi^+)$–$M(K^{*0})| < 55$ MeV; cluster in the electromagnetic calorimeter with $E_T > 4\,\text{GeV}$;
- geometrical cuts: $\chi^2 < 9$ of secondary vertex fit; $|\Delta(Z)| > 1.5\,\text{mm}$ between primary and secondary vertex; impact parameters of both tracks $> 400\mu$m; the angle between the momentum vector and the line joining primary and secondary vertex smaller than 0.1 rad; the angle θ between B_d^0 and K^- in the K^{*0} rest frame $|\cos\theta| < 0.6$;
- $p_T > 4\,\text{GeV}$ of reconstructed B_d^0.

The mass resolution obtained at the particle-level study is 67 MeV. The mass window taken for estimates is 200 MeV around the nominal B_d^0 mass. Assuming $B(B_d^0 \to K^{*0}\gamma) = (4.9 \pm 2.0) \times 10^{-5}$, the expected number of signal-events after 1 year running is 26000, with $S/B \sim 1$. This will be sufficient to measure the branching fraction with high accuracy. The expected accuracy in the CP asymmetry measurement is $\delta_{CP} = 0.01$. The SM predicts a CP asymmetry of order 1%.

8.3 $B \to K^* \mu^+ \mu^-$

Like with $B \to K^* \gamma$, we can only review the essentials and put emphasis on recent developments in theory and the specifics for the LHC experiments. A slightly more detailed discussion and relevant references can be found in the BaBar physics book [6]. The current state-of-the-art of perturbation theory is summarized in Ref. [167]. The motivation for studying this decay is either, assuming the SM to be correct, the measurement of the CKM matrix element $|V_{ts}|$, or the search for manifestations of new physics in non-standard values of the Wilson-coefficients. A very suitable observable for the latter purpose is the forward-backward asymmetry which is independent of CKM matrix elements and, due to extremely small event numbers, only accessible at the LHC. Of all the rare decay channels discussed in this section, $B \to K^* \mu^+ \mu^-$ is definitely the one whose detailed study is only possible at the LHC and which has the potential for high impact both on SM physics and beyond.

8.3.1 Theoretical Framework

The presentation in this section follows closely Ref. [168]; for other relevant recent papers treating $B \to K^* \mu^+ \mu^-$, see [169].

At the quark-level, the effective Hamiltonian (8.1) leads to the following decay amplitude:

$$\begin{aligned}\mathcal{A}(b \to s\mu^+\mu^-) = \frac{G_F \alpha}{\sqrt{2}\pi} V_{ts}^* V_{tb} \Big\{ & C_9^{\text{eff}}(s) \, [\bar{s}\gamma_\alpha L b] \, [\bar{\mu}\gamma^\alpha \mu] + C_{10} \, [\bar{s}\gamma_\alpha L b] \, [\bar{\mu}\gamma^\alpha \gamma_5 \mu] \\ & -2 m_b C_7^{\text{eff}} \left[\bar{s} i \sigma_{\alpha\nu} \frac{q^\nu}{s} R b \right] [\bar{\mu}\gamma^\alpha \mu] \Big\} . \end{aligned} \tag{8.17}$$

Here, $L/R = (1 \mp \gamma_5)/2$, $s = q^2$, $q = p_+ + p_-$, where $p_\pm$ are the four-momenta of the leptons. We neglect the strange quark mass, but keep the leptons massive. Already the free quark decay amplitude $\mathcal{A}(b \to s\mu^+\mu^-)$ contains certain long-distance effects which usually are absorbed into a redefinition of the Wilson-coefficient C_9. To be specific, we define, for exclusive decays, the *momentum-dependent* effective coefficient of the operator $\mathcal{O}_9 = e^2/(16\pi^2)(\bar{s}\gamma_\alpha L b)(\bar{\mu}\gamma^\alpha \mu)$ as

$$C_9^{\text{eff}}(s) = C_9 + Y(s), \tag{8.18}$$

where $Y(s)$ stands for matrix elements of four-quark operators. Formulas can be found in [170]. The prominent contribution to $Y(s)$ comes from the $c\bar{c}$ resonances J/ψ, ψ', ψ'' which show up as peaks in the dimuon spectrum, but are irrelevant for the short-distance physics one is interested in. Note that the effective coefficient depends on the process being considered and is, in particular, not the same for exclusive and inclusive decays: in the latter ones, also virtual and bremsstrahlung corrections to $\langle \mu^+\mu^- s|\mathcal{O}_9|b\rangle$, usually denoted by $\omega(s)$, are included, whereas for exclusive decays, they are contained in the hadronic matrix elements to be defined below. For s far below the $c\bar{c}$ threshold, perturbation theory, augmented by non-perturbative power-corrections in $1/m_c^2$, is expected to yield a reliable estimate for long-distance effects in C_9^{eff}. In contrast to inclusive decays, however, the corresponding $1/m_c^2$ terms have not yet been worked out for exclusive decays. To date, one has to rely on phenomenological prescriptions for incorporating non-perturbative contributions to $Y(s)$ [171]. The resulting uncertainties on C_9^{eff} and on various distributions in inclusive decays have been worked out in Refs. [170, 167] to which we refer for a detailed discussion.

Other long-distance corrections, specific for the exclusive decay $B \to K^* \mu^+ \mu^-$, are described in terms of matrix elements of the quark operators in (8.17) between meson states and can be parametrized in terms of form factors. Denoting by ϵ_μ the polarization vector of the K^* vector meson, we define

$$\begin{aligned}\langle K^*(p)|(V-A)_\mu|B(p_B)\rangle = & -i\epsilon_\mu^*(m_B + m_{K^*}) A_1(s) + i(p_B+p)_\mu (\epsilon^* p_B) \frac{A_2(s)}{m_B + m_{K^*}} \\ & + i q_\mu (\epsilon^* p_B) \frac{2 m_{K^*}}{s} \, (A_3(s) - A_0(s)) + \epsilon_{\mu\nu\rho\sigma} \epsilon^{*\nu} p_B^\rho p^\sigma \frac{2V(s)}{m_B + m_{K^*}} , \end{aligned}$$

	A_1	A_2	A_0	V	T_1	T_2	T_3
$F(0)$	0.337	0.282	0.471	0.457	0.379	0.379	0.260
c_1	0.602	1.172	1.505	1.482	1.519	0.517	1.129
c_2	0.258	0.567	0.710	1.015	1.030	0.426	1.128

Table 25: Central values of parameters for the parametrization (8.20) of the $B \to K^*$ form factors. Renormalization scale for T_i is $\mu = m_b$.

$$\begin{aligned}\langle K^*(p)|\bar{s}\sigma_{\mu\nu}q^\nu(1+\gamma_5)b|B(p_B)\rangle &= i\epsilon_{\mu\nu\rho\sigma}\epsilon^{*\nu}p_B^\rho p^\sigma\, 2T_1(s)\\ &+T_2(s)\left\{\epsilon_\mu^*(m_B^2-m_{K^*}^2)-(\epsilon^* p_B)\,(p_B+p)_\mu\right\}+T_3(s)(\epsilon^* p_B)\left\{q_\mu-\frac{s}{m_B^2-m_{K^*}^2}\,(p_B+p)_\mu\right\}\end{aligned} \tag{8.19}$$

with

$$A_3(s)=\frac{m_B+m_{K^*}}{2m_{K^*}}\,A_1(s)-\frac{m_B-m_{K^*}}{2m_{K^*}}\,A_2(s),\qquad A_0(0)=A_3(0),\qquad T_1(0)=T_2(0).$$

The form factors T_i are renormalization-scale dependent. All signs are defined in such a way as to render the form factors positive. The physical range in s extends from $s_{min}=0$ to $s_{max}=(m_B-m_{K^*})^2$. As described in the last subsection for the $B\to K^*\gamma$ form factor T_1, the above form factors are essentially non-perturbative. Lacking results from lattice calculations, we quote the form factors as calculated from QCD sum rules on the light-cone [126, 35], in the parametrization suggested in [168], where also a discussion of the theoretical uncertainties can be found. The form factors can be parametrized as

$$F(s)=F(0)\exp(c_1\hat{s}+c_2\hat{s}^2) \tag{8.20}$$

with $\hat{s}=s/m_B^2$. The central values of the parameters c_i are given in Tab. 25.

Let us now turn to the various decay distributions relevant for the phenomenological analysis. For lack of space, we cannot give detailed expressions for decay amplitudes and spectra in terms of the hadronic matrix elements (8.19); they can be found in [168]. Besides the total branching fraction and the spectrum in the dimuon mass, it is in particular the forward-backward asymmetry that is interesting for phenomenology. It is defined as

$$A_{FB}(s)=\frac{1}{d\Gamma/ds}\left(\int_0^1 d(\cos\theta)\frac{d^2\Gamma}{ds\,d\cos\theta}-\int_{-1}^0 d(\cos\theta)\frac{d^2\Gamma}{ds\,d\cos\theta}\right), \tag{8.21}$$

where θ is the angle between the momenta of the B meson and the μ^+ in the dilepton centre-of-mass system. The asymmetry is governed by

$$A_{FB}\propto C_{10}\left[\mathrm{Re}\left(C_9^{\mathrm{eff}}\right)V(s)A_1(s)+\frac{\hat{m}_b}{\hat{s}}\,C_7^{\mathrm{eff}}\left\{V(s)T_2(s)\,(1-\hat{m}_{K^*})+A_1(s)T_1(s)\,(1+\hat{m}_{K^*})\right\}\right]. \tag{8.22}$$

In the SM, A_{FB} exhibits a zero at $s=s_0$, given by

$$\mathrm{Re}\left(C_9^{\mathrm{eff}}(s_0)\right)=-\frac{\hat{m}_b}{\hat{s}}\,C_7^{\mathrm{eff}}\left\{\frac{T_2(s_0)}{A_1(s_0)}\,(1-\hat{m}_{K^*})+\frac{T_1(s_0)}{V(s_0)}\,(1+\hat{m}_{K^*})\right\}. \tag{8.23}$$

The forward-backward asymmetry has a zero if and only if

$$\mathrm{sign}(C_7^{\mathrm{eff}}\mathrm{Re}\,C_9^{\mathrm{eff}})=-1. \tag{8.24}$$

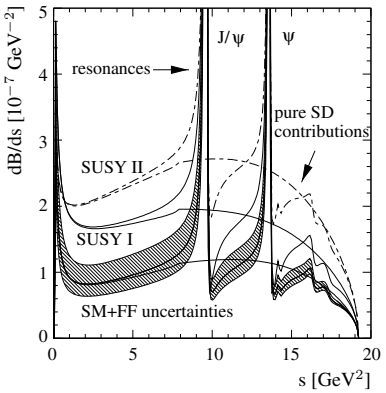

Fig. 54: Dimuon-mass spectrum of $B \to K^*\mu^+\mu^-$ in the SM and two SUSY models

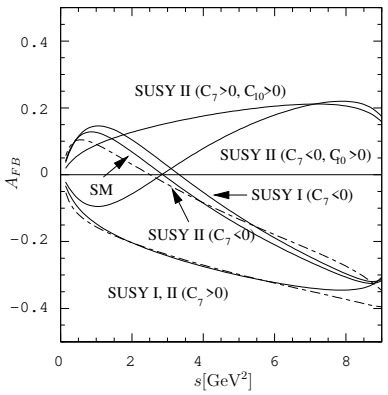

Fig. 55: Forward-backward asymmetry of $B \to K^*\mu^+\mu^-$ in the SM and two SUSY models.

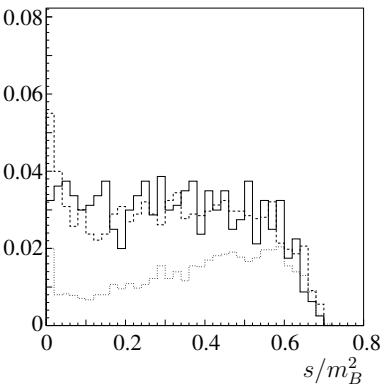

Fig. 56: ATLAS' dilepton-mass distribution for 3 data-sets: solid line: PYTHIA, dashed: GI, dotted: ISGW2.

It is interesting to observe that in the Large Energy Effective Theory (LEET) [172], both ratios of the form factors appearing in Eq. (8.23) have essentially no hadronic uncertainty, i.e. all dependence on intrinsically non-perturbative quantities cancels, and one has simply

$$\frac{T_2(s)}{A_1(s)} = \frac{1+\hat{m}_{K^*}}{1+\hat{m}_{K^*}^2-\hat{s}}\left(1-\frac{\hat{s}}{1-\hat{m}_{K^*}^2}\right), \qquad \frac{T_1(s)}{V(s)} = \frac{1}{1+\hat{m}_{K^*}}\,. \tag{8.25}$$

These relations are fulfilled by QCD sum rules on the light-cone to 2% accuracy, which indicates that corrections to the LEET limit are extremely small. In that limit, one thus has a particularly simple form for the equation determining s_0, namely

$$\mathrm{Re}(C_9^{\mathrm{eff}}(s_0)) = -2\,\frac{\hat{m}_b}{\hat{s}_0}\,C_7^{\mathrm{eff}}\frac{1-\hat{s}_0}{1+\hat{m}_{K^*}^2-\hat{s}_0}\,. \tag{8.26}$$

Thus, the precision of the zero of the forward-backward asymmetry in $B \to K^*\mu^+\mu^-$ is determined essentially by the precision of the ratio of the effective coefficients and m_b and is *largely independent of hadronic uncertainties*. The insensitivity of s_0 to the decay form factors in $B \to K^*\mu^+\mu^-$ is a remarkable result, which has first been observed in [173] by scanning over a number of form factor models. LEET puts this observation on theoretically more rigorous grounds, although (8.25), and consequently (8.26) are expected to be modified by hard perturbative QCD corrections. In the SM, one finds $s_0 \approx 2.9\,\mathrm{GeV}^2$ at $\mu = 4.8\,\mathrm{GeV}$. From Eq. (8.23) it also follows that there is no zero below the $c\bar{c}$ resonances if both C_9^{eff} and C_7^{eff} have the same sign as predicted in some beyond-the-SM models. Thus, condition (8.24) provides a discrimination between the SM and certain models with new physics. Due to space limitations we cannot discuss in detail the possible impact of particular beyond-the-SM scenarios on the decay distributions introduced above. To illustrate the fact that large effects are indeed possible, we show, in Figs. 54 and 55, the results for the dimuon spectrum and the forward-backward asymmetry obtained in [168] for several SUSY-extensions of the SM.

Note that the above formulas and considerations cannot immediately be applied to the decay $B \to \rho\mu^+\mu^-$, whose measurement could, in principle, together with that of $B \to K^*\mu^+\mu^-$, be used to determine the ratio of CKM matrix elements $|V_{ts}/V_{td}|$, as an alternative to the determination from B mixing. The problem lies in new contributions to C_9^{eff} originating from light-quark loops and associated with the presence of low-lying resonances, for instance ρ and ω, in the dimuon spectrum. These contributions are CKM-suppressed in $B \to K^*\mu^+\mu^-$, so that the corresponding uncertainties can be neglected, but they are unsuppressed in $B \to \rho\mu^+\mu^-$ decays. The problematic part in that is that the theory tools that allow one to treat $c\bar{c}$ resonance contributions to $B \to K^*\mu^+\mu^-$ are not applicable any more: perturbation theory does only work in the unphysical region $s < 0$, and an operator-product expansion which would

indicate potential power-suppressed terms also fails. No satisfactory solution to that problem is presently available.

Finally, we note that the analysis of $B_s \to \phi\mu^+\mu^-$ parallels exactly that of $B_d \to K^*\mu^+\mu^-$; the corresponding form factors can be found in Ref. [35]. Also semimuonic decays with a pseudoscalar meson in the final state, e.g. $B_d \to K\mu^+\mu^-$ and $B_d \to \pi\mu^+\mu^-$, are, from a theoretical point of view, viable sources for information on short-distance physics and CKM matrix elements. Their experimental detection is, however, extremely difficult due to the overwhelming combinatorial background; no experimental feasibility studies exist to date.

8.3.2 Experimental Considerations

As with $B \to \mu^+\mu^-$, the semimuonic decays $B_d^0 \to K^*\mu^+\mu^-$ are "self-triggering" channels thanks to the presence of two muons with high p_T in the final state. Particle identification helps decisively in separating the final-state hadrons. All three experiments assume the branching ratio $B(B_d^0 \to K^{*0}\mu^+\mu^-) = 1.5 \times 10^{-6}$ for estimating the number of events to be observed.

ATLAS have investigated form factor effects on the detection of $B_d^0 \to K^{*0}\mu^+\mu^-$; details of the analysis can be found in [174]. Two different parametrizations of the hadronic matrix elements (8.19), GI and ISGW2, were implemented into PYTHIA and the final numbers of expected events after trigger-cuts were evaluated for these two samples of signal-events. The dimuon mass distribution is shown in Fig. 56 for the case of the phase-space decay, GI and ISGW2 parametrizations. It was found that the matrix elements practically do not change the inclusive parameters of the muons and the K^{*0} meson, which is important for triggering these events. They do, however, strongly influence the spectrum in the dimuon mass and the forward-backward asymmetry. Although quark model calculations of form factors like GI and ISGW2 may serve as rough guidelines for first estimates, they do not reflect the modern state-of-the-art of theoretical calculations. For this reason, it is important to extend existing studies, taking advantage of the recent developments in the theoretical calculation of hadronic matrix elements as discussed in Sec. 8.3.1, and in particular to use only such model calculations that reproduce the model-independent results for certain form factor ratios like (8.25).

The ATLAS collaboration has studied the decays $B_d^0 \to \rho^0\mu^+\mu^-$, $B_d^0 \to K^{*0}\mu^+\mu^-$ and $B_s^0 \to \phi^0\mu^+\mu^-$. All these channels were fully simulated and reconstructed in the inner detector. As possible background, the following reactions have been considered: B_d^0 meson decays to $J/\psi K_S^0$, $\omega^0\mu^+\mu^-$, reflection of $B_d^0 \to \rho^0\mu^+\mu^-$ and $B_d^0 \to K^{*0}\mu^+\mu^-$ to other signal-channels; B_s^0 meson decays to $K^{*0}(\phi)\mu^+\mu^-$, semimuonic decays of one of the b quarks and semimuonic decays of both b quarks. An additional minimum bias of 2.4 events in the precision tracker and 3.2 events in the transition radiation tracker were taken into account when studying the signal and background. The expected results for observing these three channels are shown in Fig. 57.

Assuming the SM to be valid, the measurement of the branching fractions of the decays $B_d^0 \to \rho^0\mu^+\mu^-$ and $B_d^0 \to K^{*0}\mu^+\mu^-$ gives, in principle, the possibility to extract the ratio of the CKM elements $|V_{td}|/|V_{ts}|$ using the following equation:

$$\frac{N(B_d^0 \to \rho^0\mu^+\mu^-)}{N(B_d^0 \to K^{*0}\mu^+\mu^-)} = k_d \frac{|V_{td}|^2}{|V_{ts}|^2} \,. \tag{8.27}$$

The quantity k_d depends on form factors and Wilson-coefficients and also on the experimental cuts. Although there exist claims in the literature that, with proper cuts, k_d may be calculated with small hadronic uncertainties, see e.g. [175], these papers tend to underestimate the uncertainty associated with the impact on $c\bar{c}$ resonances on the spectrum (for $B_d^0 \to \rho^0\mu^+\mu^-$, there are also $u\bar{u}$ resonances whose contributions are often completely ignored). Our present knowledge of these long-distance effects in C_9^{eff} is, as has also been discussed in the theory subsection, unsatisfactory and calls for improved theory studies.

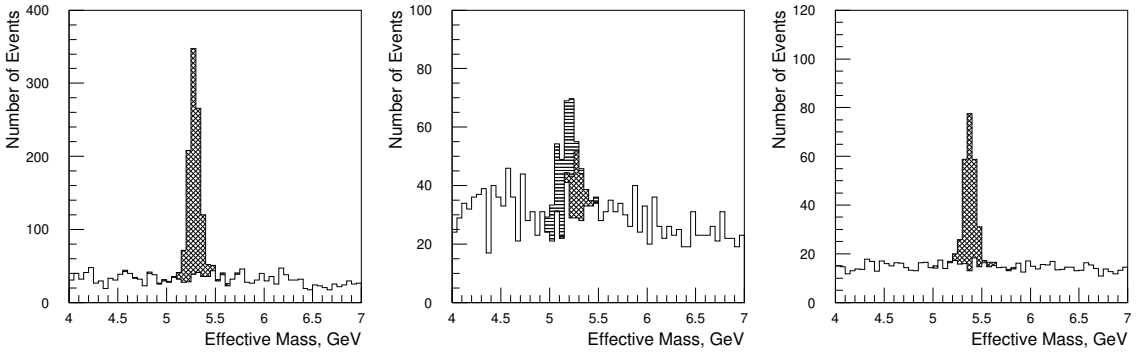

Fig. 57: $B_d^0 \to K^{*0}\mu^+\mu^-$ (left), $B_d^0 \to \rho^0\mu^+\mu^-$ (centre) and $B_s^0 \to \phi^0\mu^+\mu^-$ (right) signals with background as simulated by ATLAS. The cross-hatched histogram shows the $B_d^0 \to \rho^0\mu^+\mu^-$ signal, and the horizontally hatched one the reflection of $B_d^0 \to K^{*0}\mu^+\mu^-$ to $B_d^0 \to \rho^0\mu^+\mu^-$.

Interval	$\hat{s}_{min} \div 0.14$	$0.14 \div 0.33$	$0.55 \div \hat{s}_{max}$
ATLAS δA_{FB} (3 years)	5%	4.5%	6.5%
LHCb δA_{FB} (1 year)	2.4%	2.4%	5.8%
SM A_{FB}	10%	–14%	–29 %
MSSM A_{FB}	$(-17 \div 0.5)\%$	$(-35 \div -13)\%$	$(-33 \div -29)\%$

Table 26: Expected precision for asymmetry measurements at ATLAS and LHCb, for 3 and 1 years running, respectively, at low luminosity and assuming SM branching ratios; the experimental numbers rely on [176] and the theoretical predictions on the form factors in the GI parametrization and MSSM parameters as discussed in [177]. The kinematic limits are given by $\hat{s}_{min} = 4m_\mu^2/m_B^2$ and $\hat{s}_{max} = (m_B - m_{K^*})^2/m_B^2$.

ATLAS also studied the prospects for measuring the forward-backward (FB) asymmetry A_{FB}, defined in (8.21). Experimentally, the following quantity will be measured:

$$\langle A_{FB}\rangle_{[s_1,s_2]} = \frac{\langle N_F\rangle_{[s_1,s_2]} - \langle N_B\rangle_{[s_1,s_2]}}{\langle N_F\rangle_{[s_1,s_2]} + \langle N_B\rangle_{[s_1,s_2]}}\,, \tag{8.28}$$

where $\langle N_F\rangle_{[s_1,s_2]}$ and $\langle N_B\rangle_{[s_1,s_2]}$ are the numbers of positively charged leptons (including those from background) moving in the forward and backward directions of the B meson, respectively, in the range of the squared dimuon mass $s \in [s_1, s_2]$. In Fig. 55, we show the SM prediction for A_{FB} together with predictions in several SUSY extensions of the SM, which are characterized by the possibility that the Wilson-coefficients $C_7^{\rm eff}$ and/or $C_9^{\rm eff}$ can change sign with respect to the SM. As discussed in the previous subsection, the behaviour of the asymmetry with s depends crucially on these signs. For example, if the asymmetry turns out to be negative at small s, then this means that there is new physics beyond the SM.

The precision for asymmetry measurements in three different s intervals was estimated by ATLAS. The data are presented in Tab. 26, together with asymmetry values in the SM and one exemplary SUSY model, integrated over the corresponding intervals in $\hat{s} = s/m_B^2$. The expected accuracy of the asymmetry measurement with the ATLAS detector will be sufficient to distinguish between the SM and some of its extensions. It should, however, be stressed that new-physics effects *not* yielding sign-flips of the Wilson-coefficients do not change A_{FB} dramatically as compared to the SM.

LHCb has also performed an analysis of $B_d^0 \to K^{*0}\mu^+\mu^-$. The matrix elements reproducing the correct dimuon mass distribution were implemented into PYTHIA. The detector response for both signal- and background-events was simulated and the charged particles were reconstructed in the detector. LHCb expects to observe 4500 $B_d^0 \to K^{*0}\mu^+\mu^-$ events per year. For background-studies, the following reactions were simulated with PYTHIA: $B_d^0 \to K^{*0}\mu^+\mu^-$, $B_d^0 \to J/\psi(K^{*0}, K_S^0, \phi, K^+)$, with the subsequent decay of J/ψ into two muons, inclusive $B \to 4\pi$, $b \to \mu X, \overline{b} \to \mu X$ and $B \to \mu D(\mu X)X$. The

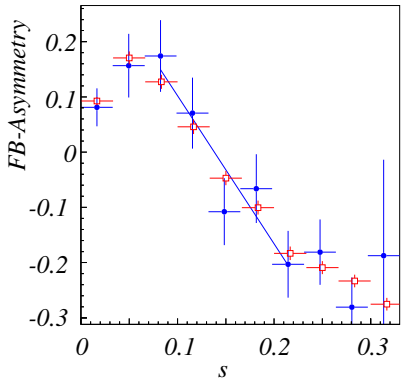

Fig. 58: LHCb fit of the FB-asymmetry A_{FB} for $B \to K^* \mu^+ \mu^-$ around the zero $\hat{s}_0$ with $A_{FB}(\hat{s}_0) = 0$. Squares denote generated and dots reconstructed data (one year statistics). The linear fit of reconstructed data intersects at 0.138 ± 0.035 (only statistical error).

Channel	B	ATLAS		CMS	LHCb	
		Signal	BG	Signal	Signal	BG
$B_d^0 \to \rho^0 \mu^+ \mu^-$	10^{-7}	222	950	1050	not yet estimated	
$B_d^0 \to K^{*0} \mu^+ \mu^-$	1.5×10^{-6}	1995	290	12600	22350	1400 ($<$ 4300 95% C.L.)
$B_s^0 \to \phi^0 \mu^+ \mu^-$	10^{-6}	411	140	3600	not yet estimated	

Table 27: Expected signal- and background-statistics for rare semimuonic decays, for 3 years' running of ATLAS and CMS at low luminosity and 5 years' of LHCb. The CMS simulation was done at the particle level only.

total number of background-events is expected to be 280. The large signal-statistics with very low background gives a nice possibility to study this channel in detail. LHCb also evaluated the sensitivity of A_{FB} measurements. The results are shown in the Tab. 26. Promising results were obtained by LHCb for measuring the position of the zero of A_{FB}, $\hat{s}_0$ with $A_{FB}(\hat{s}_0) = 0$. As discussed in the previous subsection, the position of the zero is proportional to the ratio of two Wilson-coefficients, $C_9^{\text{eff}}/C_7^{\text{eff}}$, with only small hadronic uncertainties from form factors. Note, however, that it is the *effective* Wilson-coefficients that determine $\hat{s}_0$ and that these coefficients encode both short-distance SM and – potentially – new physics effects and long-distance QCD effects, which latter ones *do* come with a certain hadronic uncertainty that to date has not been investigated in sufficient detail. LHCb simulated the expected measurements of the asymmetry, see Fig. 58, and made a linear fit of the "experimental points". It is shown that $\hat{s}_0$ can be measured with 25% accuracy, which leads to a 4% error in extracting the ratio $C_9^{\text{eff}}/C_7^{\text{eff}}$.

The CMS collaboration studied three rare B meson decay channels, $B_d^0 \to K^{*0} \mu^+ \mu^-$, $B_d^0 \to \rho^0 \mu^+ \mu^-$, $B_s^0 \to \phi^0 \mu^+ \mu^-$, at the particle level. No full simulation of the signal and background in the CMS detector has been performed yet. Secondary vertex reconstruction was however studied in detail. The main source of uncertainty in the CMS evaluation is the efficiency of higher-level triggering of dimuons with continuum mass distribution. The complete event reconstruction, using object-oriented techniques, the implementation of various higher trigger level strategies and the evaluation of triggering efficiencies, is now underway in CMS. The sources of background considered are $B^0 \to J/\psi(\mu^+\mu^-)X$, $B^0 \to \mu Y \to \mu\mu + X$, reflection of $B_s^0 \to \phi^0 \mu^+ \mu^-$ and $B_d^0 \to K^{*0} \mu^+ \mu^-$ to other signal-channels and semimuonic decays of both b quarks.

The numbers of signal- and background-events expected by ATLAS, CMS and LHCb are given in Tab. 27.

8.4 Inclusive Decays

The inclusive decay mode $B \to X_s \gamma$ has received much attention in connection with its measurement at CLEO, $B(B \to X_s \gamma) = (3.15 \pm 0.35 \pm 0.32 \pm 0.26) \times 10^{-4}$ [178], which should become much more

accurate with data being taken at the e^+e^- B factories. A state-of-the-art review on inclusive decays can be found in the corresponding chapter of the BaBar physics book [6]. The experimental environment of a hadronic machine makes it very hard to measure inclusive decays. Nevertheless, the D0 collaboration at Fermilab was able to set a 90% CL bound $B(B \to X_s\mu^+\mu^-) < 3.2 \times 10^{-4}$ [179], which should be compared to the corresponding CLEO [180] result of 5.8×10^{-5} and the SM expectation of 6×10^{-6}. In the D0 analysis, no displaced vertex was required for the muon pair, contrary to the CDF analysis of the exclusive $B \to K^*\mu^+\mu^-$ mode [181], where a sensitivity of order 10^{-6} has been reached. It is an interesting question to ask whether LHC could improve the D0 result (e.g. by requiring a displaced vertex) and whether it could possibly reach the sensitivity required for measuring the branching ratios of $B \to X_s\gamma$ and $B \to X_s\mu^+\mu^-$ as predicted in the SM.

The theoretical advantage of the inclusive decays $B \to X_s\gamma$ and $B \to X_s\mu^+\mu^-$ over particular exclusive channels lies in the fact that non-perturbative contributions to the inclusive modes can be calculated in a model-independent way with the help of the Operator Product Expansion (OPE) within the Heavy Quark Effective Theory (HQET) [182]. Actually, this statement is true only at the leading order in hard strong interactions (i.e. in $\alpha_s(m_b)/\pi$) and only after imposing certain kinematic cuts (see e.g. [167, 163]). Even with these restrictions, the accuracy of theoretical predictions for the inclusive branching ratios is expected to be better than in the exclusive case.

The theoretical analysis of $\bar{B} \to X_s\gamma$ proceeds along the same lines as in the $\bar{B} \to \bar{K}^*\gamma$ case, up to Eq. (8.12), where $\bar{K}^*$ has to be replaced by any $S = -1$ hadronic state X_s. Then, the modulus squared of the amplitude is taken, and a sum over all the states X_s is performed. The obtained sum can be related via the optical theorem to the imaginary part of the $\bar{B}\gamma \to \bar{B}\gamma$ elastic scattering amplitude, analogously to what is done in the analysis of $\bar{B} \to X_{u,c}e\bar{\nu}$ [183]. After OPE and calculating matrix elements of several local operators between $\bar{B}$ meson states at rest, one finds that the "subtracted" branching ratio

$$B(\bar{B} \to X_s\gamma)^{\text{subtracted }\psi}_{E_\gamma > E_{\rm cut}} \equiv B(\bar{B} \to X_s\gamma)_{E_\gamma > E_{\rm cut}} - B(\bar{B} \to X^{(1)}_{\text{no charm}}\psi) \times B(\psi \to X^{(2)}_{\text{no charm}}\gamma) \quad (8.29)$$

is given in terms of the purely perturbative b quark decay width, up to small non-perturbative corrections

$$\frac{\Gamma(\bar{B} \to X_s\gamma)^{\text{subtracted }\psi}_{E_\gamma > E_{\rm cut}}}{\Gamma(\bar{B} \to X_ce\bar{\nu}_e)} \simeq \frac{\Gamma(b \to X_s\gamma)^{\text{perturbative NLO}}_{E_\gamma > E_{\rm cut}}}{\Gamma(b \to X_ce\bar{\nu}_e)^{\text{perturbative NLO}}} \times \\ \times \left[1 + (\mathcal{O}(\Lambda^2/m_b^2) \simeq 1\%) + (\mathcal{O}(\Lambda^2/m_c^2) \simeq 3\%)\right]. \quad (8.30)$$

The normalization to the semileptonic rate has been used here to cancel uncertainties due to m_b^5, CKM-angles and some of the non-perturbative corrections. One has to keep in mind that (8.30) becomes a bad approximation for $E_\gamma^{\rm cut} \ll 1$ GeV, and that non-perturbative corrections grow dramatically when $E_\gamma^{\rm cut} > 2$ GeV. Moreover, non-perturbative effects arising at $\mathcal{O}(\alpha_s(m_b))$ are not included in (8.30). Estimating the size of such non-perturbative effects requires further study, see Ref. [163]. For $E_{\rm cut} = 1$ GeV, Eq. (8.30) gives

$$B(\bar{B} \to X_s\gamma)^{\text{subtracted }\psi}_{E_\gamma > E_{\rm cut}} = (3.29 \pm 0.33) \times 10^{-4}, \quad (8.31)$$

where the dominant uncertainties originate from the uncalculated $\mathcal{O}(\alpha_s^2)$ effects and from the ratio m_c/m_b in the semileptonic decay (around 7% each).

The calculation of $\bar{B} \to X_s\mu^+\mu^-$ for small dimuon invariant mass is conceptually analogous to $\bar{B} \to X_s\gamma$, but technically more complicated, because more operators become important. Here, we shall quote only the numerical estimate [167]

$$B(B \to X_s\mu^+\mu^-)_{s\in[0.05m_b^2, 0.25m_b^2]} = (1.46 \pm 0.19) \times 10^{-6}, \quad (8.32)$$

where only the error from μ-dependence of the perturbative amplitude is included.

8.5 Conclusions

The LHC experiments will be able to make precise measurements of rare radiative, semimuonic and muonic B decays. ATLAS and CMS will measure rare decays in the central η region, which will be complementary to the data to be taken by LHCb. A first assessment of LHC's potential to measure rare B decays has shown that it will be possible to

- observe $B_s^0 \to \mu^+\mu^-$, measure its branching ratio, which is of order 10^{-9} in the SM, and perform a high sensitivity search for $B_d^0 \to \mu^+\mu^-$;
- measure the branching ratio and decay characteristics of $B_d^0 \to K^{*0}\gamma$ at LHCb;
- measure the branching ratios of $B_s^0 \to \phi^0\mu^+\mu^-$, $B_d^0 \to \rho^0\mu^+\mu^-$ and $B_d^0 \to K^{*0}\mu^+\mu^-$ and study the dynamics of these decays;
- measure the FB-asymmetry in $B_d^0 \to K^{*0}\mu^+\mu^-$, which allows the distinction between the SM and a large class of SUSY models.

Studying rare muonic decays at high luminosity with the ATLAS and CMS detectors would significantly improve the results that can be obtained at low luminosity.

Open questions to be discussed in the future include:

- assessment of the combined performance of LHC experiments on rare muonic and semimuonic decays;
- studies of CP asymmetries in rare semileptonic B decays at LHC;
- evaluation of the potential of ATLAS, CMS and LHCb to measure inclusive $B_{d,s}^0 \to \mathrm{X}\mu^+\mu^-$ branching ratios;
- detection of rare decays with a τ in the final state;
- feasibility study for measuring semimuonic decays with a pseudoscalar meson in the final state, e.g. $B_d \to \pi\mu^+\mu^-$, $B_d \to K\mu^+\mu^-$.

From the theory point of view, the most urgent question left open is the precise assessment of long-distance effects both in the radiative B decays $B \to (K^*, \rho)\gamma$ and in the semimuonic ones, encoded in the effective Wilson-coefficient C_9^{eff}; the lack of knowledge of these effects limits the precision with which CKM matrix elements and short-distance coefficients can be extracted from semimuonic decays. Other tasks remaining are the improvement of form factor calculations, for instance from lattice, and the parametrization of form factors in a form that includes as much known information on the positions of poles and cuts as possible. Also, the possible size of CP asymmetries in semimuonic decays deserves further study; only few papers treat that subject, see e.g. [184].

9 THEORETICAL DESCRIPTION OF NON-LEPTONIC DECAYS[23]

Exclusive non-leptonic B decays form an important part of LHC's B physics programme and at the same time pose a big challenge for theory. In the standard approach using an effective weak Hamiltonian, non-leptonic decay amplitudes are reduced to products of short-distance Wilson-coefficients and hadronic matrix elements. The calculation of the latter ones requires genuine knowledge of non-perturbative QCD and is often done in the so-called factorization approximation, where a matrix element over typically a four-quark operator is "factorized" into a product of matrix elements over current operators, which are much easier to calculate:

$$\langle J/\psi K_S \mid (\bar{c}\gamma_\mu c)(\bar{s}\gamma^\mu b) \mid B\rangle \to \langle J/\psi \mid (\bar{c}\gamma_\mu c) \mid 0\rangle \times \langle K_S \mid (\bar{s}\gamma^\mu b) \mid B\rangle\,.$$

The factorization approximation is, of course, not exact and the assessment of "non-factorizable contributions", including FSI phases, is a fundamental problem of strong interactions, which affects both the extraction of weak phases from CP asymmetries, like $\mathcal{A}_{\mathrm{CP}}(B \to \pi\pi)$, and the determination of CKM

[23] Section coordinator: P. Ball, with help from M. Beneke, G. Buchalla, I. Caprini and A. Khodjamirian.

angles or new physics from rare decays. Whereas in Secs. 3 to 5 a pragmatic approach has been presented which aims at constraining strong-interaction effects from experiment, it remains a big challenge for theory to *predict* these effects from first principles. For this reason we devote a separate section to review several ansätze for solving or rather approaching the problem, although it is to be admitted that a complete solution is still far beyond our power. In three subsections we discuss the calculation of non-factorizable contributions to $B \to J/\psi K^{(*)}$ from QCD sum rules on the light-cone [185, 186], a method for obtaining information on the strong phase in $B \to \pi\pi$ from dispersion relations [187] and, finally, an approach that applies the methods developed for hard exclusive QCD reactions to certain B decays in the heavy quark limit $m_b \to \infty$ [76]. We would like to stress, however, that the problem of how to calculate non-factorizable contributions and, in particular, FSI phases, is very challenging indeed and that a lot of theory work remains to be done. We thus can present, instead of a coherent picture, only facettes, albeit scintillating ones.

9.1 Non-Factorizable Contributions to $B \to J/\psi K^{(*)}$

The non-factorizable contributions to the amplitudes of $B \to J/\psi K^{(*)}$ decays have recently been estimated [185, 186] using operator product expansion (OPE) and QCD light-cone sum rules. In this subsection, we outline the main results of this study.

With the effective Hamiltonian (8.1), the matrix element of $B \to J/\psi K^{(*)}$ has the following form:

$$\langle K^{(*)} J/\psi \mid \mathcal{H}^s_{\rm eff} \mid B\rangle = 4\,\frac{G_F}{\sqrt{2}} V_{cb}V^*_{cs}\Bigg[\left(C_1(\mu)+\frac{C_2(\mu)}{3}\right)\langle K^{(*)}J/\psi \mid O^s_1(\mu)\mid B\rangle + \frac{1}{2}\,C_2(\mu)\langle K^{(*)}J/\psi \mid \widetilde{O}^s_1(\mu)\mid B\rangle\Bigg]. \tag{9.1}$$

The explicit form of the four-quark operators $O^s_{1,2}$ is given in (8.10). The operator

$$\widetilde{O}^s_1 = (\bar c\Gamma^\rho \frac{\lambda^a}{2} c)(\bar s \Gamma_\rho \frac{\lambda^a}{2} b)$$

with $\Gamma_\rho = \gamma_\rho(1-\gamma_5)$ originates from the Fierz rearrangement of O^s_2. In the factorization approximation, the matrix elements of $\widetilde{O}^s_1$ vanish and the matrix elements of O^s_1 are split into the product

$$\langle K^{(*)} J/\psi \mid O^s_1(\mu)\mid B\rangle = \frac{1}{4}\,\langle J/\psi \mid \bar c\Gamma^\rho c \mid 0\rangle\langle K^{(*)} \mid \bar s\Gamma_\rho b \mid B\rangle\,, \tag{9.2}$$

involving simpler matrix elements of quark currents: $\langle 0 \mid \bar c\Gamma^\rho c \mid J/\psi(p)\rangle = f_\psi m_\psi \epsilon^\rho_\psi$ and

$$\langle K(p) \mid \bar s\Gamma_\rho b \mid B(p_B)\rangle = f_+(s)(p_{B\rho}+p_\rho) + f_-(s) q_\rho. \tag{9.3}$$

The form factor decomposition of the matrix element $\langle K^{(*)}(p) \mid \bar s\Gamma^\rho b \mid B(p_B)\rangle$ can be found in (8.19). In the above, $q = p_B - p$, $s = q^2$, f_ψ is the J/ψ decay constant, ϵ_ψ , ϵ_{K^*} are the polarization vectors of J/ψ and K^*, respectively, and $f_\pm$ are the form factors for $B \to K$. For the numerical analysis we use the form factors as calculated from QCD sum rules on the light-cone [188, 35, 126, 168].

The short-distance coefficients $C_{1,2}(\mu)$ and the matrix elements entering (9.1) are scale-dependent, whereas the decay constants and form factors determining the right-hand side of (9.2) are physical scale-independent quantities. Therefore, factorization can at best be an approximation valid at one particular scale. In fact, in both $B \to J/\psi K$ and $B \to J/\psi K^*$, factorization does not work at $\mu = \mathcal{O}(m_b)$ and is unable to reproduce both partial widths and their ratio as can be seen from Tab. 28. Factorization in these channels has to be generalized by replacing the short-distance coefficient $C_1(\mu) + C_2(\mu)/3$ by effective coefficients a_2 which are supposed to be scale-independent and incorporate possible non-factorizable

Decay Parameter	(a)	(b)	Experiment
$\Gamma(B \to J/\psi K)$ (in 10^8 sec^{-1})	1.0 ÷ 1.5	0.15 ÷ 0.2	$\begin{cases}5.8 \pm 0.8\ (B^0)[64]\\ 6.1 \pm 0.6\ (B^\pm)[64]\end{cases}$
$\Gamma(B \to J/\psi K^*)$ (in 10^8 sec^{-1})	3.9 ÷ 6.0	0.6 ÷ 0.9	$\begin{cases}9.7 \pm 1.1\ (B^0)[64]\\ 9.0 \pm 1.6\ (B^\pm)[64]\end{cases}$
$\Gamma(B \to J/\psi K^*)/\Gamma(B \to J/\psi K)$	2.6 ÷ 6.2		1.45 ± 0.26 [107]
$P_L = \Gamma_L/\Gamma$	0.475 ÷ 0.465		$\begin{cases}0.52 \pm 0.08$[107]$\\ 0.65 \pm 0.11$[86, 107]$\end{cases}$
$\left\|a_2^{B\psi K}\right\|$	0.14	0.055	$0.31 \pm 0.02 \pm 0.03$
$\left\|a_{2,1}^{B\psi K^*}\right\|$	0.14	0.055	$0.18^{+0.03}_{-0.04} \pm 0.02$
$\left\|a_{2,2}^{B\psi K^*}\right\|$	0.14	0.055	$\begin{cases}0.13^{+0.09}_{-0.10} \pm 0.01\\ 0.69^{+0.07}_{-0.08} \pm 0.05\end{cases}$
$\|a_{2,V}^{B\psi K^*}\|$	0.14	0.055	$0.16^{+0.04}_{-0.05} \pm 0.02$

Table 28: $B \to J/\psi K^{(*)}$ decay characteristics calculated in naive factorization approximation, neglecting non-factorizable contributions and taking $C_{1,2}(\mu)$ from [6] in NLO at (a) $\mu = m_b$, (b) $\mu = m_b/2$ and compared with experiment. The intervals of theoretical predictions reflect the uncertainties in the $B \to K$ and $B \to K^*$ form factors taken from [168].

effects. The most general decomposition of the matrix elements in (9.1) includes one effective coefficient for $B \to J/\psi K$ and three for $B \to J/\psi K^{(*)}$ (one for each partial wave):

$$\langle K(p)J/\psi(q) \mid \mathcal{H}^s_{\text{eff}} \mid B(p_B)\rangle = \sqrt{2}G_F V_{cb}V_{cs}^* a_2^{B\psi K} f_\psi f_+ m_\psi (\epsilon_\psi^* \cdot p)\,, \tag{9.4}$$

$$\begin{aligned}\langle K^*(p)J/\psi(q) \mid \mathcal{H}^s_{\text{eff}} \mid B(p_B)\rangle = \frac{G_F}{\sqrt{2}} V_{cb}V_{cs}^* m_\psi f_\psi \epsilon_\psi^{*\rho}\Big[&- i(m_B + m_{K^*})\epsilon^*_{K^*\rho} a_{2,1}^{B\psi K^*} A_1(s)\\ &+ i\frac{(\epsilon^*_{K^*}\cdot q)(p_B+p)_\rho}{m_B+m_{K^*}} a_{2,2}^{B\psi K^*} A_2(s) + 2\frac{\epsilon_{\rho\nu\alpha\beta}\epsilon^{*\nu}_{K^*} q^\alpha p^\beta}{m_B+m_{K^*}} a_{2,V}^{B\psi K^*} V(s)\Big]\end{aligned} \tag{9.5}$$

From experimental data we obtain estimates for these coefficients as displayed in Tab. 28. Only the absolute values of $a_2^{B\psi K}$ and $a_{2,i}^{B\psi K^*}$ $(i = 1, 2, V)$ can be extracted, whereas the relative sign of $a_{2,2}^{B\psi K^*}$ and $a_{2,1}^{B\psi K^*}$ turns out to be positive with a twofold ambiguity for the coefficient $a_{2,2}^{B\psi K^*}$. It is important to notice that experimental data themselves signal non-universality of the a_2-coefficients, although the accuracy still has to be improved.

Now we turn to describing how these coefficients can be estimated theoretically. The main non-factorizable contributions to a_2 come from the matrix elements of $\widetilde{O}_1^s$, which are parametrized in the form [185]

$$\langle KJ/\psi \mid \widetilde{O}_1^s(\mu) \mid B\rangle = 2 f_\psi m_\psi \tilde{f}(\mu)(\epsilon_\psi^* \cdot p)\,, \tag{9.6}$$

$$\begin{aligned}\langle K^*J/\psi \mid \widetilde{O}_1^s(\mu) \mid B\rangle = m_\psi f_\psi \epsilon_\psi^{*\rho}\Big[&- i(m_B + m_{K^*})\epsilon^*_{K^*\rho}\widetilde{A}_1(s)\\ &+ i\,\frac{(\epsilon^*_{K^*}\cdot q)(p_B+p)_\rho}{m_B+m_{K^*}}\widetilde{A}_2(s) + 2\,\frac{\epsilon_{\rho\nu\alpha\beta}\epsilon^{*\nu}_{K^*} q^\alpha p^\beta}{m_B+m_{K^*}}\widetilde{V}(s)\Big].\end{aligned} \tag{9.7}$$

$a_2^{B\psi K}$ can be expressed as

$$a_2^{B\psi K} = C_1(\mu) + \frac{C_2(\mu)}{3} + 2C_2(\mu)\,\frac{\tilde{f}(\mu)}{f_+(m_\psi^2)} + ... \tag{9.8}$$

and similar expressions for $a_{2,1}^{B\psi K^*}$, $a_{2,2}^{B\psi K^*}$ and $a_{2,V}^{B\psi K^*}$ with the ratios $\widetilde{A}_1/A_1(m_\psi^2)$, $\widetilde{A}_2/A_2(m_\psi^2)$ and $\widetilde{V}/V(m_\psi^2)$, respectively, replacing $\tilde{f}(\mu)/f_+(m_\psi^2)$. In the above, the ellipses denote neglected non-factorizable contributions of O_2^s, which are supposed to be subdominant. The non-factorizable amplitudes $\tilde{f}_{B\psi K}$, $\widetilde{A}_{1,2}$ and $\widetilde{V}$ have been estimated in Ref. [186] following the approach suggested in

Ref. [189] and using OPE. In this report we do not have the space to explain the method in detail, but simply state the results. At the current level of accuracy, one predicts the following ranges of non-factorizable amplitudes:

$$\tilde{f}(\mu_0) \;=\; -(0.06 \pm 0.02)\,, \tag{9.9}$$

$$\widetilde{A}_1(\mu_0) = 0.0050 \pm 0.0025,\;\; \widetilde{A}_2(\mu_0) \;=\; -(0.002 \pm 0.001),\;\; \widetilde{V}(\mu_0) = -(0.09 \pm 0.04)\;. \tag{9.10}$$

These estimates reveal substantial non-universality in absolute values and difference in signs of the non-factorizable amplitudes. Although the ratios of these amplitudes to form factors, e.g. $\tilde{f}(\mu_0)/f_+(m_\psi^2) \simeq 0.1$ are small, they have a strong impact on the coefficients a_2 because of a strong cancellation in $C_1(\mu_0) + C_2(\mu_0)/3 \simeq 0.055$, $\mu_0 = 2m_c = 2.6\,\text{GeV}$ (which is numerically close to $m_b/2$) being the relevant scale in the process. From (9.8) and the corresponding relations for the other a_2, we obtain:

$$a_2^{B\psi K} = -(0.09 \div 0.23),\;\; a_{2,1}^{B\psi K^*} = 0.07 \div 0.09,\;\; a_{2,2}^{B\psi K^*} = 0.04 \div 0.05,\;\; a_{2,V}^{B\psi K^*} = -(0.05 \div 0.26)\,, \tag{9.11}$$

where an additional $\pm(10 \div 20)\%$ uncertainty from the form factors should be added. Although in comparison with the experimental numbers for $|a_2^{B\psi K}|$ and $|a_{2,1}^{B\psi K^*}|$, the estimates (9.11) fall somewhat short, the gap between naive factorization at $\mu = m_b/2$ and experiment is narrowed considerably. Note also that the sum rule estimates for $a_2^{B\psi K}$ and $a_{2,V}^{B\psi K^*}$ yield negative sign for these two coefficients in contradiction to the global fit of the factorized decay amplitudes to the data [138], yielding a universal positive a_2. For $a_{2,2}^{B\psi K^*}$ and $a_{2,V}^{B\psi K^*}$, the estimates in (9.11) are not very conclusive in view of the large experimental uncertainties of these two coefficients. Clearly, further improvements in the sum rules are needed to achieve more accurate estimates. Nevertheless, the above calculation has demonstrated that for future theoretical studies of exclusive non-leptonic decays of heavy mesons QCD sum rule techniques provide new ways to go beyond factorization.

9.2 Dispersion Relations for B Non-Leptonic Decays into Light Pseudoscalar Mesons

Rescattering effects in non-leptonic B decays into light pseudoscalar mesons were investigated in [187] by the method of dispersion relations in terms of the external masses. Defining the weak decay amplitude $A_{B\to P_1P_2} = A(m_B^2, m_1^2, m_2^2)$, where P_1, P_2 are pseudoscalar mesons, one can show [187] that the weak amplitude satisfies the following dispersion representation:

$$A(m_B^2, m_1^2, m_2^2) = A^{(0)}(m_B^2, m_1^2, m_2^2) \;+\; \frac{1}{\pi}\int\limits_0^{(m_B-m_2)^2} \mathrm{d}z\, \frac{\text{Disc}\, A(m_B^2, z, m_2^2)}{z - m_1^2 - i\epsilon}\,. \tag{9.12}$$

The first term in this representation is the amplitude in the factorization limit, while in the second term the dispersion variable is the mass squared of the meson which does not contain the spectator quark. The representation (9.12) allows one to recover the amplitude in the factorization approximation when the strong rescattering is switched off, which is a reasonable consistency condition. As shown in [187], in the two-particle approximation (9.12) can be written as

$$A_{B\to P_1P_2} = A^{(0)}_{B\to P_1P_2} \;+\; \frac{1}{2}\sum_{\{P_3P_4\}} \Gamma_{P_3P_4;P_1P_2}\bar{A}_{B\to P_3P_4} + \frac{1}{2}\sum_{\{P_3P_4\}} \overline{\Gamma}_{P_3P_4;P_1P_2}A_{B\to P_3P_4}\,. \tag{9.13}$$

In this relation $A^{(0)}_{B\to P_1P_2}$ is the amplitude in the factorization limit, $\bar{A}_{B\to P_3P_4}$ is obtained from $A_{B\to P_3P_4}$ by changing the sign of the strong phases, the coefficients $\Gamma_{P_3P_4;P_1P_2}$ are computed as dispersive integrals

$$\Gamma_{P_3P_4;P_1P_2} = \frac{1}{\pi}\int\limits_0^{(m_B-m_2)^2} \mathrm{d}z\, \frac{C_{P_3P_4;P_1P_2}(z)}{z - m_1^2 - i\epsilon}\,, \tag{9.14}$$

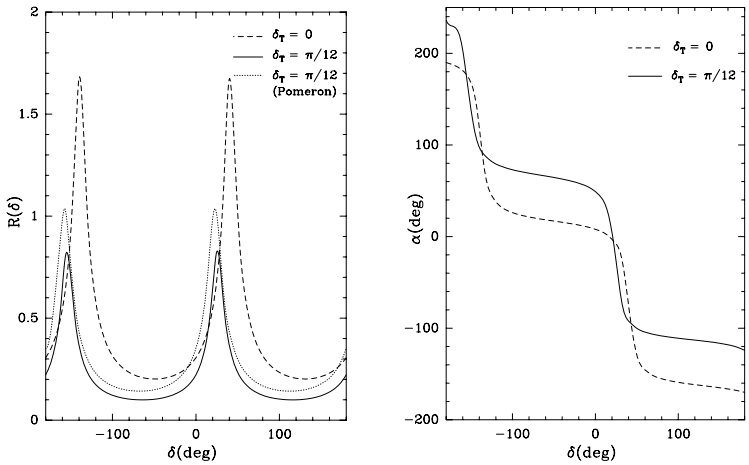

Fig. 59: The ratio $R = |A_P/A_T|$ (left) and the weak phase α (right), as functions of the strong phase difference δ, solid curve $\delta_T = \pi/12$, dashed curve $\delta_T = 0$.

and $\overline{\Gamma}_{P_3P_4;P_1P_2}$ are defined as in (9.14), with the numerator C replaced by C^*, where

$$C_{P_3P_4;P_1P_2}(z) = \frac{1}{2}\int \frac{\mathrm{d}^3\mathbf{k}_3}{(2\pi)^3 2\omega_3}\frac{\mathrm{d}^3\mathbf{k}_4}{(2\pi)^3 2\omega_4}(2\pi)^4\delta^{(4)}(p-k_3-k_4)\mathcal{M}_{P_3P_4\to P_1P_2}(s,t)\,. \tag{9.15}$$

The strong amplitudes $\mathcal{M}_{P_3P_4;P_1P_2}(s,t)$ entering this expression are evaluated for an off-shell meson P_1 of mass squared equal to z, at the c.m. energy squared $s = m_B^2$, which is high enough to justify the application of Regge-theory. A detailed calculation [187] takes into account both the t-channel trajectories describing the scattering at small angles and the u-channel trajectories describing the scattering at large angles.

Let us apply the dispersive formalism to the decay $B^0 \to \pi^+\pi^-$, taking as intermediate states in the dispersion relation (9.13) the pseudoscalar mesons $\pi^+\pi^-$, $\pi^0\pi^0$, K^+K^-, $K^0\bar{K}^0$, $\eta_8\eta_8$, $\eta_1\eta_1$ and $\eta_1\eta_8$. Assuming SU(3) flavour-symmetry and keeping only the contribution of the dominant quark topologies, the dispersion relation (9.13) becomes an algebraic equation involving tree and penguin amplitudes, A_T and A_P. With the Regge parameters discussed in [187], this relation can be written as

$$\begin{aligned} A(B^0\to\pi^+\pi^-)/A_T =& \mathrm{e}^{i\gamma} + R\mathrm{e}^{i\delta}\mathrm{e}^{-i\beta} \\ =& \frac{\mathrm{e}^{-i\delta_T}}{A_T}\left[A_T^{(0)}\mathrm{e}^{i\gamma} + A_P^{(0)}\mathrm{e}^{-i\beta}\right] - \left[(0.01+1.27\,i) + (0.75-1.01\,i)\,\mathrm{e}^{-2i\delta_T}\right]\,\mathrm{e}^{i\gamma} \\ &+R\left[-(1.97+2.64\,i)\,\mathrm{e}^{i\delta} - (1.79-2.00i)\,\mathrm{e}^{-i\delta}\mathrm{e}^{-2i\delta_T}\right]\,\mathrm{e}^{-i\beta}\,. \end{aligned} \tag{9.16}$$

Here $A_T^{(0)}$ and $A_P^{(0)}$ are the amplitudes in the factorization approximation, $R = |A_P/A_T|$ and $\delta = \delta_P - \delta_T$, δ_T (δ_P) being the strong phase of A_T (A_P), respectively. It is seen that the weak angles appear in the combination $\gamma + \beta = \pi - \alpha$. Solving the complex equation (9.16) for R and α, we derive their expressions as functions of δ_T and δ. The evaluation of these expressions requires also the knowledge of the ratios $A_P^{(0)}/A_T^{(0)}$ and $A_T^{(0)}/A_T$. In Fig. 59 we represent R and α as functions of the phase difference δ, for two values of δ_T, using as input $A_P^{(0)}/A_T^{(0)} = 0.08$ and $A_T^{(0)}/A_T \approx 0.9$ [76]. Values of the ratio R less than one are obtained for both $\delta_T = 0$ and $\delta_T = \pi/12$. The dominant contribution is given by the elastic channel, more precisely by the Pomeron, as is seen in Fig. 59, where the dotted curve shows the ratio R for $\delta_T = \pi/12$, keeping only the contribution of the Pomeron in the Regge amplitudes.

The above results show that the dispersive formalism is consistent with the treatment based on factorization and perturbative QCD in the heavy quark limit presented in Ref. [76], supporting therefore the physical idea of parton-hadron duality. From a practical point of view, the dispersion representations

in the external mass provide a set of algebraic equations for on-shell decay amplitudes, leading to non-trivial constraints on the hadronic parameters.

9.3 QCD Factorization for Exclusive Non-Leptonic B Decays

The theory of hadronic B decay matrix elements is a crucial basis for precision flavour physics with non-leptonic modes, which is one of the central goals of the B physics programme at the LHC. A new, systematic approach towards this problem, going beyond previous attempts, was recently proposed in [76]. It solves the problem of how to calculate non-factorizable contributions, and in particular FSIs, in the heavy quark limit and constitutes a promising approach, complementary to the one discussed in the preceding sections. In this approach, the statement of QCD factorization in the case of $B \to \pi\pi$, for instance, can be schematically written as

$$A(B \to \pi\pi) = \langle \pi | j_1 | B \rangle \, \langle \pi | j_2 | 0 \rangle \cdot \left[1 + \mathcal{O}(\alpha_s) + \mathcal{O}\left(\frac{\Lambda_{\rm QCD}}{m_B} \right) \right] . \tag{9.17}$$

Up to corrections suppressed by $\Lambda_{\rm QCD}/m_B$ the amplitude is calculable in terms of simpler hadronic objects: It factorizes, to lowest order in α_s, into matrix elements of bilinear quark currents ($j_{1,2}$). To higher order in α_s, but still to leading order in $\Lambda_{\rm QCD}/m_B$, there are 'non-factorizable' corrections, which are however governed by hard-gluon exchange. They are therefore again calculable in terms of few universal hadronic quantities. More explicitly, the matrix elements of four-quark operators Q_i are expressed by the factorization formula

$$\langle \pi(p')\pi(q) | Q_i | \bar{B}(p) \rangle = f^{B\to\pi}(q^2) \int_0^1 dx \, T_i^I(x) \Phi_\pi(x) + \int_0^1 d\xi dx dy \, T_i^{II}(\xi, x, y) \Phi_B(\xi) \Phi_\pi(x) \Phi_\pi(y), \tag{9.18}$$

which is valid up to corrections of relative order $\Lambda_{\rm QCD}/m_b$. Here $f^{B\to\pi}(q^2)$ is a $B \to \pi$ form factor [185, 126] evaluated at $q^2 = m_\pi^2 \approx 0$, and Φ_π (Φ_B) are leading-twist light-cone distribution amplitudes of the pion (B meson). The $T_i^{I,II}$ denote hard-scattering kernels, which are calculable in perturbation theory. The corresponding diagrams are shown in Fig. 60.

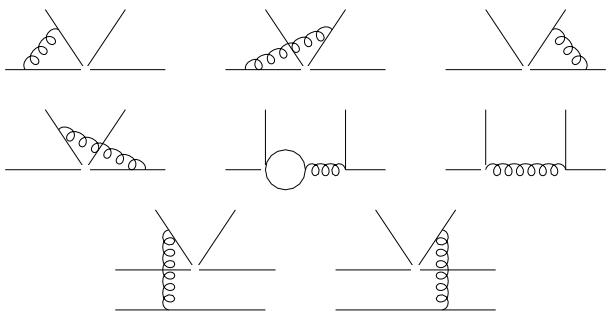

Fig. 60: Order α_s corrections to the hard scattering kernels T_i^I (first two rows) and T_i^{II} (last row). In the case of T_i^I, the spectator quark does not participate in the hard interaction and is not drawn. The two lines directed upwards represent the two quarks forming the emitted pion. T_i^I starts at $\mathcal{O}(\alpha_s^0)$, T_i^{II} at $\mathcal{O}(\alpha_s^1)$.

This treatment of hadronic B decays is based on the analysis of Feynman diagrams in the heavy quark limit, utilizing consistent power counting to identify the leading contributions. The framework is very similar in spirit to more conventional applications of perturbative QCD in exclusive hadronic processes with a large momentum transfer, as the pion electromagnetic form factor [190, 191, 192]. It may be viewed as a consistent formalization of Bjorken's colour transparency argument [127]. In addition the method includes, for $B \to \pi\pi$, the hard non-factorizable spectator interactions, penguin contributions and rescattering effects. As a corollary, one finds that strong rescattering phases are either of $\mathcal{O}(\alpha_s)$, and calculable, or power suppressed. In any case they vanish therefore in the heavy quark limit.

QCD factorization is valid for cases where the emitted particle (the meson created from the vacuum in the weak process, as opposed to the one that absorbs the b quark spectator) is a small size colour-singlet object, e.g. either a fast light meson (π, ϱ, K, K^*) or a J/ψ. For the special case of the ratio $\Gamma(B \to D^*\pi)/\Gamma(B \to D\pi)$ the perturbative corrections to naive factorization have been evaluated in [193] using a formalism similar to the one described above. Note that factorization cannot be justified in this way if the emitted particle is a heavy-light meson ($D^{(*)}$), which is not a compact object and has strong overlap with the remaining hadronic environment.

9.3.1 Final State Interactions

A general issue in hadronic B decays, with important implications for CP violation, is the question of FSIs. When discussing this problem, we may choose a partonic or a hadronic language. The partonic language can be justified by the dominance of hard rescattering in the heavy quark limit. In this limit the number of physical intermediate states is arbitrarily large. We may then argue on the grounds of parton-hadron duality that their average is described well enough (say, up to $\Lambda_{\rm QCD}/m_b$ corrections) by a partonic calculation. This is the picture implied by (9.18). The hadronic language is in principle exact. However, the large number of intermediate states makes it almost impossible to observe systematic cancellations, which usually occur in an inclusive sum of intermediate states.

Consider again the decay of a B meson into two pions. Unitarity implies $\mathrm{Im}\, A(B \to \pi\pi) \sim \sum_n A(B \to n) A^*(n \to \pi\pi)$. The elastic rescattering contribution ($n = \pi\pi$) is related to the $\pi\pi$ scattering amplitude, which exhibits Regge behaviour in the high-energy ($m_b \to \infty$) limit. Hence the soft, elastic rescattering phase increases slowly in the heavy quark limit [194]. On general grounds, it is rather improbable that elastic rescattering gives an appropriate description at large m_b. This expectation is also borne out in the framework of Regge behaviour, see [194], where the importance of inelastic rescattering is emphasized. However, the approach pursued in [194] leaves open the possibility of soft rescattering phases that do not vanish in the heavy quark limit, as well as the possibility of systematic cancellations, for which the Regge language does not provide an appropriate theoretical framework.

Eq. (9.18) implies that such systematic cancellations do occur in the sum over all intermediate states n. It is worth recalling that such cancellations are not uncommon for hard processes. Consider the example of $e^+e^- \to$ hadrons at large energy q. While the production of any hadronic final state occurs on a time-scale of order $1/\Lambda_{\rm QCD}$ (and would lead to infrared divergences if we attempted to describe it in perturbation theory), the inclusive cross section given by the sum over all hadronic final states is described very well by a $q\bar{q}$ pair that lives over a short time-scale of order $1/q$. In close analogy, while each particular hadronic intermediate state n cannot be described in terms of partons, the sum over all intermediate states is accurately represented by a $q\bar{q}$ fluctuation of small transverse size of order $1/m_b$, which therefore interacts little with its environment. Note that precisely because the $q\bar{q}$ pair is small, the physical picture of rescattering is very different from elastic $\pi\pi$ scattering – hence the Regge picture is difficult to justify in the heavy quark limit.

As is clear from the discussion, parton-hadron duality is crucial for the validity of (9.18) beyond perturbative factorization. A quantitative proof of how accurately duality holds is a yet unsolved problem in QCD. Short of a solution, it is worth noting that the same (often implicit) assumption is fundamental to many successful QCD predictions in jet and hadron-hadron physics or heavy quark decays.

9.3.2 QCD Factorization in $B \to \pi\pi$

Let us finally illustrate one phenomenological application of QCD factorization in the heavy quark limit for $\bar{B} \to \pi^+\pi^-$ [76]. The $\bar{B}_d \to \pi^+\pi^-$ decay amplitude A reads

$$A = i\frac{G_F}{\sqrt{2}} m_B^2 f_+(0) f_\pi |\lambda_c| \cdot [R_b e^{-i\gamma} \left(a_1^u(\pi\pi) + a_4^u(\pi\pi) + a_6^u(\pi\pi) r_\chi\right) - \left(a_4^c(\pi\pi) + a_6^c(\pi\pi) r_\chi\right)]. \quad (9.19)$$

$a_1^u(\pi\pi)$	$a_4^u(\pi\pi)$	$a_4^c(\pi\pi)$	$a_6^p(\pi\pi)r_\chi$
$1.038 + 0.018i$	$-0.029 - 0.015i$	$-0.034 - 0.008i$	–
(1.020)	(-0.020)	(-0.020)	(-0.030)

Table 29: QCD coefficients $a_i^p(\pi\pi)$ for $\bar{B} \to \pi^+\pi^-$ at NLO (renormalization scale $\mu = m_b$). Leading order values are shown in parenthesis for comparison.

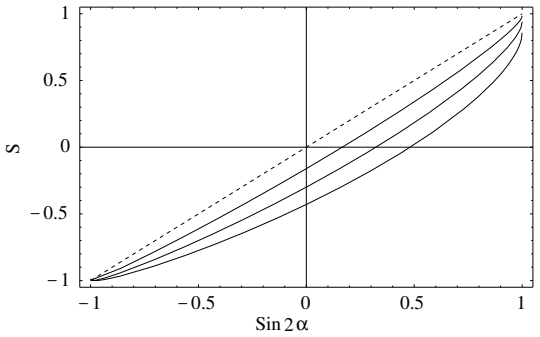

Fig. 61: Coefficient of $-\sin(\Delta M_{B_d} t)$ vs. $\sin 2\alpha$. $\sin 2\beta = 0.7$ has been assumed. See text for explanation.

Here R_b is the ratio of CKM matrix elements defined in (1.9), γ is the phase of V_{ub}^*, and we will use $|V_{cb}| = 0.039 \pm 0.002$, $|V_{ub}/V_{cb}| = 0.085 \pm 0.020$. We also take $f_\pi = 131\,\text{MeV}$, $f_B = (180 \pm 20)\,\text{MeV}$, $f_+(0) = 0.275 \pm 0.025$, and $\tau(B_d) = 1.56\,\text{ps}$; $\lambda_c \equiv V_{cd}^* V_{cb}$. The contribution of $a_6^p(\pi\pi)$ is multiplied by $r_\chi = 2m_\pi^2/(m_b(m_u + m_d)) \sim \Lambda_{\rm QCD}/m_b$. It is thus formally power suppressed, but numerically relevant since $r_\chi \approx 1$. The coefficients a_i are estimated in Tab. 29. We then find for the branching fraction

$$B(\bar{B}_d \to \pi^+\pi^-) = 6.5\,[6.1] \cdot 10^{-6} \left| e^{-i\gamma} + 0.09\,[0.18]\, e^{i \cdot 12.7\,[6.7]^\circ} \right|^2. \tag{9.20}$$

The default values correspond to $a_6^p(\pi\pi) = 0$, the values in brackets use $a_6^p(\pi\pi)$ at leading order. The predictions for the $\pi^+\pi^-$ final state are relatively robust, with errors of the order of $\pm\,30\%$ due to the input parameters. The direct CP asymmetry in the $\pi^+\pi^-$ mode is approximately $4\% \times \sin\gamma$.

As a further example, we use the factorization formula to compute the time-dependent, mixing-induced asymmetry in $B_d \to \pi^+\pi^-$ decay,

$$\mathcal{A}(t) = -S \cdot \sin(\Delta M_{B_d} t) + C \cdot \cos(\Delta M_{B_d} t). \tag{9.21}$$

In the absence of a penguin contribution (defined as the contribution to the amplitude which does not carry the weak phase γ in standard phase conventions), $S = \sin 2\alpha$ (where α refers to one of the angles of the CKM unitarity triangle) and $C = 0$. Fig. 61 shows S as a function of $\sin 2\alpha$ with the amplitudes computed according to (9.18) and (9.19). The central of the solid lines refers to the heavy quark limit including α_s corrections to naive factorization and including the power-suppressed term $a_6 r_\chi$ that is usually also kept in naive factorization. The other two solid lines correspond to dropping this term or multiplying it by a factor of 2. This exercise shows that formally power-suppressed terms can be non-negligible, but it also shows that a measurement of S can be converted into a range for $\sin 2\alpha$ which may already provide a very useful constraint on CP violation.

More work remains to be done. The proof of factorization has to be completed. Power corrections are an important issue, as m_b is not arbitrarily large. There exist 'chirally enhanced' corrections $\sim r_\chi$. All such terms can be identified, but they involve non-factorizable soft gluons. The size of these terms has to be estimated to arrive at a realistic phenomenology. If this can be done, one may expect promising constraints and predictions for a large number of non-leptonic two-body final states. We emphasize in particular the experimentally attractive possibility to determine $\sin 2\alpha$ from $B \to \pi^+\pi^-$ decays alone.

10 B_c PHYSICS[24]

The B_c^+ meson is the lowest lying bound state of two heavy quarks, $\bar{b}$ and c. The QCD dynamics of this state is therefore similar to that of quarkonium systems, such as the $\bar{b}b$ or $\bar{c}c$ families, which are approximately non-relativistic. In contrast to the common quarkonia, however, B_c carries open flavour and the ground state is stable under strong interactions. In fact, B_c is the only hadron combining these features and forming a flavoured, weakly decaying quarkonium. Since the complicated interplay of strong and weak forces is the key problem in the theoretical analysis of weak decays of hadrons, the quarkonium-like B_c provides us with a very interesting special case to study such a general question. Tools for calculation, for example heavy quark expansions, non-relativistic QCD (NRQCD), factorization, which are important in many areas of heavy flavour physics, can be tested in a complementary setting.

The observation of the B_c meson by the CDF Collaboration in the channel $B_c \to J/\psi l\nu$, with measured mass and lifetime [195]

$$M_{B_c} = 6.40 \pm 0.39\,(\text{stat}) \pm 0.13\,(\text{syst})\,\text{GeV}, \quad \tau_{B_c} = 0.46^{+0.18}_{-0.16}\,(\text{stat}) \pm 0.03\,(\text{syst})\,\text{ps}, \tag{10.22}$$

opened up the experimental investigations of the $\bar{b}c$ hadronic system. B_c physics can also be pursued at the LHC, where a copious production of the B_c meson and of its radial and orbital excitations is expected [47] (see also [196] for a recent review). No full experimental studies have been performed yet, and thus we concentrate on a brief summary of B_c decay properties, collecting useful information and illustrating a range of opportunities that may be pursued in this field. We also shortly summarize the present status of experimental studies.

10.1 B_c Lifetime and Inclusive Decays

The total decay rate of the B_c can be computed starting from a heavy-quark expansion of the transition operator, supplemented by NRQCD. This framework is familiar from the study of ordinary, heavy-light b hadron lifetimes [19], with the basic difference that in the heavy-light case the rôle of NRQCD is played by heavy-quark effective theory (HQET). For B_c the characteristic features of NRQCD result in a particularly intuitive expression for the total rate:

$$\Gamma_{B_c} = \Gamma_b \left(1 - \frac{v_b^2}{2}\right) + \Gamma_c \left(1 - \frac{v_c^2}{2}\right) + \Delta\Gamma_{PI} + \Delta\Gamma_{WA} + \mathcal{O}(v^4)\,. \tag{10.23}$$

Eq. (10.23) is written as an expansion in the heavy quark velocities v, complete through order v^3. To lowest order, v^0, we have $\Gamma_{B_c} = \Gamma_b + \Gamma_c$, the sum of the free decay rates of the heavy quark constituents $\bar{b}$ and c. The first bound state corrections arise at $\mathcal{O}(v^2)$ only and are equivalent to time-dilatation. The effect of binding compels the heavy quarks to move around each other, thus retarding their decay. At $\mathcal{O}(v^3)$ there are two terms. First, a correction from Pauli interference (PI) of the two c quarks in the final state of $(c)\bar{b} \to (c)\bar{c}c\bar{s}$ decay. Second, a contribution from the weak annihilation of the constituents $\bar{b}c$, either into hadrons or into leptons, the latter dominated by $B_c \to \tau\nu$. A numerical analysis of (10.23) gives the estimate [197]

$$\tau_{B_c} \equiv \frac{1}{\Gamma_{B_c}} = (0.4 - 0.7)\,\text{ps}\,, \tag{10.24}$$

with a large uncertainty from the heavy quark masses (m_c), but in agreement with the measurement (10.22). The same framework can be used to calculate other inclusive decay properties of B_c, for instance the semileptonic branching fraction $B(B_c \to Xe\nu)$, which turns out to be $\sim 12\%$. More details and references can be found in [197, 198, 199].

[24] Section coordinators: G. Buchalla, P. Colangelo and F. De Fazio, with acknowledgements for V.V. Kiselev and A. Likhoded for useful discussions.

10.2 Leptonic and Radiative Leptonic B_c Decays

The purely muonic B_c branching ratio is determined by the decay constant f_{B_c}:

$$B(B_c \to \mu\nu) = \tau_{B_c} \frac{G_F^2}{8\pi} |V_{cb}|^2 f_{B_c}^2 M_{B_c}^3 \left(\frac{m_\mu}{M_{B_c}}\right)^2 \left(1 - \frac{m_\mu^2}{M_{B_c}^2}\right)^2$$
$$= 6.8 \times 10^{-5} \frac{M_{B_c}}{6.28\,\mathrm{GeV}} \left(\frac{|V_{cb}|}{0.04}\right)^2 \left(\frac{f_{B_c}}{400\,\mathrm{MeV}}\right)^2 \frac{\tau_{B_c}}{0.46\,\mathrm{ps}}\,. \qquad (10.25)$$

The value of f_{B_c} has been computed by lattice NRQCD: $f_{B_c} = (420 \pm 13)\,\mathrm{MeV}$ [200], QCD Sum Rules: $f_{B_c} = (360 \pm 60)\,\mathrm{MeV}$ [201, 202], and various quark models with predictions in the range $f_{B_c} = [430 - 570]\,\mathrm{MeV}$ [203].

The photon emission in the radiative muonic decay $B_c \to \mu\nu\gamma$ removes the helicity suppression of the purely muonic mode. In the non-relativistic limit, the radiative muonic decay width is also determined by f_{B_c} [204]. In this limit one obtains the ratio $\Gamma(B_c \to \mu\nu\gamma)/\Gamma(B_c \to \mu\nu) \simeq 0.8$. Corrections to this result within a relativistic quark model have been discussed in [205].

10.3 Semileptonic B_c Decay Modes

The calculation of the matrix elements governing the exclusive semileptonic B_c decay modes has been carried out using QCD sum rules [202, 206] and quark models [207, 208]. The predictions for the various exclusive decay rates are reported (in rather conservative ranges) in Tab. 30, with the conclusion that the semileptonic B_c decay width is dominated by the modes induced by the charm decay.

Channel	$\Gamma(10^{-15}$ GeV)	B
$B_c^+ \to B_s e^+ \nu$	$11 - 61$	$[8 - 42] \times 10^{-3}$
$B_c^+ \to B_s^* e^+ \nu$	$30 - 79$	$[21 - 55] \times 10^{-3}$
$B_c^+ \to B_d e^+ \nu$	$1 - 4$	$[7 - 28] \times 10^{-4}$
$B_c^+ \to B_d^* e^+ \nu$	$2 - 6$	$[14 - 42] \times 10^{-4}$
$B_c^+ \to \eta_c e^+ \nu$	$2 - 14$	$[14 - 98] \times 10^{-4}$
$B_c^+ \to J/\psi e^+ \nu$	$22 - 35$	$[15 - 24] \times 10^{-3}$
$B_c^+ \to \eta_c' e^+ \nu$	$0.3 - 0.7$	$[2 - 5] \times 10^{-4}$
$B_c^+ \to \psi' e^+ \nu$	$1 - 2$	$[7 - 14] \times 10^{-4}$
$B_c^+ \to D^0 e^+ \nu$	$0.01 - 0.09$	$[7 - 63] \times 10^{-6}$
$B_c^+ \to D^{*0} e^+ \nu$	$0.1 - 0.3$	$[7 - 21] \times 10^{-5}$

Table 30: Semileptonic B_c^+ decay widths and branching fractions ($\tau_{B_c} = 0.46$ ps).

The calculation of the semileptonic matrix elements can be put on a firmer theoretical ground taking into account the decoupling of the spin of the heavy quarks of the B_c meson, as well as of the meson produced in the semileptonic decays, i.e. mesons belonging to the $\bar{c}c$ family ($\eta_c, J/\psi$, etc.) and mesons containing a single heavy quark ($B_s^{(*)}$, $B_d^{(*)}$, $D^{(*)}$). The decoupling occurs in the heavy quark limit ($m_b, m_c \gg \Lambda_{QCD}$); it produces a symmetry, the heavy quark spin symmetry, allowing to relate, near the zero-recoil point, the form factors governing the B_c decays into a 0^- and 1^- final meson to a few invariant functions [209]. Examples are the processes $B_c \to (B_s, B_s^*)\mu\nu$ and $B_c \to (B_d, B_d^*)\mu\nu$, where the energy released to the final hadronic system is much less than m_b, thus leaving the b quark almost unaffected. The final B_a meson ($a = d, s$) keeps the same B_c four-velocity v, apart from a small residual momentum q. Defining $p_{B_c} = M_{B_c} v$ and $p_{B_a} = M_{B_a} v + q$, one has:

$$\langle B_a, v, q | V_\mu | B_c, v \rangle = \sqrt{2M_{B_c} 2M_{B_a}} [\Omega_1^a \, v_\mu + a_0 \, \Omega_2^a \, q_\mu],$$

$$\langle B_a^*, v, q, \epsilon | V_\mu | B_c, v \rangle \, = \, -i \, \sqrt{2M_{B_c} 2M_{B_a^*}} \, a_0 \, \Omega_2^a \, \epsilon_{\mu\nu\alpha\beta} \epsilon^{*\nu} q^\alpha v^\beta ,$$
$$\langle B_a^*, v, q, \epsilon | A_\mu | B_c, v \rangle \, = \, \sqrt{2M_{B_c} 2M_{B_a^*}} [\Omega_1^a \, \epsilon_\mu^* + a_0 \, \Omega_2^a \, \epsilon^* \cdot q \, v_\mu], \qquad (10.26)$$

i.e. only two form factors are needed to describe the previous transitions. The scale parameter a_0 is related to the B_c Bohr radius [209]. For the B_c transitions into a $\bar{c}c$ meson, $B_c \to (\eta_c, J/\psi)\mu\nu$, spin symmetry implies that the semileptonic matrix elements can be expressed, near the zero-recoil point, in terms of a single form factor:

$$\langle \eta_c, v, q | V_\mu | B_c, v \rangle = \sqrt{2M_{B_c} 2M_{\eta_c}} \, \Delta \, v_\mu \, , \quad \langle J/\psi, v, q, \epsilon | A_\mu | B_c, v \rangle = \sqrt{2M_{B_c} 2M_{J/\psi}} \, \Delta \, \epsilon_\mu^* \, . \quad (10.27)$$

Model-independent results exist in the heavy-quark limit for Δ and Ω_1^a at the zero-recoil point [209]. Additional information on the form factors Δ and Ω_i^a is available from quark models [208, 210] and NRQCD sum rules [211]. The related predictions are included in the ranges reported in Tab. 30. Moreover, spin symmetry implies relations between B_c decays to pseudoscalar and vector states, near the non-recoil point, that can be experimentally tested at the LHC [210].

10.4 Non-Leptonic Decay Modes

Two-body non-leptonic decays are of prime importance for the measurement of the B_c mass. In particular, decay modes with a J/ψ in the final state are suitable for an efficient background-rejection.

The non-leptonic B_c decay rates have been computed in the factorization approximation, using various parametrizations of the semileptonic form factors and different prescriptions for the parameters a_1 and a_2 appearing in the factorized matrix elements [207, 208, 210]. Predictions for the various decay modes, induced by the beauty and charm quark transitions, are reported in Tabs. 31 and 32, respectively, using $M_{B_c} = 6.28$ GeV. For several modes, ranges of values for the branching fractions are reported; they are obtained considering the spread of predictions by different approaches, and suggest the size of the theoretical uncertainty for each decay mode.

Channel	B	Channel	B
$B_c^+ \to \eta_c \pi^+$	$[3-25] \times 10^{-4}$	$B_c^+ \to \eta_c K^+$	$[2-17] \times 10^{-5}$
$B_c^+ \to \eta_c \rho^+$	$[7-60] \times 10^{-4}$	$B_c^+ \to \eta_c K^{*+}$	$[4-31] \times 10^{-5}$
$B_c^+ \to \eta_c a_1^+$	9×10^{-4}	$B_c^+ \to \eta_c K_1^+$	5×10^{-5}
$B_c^+ \to J/\psi \pi^+$	$[1-2] \times 10^{-3}$	$B_c^+ \to J/\psi K^+$	$[7-17] \times 10^{-5}$
$B_c^+ \to J/\psi \rho^+$	$[4-7] \times 10^{-3}$	$B_c^+ \to J/\psi K^{*+}$	$[2-4] \times 10^{-4}$
$B_c^+ \to J/\psi a_1^+$	5×10^{-3}	$B_c^+ \to J/\psi K_1^+$	3×10^{-4}
$B_c^+ \to \psi' \pi^+$	$[2-3] \times 10^{-4}$	$B_c^+ \to \psi' K^+$	$[1-2] \times 10^{-5}$
$B_c^+ \to \psi' \rho^+$	$[5-8] \times 10^{-4}$	$B_c^+ \to \psi' K^{*+}$	$[3-4] \times 10^{-5}$
$B_c^+ \to \psi' a_1^+$	6×10^{-4}	$B_c^+ \to \psi' K_1^+$	3×10^{-5}
$B_c^+ \to D^+ \bar{D}^0$	$[1-12] \times 10^{-5}$	$B_c^+ \to D_s^+ \bar{D}^0$	$[6-62] \times 10^{-7}$
$B_c^+ \to D^+ \bar{D}^{*0}$	$[1-12] \times 10^{-5}$	$B_c^+ \to D_s^+ \bar{D}^{*0}$	$[6-62] \times 10^{-7}$
$B_c^+ \to D^{*+} \bar{D}^0$	$[8-10] \times 10^{-5}$	$B_c^+ \to D_s^{*+} \bar{D}^0$	$[5-6] \times 10^{-6}$
$B_c^+ \to D^{*+} \bar{D}^{*0}$	$[1-2] \times 10^{-4}$	$B_c^+ \to D_s^{*+} \bar{D}^{*0}$	$[8-11] \times 10^{-6}$
$B_c^+ \to \eta_c D_s$	$[5-7] \times 10^{-3}$	$B_c^+ \to \eta_c D^+$	$[5-8] \times 10^{-5}$
$B_c^+ \to \eta_c D_s^*$	$[4-6] \times 10^{-4}$	$B_c^+ \to \eta_c D^{*+}$	$[2-6] \times 10^{-5}$
$B_c^+ \to J/\psi D_s$	$[2-3] \times 10^{-3}$	$B_c^+ \to J/\psi D^+$	$[5-13] \times 10^{-5}$
$B_c^+ \to J/\psi D_s^*$	$[6-12] \times 10^{-3}$	$B_c^+ \to J/\psi D^{*+}$	$[2-4] \times 10^{-4}$

Table 31: Branching fractions of B_c^+ non-leptonic decays induced by $b \to c, u$ transitions.

Channel	B	Channel	B
$B_c^+ \to B_s\pi^+$	$[4-17]\times10^{-2}$	$B_c^+ \to B_sK^+$	$[3-12]\times10^{-3}$
$B_c^+ \to B_s\rho^+$	$[2-7]\times10^{-2}$	$B_c^+ \to B_sK^{*+}$	$[5-9]\times10^{-5}$
$B_c^+ \to B_s^*\pi^+$	$[3-7]\times10^{-2}$	$B_c^+ \to B_s^*K^+$	$[2-5]\times10^{-3}$
$B_c^+ \to B_s^*\rho^+$	$[14-19]\times10^{-2}$		
$B_c^+ \to B_d\pi^+$	$[2-4]\times10^{-3}$	$B_c^+ \to B_dK^+$	$[2-3]\times10^{-4}$
$B_c^+ \to B_d\rho^+$	$[2-7]\times10^{-3}$	$B_c^+ \to B_dK^{*+}$	$[4-20]\times10^{-5}$
$B_c^+ \to B_d^*\pi^+$	$[2-4]\times10^{-3}$	$B_c^+ \to B_d^*K^+$	$[1-3]\times10^{-4}$
$B_c^+ \to B_d^*\rho^+$	$[1-2]\times10^{-2}$	$B_c^+ \to B_d^*K^{*+}$	$[4-6]\times10^{-4}$

Table 32: Branching fractions of B_c^+ decays induced by $c \to s, d$ transitions.

10.5 B_c Decays induced by FCNC Transitions

Among the rare B_c decay processes that have been discussed in the literature are the radiative decays $B_c \to B_u^*\gamma$ and $B_c \to D_s^*\gamma$, induced at the quark level by the $c \to u\gamma$ and $b \to s\gamma$ transitions, respectively [212]. The interest for the former decay mode is related to the possibility of studying the $c \to u$ electromagnetic penguin transition, which in the charm mesons is overwhelmed by long-distance contributions. In the case of B_c, long- and short-distance contributions have been estimated to be of comparable size, and the branching fraction $B(B_c \to B_u^*\gamma)$ is predicted, in the SM, at the level of 10^{-8}.

10.6 CP Violation in B_c Decays

B_c decays can give information about CP violation and the weak CKM phases. Promising channels are $B_c^\pm \to (\bar{c}c)D^\pm$, in particular the one where the charmonium state is a J/ψ, whose decay mode to $\mu^+\mu^-$ can be easily identified. In this case, CP violation is due to the difference between the weak phases of the tree and penguin diagrams contributing to the decay. The CP asymmetry $\mathcal{A}(B_c^\pm \to J/\psi D^\pm)$ has been estimated: $\mathcal{A}(B_c^\pm \to J/\psi D^\pm) \simeq 4\times10^{-3}$ [213]. Interesting channels are also those with a light meson in the final state, e.g. $B_c \to D\rho$ and $B_c \to D\pi$. However, in this case the sizeable rôle played by the annihilation mechanism makes it difficult to predict the decay rates and the CP asymmetries. Decay modes such as $B_c \to D^0D_s$ can also be considered, although considerable difficulties would be met in the experimental detection of D_s and in the removal of the background from B_u decays.

Finally, the decay $B_c^+ \to B_s^{(*)}l^+\nu$ has been proposed as an interesting source of flavour-tagged B_s mesons for the study of mixing and CP violation in the B_s sector [198].

10.7 Experimental Considerations

ATLAS have studied the reconstruction of B_c mesons using the decays $B_c \to J/\psi\pi$ and $B_c \to J/\psi\ell\nu$, with $J/\psi \to \mu^+\mu^-$ (see [37]). For this study, the following branching ratios have been assumed: $B(B_c \to J/\psi\pi) = 0.2\times10^{-2}$ and $B(B_c \to J/\psi\mu\nu) = 2\times10^{-2}$. It is estimated that after 3 years of running at low luminosity, it will be possible to fully reconstruct 12000 $B_c \to J/\psi\pi$ events and 3×10^6 events in the $B_c \to J/\psi\mu\nu$ channel. The statistics would allow a very precise determination of the B_c mass and lifetime.

10.8 Concluding Remarks

The B_c meson is of particular interest as a unique case to study the impact of QCD dynamics on weak decays. Applications in flavour physics (CKM parameters, rare decays, B_s flavour tagging) have also been considered in the literature. Important theoretical questions that need further attention are the issues of quark-hadron duality for inclusive decays and, for exclusive modes, the importance of corrections to the heavy-quark and non-relativistic limits, as well as corrections to the factorization approximation. The experimental feasibility for various observables needs likewise to be assessed in more detail. The aim

of the present section has been to give a flavour of the special opportunities that exist, from a theoretical perspective, in studying the physics of the B_c. Some of these are realizable at the LHC, where it will be possible to investigate also the production, spectrum, lifetimes and decays of baryons containing two heavy quarks [214]. It is to be hoped that the results summarized in this section will trigger more detailed experimental studies.

11 CONCLUSIONS[25]

The studies presented at and initiated by the workshop have clearly shown that the LHC is very well equipped and prepared to pursue a rigorous b physics programme. The main emphasis in the studies presented here has been on exploring LHC's potential for measuring CP violating phenomena and, on the theory side, on enabling a meaningful extraction of information on the underlying mechanism on CP violation in the SM. Most of the presented "strategies" aim at extracting the three angles of the unitarity triangle, α, β and γ, as well as $\delta\gamma$, in as many different ways as possible; any significant discrepancy between the extracted values or with the known lengths of the sides of the triangle would constitute evidence for new physics. Apart from detailed studies of the e^+e^- B factory "benchmark modes", also the hadron collider "gold-plated" mode $B_s \to J/\psi\phi$ has been studied, and new strategies for measuring β and γ from B_s decays, which cannot be accessed at e^+e^- B factories, have been developed. We conclude that the three experiments are well prepared to solve the "mystery of CP violation" (p. 1).

Another important goal to be pursued is the measurement of B mixing parameters, and the studies summarized in this report make clear that all three LHC experiments have excellent potential. There is sensitivity in one year's operation to a mass difference in the B_s system far beyond the SM expectation, and similarly good prospects for a rapid measurement of the width difference.

The second focus of the workshop was the assessment of LHC's reach in rare decays. The discussion centred on decay modes with the favourable experimental signature of two muons or one photon in the final state. It has been demonstrated that the decay $B_s \to \mu^+\mu^-$ with a SM branching ratio of $\sim 10^{-9}$ can be seen within one year's running. It has also been shown that decay spectra of semimuonic rare decays like $B \to K^*\mu^+\mu^-$ are accessible, which opens the possibility to extract information on short-distance (new) physics in a theoretically controlled way. LHC's full potential for rare decays has, however, not yet been fully plumbed, and further studies, in particular about the feasibility of inclusive measurements, are ongoing.

Of the many other possible b physics topics, only a few could be marked out, and we have reported some recent developments in the theoretical description of non-leptonic decays and discussed a few issues in B_c physics. The exploration of other exciting topics, such as physics with b, baryons or (non-rare) semileptonic decays, to name only a few, has to await a second round of workshops.

References

[1] J.H. Christenson et al., Phys. Rev. Lett. **13**, 138 (1964).

[2] P. Eerola, hep–ex/9910067.

[3] G.C. Branco, L. Lavoura and J.P. Silva, *CP Violation*, Clarendon Press, Oxford, UK, 1999.

[4] For reviews, see e.g. Y. Nir, hep–ph/9911321; M. Gronau, hep–ph/9908343; R. Fleischer, hep–ph/9908340.

[5] A.J. Buras, hep–ph/9905437.

[6] "The BaBar Physics Book", eds. P.F. Harrison and H.R. Quinn, SLAC Report 504 (1998).

[7] N. Cabibbo, Phys. Rev. Lett. **10**, 531 (1963).

[8] M. Kobayashi and T. Maskawa, Prog. Th. Phys. **49**, 652 (1973).

[9] C. Jarlskog, Phys. Rev. Lett. **55**, 1039 (1985); Z. Phys. **C29**, 491 (1985).

[25] Section coordinators: P. Ball, R. Fleischer, G.F. Tartarelli, P. Vikas and G. Wilkinson.

[10] For reviews, see, for instance, Y. Grossman, Y. Nir and R. Rattazzi, hep–ph/9701231;
M. Gronau and D. London, Phys. Rev. **D55**, 2845 (1997);
Y. Nir and H.R. Quinn, Annu. Rev. Nucl. Part. Sci. **42**, 211 (1992);
R. Fleischer, hep–ph/9709291;
L. Wolfenstein, Phys. Rev. **D57**, 6857 (1998).

[11] L. Wolfenstein, Phys. Rev. Lett. **51**, 1945 (1983).

[12] A.J. Buras, M.E. Lautenbacher and G. Ostermaier, Phys. Rev. **D50**, 3433 (1994).

[13] R. Aleksan, B. Kayser and D. London, Phys. Rev. Lett. **73**, 18 (1994).

[14] L.L. Chau and W.-Y. Keung, Phys. Rev. Lett. **53**, 1802 (1984);
C. Jarlskog and R. Stora, Phys. Lett. **B208**, 268 (1988).

[15] R. Fleischer, Z. Phys. **C62**, 81 (1994).

[16] R. Fleischer, Phys. Lett. **B321**, 259 (1994); Phys. Lett. **B332**, 419 (1994).

[17] R. Fleischer, Int. J. Mod. Phys. **A12**, 2459 (1997).

[18] G. Buchalla, A.J. Buras and M.E. Lautenbacher, Rev. Mod. Phys. **68**, 1125 (1996).

[19] I. Bigi et al., hep–ph/9401298.

[20] B. Blok, M. Shifman and D.-X. Zhang, Phys. Rev. **D57**, 2691 (1998); (E) Phys. Rev. **D59**, 019901 (1999).

[21] I. Bigi et al., Phys. Rev. **D59**, 054011 (1999);
I. Bigi and N. Uraltsev, Phys. Rev. **D60**, 114034 (1999); Phys. Lett. **B457**, 163 (1999).

[22] B. Grinstein and R. Lebed, Phys. Rev. **D57**, 1366 (1998); Phys. Rev. **D59**, 054022 (1999).

[23] M. Beneke et al., Phys. Lett. **B459**, 631 (1999).

[24] S. Hashimoto et al., hep–ph/9912318.

[25] I. Dunietz, Phys. Rev. **D52**, 3048 (1995).

[26] R. Fleischer and I. Dunietz, Phys. Rev. **D55**, 259 (1997).

[27] R. Fleischer and I. Dunietz, Phys. Lett. **B387**, 361 (1996).

[28] R. Fleischer, Phys. Rev. **D58**, 093001 (1998).

[29] A. Alavi-Harati et al. (KTeV Coll.), Phys. Rev. Lett. **83**, 22 (1999);
V. Fanti et al. (NA48 Coll.), Phys. Lett. **B465**, 335 (1999).

[30] M. Gronau and D. Wyler, Phys. Lett. **B265**, 172 (1991).

[31] M. Gronau, J.L. Rosner and D. London, Phys. Rev. Lett. **73**, 21 (1994).

[32] O.F. Hernández et al., Phys. Lett. **B333**, 500 (1994); Phys. Rev. **D50**, 4529 (1994).

[33] D. Atwood, I. Dunietz and A. Soni, Phys. Rev. Lett. **78**, 3257 (1997).

[34] For an overview, see R. Fleischer, hep–ph/9908341.

[35] P. Ball and V.M. Braun, Phys. Rev. **D58**, 094016 (1998).

[36] The ATLAS Coll., *ATLAS Technical Proposal,* CERN/LHCC/94-43.

[37] The ATLAS Coll., *ATLAS Detector and Physics Performance Technical Design Report,* CERN/LHCC/99-14 and CERN/LHCC/99-15. In particular, the *Inner Detector* is described in Vol. I, Chapter 3, pp. 53–98 and the B physics performance in Vol. II, Chapter 17, pp. 561–618.

[38] The CMS Coll., *CMS Technical Proposal,* CERN/LHCC/94-38.

[39] The LHCb Coll., *LHCb Technical Proposal*, CERN/LHCC/98-4.

[40] The ATLAS Coll., *Inner Detector Technical Design Report,* CERN/LHCC/97-16 and CERN/LHCC/97-17; *Pixel Detector Technical Design Report,* CERN/LHCC/98-13.

[41] The CMS Coll., *The Tracker System Project Technical Design Report,* CERN/LHCC/98-6.

[42] The ATLAS Coll., *Calorimeter Performance Technical Design Report,* CERN/LHCC/96-40; *Liquid Argon Calorimeter Technical Design Report,* CERN/LHCC/96-41; *Tile Calorimeter Technical*

Design Report, CERN/LHCC/96-42.

[43] The CMS Coll., *The Hadronic Calorimeter Technical Design Report,* CERN/LHCC/97-31; *The Electromagnetic Calorimeter Technical Design Report,* CERN/LHCC/97-33.

[44] The ATLAS Coll., *Muon Spectrometer Technical Design Report,* CERN/LHCC/97-22.

[45] The CMS Coll., *Muon Technical Design Report,* CERN/LHCC/97-32.

[46] T. Sjöstrand, Comp. Phys. Comm. **82**, 74 (1994).

[47] See the Chapter on B production in this Book, hep–ph/0003142.

[48] H.L. Lai et al. (CTEQ Coll.), Phys. Rev. **D51**, 4763 (1995).

[49] GEANT 3.21, CERN Program Library Long Write-up W5013.

[50] S. Banerjee et. al., CMS Note CMS-NOTE-1999-056.

[51] The ATLAS Coll., *Trigger Performance Status Report,* CERN/LHCC/98-15.

[52] G. Wrochna, CMS Note CMS-CR-1996-002.

[53] The ATLAS Coll., *Level-1 Trigger Technical Design Report,* CERN/LHCC/98-14.

[54] J. Pilszka and G. Wrochna, CMS Note CMS-NOTE-1998-075.

[55] The ATLAS Coll., *DAQ, Event Filter, Level-2 and DCS Technical Progress Report,* CERN/LHCC/98-16.

[56] Y. Coadou et al., ATLAS Note ATL-PHYS-99-022.

[57] Y. Lemoigne and V. Roinishvili, CMS Note CMS-NOTE-2000-018.

[58] M. Gronau, A. Nippe and J.L. Rosner, Phys. Rev. **D47**, 1988 (1993).

[59] The ALEPH Coll., Phys. Lett. **B425**, 215 (1998);
The DELPHI Coll., Phys. Lett. **B345**, 598 (1995);
The OPAL Coll., Z. Phys. **C66**, 19 (1995).

[60] A.B. Carter and A.I. Sanda, Phys. Rev. Lett. **45**, 952 (1980); Phys. Rev. **D23**, 1567 (1981);
I.I. Bigi and A.I. Sanda, Nucl. Phys. **B193**, 85 (1981).

[61] R. Fleischer, Eur. Phys. J. **C10**, 299 (1999).

[62] Y. Nir and D. Silverman, Nucl. Phys. **B345**, 301 (1990).

[63] K. Ackerstaff et al. (OPAL Coll.), Eur. Phys. J. **C5**, 1998 (379);
F. Abe et al. (CDF Coll.), Phys. Rev. Lett. **81**, 1998 (5513) (for an updated analysis, see Preprint CDF/PUB/BOTTOM/CDF/4855);
R. Forty et al. (ALEPH Coll.), Preprint ALEPH 99-099.

[64] C. Caso et al. (PDG), Eur. Phys. J. **C3**, 1 (1998).

[65] M. Gronau, Phys. Lett. **B300**, 163 (1993);
J.P. Silva and L. Wolfenstein, Phys. Rev. **D49**, R1151 (1994);
R. Aleksan et al., Phys. Lett. **B356**, 95 (1995);
A.J. Buras and R. Fleischer, Phys. Lett. **B360**, 138 (1995);
F. DeJongh and P. Sphicas, Phys. Rev. **D53**, 4930 (1996);
M. Ciuchini et al., Nucl. Phys. **B501**, 271 (1997);
P.S. Marrocchesi and N. Paver, Int. J. Mod. Phys. **A13**, 251 (1998);
A. Ali, G. Kramer and C.D. Lü, Phys. Rev. **D59**, 014005 (1999).

[66] J. Charles, Phys. Rev. **D59**, 054007 (1999).

[67] M. Gronau and D. London, Phys. Rev. Lett. **65**, 3381 (1990).

[68] A.J. Buras and R. Fleischer, Eur. Phys. J. **C11**, 93 (1999).

[69] M. Gronau, D. Pirjol and T.M. Yan, Phys. Rev. **D60**, 034021 (1999).

[70] Y. Grossman and H.R. Quinn, Phys. Rev. **D58**, 017504 (1998).

[71] H. Lipkin et al., Phys. Rev. **D44**, 1454 (1991).

[72] A. Snyder and H.R. Quinn, Phys. Rev. **D48**, 2139 (1993).
[73] D.E. Jaffe (CLEO Coll.), hep–ex/9910055.
[74] R. Fleischer, hep–ph/0001253.
[75] R. Fleischer and T. Mannel, Phys. Lett. **B397**, 269 (1997).
[76] M. Beneke et al., Phys. Rev. Lett. **83**, 1914 (1999).
[77] R. Aleksan et al., Nucl. Phys. **B361**, 141 (1991).
[78] S. Versillé, PhD thesis, Université de Paris-Sud (April 1999). Available (in French) at the URL `http://www-lpnhep.in2p3.fr/babar/public/versille/Thesis/`.
[79] J. Charles, PhD thesis, Université de Paris-Sud (April 1999). Available (in French) at the URL `http://qcd.th.u-psud.fr/preprints_labo/physique_particule/art1999/art1999.html`.
[80] S. Versillé, J. Charles, R.N. Cahn and F. le Diberder, in preparation.
[81] R.G. Sachs, Preprint EFI-85-22 (1985) (unpublished);
I. Dunietz and R.G. Sachs, Phys. Rev. **D37**, 3186 (1988); (E) Phys. Rev. **D39**, 3515 (1989);
I. Dunietz, Phys. Lett. **B427**, 179 (1998).
[82] R. Aleksan, I. Dunietz and B. Kayser, Z. Phys. **C54**, 653 (1992).
[83] M. Gronau and D. London, Phys. Lett. **B253**, 483 (1991).
[84] M. Athanas et al. (CLEO Coll.), Phys. Rev. Lett. **80**, 5493 (1998).
[85] I. Dunietz, Phys. Lett. **B270**, 75 (1991).
[86] M.P. Schmidt (CDF Coll.), hep–ex/9906029.
[87] A.S. Dighe et al., Phys. Lett. **B369**, 144 (1996).
[88] A.S. Dighe, I. Dunietz and R. Fleischer, Eur. Phys. J. **C6**, 647 (1999).
[89] I. Dunietz, R. Fleischer and U. Nierste, in preparation.
[90] D. Silverman, Phys. Rev. **D58**, 095006 (1998).
[91] P. Ball and R. Fleischer, Phys. Lett. **B475**, 111 (2000).
[92] J.L. Rosner, Phys. Rev. **D42**, 3732 (1990).
[93] R. Fleischer, Phys. Rev. **D60**, 073008 (1999).
[94] A.S. Dighe, I. Dunietz and R. Fleischer, Phys. Lett. **B433**, 147 (1998).
[95] Y. Grossman and H.R. Quinn, Phys. Rev. **D56**, 7259 (1997);
J. Charles et al., Phys. Lett. **B425**, 375 (1998);
B. Kayser and D. London, hep–ph/9909560.
[96] See, e.g. D. Chang, Nucl. Phys. **B214**, 435 (1983);
G. Ecker and W. Grimus, Nucl. Phys. **B258**, 328 (1985); Z. Phys. **C30**, 293 (1986).
[97] J.-M. Frère et al., Phys. Rev. **D46**, 337 (1992).
[98] P. Ball, J.-M. Frère and J. Matias, hep–ph/9910211.
[99] A. Ali and D. London, Eur. Phys. J. **C9**, 687 (1999).
[100] G. Barenboim et al., Phys. Rev. **D60**, 016003 (1999).
[101] Y. Grossman, Phys. Lett. **B380**, 99 (1996).
[102] P. Kooijman and N. Zaitsev, LHCb NOTE 98-067, and N. Zaitsev, private communication.
[103] M.Smizanska for the ATLAS Coll., Talk given at the 6th Conference on B Physics with Hadron Machines, June 1999, Bled. To be published in Nucl. Instrum. Meth. A.
[104] P. Galumian, private communication.
[105] A. Dighe and S. Sen, Phys. Rev. **D59**, 074002 (1999).
[106] M. Bauer, B. Stech and M. Wirbel, Z. Phys. **C29**, 637 (1985); Z. Phys. **C34**, 103 (1987).
[107] C.P. Jessop et al. (CLEO Coll.), Phys. Rev. Lett. **79**, 4533 (1997).

[108] M. Beneke, G.Buchalla and I.Dunietz, Phys. Rev. **D54**, 4419 (1996).

[109] For overviews, see R. Fleischer, hep–ph/9904313; M. Neubert, hep–ph/9909564.

[110] R. Fleischer, Phys. Lett. **B459**, 306 (1999).

[111] I. Dunietz, Proceedings of the Workshop on B Physics at Hadron Accelerators, Snowmass (CO), USA, eds. P. McBride and C. Shekhar Mishra, p. 83.

[112] H.J. Lipkin, Phys. Lett. **B415**, 186 (1997).

[113] A.J. Buras, R. Fleischer and T. Mannel, Nucl. Phys. **B533**, 3 (1998).

[114] R. Fleischer, Eur. Phys. J. **C6**, 451 (1999).

[115] R. Fleischer, Phys. Lett. **B435**, 221 (1998).

[116] D. Pirjol, Phys. Rev. **D60**, 054020 (1999).

[117] Y. Kwon et al. (CLEO Coll.), hep–ex/9908029; hep–ex/9908039.

[118] R. Fleischer and T. Mannel, Phys. Rev. **D57**, 2752 (1998).

[119] M. Neubert and J.L. Rosner, Phys. Lett. **B441**, 403 (1998).

[120] R. Fleischer, Phys. Lett. **B365**, 399 (1996).

[121] M. Gronau and J.L. Rosner, Phys. Rev. **D57**, 6843 (1998).

[122] M. Neubert and J.L. Rosner, Phys. Rev. Lett. **81**, 5076 (1998).

[123] A.J. Buras and R. Fleischer, Phys. Lett. **B365**, 390 (1996).

[124] J. Schwinger, Phys. Rev. Lett. **12**, 630 (1964);
R.P. Feynman, in "Symmetries in Particle Physics", ed. A. Zichichi (Acad. Press 1965);
O. Haan and B. Stech, Nucl. Phys. **B22**, 448 (1970);
D. Fakirov and B. Stech, Nucl. Phys. **B133**, 315 (1978);
L.L. Chau, Phys. Rept. **95**, 1 (1983).

[125] A. Khodjamirian, R. Rückl and C.W. Winhart, Phys. Rev. **D58**, 054013 (1998);
E. Bagan, P. Ball and V.M. Braun, Phys. Lett. **B417**, 154 (1998).

[126] P. Ball, JHEP **9809**, 005 (1998).

[127] J.D. Bjorken, Nucl. Phys. Proc. Suppl. **11**, 325 (1989); Proceedings of the SLAC Summer Institute 1990, p. 167.

[128] L. Wolfenstein, Phys. Rev. **D52**, 537 (1995);
J.-M. Gérard and J. Weyers, Eur. Phys. J. **C7**, 1 (1999);
A.F. Falk et al., Phys. Rev. **D57**, 4290 (1998);
D. Atwood and A. Soni, Phys. Rev. **D58**, 036005 (1998).

[129] M. Neubert, Phys. Lett. **B424**, 152 (1998).

[130] M. Gronau and J.L. Rosner, Phys. Rev. **D58**, 113005 (1998).

[131] M. Neubert, JHEP **9902**, 014 (1999).

[132] N.G. Deshpande and X.G. He, Phys. Rev. Lett. **74**, 26 (1995); (E) Phys. Rev. Lett. **74**, 4099 (1995).

[133] M. Gronau et al., Phys. Rev. **D52**, 6374 (1995).

[134] M. Gronau and D. Pirjol, Phys. Lett. **B449**, 321 (1999); Phys. Rev. **D61**, 013005 (2000);
K. Agashe and N.G. Deshpande, Phys. Lett. **B451**, 215 (1999); Phys. Lett. **B454**, 359 (1999).

[135] R. Fleischer and T. Mannel, hep–ph/9706261;
R. Fleischer, in Ref. [10]; M. Neubert, in Ref. [131];
D. Choudhury, B. Dutta and A. Kundu, Phys. Lett. **B456**, 185 (1999);
X.G. He, C.L. Hsueh and J.Q. Shi, Phys. Rev. Lett. **84**, 18 (2000).

[136] Y. Grossman, M. Neubert and A.L. Kagan, hep–ph/9909297.

[137] R. Fleischer and J. Matias, Phys. Rev. **D61**, 074004 (2000).

[138] M. Neubert and B. Stech, hep–ph/9705292.

[139] E. Jenkins and M.J. Savage, Phys. Lett. **B281**, 331 (1992).

[140] B. Grinstein et al., Nucl. Phys. **B380**, 369 (1992).

[141] L. Lellouch and C.-J.D. Lin (UKQCD Coll.), Nucl. Phys. Proc. Suppl. **73**, 357 (1999) [hep–lat/9809018].

[142] R. Fleischer, Z. Phys. **C58**, 483 (1993);
G. Kramer, W.F. Palmer and H. Simma, Z. Phys. **C66**, 429 (1995).

[143] M. Bander, D. Silverman and A. Soni, Phys. Rev. Lett. **43**, 242 (1979).

[144] A.J. Buras, M. Jamin and P.H. Weisz, Nucl. Phys. **B347**, 491 (1990).

[145] S. Aoki, hep–ph/9912288; S. Hashimoto, hep–lat/9909136; L. Lellouch, hep–ph/9906497; J.M. Flynn and C.T. Sachrajda, hep–lat/9710057.

[146] C. Bernard, T. Blum and A. Soni, Phys. Rev. **D58**, 014501 (1998);
L. Lellouch and C.J. Lin (UKCD Coll.), hep–ph/9912322.

[147] S. Hashimoto et al., Phys. Rev. **D60**, 094503 (1999).

[148] R. Gupta, T. Bhattacharya and S. Sharpe, Phys. Rev. **D55**, 4036 (1997).

[149] G. Blaylock, hep–ex/9912038;
see also `http://www.cern.ch/LEPBOSC/combined_results/summer_1999/`.

[150] H.-G. Moser and A. Roussarie, Nucl. Instrum. Meth. **A384**, 491 (1997).

[151] A. Starodumov and Z. Xie, CMS NOTE 1999/006.

[152] Z. Xie, F. Palla and A. Starodumov, CMS NOTE in preparation.

[153] R. Ammar et al. (CLEO Coll.), Phys. Rev. Lett. **71**, 674 (1993).

[154] Y. Grossman, Z. Ligeti and E. Nardi, Phys. Rev. **D55**, 2768 (1997).

[155] W. Skiba and J. Kalinowski, Nucl. Phys. **B404**, 3 (1993).

[156] T. Inami and C.S. Lim, Prog. Th. Phys. **65**, 297 (1981); (E) 1772.

[157] D. Atwood, L. Reina and A. Soni, Phys. Rev. **D55**, 3156 (1997);
K.S. Babu and C. Kolda, Phys. Rev. Lett. **84**, 228 (2000).

[158] A. Nikitenko, A. Starodumov and N. Stepanov, CMS-NOTE-1999-039 (hep–ph/9907256).

[159] C. Greub, T. Hurth and D. Wyler, Phys. Rev. **D54**, 3350 (1996);
C. Greub and T. Hurth, Phys. Rev. **D56**, 2934 (1997).

[160] K. Chetyrkin, M. Misiak and M. Münz, Phys. Lett. **B400**, 206 (1997); (E) **B425**, 414 (1998).

[161] M.B. Voloshin, Phys. Lett. **B397**, 275 (1997).

[162] A. Khodjamirian et al., Phys. Lett. **B402**, 167 (1997).

[163] M. Misiak, hep–ph/0002007.

[164] A. Khodjamirian, G. Stoll and D. Wyler, Phys. Lett. **B358**, 129 (1995);
A. Ali and V.M. Braun, Phys. Lett. **B359**, 223 (1995).

[165] B. Grinstein and D. Pirjol, hep–ph/0002216.

[166] G. Kostina and P. Pakhlov, LHCb Note LHCB/97–022
(`http://lhcb.cern.ch/notes/postscript/97notes/97-022.ps`).

[167] C. Bobeth, M. Misiak and J. Urban, hep–ph/9910220.

[168] A. Ali et al., Phys. Rev. **D61**, 074024 (2000).

[169] D. Melikhov, N. Nikitin and S. Simula, Phys. Rev. **D57**, 6814 (1998); Phys. Lett. **B430**, 332 (1998); Phys. Lett. **B442**, 381 (1998);
T.M. Aliev, C.S. Kim and Y.G. Kim, hep–ph/9910501;
C.S. Kim, Y.G. Kim and C.D. Lu, hep–ph/0001151.

[170] A. Ali and G. Hiller, Eur. Phys. J. **C8**, 619 (1999); Phys. Rev. **D60**, 034017 (1999).

[171] A. Ali, T. Mannel and T. Morozumi, Phys. Lett. **B273**, 505 (1991);

F. Krüger and L.M. Sehgal, Phys. Lett. **B380**, 199 (1996);
Z. Ligeti, I.W. Stewart and M.B. Wise, Phys. Lett. **B420**, 359 (1998).

[172] J. Charles et al., Phys. Rev. **D60**, 014001 (1999).

[173] G. Burdman, Phys. Rev. **D57**, 4254 (1998).

[174] D. Melikhov et al., ATLAS Note ATL–PHYS–98–123.

[175] T.M. Aliev, C.S. Kim and M. Savci, Phys. Lett. **B441**, 410 (1998).

[176] N. Nikitin, F. Rizatdinova and L. Smirnova, Phys. Atom. Nucl. **62**, 1697 (1999) [Yad. Fiz. **62**, 1823 (1999)].

[177] P. Cho, M. Misiak and D. Wyler, Phys. Rev. **D54**, 3329 (1996).

[178] S. Ahmed et al. (CLEO Coll.), hep–ex/9908022.

[179] B. Abbott et al. (D0 Coll.), Phys. Lett. **B423**, 419 (1998).

[180] S. Glenn et al. (CLEO Coll.), Phys. Rev. Lett. **80**, 2289 (1998).

[181] T. Affolder et al. (CDF Coll.), Phys. Rev. Lett. **83**, 3378 (1999).

[182] A.F. Falk, M. Luke and M.J. Savage, Phys. Rev. **D49**, 3367 (1994).

[183] J. Chay, H. Georgi and B. Grinstein, Phys. Lett. **B247**, 399 (1990).

[184] T.M. Aliev, D.A. Demir and M. Savci, hep–ph/9912525.

[185] A. Khodjamirian and R. Rückl, hep–ph/9801443.

[186] A. Khodjamirian and R. Rückl, hep–ph/9807495;
A. Khodjamirian, R. Rückl and C.W. Winhart, in preparation.

[187] I. Caprini, L. Micu and C. Bourrely, Phys. Rev. **D60**, 074016 (1999); hep–ph/9910297.

[188] V.M. Belyaev, A. Khodjamirian and R. Rückl, Z. Phys. **C60**, 349 (1993).

[189] B. Blok and M. Shifman, Nucl. Phys. **B389**, 534 (1993).

[190] G.R. Farrar and D.R. Jackson, Phys. Rev. Lett. **43**, 246 (1979).

[191] A.V. Efremov and A.V. Radyushkin, Phys. Lett. **B94**, 245 (1980).

[192] G.P. Lepage and S.J. Brodsky, Phys. Rev. **D22**, 2157 (1980).

[193] H.D. Politzer and M.B. Wise, Phys. Lett. **B257**, 399 (1991).

[194] J.F. Donoghue et al., Phys. Rev. Lett. **77**, 2178 (1996).

[195] F. Abe et al. (CDF Coll.), Phys. Rev. Lett. **81**, 2432 (1998); Phys. Rev. **D58**, 112004 (1998).

[196] S.S. Gershtein et al., hep–ph/9803433.

[197] M. Beneke and G. Buchalla, Phys. Rev. **D53**, 4991 (1996).

[198] C. Quigg, in Proc. of the Workshop on B Physics at Hadron Accelerators, Snowmass (CO), USA, 1993, eds. P. McBride and C.S. Mishra.

[199] I.I. Bigi, Phys. Lett. **B371**, 105 (1996).

[200] B.D. Jones and R.M. Woloshyn, Phys. Rev. **D60**, 014502 (1999).

[201] V.V. Kiselev and A. Tkabladze, Sov. J. Nucl. Phys. **50**, 1063 (1989);
T.M. Aliev and O. Yilmaz, Nuovo Cim. **105A**, 827 (1992);
M. Chabab, Phys. Lett. **B325**, 205 (1994).

[202] P. Colangelo, G. Nardulli and N. Paver, Z. Phys. **C57**, 43 (1993);
E. Bagan et al., Z. Phys. **C64**, 57 (1994).

[203] S. Godfrey and N. Isgur, Phys. Rev. **D32**, 189 (1985);
P. Colangelo, G. Nardulli and M. Pietroni, Phys. Rev. **D43**, 3002 (1991);
E. Eichten and C. Quigg, Phys. Rev. **D49**, 5845 (1994);
S.S. Gershtein et al., Phys. Rev. **D51**, 3613 (1995);
L.P. Fulcher, Phys. Rev. **D60**, 074006 (1999).

[204] G. Chiladze, A.F. Falk and A.A. Petrov, Phys. Rev. **D60**, 034011 (1999).

[205] P. Colangelo and F. De Fazio, Mod. Phys. Lett. **A33**, 2303 (1999).

[206] V.V. Kiselev and A. Tkabladze, Phys. Rev. **D48**, 5208 (1993).

[207] D. Du and Z. Wang, Phys. Rev. **D39**, 1342 (1989);
M. Lusignoli and M. Masetti, Z. Phys. **C51**, 549 (1991).

[208] C.H. Chang and Y.Q. Chen, Phys. Rev. **D49**, 3399 (1994);
J.F. Liu and K.T. Chao, Phys. Rev. **D56**, 4133 (1997).

[209] E. Jenkins et al., Nucl. Phys. **B390**, 463 (1993).

[210] M.A. Sanchiz-Lozano,Nucl. Phys. **B440**, 251 (1995);
M. Galdon and M.A. Sanchiz-Lozano, Z. Phys. **C71**, 277 (1996);
P. Colangelo and F. De Fazio, Phys. Rev. **D61**, 034012 (2000).

[211] V.V. Kiselev, A.K. Likhoded and A.I. Onishchenko, hep–ph/9905359.

[212] D. Du, X. Li and Y. Yang, Phys. Lett. **B380**, 193 (1996);
S. Fajfer, D. Prelovsek and P. Singer, Phys. Rev. **D59**, 114003 (1999);
T.M. Aliev and M. Savci, hep–ph/9908203.

[213] M. Masetti, Phys. Lett. **B286**, 160 (1992);
Y.S. Dai and D.S. Du, Eur. Phys. J. **C9**, 557 (1999).

[214] E. Bagan et al., Phys. Lett. **B287**, 176 (1992); Phys. Lett. **B301**, 243 (1993);
D.B. Lichtenberg, R. Roncaglia and E. Predazzi,Phys. Rev. **D52**, 1722 (1995);
S.S. Gershtein et al., Heavy Ion Phys. **9**, 133 (1999);
V.V. Kiselev, A.K. Likhoded and A.I. Onishchenko, hep–ph/9901224.